The role of protein phosphorylation in acclimation processes in the cyanobacterium *Synechocystis* sp. PCC 6803

Zur Erlangung des akademischen Grades

doctor rerum naturalium (Dr. rer. nat.)

der Mathematisch-Naturwissenschaftlichen Fakultät der Universität Rostock

vorgelegt von Thomas Barske

geb. am 03.06.1990 in Neustrelitz

Rostock, Juli 2024

https://doi.org/10.18453/rosdok_id00005006

Die Rolle der Proteinphosphorylierung bei Akklimatisierungsprozessen im Cyanobakterium *Synechocystis* sp. PCC 6803

Zur Erlangung des akademischen Grades

doctor rerum naturalium (Dr. rer. nat.)

der Mathematisch-Naturwissenschaftlichen Fakultät der Universität Rostock

vorgelegt von Thomas Barske

geb. am 03.06.1990 in Neustrelitz

Rostock, Juli 2024

Gutachter:

1. Prof. Dr. Martin Hagemann, Universität Rostock, MNF/ IfBi / Pflanzenphysiologie

2. Prof. Dr. Karl Forchhammer, Universität Tübingen, Mikrobiologie/Organismische Interaktionen

Tag der Einreichung: 16.07.2024

Tag der Verteidigung: 08.11.2024

Summary

Cyanobacteria present a remarkable capability in acclimating to fluctuating environmental conditions and therefore, were able to inhabit all kinds of diverse habitats. Their diversity in responding to rapidly changing conditions is highlighted by their complexity in signal perception systems. The model organism *Synechocystis* sp. PCC 6803 (*Synechocystis*) can adopt a photoautotrophic, photo-mixotrophic and heterotrophic lifestyle. The underlying coherent decision making between heterotrophy (catabolism) and photoautotrophy (anabolism) mode of lifestyle requires an adaptable regulatory network. Rapid signal transmission through post translational modification, particularly through protein phosphorylation, is essential for adequate cellular responses. We hypothesized that a switch from carbon anabolism towards carbon catabolism in constant light can be mainly regulated by modifications of enzyme activities due to differential phosphorylation states. In this thesis the physiological importance of protein phosphorylation in *Synechocystis* under fluctuating inorganic carbon (Ci) conditions was studied. A global proteome and phospho-proteome study with *Synechocystis* WT (F) was conducted with HC (high CO_2) to LC (low CO_2) shifted cells. We thereby comparatively analyzed alterations on a proteome and phospho-proteome level of short-term and long-term acclimated cells. 200 phosphorylation-events (p-events) on 105 proteins were detected with an extensive number of transiently modified p-events upon changing Ci. Among, proteins with significant alterations corresponded to proteins associated with CCM (i.e., CmpA, CmpB), photosynthesis (i.e., PsaD, CpcA), DNA replication (i.e., DnaX, SbcC, NusG) and regulatory proteins (e.g., CP12, P_{II}). The twelve serine/threonine protein kinases (SpkA-L) of *Synechocystis* were analyzed in their role in the acclimation to different environmental conditions. Kinase deficient mutants, indicating a Ci related phenotype, were studied in detail. The phenotypes of Δ*spkB* and Δ*spkC* highlighted that the protein kinases SpkB, SpkC are promising candidates in regulating carbon allocation. Δ*spkB* and Δ*spkC* showed significantly reduced growth in a HC LC shift growth experiments with Δ*spkB* presenting additional impairment in glucose utilization. Global proteome and phospho-proteome studies were applied to reveal potential kinase/target relationships. The global phospho-proteome of Δ*spkB* showed lowered P_{II} phosphorylation. Altered P_{II} phosphorylation could further be verified *in vivo* concluding a potential regulatory role of SpkB in C/N homeostasis. Additionally, SpkC was found to be differentially phosphorylated in WT (F) in response to LC. The Δ*spkC* mutant was significantly impacted under HC LC shift and the global phospho-proteome of Δ*spkC* presented abolished p-events on CmpA and CmpB of the high affinity HCO_3^- transporter BCT1 followed by a significantly lowered affinity to HCO_3^-. This result suggested a role of SpkC in modulating rapid low Ci induced HCO_3^- transport.

Zusammenfassung

Cyanobakterien verfügen über die bemerkenswerte Fähigkeit, sich and wechselnde Umweltbedingungen anpassen zu können und waren daher in der Lage, die unterschiedlichsten Lebensräume zu besiedeln. Ihre Fähigkeit auf rasch schwankende Umweltbedingungen reagieren zu können, wird durch ihre komplexen Signalwahrnehmungssysteme unterstrichen. Der Modellorganismus *Synechocystis* sp. PCC 6803 lebt sowohl photoautotroph, photomixotroph als auch heterotroph. Die zugrunde liegende kohärente Entscheidungsfindung zwischen Heterotrophie (Katabolismus) und Photoautotrophie (Anabolismus) erfordert ein anpassungsfähiges regulatorisches Netzwerk. Eine schnelle Signalübersetzung durch Posttranslationale Modifizierung, insbesondere durch Proteinphosphorylierung, ist für die schnelle zelluläre Reaktion von wesentlicher Bedeutung. Die Hypothese wurde aufgestellt, dass ein Wechsel vom Kohlenstoff-Anabolismus zum Kohlenstoff-Katabolismus bei konstantem Licht hauptsächlich durch Modifikationen der Enzymaktivitäten aufgrund unterschiedlicher Phosphorylierungszustände reguliert werden kann. In dieser Arbeit wurde die physiologische Bedeutung der Proteinphosphorylierung in *Synechocystis* unter fluktuierenden anorganischen Kohlenstoff (Ci) Bedingungen untersucht. Eine Proteom- und Phospho-Proteom-Studie mit *Synechocystis* WT (F) wurde durchgeführt, welches von HC (hoher CO_2-Gehalt) in LC (niedriger CO_2-Gehalt) überführt wurde. Die Veränderungen auf Proteom- und Phospho-Proteom-Ebene von kurz- und langfristig akklimatisierten Zellen wurden verglichen. 200 Phosphorylierungs-Ereignisse an 105 Proteinen wurden registriert. Unter diesen konnten signifikante Phosphorylierungs-Veränderungen bei Proteinen, die mit dem CCM (z.B. CmpA, CmpB), Photosynthese (z.B. PsaD, CpcA), DNA-Replikation (z.B. DnaX, SbcC, NusG) und regulatorischen Proteinen (z. B. CP12, PII) in Verbindung stehen, gefunden werden. Die zwölf Serin/Threonin Proteinkinasen (SpkA-L) von *Synechocystis* wurden auf ihre Rolle in der Akklimatisierung an verschiedene Umweltbedingungen untersucht. Mutanten, die einen Ci-bezogenen Phänotyp aufwiesen, wurden im Detail untersucht. Die Phänotypen von Δ*spkB* und Δ*spkC* machten deutlich, dass die Proteinkinasen SpkB und SpkC vielversprechende Kandidaten für die Regulierung der Kohlenstoff-Verteilung sind. Δ*spkB* und Δs*pkC* zeigten im Wechsel von HC zu LC ein signifikant reduziertes Wachstum, wobei Δ*spkB* eine zusätzliche Beeinträchtigung der Glukose-Verstoffwechslung aufwies. Proteom- und Phospho-Proteom-Studien wurden durchgeführt, um potenzielle Kinase-Substrat-Beziehungen aufzudecken. Das Phospho-Proteom von Δ*spkB* zeigte eine verringerte PII-Phosphorylierung auf. Diese konnte auch *in vivo* nachgewiesen werden, was auf eine mögliche regulatorische Rolle von SpkB bei der C/N-Homöostase schließen lässt. Außerdem wurde festgestellt, dass SpkC in WT (F) nach dem Transfer von HC zu LC verändert phosphoryliert vorlag. Δ*spkC* zeigte in LC ein signifikant

reduziertes Wachstum. Im Δ*spkC* Phospho-Proteom konnten die Phosphorylierungs-Ereignisse an CmpA und CmpB nicht nachgewiesen, welches von einer signifikant verringerten Affinität zu HCO_3^- in der Mutante begleitet war. Die Ergebnisse weisen auf eine Rolle von SpkC in der Modulierung des schnellen, durch niedriges Ci induzierten, HCO_3^- Transports hin.

I Table of content

II List of Tables

III List of Figures

IV Abbreviations

2OG	2-oxoglutaric acid
2PG	2-Phosphoglyceric acid
3PGA	3-Phosphoglyceric acid
AA	amino acid
ADP	adenosine diphosphate
Ala	alanine
Arg	arginine
Arg	argenine
Asn	asparagine
Asp	aspartic acid
ATP	adenosine triphosphate
B. Subtilis	*Bacilus subtilis*
bp	base pairs
C	carbon
CA	carbonic anhydrase
CBB	Calvin-Benson-Bassham cycle
CCM	carbon concentrating mechanism
Chl *a*	chlorophyll *a*
Ci	inorganic carbon
CoA	coenzyme A
Cys	cysteine
$Cytb_6f$	cytochrome b_6f complex
Da	Dalton
ddH_2O	double destilated water
de novo	from the beginning
DNA	desoxyribonucleic acid
E. coli	*Escherichia coli*
ED	Entner-Doudoroff pathway
EMP	Embden-Meyerhof-Parnas pathway
FD	ferredoxin
FNR	ferredoxin-NADP reductase
gDNA	genomic DNA
Gln	glutamine

Glu	glutamic acid
Gluc	glucose
Gly	glycine
GOGAT	glutamine-oxoglutarate amidotransferase
GOI	gene of intrest
GS	glutamine synthetase
GTP	guanosine triphosphate
HC	high carbon
HCO_3^-	bicarbonate
Hik	histidine kinase
His	histidine
HRP	horse reddish peroxidase
Ile	isoleucine
in silico	on a computer
in vivo	within the living
$Km^R/Sp^R/Gm^R$	kanamycin/ spectinomycin/ gentamycin resistance
LC	low carbon; ambient air
Leu	leucine
Lys	lysine
M. xanthus	*Myxococcus xanthus*
MBP	myelin basic protein
Met	methionine
MP	milk powder
MS	mass spectrometry
N	nitrogen
N_2	atmospheric nitrogen
NADP+	nicotinamide adenine dinucleotide phosphate
NO_3^-	nitrate
OD	optical densitiy
ON	over night
OPP	oxidative pentose phosphate pathway
P	phosphorus
p-event	phosphorylation event
p-occupancy	phosphorylation occupancy
p-phoshorlyation	protein phosphorylation

p-proteins	phospho-proteins
PB	phycobiliproteins
PBS	phycobilisome
PC	plastocyanin
PCR	polymerase chain reaction
PEP	phosphoenolpyruvic acid
Phe	phenylalanine
PK	phosphoketolase pathway
PKL	protein kinase like
PQ	plastoquinone
PQH_2	plastohydroquinone
Pro	proline
PSI	photosystem I
PSII	photosystem II
PTM	post translational modification
PVDF	Polyvinylidene fluoride or polyvinylidene difluoride
Q_a	quinone A
RNA	ribonucleic acid
ROS	reactive oxygen species
rpm	revelations per minute
RR	response regulator
RT	room temperatur
RuBisCo	ribulose 1,5-bisphosphate carboxylase/oxygenase
S/Ser	serine
spk/Spk	serine/threonine protein kinase (gene/protein)
Synechocystis	*Synechocystis* sp. PCC 6803
T/Thr	threonine
TCA	tricarboxylic acid cycle
TCS	two component system
Trp	tryptophan
TU	transcriptive unit
v/v	volume/volume
Val	valine
w/v	weight/volume
Y/Tyr	tyrosine

1 Introduction

1.1 The need to study cyanobacteria

Despite their rich diversity, chloroplasts which are found in the kingdom of *Plantae,* comprising green plants, red algae, green algae and glaucophytes, are derived from a single endosymbiotic event approximately 1.5 billion years ago, in which a free-living cyanobacterium was engulfed by a heterotrophic eukaryotic cell (Cavalier-Smith, 2000; Weber et al., 2006; Chan & Bhattacharya, 2010). However, instead of digesting the engulfed cyanobacteria, this ancient event was followed by horizontal gene transfer from the endosymbiont to the host nucleus. Consequently, this process led to the evolution of a stable photosynthetic organelle, the plastids we know today (Weber et al., 2006). In fact, oxygenic photosynthesis evolved 2.7 billon years ago in cyanobacteria (Hohmann-Marriott & Blankenship, 2011). Since then, cyanobacteria continued to evolve and through their outstanding capability to adjust to changing environmental conditions inhabited all kinds of diverse habitats in which some light is available (Houmard, 1995). Today, cyanobacteria are contributing to almost one quarter of globally fixed CO_2 and additionally are important assimilators of atmospheric N_2 (Kasting & Siefert, 2002; Durall & Lindblad, 2015). Lately, through increasing concern about climate change and the exploration for sustainable energy sources raised much interest in photoautotrophic cyanobacteria as chassis to produce biofuels and chemical feedstock (Angermayr et al., 2009; Ducat et al., 2011; Hagemann & Hess, 2018). Thus, bioengineered cyanobacteria were trialed to manufacture products such as ethanol (Deng & Coleman, 1999; Z. Gao et al., 2012), isobutyraldehyde and isobutanol (Atsumi et al., 2009), fatty acids (X. Liu et al., 2011), sucrose (Ducat et al., 2012), hydroxy propionate (Y. Wang et al., 2016) and isoprene (Lindberg et al., 2010; Pade et al., 2016). However, production yields remained low, making the production of bio-compounds not yet economically feasible (Hagemann & Hess, 2018).

1.1.1 Model organism *Synechocystis* sp. PCC 6803

The unicellular cyanobacterial model organism *Synechocystis* sp. PCC 6803 (hereafter *Synechocystis*) was first isolated from a freshwater lake in Berkley in 1968 and became part of the Pasteur Culture Collection (PCC) (Rippka et al., 1979; Zavřel et al., 2017). Although being classified as a freshwater cyanobacterium, *Synechocystis* can be found in a variety of different habitats e.g., coastal areas and even areas of high salinity (Reed & Stewart, 1985; Pattanayak et al., 2015). *Synechocystis* can live in different modes of lifestyle i.e.,

photoautotrophically, mixotrophically (X. Chen et al., 2016), and light-activated heterotrophically (Anderson & McIntosh, 1991) on an external carbon source (e.g., glucose) (Rippka et al., 1979) even though many other cyanobacteria are obligated photoautotrophs. *Synechocystis* is a non-diazotrophic cyanobacterium, meaning it is unable to fix atmospheric nitrogen (N_2) and can only grow on combined nitrogen sources, usually with nitrate (NO_3^-). *Synechocystis* was the first fully sequenced photoautotrophic organism (Kaneko et al., 1996; Kaneko & Tabata, 1997). Through its natural competency, it can take up foreign DNA and incorporate it into its own genome by homologous recombination (Grigorieva & Shestakov, 1982) *Synechocystis* is suitable for genetic manipulation (Ikeuchi & Satoshi Tabata, 2001) thereby, making it a great tool to study general metabolism which created an interest in its use in biotechnological application (e.g., Hagemann & Hess, 2018). Moreover, *Synechocystis* can naturally produce carbon biopolymers such as glycogen (Gründel et al., 2012), polyhydroxy butyrate (PHB) (Schlebusch & Forchhammer, 2010) and cyanophycin (Watzer et al., 2015), which are of biotechnological interest.

1.2 Photosynthesis in cyanobacteria

Almost all life on earth, directly or indirectly, depends on energy derived from the sun and thus, underlines the importance of the biological process of photosynthesis that harvests and converts the sun's energy into energy-rich organic compounds (Blankenship, 2002). Cyanobacteria are the only prokaryotes capable of performing oxygenic photosynthesis. In this process inorganic carbon (Ci), either as carbon dioxide (CO_2) or bicarbonate (HCO_3^-), is effectively converted to organic compounds driven by light energy. The light dependent reaction is taking place in the thylakoid membrane in most cyanobacteria (Figure 1) (Vermaas, 2001). Photosynthesis involves two light-driven reactions: (i) oxidation of water with the consequent release of oxygen (O_2) carried out by photosystem II (PSII) and, the reduction of ferredoxin (FD) performed by PSI (Hill & Bendall, 1960; Vermaas, 2001; Lea-Smith et al., 2016). The reaction initiates at PSII, a multimeric protein complex consisting of an antenna complex, the reaction center and the oxygen evolving complex. The membrane complex cytochrome (Cyt) b_6f facilitates electron transport between PSII to PSI. The protein complexes are connected by mobile redox carriers i.e., plastoquinone (PQ) between PSII and $Cytb_6f$ and plastocyanin (PC) between $Cytb_6f$ and PSI. ATP-synthase is driven by the proton gradient over the thylakoid membrane (Mitchell, 1961), which is generated in parallel to the vectorial electron transport. In the linear electron transport chain, $NADP^+$ the final electron acceptor (Herva et al., 2003). Alternatively, FD can donate electrons back to $Cytb_6f$ through PQ and create a cyclic electron flow to produce more ATP.

In cyanobacteria, light energy is captured by a vast membrane-extrinsic complex named phycobilisomes (PBS) mainly associated with PSII and chlorophyll a (Chl*a*) bound to antennae proteins in PSII and PSI (Bhatti et al., 2020; Calzadilla & Kirilovsky, 2020). PBS consist of water soluble phycobiliproteins (PB) and linker proteins (Figure 1). In *Synechocystis,* PBS are organized in hemi-discoidal structures with stacks of allophycocyanin trimers and peripheral phycocyanin rods. PBS funnel the captured light energy mainly to PSII (Bryant & Frigaard, 2006; N. K. Singh et al., 2015). If the absorbed light exceeds the energy consumption for cellular processes can lead to the over-reduction of the entire photosynthetic chain which in turn promotes the formation of reactive oxygen species (ROS) at PSII and PSI (Bhatti et al., 2020; Calzadilla & Kirilovsky, 2020). Cyanobacteria can rapidly alter their photosynthetic complexes in response to light in a process termed state transition. This activity redistributes the excitation energy via reversible migration of PBS between PSII and PSI and thereby decreases or increases the activity of the photosystems (Allen et al., 1985; Allen & Holmes, 1986; Mullineaux & Allen, 1988; Mullineaux et al., 1997).

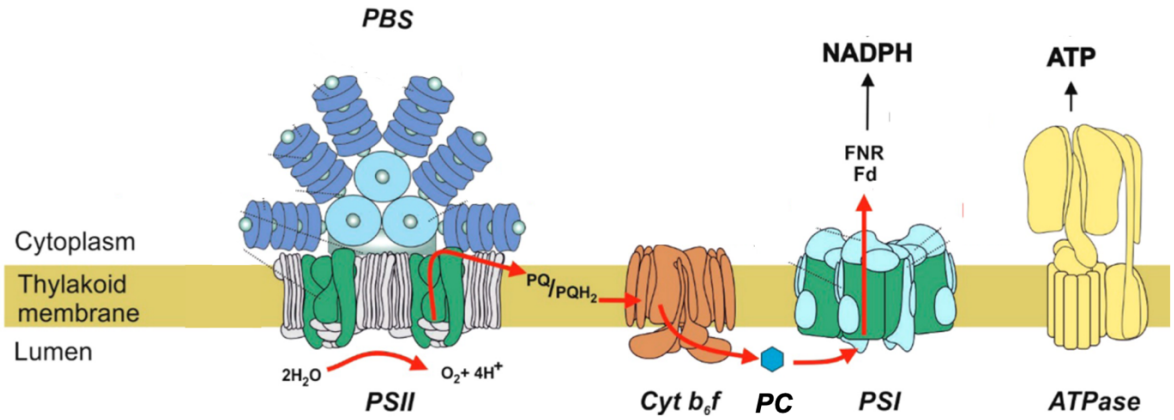

Figure 1: Overview of the photosynthetic electron transport chain in cyanobacteria. Electron transport during the light reaction of photosynthesis takes place in the thylakoid membrane. Shown are four integral membrane complexes photosystem II and I (PSII, PSI), Cytochrome (Cyt) b_6f and the ATP-synthase (ATPase) together with the ferredoxin-NADP reductase (FNR), the mobile electron carriers plastoquinone (PQ, PQH_2) and plastocyanin (PC). Light energy is captured by a membrane-extrinsic complex named phycobilisomes (PBS) mainly associated with PSII. (Figure modified from Angeleri et al., 2016).

1.3 Ci assimilation in cyanobacteria

The CO_2 fixing enzyme ribulose 1,5-bisphosphate carboxylase/oxygenase (RuBisCO) in the photosynthetic Calvin-Benson-Bassham (CBB) cycle evolved under relatively high levels of atmospheric CO_2 concentrations (0.6%) and virtual O_2-free conditions, thus RuBisCO shows a rather low affinity towards CO_2 and low specificity of CO_2 over O_2 (Hagemann et al., 2021). Hence, cyanobacteria had to adapt to today's Earth atmosphere which contains 0.04% CO_2 and 20% O_2 (Rae et al., 2013). To overcome low CO_2 affinity and suppressing the futile

oxygenase reaction of RuBisCO, cyanobacteria evolved a Ci concentrating mechanism (CCM) (Figure 2), which increases cellular CO_2 levels in the proximity of RuBisCO (Tcherkez et al., 2006; Burnap et al., 2015; Raven et al., 2017). The CCM in *Synechocystis* is taking up Ci either in the form of CO_2 or HCO_3^- and accumulates high HCO_3^- levels in the cytoplasm, which is then diffusing into the microcompartment carboxysome, where RuBisCO is situated and the HCO_3^- is converted to a locally high concentration of CO_2 through the activity of carbonic anhydrase (CA) (Rae et al., 2013; Burnap et al., 2015). *Synechocystis* possesses three HCO_3^- uptake transporters: (i) the constitutively expressed Na^+ HCO_3^- symporter BicA (Price et al., 2004), (ii) the low Ci induced ABC-type transporter BCT1 (Omata et al., 1999) and (iii) the Na^+ HCO_3^- symporter SbtA (Shibata et al., 2002). Additionally, CO_2 can be converted into HCO_3^- by either the constitutively expressed Ndh1-4 or the low Ci induced Ndh1-3 complex (Shibata et al., 2001). The expression of CCM related genes is under the control of the transcription factors NdhR (CcmR) (Figge et al., 2001; H. L. Wang et al., 2004), CmpR (Omata et al., 2001), CyAbrB2 (Shalev-Malul et al., 2008; Orf, Schwarz, et al., 2016) and RbcR (Bolay et al., 2022).

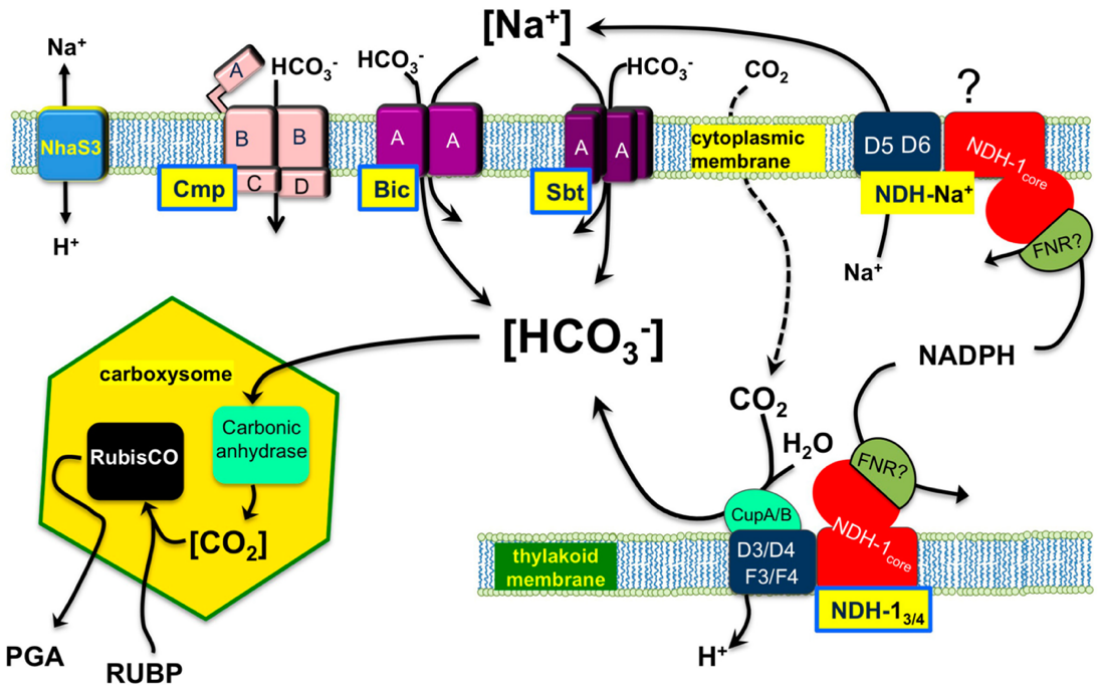

Figure 2: Overview of cyanobacterial carbon concentrating mechanism (CCM). Inorganic carbon (Ci) is taken up as either CO_2 or HCO_3^- through the constitutively expressed symporter BicA, Ndh1-4 or the low Ci induced ABC1 transporter BCT1, Ndh1-3 and the symporter SbtA. HCO_3^- is transported to the carboxysome where inwards diffusing HCO_3^- is converted to CO_2 by carbonic anhydrase (CA) creating a high CO_2 concentration in the vicinity of RuBisCO (Figure taken from Burnap et al. 2015).

1.4 Primary carbon metabolism in cyanobacteria

The primary carbon (C) metabolism is conserved throughout all domains of life (Figure 3). In oxygenic photoautotrophs such as cyanobacteria, the CBB cycle (Figure 3) is the primary route of incorporating Ci into the cellular metabolism (Bassham et al., 1954). RuBisCO is the key enzyme catalyzing the reaction of ribulose 1,5 bisphosphate either with CO_2 producing two molecules 3-phosphoglycerate (3PGA) or by reacting with O_2 and thereby generating one molecule 3PGA metabolite and one molecule of the toxic compound 2-phosphoglycolate (2PG) (e.g., Flügel et al., 2017). Two molecules of the toxic compound 2PG are efficiently recycled by the photorespiratory 2PG metabolism into one 3PGA thereby releasing CO_2 (Eisenhut et al., 2008). The CBB cycle provides carbohydrates for biosynthesis and storage (Makowka et al., 2020). Under conditions with high 3PGA proportions (e.g., HC, high CO_2 i.e., 5%), excess amounts of organic carbon will be stored in form of glycogen (Mills et al., 2020), which is consumed during the night or in a Ci limited environment to sustain the metabolism (Eisenhut et al., 2007; Gründel et al., 2012; Saha et al., 2016). *Synechocystis* possesses two main glycolytic routes to metabolize the stored organic carbon in from of glycogen: (i) the Embden-Meyerhof-Parnas (EMP) and (ii) the oxidative pentose phosphate (OPP) pathway (Makowka et al., 2020). The OPP is downregulated during the day and serves as the primary breakdown pathway under conditions promoting a heterotrophic metabolism, e.g., during the night (Pelroy & Bassham, 1972; Takahashi et al., 2008). Additional glycolytic routes have been identified in cyanobacteria i.e., the Entner-Doudoroff (ED) (X. Chen et al., 2016) and the phosphoketolase (PK) (Alagesan et al., 2013; Bachhar & Jablonsky, 2020) pathway with reports indicating a function under fluctuating light conditions or ED (Schulze et al., 2022) and a contribution to heterotrophic growth for PK pathway (Xiong et al., 2015).

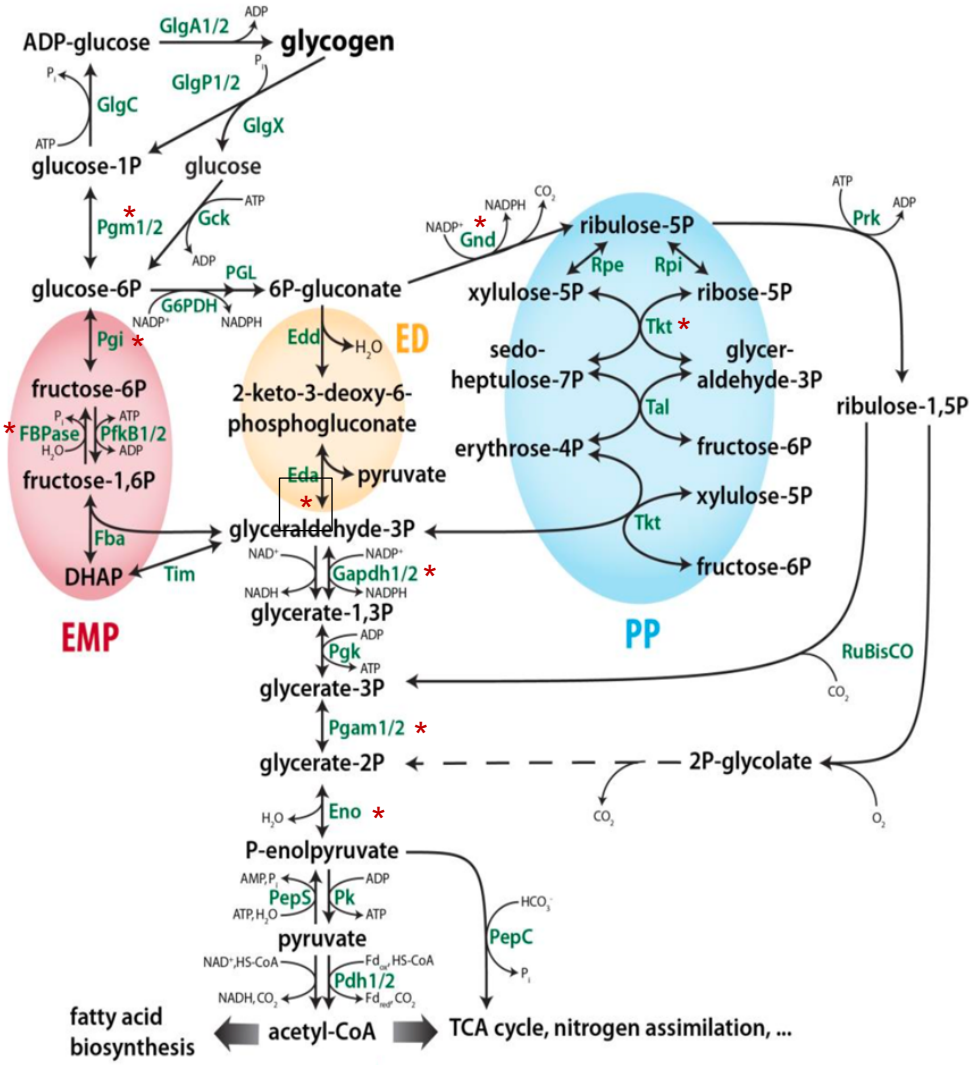

Figure 3: Overview of the primary carbon metabolism in *Synechocystis*. During the reaction of the Calvin-Benson-Bassham (CBB) cycle, CO_2 is fixed by ribulose 1,5-bisphosphate carboxylase/oxygenase (RuBisCO) to form either two molecules 3-phosphoglycerate (3PGA) or one molecule 3PGA together with one molecule of the toxic compound 2-phosphoglycolate (2PG). 2PG is efficiently recycled by the 2PG-metabolism. 3PGA can either be used in the lower metabolism or excess amounts can be stored in form of glycogen. Under Ci limitation, glycogen is again mobilized via two glycolytic routes: (i) Embden-Meyerhof-Parnas (EMP; red) and (ii) the oxidative pentose phosphate (OPP; blue) pathway. Red asterisk (*) indicate confirmed phospho-proteins (Yang et al., 2013; Mikkat et al., 2014; Spät et al., 2015; Z. Chen et al., 2015; Angeleri et al., 2016; Toyoshima et al., 2020); (Figure adapted from Koch et al., 2019).

The product of carbohydrate oxidation, pyruvate, is entering the tricarboxylic acid cycle (TCA, Krebs cycle) as acetyl-CoA (H. A. Krebs, 1970). In cyanobacteria, the TCA cycle (Figure 4) has been shown to be incomplete because of the missing 2-oxogluterate (2OG) dehydrogenase complex with only recently discovered shunts completing the TCA cycle (S. Zhang & Bryant, 2011). In bacteria the TCA cycle fulfills two main tasks: (i) by oxidizing acetyl-CoA, derived from the primary C metabolism, generating CO_2 and NADH thereby delivering

electrons for oxidative phosphorylation and (ii) to produce 2OG as a precursor for N assimilation (Steinhauser et al., 2012; Jablonsky et al., 2016). N is assimilated via the coupled glutamine synthetase (GS)- glutamine-oxoglutarate amidotransferase (GOGAT) and yields the amino acid (AA) glutamine with 2OG as the central building block (Meeks et al., 1977). Thus, 2OG is connecting C and N metabolism (Forchhammer & Selim, 2019).

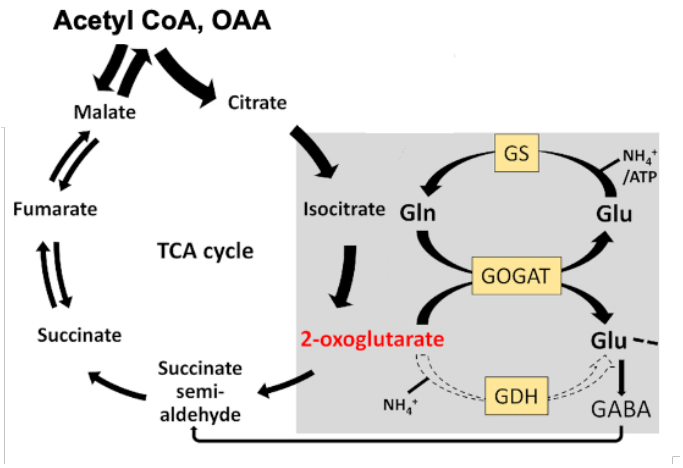

Figure 4: Overview of the TCA cycle and nitrogen assimilation in *Synechocystis*. Fixed Ci is introduced into the tricarboxylic acid (TCA) cycle via acetyl-CoA, where it gets oxidized to produce electrons for oxidative phosphorylation and to produce 2-oxogluterate (2OG). 2OG is the precursor of N assimilation and thereby connects C and N metabolism with each other. N is assimilated via the coupled glutamine synthetase (GS)- glutamine-oxoglutarate amidotransferase (GOGAT) and yields the AA glutamine with 2OG serving as carbon precursor. (Figure adapted from Forchhammer & Selim, 2019)

1.4.1 Regulation of the primary carbon metabolism in *Synechocystis*

Synechocystis has been characterized of being capable of thriving in various lifestyle modes i.e., photoautotrophically, heterotrophically, and mixotrophically (X. Chen et al., 2016). To accommodate appropriate metabolic fluxes, the primary C metabolism needs to be able to flexibly acclimate itself towards changing environmental conditions e.g., changes in light quantity and quality (e.g., day/night, shading), nutrient availability (e.g., C, N, P), or changes in temperature (e.g., heat stress, cold stress). To avoid futile cycles within the metabolic network, a multilayered regulatory system is needed to effectively respond to changes in the environment. Regulatory mechanisms for the primary C metabolism are scarcely understood. Transcriptional regulation was thought to be the prevalent mode of regulation in bacteria and its pivotal role in regulating CCM and N assimilation in *Synechocystis* was demonstrated (Ohashi et al., 2011; Burnap et al., 2015). The RNA polymerase σ-factor SigE is a positive regulator of genes involved in carbohydrate catabolism in dark acclimated cells in a heterotrophic lifestyle and shows a circadian oscillation reaching its peak in light/dark transition

(Osanai et al., 2005, 2009, 2011). Mutant studies on histidine kinase (Hik) 8, an ortholog to circadian clock protein SasA, has been identified to have a role in the control of the C metabolism in response to light mediated redox changes (A. K. Singh et al., 2004; Osanai et al., 2015). Likely, Hik8 interacts with the response regulator (Rre) 37 (Osanai et al., 2014). A mutant defective in Rre37 presented a defect in light-activated heterotrophic growth (Osanai et al., 2014). Furthermore, Hik37 seems to be involved in glucose (Gluc) mediated catabolism (L. Gao et al., 2014). The transcription factor RpaA is involved in SigE degradation in the dark and stimulates transcription of enzymes of glycogen and Gluc metabolism (Iijima et al., 2015; Köbler et al., 2018) and together with the proposed clock complex KaiAB1C1-SasA RpaA affects the switch from autotrophy to the usage of stored carbon (Scheurer et al., 2021).

Post translational modifications (PTM) i.e., covalent modifications, protein-protein interactions and effector metabolite binding became of interest as a regulatory mechanism in bacterial C allocation and have been reported to play a vital role in coordinating glycolytic fluxes in animal and plant cells (e.g., Zaffagnini et al., 2013; van Heerden et al., 2015). GlnB (P_{II}) is one of the best characterized regulatory proteins in *Synechocystis* (Forchhammer et al., 2022). By binding 2OG, ATP and/or ADP, P_{II} can integrate information about the C/N balance and of the energy state of the cell and adjust C and N fluxes accordingly (Forchhammer & Selim, 2019). Recently, P_{II} has been demonstrated to interact with the small protein PirC (Orthwein et al., 2021). PirC is said to be released from P_{II} under N limitation and interacts with the phosphoglycerate mutase 1 (Pgam1) and thus blocking fluxes into the lower glycolysis and thereby favoring anabolic glycolytic routes and the formation of glycogen. The small, disordered protein CP12 known to bind the CBB enzymes glyceraldehyde 3-phosphate dehydrogenase 2 (GapDH2) and phosphoribulokinase (PRK) under oxidative conditions is modulating CBB and OPP activity under redox changing conditions (Gurrieri et al., 2021; Lucius et al., 2022). Shifting *Synechocystis* from high carbon (HC) to low carbon (LC) led to no apparent changes in transcript abundancies of metabolic enzymes (Klähn et al., 2015; Orf et al., 2015) but was accompanied by a shift in the metabolic signature that highlights the efficiency of PTM (Orf, Timm, et al., 2016). According to kinetic models, metabolic changes mainly occur through substrate dependent enzymatic activities combined with specific action of isoenzymes at metabolic branching points and the underlying regulation by PTM (Jablonsky et al., 2016).

Phospho-proteomic experiments revealed an ever-increasing number of phosphoproteins (p-proteins) in *Synechocystis* (Mikkat et al., 2014; Spät et al., 2015; Z. Chen et al., 2015; Angeleri et al., 2016; Toyoshima et al., 2020) amongst, many were found to be enzymes in the primary C metabolism e.g., GapDH2, Pgam1, Eno (Figure 3) (Mikkat et al., 2014). The physiological

relevance of the identified phosphorylation events (p-events) remains elusive. New evidence for the glycogen metabolism enzyme phosphoglucomutase 1 (Pgm1) revealed the importance of PTM on serine 47 (S47) during nitrogen starvation and its concomitant role in modulating its activity (Doello et al., 2022). Additionally, it was discovered that regulatory proteins such as P_{II} (Forchhammer & Tandeau De Marsac, 1994) and CP12 (Spät et al., 2018) are prone to p-phosphorylation and furthermore, presenting changes in their phosphorylation status under changing environmental conditions (Forchhammer & Tandeau De Marsac, 1994; Schwarz et al., 2014; Spät et al., 2018). These results clarify the significance of PTM in form of p-phosphorylation as a hallmark in metabolic regulation in *Synechocystis*.

1.5 Posttranslational protein modification

PTM are covalent modifications on AA after DNA to RNA transcription and consequent translation into proteins to extend the information content of the 20 proteogenic AA (Walsh et al., 2005; Macek et al., 2019). PTM are not genetically encoded however, they can influence protein folding, activity, stability, protein interaction capabilities and cellular localization (Prabakaran et al., 2012; Mijakovic et al., 2016). Protein modification is taking place on approximately half of all proteinogenic AA. AA with hydroxy-, amino- or thiol groups such as serine (Ser), threonine (Thr), tyrosine (Tyr), histidine (His), aspartate (Asp), asparagine (Asn), lysine (Lys), arginine (Arg) and cysteine (Cys) are among the most modified (Macek et al., 2019). Two categories of PTM can occur: (i) the enzyme catalyzed reversible covalent attachment of a small group i.e., in form of methylation (methyl group, 14 Da), acetylation (acetyl group, 42 Da) or p-phosphorylation (phosphate group, 80 Da), to even larger more complex modifications e.g., oligosaccharide structures (2-3 kDa) or polypeptide chains (up to 10 kDa) like ubiquitin in eukaryotes and ubiquitin-like protein (Pup) in prokaryotes and (ii) by irreversible covalent cleavage of protein backbones by proteases or less commonly, by autocatalytic cleavage (Walsh et al., 2005; Pearce et al., 2008; Macek et al., 2019). However, most PTM are sub-stoichiometric and therefore, not present on all molecules of a given protein, enabling the cell to rapidly expand the pool of modified proteins without relying on energy intensive *de novo* protein biosynthesis and degradation (Macek et al., 2019). It is well established that the vast majority of these modifications are ubiquitous across eukaryotes, archaea and bacteria (Walsh et al., 2005; Minguez et al., 2012; Cain et al., 2014; Mijakovic et al., 2016; Ramazi & Zahiri, 2021). The number of PTM and the diverse array of protein targets have challenged the dogma of molecular biology, which posited that one gene codes for one protein with a single function (Cain et al., 2014). Different PTM can occur simultaneously on multiple residues or in a tandem cascade on a peptide sequence. For instance, the tyrosine kinase Ab1 has been demonstrated to undergo phosphorylation on eleven different residues,

theoretically resulting in 40’420’800 (11!) different isoforms of a single protein (Steen et al., 2003; Walsh et al., 2005; Macek et al., 2019). The complexity of the PTM network is further compounded by the fact that even some complex modification, such as ubiquitin, can themselves undergo additional modifications e.g., phosphorylation (Koyano et al., 2014; Macek et al., 2019).

Bacteria, often seen as simple organisms, explore a vast range of PTM (Figure 5). Mass spectrometry (MS) based proteomics revealed an extensive spectrum of PTMs in eukaryotes which those also have shown to have profound effects on bacterial physiology and virulence (Szymanski et al., 2002; Cain et al., 2014). In bacteria, p-phosphorylation is the best documented and the so far best understood modification among PTM (Mijakovic et al., 2016). Large scale PTM studies in eukaryotes find thousands of modified peptides, contrasting to the much less abundant and more diverse protein modifications in bacteria (Olsen & Mann, 2013; Macek et al., 2019). Rapid progress in bacterial PTM research is best illustrated by the detection of p-events which expanded from 81 p-events in the first published phospho-proteome of *Escherichia coli* (*E. coli*) to more than 1883 in recent studies (Macek et al., 2007, 2019; Potel et al., 2018).

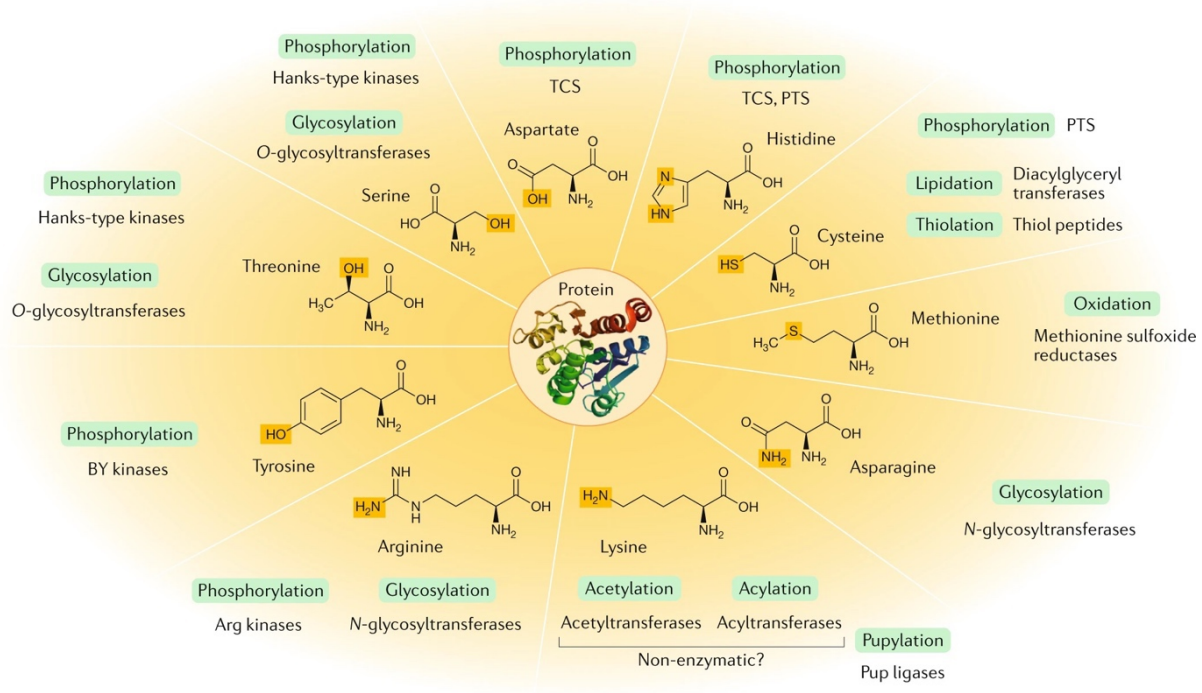

Figure 5: Overview of posttranslational modifications (PTM) in bacteria. Amino acid (AA) residues can be covalently modified. Common AA residue specific modifications in bacteria and enzymes carrying out the modification are depicted. TCS= two component system, PTS= phosphotransferase system. (Figure taken from Macek et al., 2019).

1.5.1 Protein phosphorylation in bacteria

Reversible p-phosphorylation and dephosphorylation is one of the most important PTM, catalyzed by protein kinases and phosphatases. Protein kinases are enzymes that transfer a phosphate group to specific AA on a target protein (Figure 6) (Cozzone, 1993). Typically, these kinases use the γ-phosphate of ATP as phosphate group donor, although GTP and PEP can also serve as phosphate group suppliers (Hunter, 1991, 2012). Protein kinases exhibit specificity to their acceptor AA, leading the 'Nomenclature Committee of International Union of Biochemists' to classify them into five groups based on the nature of the acceptor AA: (i) AA with alcohol groups such as Ser and Thr, which form phosphate esters, (ii) AA with phenolic groups as acceptors, namely Tyr , which also forms phosphate esters, (iii) basic AA such as His, Arg and Lys, which produce phosphoramidates, (iv) AA with acyl groups as acceptors, such as Asp and Glu, generating mixed phosphate-carboxylate acid anhydrites and (v) Cys residues, which produce thioesters (Hunter, 1991; Cozzone, 1993). This classification underscores the diverse roles and specificities of protein kinases in bacterial phosphorylation processes.

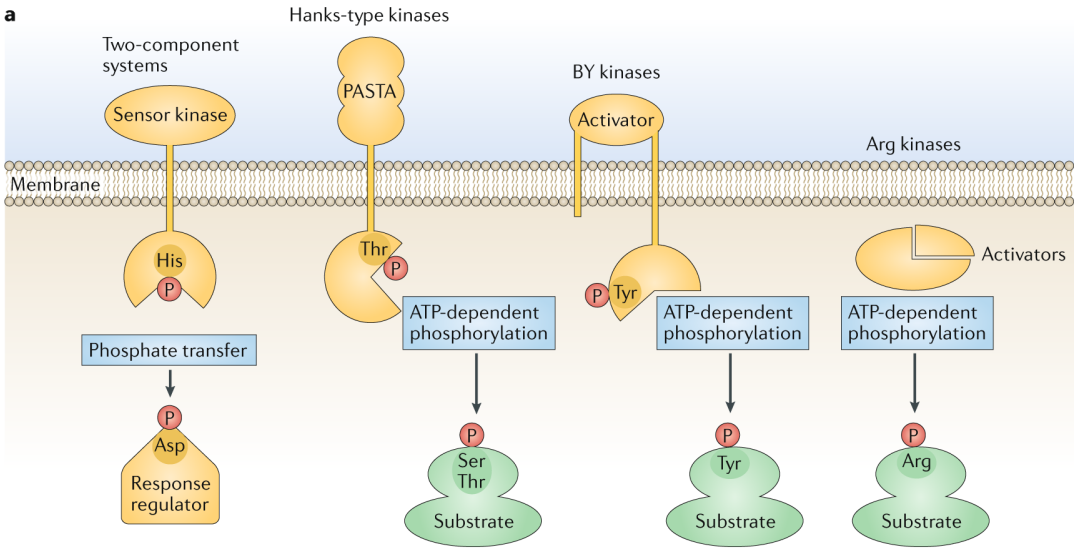

Figure 6: Overview of phosphate group transfer to AA in bacteria. Phosphate group transfer to side specific histidine (His), aspartate (Asp), serine (Ser), threonine (Thr), tyrosine (Tyr) and arginine (Arg) residues together with their respective kinases. (Figure adapted from Macek et al. 2019).

Bacterial p-phosphorylation serves as a crucial signal transduction mechanism, linking environmental stimuli to the regulation of essential physiological processes (Kobir et al., 2011). The most common type of p-phosphorylation signaling in bacteria involves two-component systems (TCS), where signals are transmitted via His autophosphorylation and consequent

Asp phosphorylation (Figure 6). This type of signaling is the predominant form of p-events in bacterial organisms (Macek et al., 2019). TCS can be found in all bacterial species and consist of a signal-sensing histidine kinase (Hik) and a response regulator (RR). Often membrane associated, upon signal perception Hik uses ATP to autophosphorylate on a His residue which in turn transfers the phosphate group onto an Asp residue on the receiver domain of a RR. The RR can harbor an additional DNA binding domain or other domains to translate the sensed signal into a stress specific response (Stock et al., 2000; Hirakawa et al., 2020). Thus, TCS mediated signal cascades enable bacteria to adapt to stress and environmental changes effectively on mostly transcriptional level (Gross et al., 1989).

Phosphoesters on Ser, Thr and Tyr are the second most common form of p-phosphorylation in bacteria (Macek et al., 2019). P-phosphorylation on Ser and Thr residues are commonly catalyzed by Hanks-type kinases, which share a strong similarity to kinases found in eukaryotes (Figure 6) (Pereira et al., 2011; Mijakovic et al., 2016; Macek et al., 2019). It should be noted that in addition to Hanks-type kinases, other kinases have been identified phosphorylating Ser and Thr residues. These are termed atypical kinases (Pérez et al., 2008; Pereira et al., 2011; Mijakovic et al., 2016). Unlike Ser and Thr phosphorylation, no eukaryotic-like Tyr kinases were identified in bacteria (Grangeasse et al., 2012). The majority of tyrosine residue phosphorylation is carried out by the protein kinase family of bacterial protein-tyrosine kinases (BY-kinases, Figure 6) (Grangeasse et al., 2012; Mijakovic et al., 2016). Arg phosphorylation was discovered recently in *Bacillus subtilis* (*B. subtilis*), where it was proven to affect factors in the stress response system. This view was only recently expanded by reports of Arg phosphorylation in *Staphylococcus aureus* (Fuhrmann et al., 2009, 2013, 2016; Elsholz et al., 2012; Schmidt et al., 2014; Junker et al., 2018). Cys thiol groups are not only prone to oxidative modification but can also undergo phosphorylation (Mijakovic et al., 2016). Cys phosphorylation has been shown to play a regulatory role in the control of transcription factors in *Staphylococcus aureus* (F. Sun et al., 2012). Phospho-Lys modification was detected *in vivo*, but little is known about their biological role. No Lys kinase has yet been identified (Bertran-Vicente et al., 2014).

Even though, His and Asp phosphorylation account for most p-events in bacteria, their thermodynamic instability renders the *in vivo* detection challenging in phospho-proteomic studies (Macek et al., 2019). The applied extraction method for phosphorylated peptides is carried out under acidic conditions (pH<4) and thus favoring p-events on Ser, Thr and Tyr residues instead of phosphorylated His and Asp residues through their low chemically stability in such environments (Macek & Mijakovic, 2011; Mijakovic & Macek, 2012; Macek et al., 2019). Quantifying relative proteins levels of perturbed biological systems depended for long

on 2-D gel-electrophoresis (Macek & Mijakovic, 2011). Therefore, early global phospho-proteome studies relied heavily on this technology to identify p-events. Technical advances in gel-free and MS based approaches resulted in the first published *in vivo* phospho-proteome of *B. subtilis* (Macek et al., 2007) and of *E. coli* (Macek et al., 2008) in an exponential growth phase. In comparison to previous gel-based methods that reported a small number or p-events, which could not be linked to specific peptides (Enami & Ishihama, 1984; Cortay et al., 1986; Lévine et al., 2006), this approach reported 103 individual phospho-peptides which could be assigned to 78 individual proteins of *B. subtilis* and 81 phospho-peptides on 79 proteins in *E. coli*, respectively. However, most of the p-events detected in phospho-proteomic studies have not been analyzed and their effect on protein function remains elusive (Mijakovic et al., 2016).

1.5.2 Serine/Threonine protein kinases in bacteria

The Ser/Thr kinase superfamily of protein kinase like (PKL) proteins includes all protein kinases and small molecule and metabolite kinases (Figure 7) (Cheek et al., 2002; Kannan et al., 2007; Lundquist et al., 2012). PKL demonstrates a diverse sequence and structural variability to meet the catalytic demands for the vast variety of target proteins. The PKL superfamily is subdivided into Hanks-type kinases and atypical protein kinases (Figure 7) (Hanks et al., 1988; Hanks & Hunter, 1995; Kannan et al., 2007).

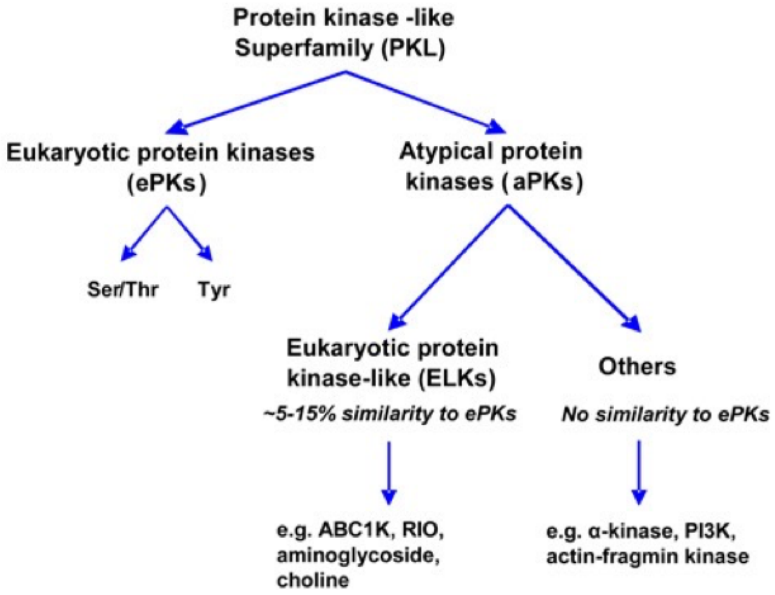

Figure 7: Grouping of the protein kinase-like (PKL) superfamily. The Ser/Thr PKL superfamily includes all protein kinases, small molecule and metabolite kinases. PKL demonstrates a diverse sequence and structural variability to meet the catalytic demands for the vast variety of target proteins. The PKL superfamily is subdivided into Hanks-kinases (**ePKs**) and atypical protein kinases (**aPKs**). (Figure adapted from Lundquist et al., 2012)

Hanks et al. (1998) defined and described the prevalent family of Ser, Thr and Tyr protein kinases in eukaryotes (Janczarek et al., 2018). Initially, this group of kinases was believed to be exclusively existing in eukaryotes but the discovery of the first bacterial Ser/Thr kinase Pkn1 in *Myxococcus xanthus* (*M. xanthus*) broke the phylogeny barrier (Muñoz-Dorado et al., 1991; Janczarek et al., 2018). The discovered enzyme shared a strong structural similarity to previously described kinases in eukaryotes. The increasing number of available prokaryotic genomes led to a rapid increase in identified kinases resembling the ones found in eukaryotes (Shi et al., 1998; Kennelly, 2002; Krupa & Srinivasan, 2005; Pérez et al., 2008; Pereira et al., 2011). Hence, the identified Ser/Thr kinases were termed eukaryotic like protein kinases in bacteria without any conclusive evidence that this family of kinases originated in eukaryotes (Pereira et al., 2011). Moreover, studies suggested that Hanks-type kinases found in eukaryotes, bacteria and archaea share an evolutionary origin leading back to the last universal common ancestor (LUCA) and that there is no evidence of horizontal gene transfer from eukaryotes to bacteria (Leonard et al., 1998; Stancik et al., 2018). Thus, the name Hanks-type kinases was suggested to be adopted for this group of kinases found in bacteria and archaea due to their monophyletic origin (Stancik et al., 2018). Typically, Hanks-kinases are organized into twelve subdomains which fold into the characteristic two-lobed catalytic core architecture (Figure 8) (Hanks et al., 1988; Hanks & Hunter, 1995; Kornev & Taylor, 2010; Pereira et al., 2011; Janczarek et al., 2018). The catalytic core is situated embedded in the cleft pocket of the two lobes (Figure 8 A). The smaller N-terminal lobe is responsible for binding and orienting ATP as phosphate group donor whereas the larger C-terminal lobe binds to the substrate and facilitates the phospho-transfer. In bacteria, protein kinases can also possess additional domains outside the conserved catalytic domain that mediate ligand binding or protein-protein interactions (e.g., penicillin-binding Ser/Thr kinase associated repeats (PASTA) and fork head-associated domains (FHA)) (Krupa & Srinivasan, 2005). Protein kinases are seen as molecular switches and are found to be either in an inactive or active state (Huse & Kuriyan, 2002; Pereira et al., 2011). The transition to an active state relies on various mechanism such as binding of allosteric effectors and subcellular location (Kornev & Taylor, 2010; Pereira et al., 2011; Janczarek et al., 2018). The activation segment (Figure 8 A, B) is the most important regulatory part of the kinase (Hanks et al., 1988; Hanks & Hunter, 1995; Kornev & Taylor, 2010; Pereira et al., 2011; Janczarek et al., 2018). Kinases achieve their active state either by autophosphorylation or transphosphorylation by another kinase of at least one Ser or Thr residue in the activation loop.

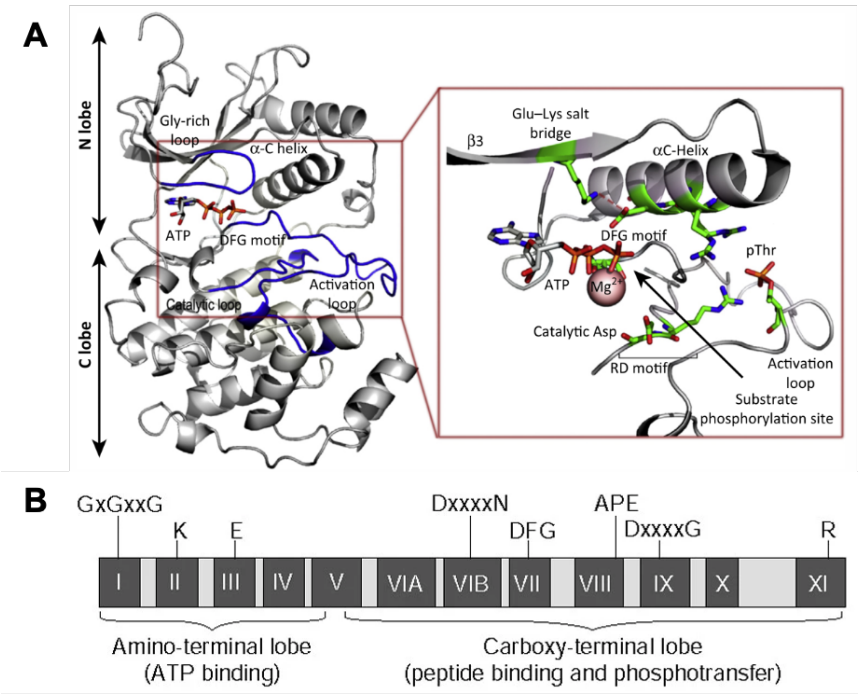

Figure 8: Overview of the structural architecture and subdomains of the catalytic domains a Hanks-type Ser/Thr kinase. (**A**) Hanks-kinases consist of N and C lobes, connected by an activation segment, termed the activation loop. The activation segment contains motifs essential for the catalytic activity of a protein kinase. (**B**) The catalytic domain is structured in twelve conserved subdomains (indicated by roman numeral I-XI) together with conserved AA residues in certain segments. (Figures adapted from (**A**) Beenstock et al., 2016 and (**B**) Hanks, 2003)

Atypical protein kinases share little or no conserved motifs with Hanks-type kinases (Scheeff & Bourne, 2005). However, crystallography studies revealed that most atypical kinases maintain a similar kinase fold. *In silico* studies in which members of the entire PKL superfamily were analyzed according to their sequence and structure revealed only a few conserved residues between Hanks-kinases and atypical kinases. Among the group of atypical kinases, there are members sharing up to 15 % sequence identity named 'Hanks-protein kinase like protein kinases' (Scheeff & Bourne, 2005; Kannan et al., 2007). Members of the former group appeared to be important regulatory kinases for bacteria (C. C. Zhang, 1996; Shi et al., 1998; Kennelly, 2002; Krupa & Srinivasan, 2005), such as ABC1/UbiB kinases (Bousquet et al., 1991; Brasseur et al., 1997; Leonard et al., 1998; Poon et al., 2000), amyloglycoside kinases (Toth et al., 2009) and others (Kannan et al., 2007; Lundquist et al., 2012).

Members of the UbiB/ABC1 family of kinases are found in bacteria, archaea and eukaryotes with all of them possessing a protein kinase like domain (Leonard et al., 1998). The UbiB protein from *E. coli* is responsible for the aerobic biosynthesis of the redox-active lipid ubiquinone and thus, marks the founding member of the UbiB/ABC1 kinase family (Poon et al., 2000). Prior, the prototypic member of the UbiB/ABC1 was analyzed in *Saccharomyces*

cerevisiae where the ABC1 defective mutant showed impaired aerobic respiration due the reduced activity of mitochondrial bc1 -complex (ABC1) but was initially not associated with a kinase function in yeast (Bousquet et al., 1991; Brasseur et al., 1997; Leonard et al., 1998; Do et al., 2001).

1.6 Protein phosphorylation in cyanobacteria

Cyanobacterial diversity and ability to adapt to changing environmental conditions is highlighted by their complexity of signal perception systems (A. Zorina, 2013). Thus, rapid signal transmission from a receptor to a receiver is essential for an adequate response to stress. Such dynamics are possible through reversible PTM i.e., in form of p-phosphorylation (Macek & Mijakovic, 2011). First demonstrated evidence of p-phosphorylation in cyanobacteria was obtained through [^{32}P] orthophosphate *in vivo* and in cell-free *in vitro* labeling experiments in *Calothrix* sp. PCC 7601 (Schuster et al., 1984), *Syncheococcus* sp. PCC 6301 (Allen et al., 1985), *Anabaeana* sp. PCC 7120 (Mann et al., 1991), *Synechocystis* sp. PCC 6803 (Bloye et al., 1992; Hagemann et al., 1993) and in *Synechococcus* sp. PCC 7942 (Forchhammer & Tandeau De Marsac, 1994). Traditionally, like in other bacteria, TCS were believed to be the predominant phosphorylation-based signal transduction mechanism in cyanobacteria (Stock et al., 2000; Los et al., 2010; Yang et al., 2013). Even though phosphorylation on Ser, Thr and Tyr residues were known to occur in cyanobacteria, studies on kinases creating phosphomonoesters were largely neglected (Mann, 1994). This ultimately changed after the discovery of a Hanks-type Ser/Thr kinase in *M. xanthus* (Muñoz-Dorado et al., 1991). Subsequently, the PCR-based strategy that was applied to identify a Hanks-kinase in *M*. *xanthus* was also employed in *Anabaena* PCC 7120 and resulted in the discovery of the first Hanks-kinase in cyanobacteria (C.-C. Zhang, 1993) followed by an increasing number of similar kinases and phosphatases found in other cyanobacteria ever since (C.-C. Zhang et al., 2005). Crosstalk between TCS and Ser/Thr protein kinases has been reported for *Synechocystis* (Z. X. Liu et al., 2015), *Synechococcus* sp. PCC 7002 (Phalip & Zhang, 2001) and *Anabaena* sp. PCC 7120 (L. Wang et al., 2002) creating complex signal transduction systems. Further insights into the role of p-phosphorylation in cyanobacteria was gained through the first successful cyanobacterial global phospho-proteome study of the marine cyanobacterium *Synechococcus* sp. PCC 7002 where 410 p-events on 245 proteins could be detected (Yang et al., 2013). The distribution of Ser/Thr and Tyr kinases and phosphatases is uneven among cyanobacteria and can vary from zero detected in some *Prochlorococcus* strains to up 56 encoding genes in the N_2 fixing bacterium *Nostoc punctiforme* PCC 73102 (Figure 9) (C.-C. Zhang et al., 2005; A. Zorina, 2013). Interestingly, freshwater cyanobacteria

contain a relatively large number of Ser/Thr and Tyr kinases and phosphatases compared to marine cyanobacteria (C.-C. Zhang et al., 2005). More stable conditions in marine habitats compared to the sessional changes in freshwater environments led to a proposed reduction in genome size of marine cyanobacteria and alongside a reduced number of regulatory and signaling genes (Dufresne et al., 2003). However, no correlation between genome size and number of Ser/Thr and Tyr kinases and phosphatases could be made (C.-C. Zhang et al., 2005).

Strain	Major traits	Genome size, Mb	Number of genes	S/T/ and Y kinase	S/T phos-phatase	Y kinase (Wzc-like)	Y phosphatase (Wzb-like)
Synechocystis PCC 6803	unicellular fresh water strain, motile	3.57	3,168	11	6	2	1
Anabaena PCC 7120	filamentous fresh water strain, N2-fixing, heterocystous	7.21	6,132	52	12	7	5
Thermosynechococcus elongates BP-1	unicellular, thermophilic, from hot spring	2.59	2,475	11	7	2	1
Gloeobacter violaceus PCC 7421	unicellular, no thylacoids, from limestone rock	4.66	4,430	15	7	6	2
Synechococcus WH 8102	unicellular marine strain, motile	2.43	2,514	0	1	1	2
Prochlorococcus marinus SS120	unicellular marine strain, low-light adapted	1.75	1,850	0	0	0	1
Prochlorococcus marinus MED4	unicellular marine strain, high-light adapted	1.66	1,694	1	0	1	1
Prochlorococcus marinus MIT9313	unicellular marine strain, low-light adapted	2.41	2,251	2	1	0	1

Figure 9: Kinase and phosphatase gene distribution among sequenced cyanobacterial genomes. Number of annotated Ser (**S**), Thr (**T**) and Tyr (**Y**) kinases and phosphatases in comparison to genome size and gene number among cyanobacteria. (Figure adapted from C.-C. Zhang et al., 2005)

Hanks-type Ser/Thr kinases in cyanobacteria often have complex domain structures and attempts have been made to group them into separate cyanobacterial kinase families according to their structural traits (C.-C. Zhang et al., 2005; X. Zhang et al., 2007; A. Zorina, 2013). X. Zhang et al. (2007) divided cyanobacterial Ser/Thr kinases into three (I-III) greater families (Figure 10) (X. Zhang et al., 2007; A. Zorina, 2013). Family [I] consists of kinases with only a catalytic domain which is further divided into three subfamilies. Subfamily [I-I] consists of soluble kinases with only one catalytic domain and a typical size fewer than 400 AA which are predominantly found in *Gloeobacter violaceus* PCC 7421, *Croscophaera watsonii* WH 8501 and in diazotrophic filamentous strains. Subfamily [I-II], which is found in unicellular cyanobacteria such as *Synechocystis* is characterized by additional transmembrane domains behind the kinase domain and Subfamily [I-III] with long unidentified domains at the C-terminus. Some kinase representatives even share multiple similarities and are clustered in multiple family branches e.g., SpkC and SpkD of *Synechocystis* (X. Zhang et al., 2007; A. Zorina, 2013). Family [II] is defined by further functional groups in addition to the kinase

domain e.g., PAS, FHA and GAF (Krupa & Srinivasan, 2005) and Family [III] which possess an additional His kinase domain on the C-terminus of the N-terminal Ser/Thr kinase domain, mainly found in *Anabaena* PCC 7120 (C.-C. Zhang et al., 2005; X. Zhang et al., 2007; A. Zorina, 2013). Ser/Thr kinases with dual kinase function are absent in unicellular cyanobacteria such as *Synechocystis* (C.-C. Zhang et al., 2005).

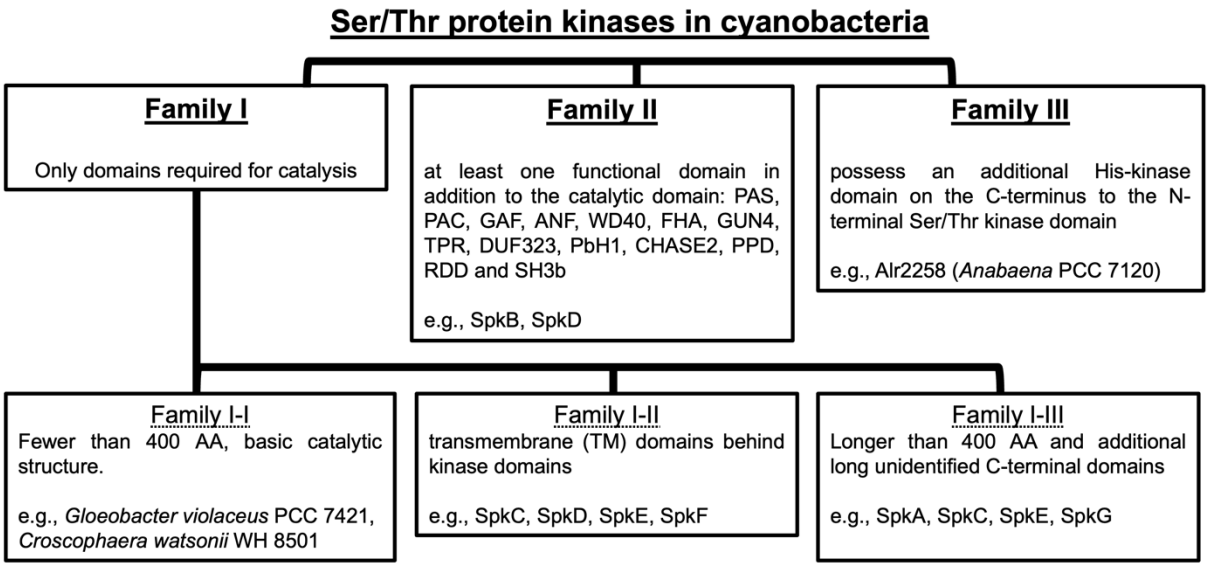

Figure 10: Grouping of cyanobacterial Ser/Thr kinases. Cyanobacterial Hanks-type Ser/Thr kinases were attempted to be grouped according to their respective structural traits. Ser/Thr kinases were clustered into three families (I-III) and subfamilies. Characteristics of each family branch is shown together with representative cyanobacteria. Clustering was performed according to C.-C. Zhang et al. (2005), X. Zhang et al. (2007) and A. Zorina. (2013).

The first cyanobacterial genome sequenced was that of the freshwater cyanobacterium *Synechocystis* (Kaneko et al., 1996; Kaneko & Tabata, 1997) and thus with the emerging interest in p-phosphorylation in bacteria, the genome of *Synechocystis* was searched for Ser/Thr and Tyr -Kinases and phosphatases similar to Hanks-kinases and Hanks-phosphatases (C.-C. Zhang et al., 1998). The search revealed that *Synechocystis* possesses twelve Ser/Thr kinases, one Tyr-kinases and seven phosphatases (C.-C. Zhang et al., 1998; Leonard et al., 1998; Shi et al., 1998). To this day, *Synechocystis* remains the cyanobacterium with the most information about the potential role of p-phosphorylation in acclimation processes through extensive phospho-proteome data sets generated under various environmental conditions (Mikkat et al., 2014; Spät et al., 2015; Z. Chen et al., 2015; Angeleri et al., 2016; Toyoshima et al., 2020). Based on earlier results on salt dependent changes on phosphorylation pattern in cell extracts of *Synechocystis* (Hagemann et al., 1993), the first 2D-gel based LC-MS coupled snapshot phospho-proteome study was performed under fluctuating salinity condition (Mikkat et al., 2014). This study was able to identify 32 p-proteins

such as P_{II}, Kai proteins and a great number of proteins taking part in the primary C metabolism i.e., PgmI, PgmII, PgI, FbaA, FbpII Eno and GapDH2 (see Figure 3). Similarly, several proteins functioning in the C metabolism were also found to be phosphorylated in other cyanobacteria e.g., *Synechococcus* sp. PCC 7002 (Yang et al., 2013) and *Nostoc flagelliforme* (W. Liang et al., 2021). Progressively, interest arose about the potential role of adaptive p-phosphorylation in acclimation processes under fluctuating environmental conditions in *Synechocystis*, which resulted in the first gel-free LC-MS/MS based comparative global phospho-proteome study under N starvation (Spät et al., 2015). This study showed an overall increase in p-events under low N conditions, among many were involved in CCM, primary C metabolism and the central regulator of C/N partitioning P_{II}. These results highlighted the overall importance of dynamic changes in p-phosphorylation when acclimating from an N containing to a N free environment. Similarly, a snapshot phospho-proteome experiment under variating light conditions was performed and discovered that some photosynthesis related proteins undergo changes in phosphorylation occupancy (p-occupancy) under changing light qualities (Z. Chen et al., 2015). Furthermore, this study showed through side specific mutations that the phosphorylation of phycocyanin β-subunit CpcB is of importance for efficient photosynthetic energy resonance transfer and state transition. In a non-comparative phospho-proteome investigation with HC and LC acclimated *Synechocystis* with the emphasis on evaluating p-phosphorylation in relation with C-fixation, photosynthesis and photoprotection displayed that most detected p-events could be clustered to those functional groups of proteins (Angeleri et al., 2016). The most recent comparative survey, a connection between alteration on proteome and phospho-proteome levels under different growth conditions was analyzed (Toyoshima et al., 2020). There, photoautotrophic, heterotrophic, heterotrophic in presence of light and mixotrophic growth condition together with growth under N-starvation (24, 48 h) of *Synechocystis* were compared on proteome and phospho-proteome level and could reveal that relatively small alterations in the proteome are accompanied with vast deviations in overall p-phosphorylation status in the cell which highlights the underlying significance of reversible p-phosphorylation in acclimation processes. Phospho-proteome analyzes proved (Yang et al., 2013; Mikkat et al., 2014; Spät et al., 2015; Z. Chen et al., 2015; Angeleri et al., 2016; Toyoshima et al., 2020) that cyanobacteria explore vast PTM in from of p-phosphorylation in order to rapidly adjust to their environment, but even though extensive data on p-events in cyanobacteria could be collected, fundamental knowledge about Ser/Thr and Tyr kinases and phosphatases and their relationship with recorded p-events remains scarce.

The overall physiological importance of p-phosphorylation in cyanobacteria has been widely acknowledged and its role in dynamic regulatory processes e.g., N metabolism, C metabolism, cell motility, osmotic stress, photosynthesis or state transition (Mann, 1994; C.-C. Zhang et

al., 2005). However, general understanding of the relationship between Ser/Thr and Tyr kinases and phosphatases in cyanobacteria and their potential targets remains fragmentary (Mikkat et al., 2014). To this date the best characterized cyanobacterial p-proteins remain the global regulatory protein P_{II} (Forchhammer et al., 2022), regulator of the C/N balance, and the circadian clock protein KaiC from *Synechococcus elongatus* PCC 7942 (Nakajima et al., 2005; Mikkat et al., 2014). On a global scope, p-phosphorylation affects all functional protein categories in *Synechocystis*, with most p-events found on proteins with unknown function followed by proteins with assigned roles in energy production and conversion (Spät et al., 2023). However there is a growing discrepancy between detected p-events and the number annotated protein kinases. Up until today approximately 500 p-proteins (Appendix Table 3) have been identified in *Synechocystis*, which is in sharp contrast to the only twelve annotated protein kinases (SpkA-L ;C.-C. Zhang et al., 1998; Leonard et al., 1998; Shi et al., 1998) . This occurrence has also been observed for other bacteria e.g., *E. coli* (Macek et al., 2008), *B. subtilis* (Macek et al., 2007) or the marine cyanobacterium *Synechococcus* sp. PCC7002 (Yang et al., 2013). Besides kinase mediated p-phosphorylation adjuvant forms of non-enzymatic (Doello et al., 2022; Neumann et al., 2022) and non-enzymatic acetyl phosphate dependent p-phosphorylation are likely occurring (Morrison et al., 2005). Strict protein kinase substrate specificity is a matter of debate. Bacterial protein kinases have a predicted relaxed substrate specificity (Kobir et al., 2011) with protein kinase recognition sides consisting of only one to three residues for efficient phosphorylation (Kobe et al., 2005; Miller & Turk, 2018). An incomplete picture of Ser/Thr protein kinases in cyanobacteria needs to be considered. Many bacterial Ser/Thr protein kinases in e.g., *Synechocystis* resemble Hanks-type kinases (C.-C. Zhang et al., 1998; Leonard et al., 1998; Shi et al., 1998), however there is a chance of evolutionary unrelated protein kinases such as the isocitrate dehydrogenase kinase/phosphatase found in *E. coli* (Zheng & Jia, 2010) to influence the overall phospho-proteome of cyanobacteria.

1.6.1 Serine/Threonine protein kinases in *Synechocystis*

The genome of *Synechocystis* (Kaneko et al., 1996; Kaneko & Tabata, 1997) harbors twelve Ser/Thr protein kinases (SpkA-L) (C.-C. Zhang et al., 1998; Leonard et al., 1998; Shi et al., 1998) which are structurally divided into PKN2 kinases and ABC1 kinases (Figure 11) (Leonard et al., 1998) respectively to their prototypic family members (Bousquet et al., 1991; Muñoz-Dorado et al., 1991; Udo et al., 1995; Brasseur et al., 1997).

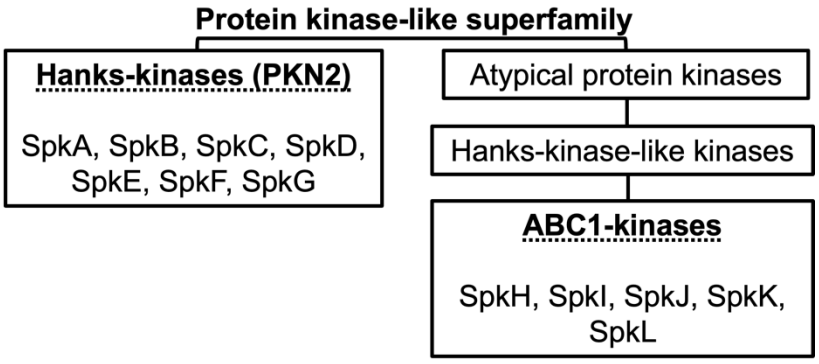

Figure 11: *Synechocystis* Ser/Thr protein kinases assigned to their prototypic family members. The twelve annotated Ser/Thr protein divided into Hanks-type (PKN2) and ABC1 kinases according to their structure. Categorization is based on the studies of C.-C. Zhang et al. (1998); Leonard et al. (1998) and Shi et al. (1998).

The PKN2 group comprises the protein kinases SpkA-G and share strong structural similarity to Hanks-kinases (Leonard et al., 1998; X. Zhang et al., 2007). According to Zhang et al. (2007) SpkF belongs to cyanobacterial kinase family [I-II] with a transmembrane domain whereas SpkA, SpkC, SpkE and SpkG (Figure 10) are grouped in family [I-III] with long stretches of undefined domains behind their catalytic domains (X. Zhang et al., 2007). The architecture of SpkB (Figure 10) is highlighted by a pentapeptide repeat motif at the C-terminus (Bateman et al., 1998) while SpkD possesses an additional SH3B domain resulting in their classification into family [II] of cyanobacterial kinases (Figure 10) (X. Zhang et al., 2007). A global proteome study located SpkC and SpkF as integral proteins in the plasma membrane (Liberton et al., 2016). Kinase activity could be detected for SpkA-G on artificial substrates i.e., histone, MBP and casein as well as autophosphorylation activity with exception of SpkE (Kamei et al., 2001, 2002, 2003; A. A. Zorina et al., 2014). Studies on SpkA showed evidence of a role in cell motility, demonstrated in the null mutant Δ*spkA* by arrest of colony movement under lateral illumination (Kamei et al., 2001). Though retaining pili, the authors proposed that SpkA might not be essential for pili biogenesis but still influences gliding motility towards a light source. This view was further expanded by a microarray analysis with Δ*spkA* where expression changes for pilin operon *pilA1-A2*, *pil5-pil6* and *pil9-pil10-pil11-slr2018* were detected and furthermore verified in Northern-blot quantification showing reduced level of *pilA9* and enhanced quantities of *pilA5* together with the observation of missing thick pili (Panichkin et al., 2006). Reports for the SpkB-deficient mutant Δ*spkB* presented a similar phenotype as Δ*spkA* with a strongly reduced gliding motility and it was suggested to stimulate motility though the null mutant still retained WT-like pili (Kamei et al., 2003). Additionally, it was demonstrated that SpkB is redox sensitive and able to phosphorylate GlyS (glycyl-tRNA synthetase subunit beta) (Mata-Cabana et al., 2012). *spkB* is highlighted by upregulation under elevated levels of hexane in microarray analysis for hexane stress responses (J. Liu et

al., 2012). For Δ*spkC* a high tolerance toward the toxic compound methylamine in low light was described (Galkin et al., 2003). A microarray assay with WT in the presence of inhibitors DCMU and DBMIB in low light characterized an induction of *spkC* transcription (Hihara et al., 2003). The group around A. Zorina et al. (2011) proposed a cascade of SpkC/F/K and its role in phosphorylating the heat shock protein GroES. Upregulation of gene expression of *spkD* was observed under LC and concomitantly, Δ*spkD* was unable to grow under ambient air (Laurent et al., 2008). The authors suggested that SpkD is involved in adjustments of TCA cycle metabolites because the supplementation of alternative Ci sources such as Gluc, phosphoglyceraldehyde and pyruvate could not rescue the mutant, only the external addition of TCA metabolites e.g., acetyl CoA, succinate and 2OG were able to revert the phenotype. Recent RNA-Seq analysis found *spkD* upregulated in the LexA mutant (Kizawa et al., 2016). A phospho-proteome study under different light conditions identified SpkD as a p-protein (Z. Chen et al., 2015). Initially suggested to be a non-functional protein kinase (Kamei et al., 2002), SpkE was reported to be required for PTM of pili proteins after biogenesis (Kim et al., 2004). The transcription profile of cold inducible genes in mutant Δ*spkE* was similar to the cold stress sensor Hik33 deficient mutant and led to the hypothesis that SpkE was an additional component in cold stress responses in *Synechocystis* (A. A. Zorina et al., 2014). Induction of gene expression of *spkF* was observed in an ethanol resistance RNA-Seq study under ethanol exposure (J. Wang et al., 2012). Furthermore, SpkC and SpkF has been shown to be prone to modification by phosphorylation upon N-starvation (Spät et al., 2015) with a reported transiently increase in phosphorylation pattern of SpkF when *Synechocystis* resuscitates after chlorosis (Spät et al., 2018). In microarray experiments with H_2O_2 treated WT, *spkG* was found to be downregulated (Li et al., 2004). Moreover, growth of Δ*spkG* was impaired under elevated NaCl concentrations and a role in regulating salt induced genes was proposed (C. Liang et al., 2011). *spkG* is transcribed in the PSII assembly protein (PAP) operon (*slr0144-slr0152*) and it could be concluded that SpkG is involved in Fd5 phosphorylation (Angeleri et al., 2018). Most recently, SpkD and SpkG were hypothesized to influence the expression of polyunsaturated fatty acid (PUFA) desaturases (G. Chen et al., 2021).

Protein kinases SpkH-L belong to Hanks-type kinase like atypical protein kinases ABC1 (Figure 11) (Leonard et al., 1998). Apart from SpkH (A. A. Zorina et al., 2023), no kinase activity for ABC1 kinases could be demonstrated. Transmembrane domains for SpkH, SpkI and SpkL have been proposed (A. A. Zorina et al., 2014). Physiologically, this group is almost undescribed. It has been demonstrated that the expression of *spkH* is light induced and significantly downregulated with addition of salt stress (Allakhverdiev et al., 2002). *spkH* was also found to be highly expressed in WT under osmotic stress in form of supplemented sorbitol (Paithoonrangsarid et al., 2004). SpkI remains the best described ABC1 kinase in

Synechocystis (Irmler & Forchhammer, 2001; L. Huang et al., 2002; X. Wang et al., 2022). Due to *spkI* locations upstream of the P_{II} phosphatase *pphA*, it was initially suspected to be involved in P_{II} phosphorylation but was proven to be non-essential for the phosphorylation of the former (Irmler & Forchhammer, 2001). A global gene expression study revealed that gene expression is induced under UV-B radiation and further intensified with light irritation (L. Huang et al., 2002). Most recent reports highlighted a WT-like growth accompanied with a higher NPQ capacity in Δ*spkI* under standard growth conditions (X. Wang et al., 2022). However, the mutant presented reduced growth and decreased net-photosynthesis in a high salt environment. Thus, Western-blot studies indicated reduced levels of major photosynthetic proteins, whereas fluorescence measurements revealed modification in PSI and $Cytb_6f$ together with impaired Q_A and state transition. Hence the authors suggested a central role in maintaining photosynthesis during salt acclimation. SpkK could be located to the thylakoid membrane (Baers et al., 2019) and is proposed to act in a cascade together with SpkC and SpkF (A. Zorina et al., 2011). *spkL* presented lower gene expression under iron starvation (Hernández-Prieto et al., 2012). No conclusive data are available for SpkJ.

1.7 Objective

Cyanobacteria represent the evolutionary origin of modern eukaryotic photoautotroph which makes them outstanding tools to study general metabolism and its regulation (Cavalier-Smith, 2000; Weber et al., 2006; Chan & Bhattacharya, 2010). Especially well suited is the model organism *Synechocystis* because it can adopt a photoautotrophic, mixotrophic and heterotrophic lifestyle (Anderson & McIntosh, 1991; X. Chen et al., 2016). Thus, the primary C metabolism (Figure 3) needs to be regulated upon changes in environmental conditions such as availability of nutrients (e.g., C, N, P), changes in light quality and quantity (e.g., day/night, shading) or temperature (e.g., heat stress, cold stress). Central for C assimilation in *Synechocystis,* like in other phototrophs, is the CO_2 fixing CBB cycle (Bassham et al., 1954), which is exporting newly fixed organic C into interconnected glycolytic routes for biosynthesis purposes such as N assimilation, or the formation of glycogen out of excess C (Mills et al., 2020). The underlying coherent decision making between heterotrophy (catabolism) and photoautotrophy (anabolism) mode of lifestyle requires therefore an adaptable regulatory network. Mechanism regulating the glycolytic fluxes in the primary C metabolism are scarcely understood. The day/night transition and its concomitant transcriptional changes are believed to influence glycolytic fluxes (A. K. Singh et al., 2004; Osanai et al., 2009, 2011, 2014, 2015; L. Gao et al., 2014; Iijima et al., 2015; Köbler et al., 2018; Scheurer et al., 2021). However, the switch from a heterotrophic to a photoautotrophic lifestyle is suggested to be also C dependent seen in a breakdown of glycogen (Eisenhut et al., 2007; Gründel et al., 2012) and

an increase in glycolytic fluxes after the switch from a HC to a LC environment during the day (X. Chen et al., 2016). Interestingly, a shift from HC to LC did not result in significant transcriptional or proteomic changes for metabolic enzymes inside the primary C metabolism of *Synechocystis* (Orf et al., 2015) but was nevertheless, followed by a significant change in the metabolic signature (Orf, Timm, et al., 2016). These findings suggest a crucial role of PTM on metabolic enzyme as an important level of regulating the primary C metabolism. Phospho-proteomics have detected an increasing number of p-proteins in *Synechocystis* (Mikkat et al., 2014; Spät et al., 2015; Z. Chen et al., 2015; Angeleri et al., 2016; Toyoshima et al., 2020). Among these, several have been identified as metabolic enzymes involved in the primary C metabolism e.g., GapDH2, Gnd, Eno and Pgm1 (Mikkat et al., 2014) which underlines an overall importance of p-phosphorylation as a regulatory mechanism.

This thesis aimed to elucidate the role of PTM, particularly p-phosphorylation in the acclimation towards changing Ci conditions. We hypothesized that a switch from C anabolism towards C catabolism under constant light is primarily regulated by modifications in enzyme activities due to differential phosphorylation states. To test this central hypothesis, we conducted a global proteome and phospho-proteome study with *Synechocystis* WT(F) cells. These cells were shifted from a HC to a LC atmosphere. We then performed a comparative analysis of the proteome and phospho-proteome changes in both short-term and long-term acclimated LC cells, relative to their HC acclimated state. Protein kinases are known to be the main enzymes in signal sensing and transduction processes under changing growth conditions. Therefore, the specific role(s) of protein kinases were analyzed. Particularly, the twelve annotated Ser/Thr protein kinases (Spk) in the genome of *Synechocystis* (C.-C. Zhang et al., 1998; Leonard et al., 1998; Shi et al., 1998) were studied in their role during the acclimation to different environmental conditions. To this end, knock-out mutants for the twelve kinase coding genes were established as tools to search for their specific functions. The obtained *spk* mutant collection was initially screened in their ability to acclimate to different environmental conditions. Among them, the focus was directed to changing Ci and organic C conditions to identify most promising candidates involved in the photoautotrophy/heterotrophy switch. Then, protein kinase deficient mutants indicating a Ci related phenotype were studied in detail. Particularly, global proteome and phospho-proteome studies were applied to reveal potential kinase/target relationships.

2 Material & Methods

2.1 Organism used in this study

2.1.1 *Synechocystis* strains

All mutant strains created and analyzed in this study were generated in S*ynechocystis* sp. PCC 6803 (WT (M)) (Rippka et al., 1979) and strain PCC 6803M (WT (F)) (Trautmann et al., 2012) background (Table 1).

Table 1: *Synechocystis* strains used and generated throughout this study.

Strain	Feature	Resistance	WT	Reference
WT(M)	*Synechocystis* sp. PCC 6803	-	M	Rippka et al., 1979
WT(F)	*Synechocystis* sp. PCC 6803M	-	F	Trautmann et al., 2012
Δ*spkA*	deletion in *sll1575*	Km	M	Bédu; Aix-Marseille Université
Δ*spkB*	insertion in *slr1697*	Km	M	Bédu; Aix-Marseille Université
Δ*spkC*	deletion in *slr0599*	Km	F	Bédu; Aix-Marseille Université
Δ*spkD*	deletion in *sll0776*	Gm	M	this study
Δ*spkE*	deletion in *slr1443*	Km	M	Bédu; Aix-Marseille Université
Δ*spkF*	deletion in s*lr1225*	Km	F	this study
Δ*spkG*	insertion in *slr0152*	Sp	M	Bédu; Aix-Marseille Université
Δ*spkH*	deletion in *sll0005*	Km	F	this study
Δ*spkI*	deletion in *sll1770*	Km	F	this study
Δ*spkJ*	deletion in *slr0889*	Km	F	this study
Δ*spkK*	deletion in *slr1919*	Km	F	this study
Δ*spkL*	deletion in *sll0095*	Km	F	this study
Δ*spkB*^{C}	complementation of Δ*slr1697*	Km/Sp	M	this study

2.1.2 *Synechocystis* cultivation

Synechocystis strains were continuously propagated on buffered solid 1.5 % BG11 bacto agar plates (2x BG11, TES pH 8.0, Rippka et al., 1979; 3% bacto agar, Becton, Dickinson and Company, USA; mixed 1:1 v/v; Table 2) without the addition of HCO_3^- in a 30 °C ambient air

(0.04% CO_2; low carbon, LC) environment under continuous light of 100 µmol m^{-2} s^{-1}. For cultivation in liquid medium, *Synechocystis* was inoculated in BG11 medium (TES pH 7.0; TES pH 8.0; Table 2) and grown either in shaking flasks (140 rpm) at 30 °C in ambient air or agitated bubbling in a water bath (30 °C) either under HC (5 % CO_2) or LC under continuous illumination (100 µmol m^{-2} s^{-1}). Antibiotics were added to the growth medium according to each mutant (kanamycin: 50 µg/ml, spectinomycin: 20 µg/ml, gentamycin: 2.5 µg/ml).

Table 2: Composition of BG11 medium for *Synechocystis* cultivation.

Chemical	Concentration	V stock H_2O [ml]	V of stock BG11 [ml]	V of stock 2x BG11 [ml]
Stock solution 1	**mM**	**100**	**1**	**2**
Ferric ammonium citrate	0.03			
Stock solution 2	**mM**	**1000**	**50**	**100**
$NaNO_3$	17.65			
K_2HPO_4	0.22			
$MgSO_4$ x $7H_2O$	0.3			
Stock solution 3	**mM**	**100**	**2**	**4**
$CaCl_2$ x $2H_2O$	0.26			
A6 trace elements	**µM**	**1000**	**1**	**2**
H_3BO_3	46			
$MnCl_2$ x $4H_2O$	9.4			
$ZnSO_4$ x $7H_2O$	0.77			
$CUSO_4$ x $5H_2O$	320			
Na_2MoO_4 x $2H_2O$	0.086			
$Co(NO_3)_2$ x $6H_2O$	0.17			
Stock solution 4	**mM**	**500**	**20**	**40**
1 M TES-KOH pH 8.0 / pH 7.0	20			
Citric acid monohydrate	0.029			
EDTA x $2H_2O$	0.003			
$Na_2S_2O_3$ x $5H_2O$	**(for 2 x BG11 only)**			**6 g**

2.1.3 *E. coli* strains

E. coli strains DH5α (Thermofisher Scientific, USA) and the methyltransferase deficient strain C2925 (New England Biolabs (NEB), USA) were used for vector amplification and propagation.

2.1.4 *E. coli* cultivation

E. coli was grown either over night at 37 °C on solid 1.5 % LB agar Plates (Carl Roth, Germany) or agitated at 200 rpm in liquid LB (Lysogeny Broth) medium (37 °C; Carl Roth, Germany). Corresponding antibiotics were added to the propagated vector (Ampicillin 100 µg/ml, Kanamycin 50 µg/ml, Spectinomycin 20 µg/ml, Gentamycin 10 µg/ml).

2.2 Chemicals and enzymes

All chemicals used in this study were purchased from Carl Roth (Karlsruhe, Germany). Enzymes were acquired from New England Biolabs (NEB, Ipswich, USA) if not indicated otherwise.

2.3 Molecular biological methods

2.3.1 Extraction of genomic DNA from *Synechocystis*

To isolate genomic DNA (gDNA) from *Synechocystis*, either 200 µl of liquid culture or scratched off cells of a solid culture plate were used. The cells were dispersed in 200 µl ddH_2O and layered with 200 µl of Tris-buffered phenol. The suspension was incubated for 10 min at 65 °C and mixed very 2 min. After heat incubation, cells cooled down and 200 µl of chloroform was added. Samples were further mixed and centrifugated for 5 min at 13.000 rpm at RT. The aqueous supernatant was transferred to a new tube and washed with 200 µl of chloroform. Centrifugation was repeated and the upper phase was transferred to a new tube. Isolated gDNA was used as template DNA for PCR reactions.

2.3.2 Polymerase chain reaction (PCR)

For *in vitro* amplification of the GOI PCR was performed. PCR allowed the continued verification of the segregation status of mutated *Synechocystis* strains as well as serving as a control mechanism throughout the cloning process. The proofreading polymerase Platinum SuperFi II (Thermofisher Scientific, USA) was applied for initial amplification of the GOI. gDNA from *Synechocystis* WT (F) and WT (M) served as gene amplification and control template. PCR with the Taq PCR Master Mix (Qiagen, Germany) was applied to confirm the segregation status of *Synechocystis* and to verify transformed *E. coli* cells. For colony PCR in *E. coli*, single colonies were picked and diluted in 20 µl DNase free water and lysed for 10 min at 95 °C. A full list of primers and primer combination can be found in the Appendix Table 1. Table 3 & 4 show standard PCR reaction setup und PCR program.

Table 3: Components required for a single PCR reaction. Master mixes were prepared for multiple reaction.

	Master Mix	SuperFi II	Master Mix	SuperFi II
Components	**Volume [µl]**		**Concentration [µM]**	
Reaction Buffer	10	2	1x	
10 mM dNTPs	-	0.4	-	0,5
Primer forward	1		0.5	
Primer reverse	1		0.5	
Template DNA	1		n/a	
Polymerase	-	0.4	1 unit	
DNase free Water	x µl to Σ 20 µl		-	

Table 4: PCR standard program.

		Master Mix	SuperFi II	Master Mix	SuperFi II
Step		**T [°C]**		**t [s]**	
Initial denaturation		95	98	5 [min]	30
Denaturation	34 cycles	95	98	60	10
Annealing		x primer specific	60	45	10
DNA elongation		72		x (1 kbp min^{-1})	x (2 kbp min^{-1})
Final elongation		72		7 [min]	

2.3.3 Agarose gel electrophoresis

DNA molecules were separated by agarose gel electrophoresis. For this purpose, 1 % (w/v) agarose was added to 1x Tris-Acetate EDTA Buffer (TAE; 50x TAE: 2 M Tris-HCl pH 8.0, 0.5 M EDTA, 5.7 % (v/v) acetic acid). The suspension was melted in the microwave. 1 drop of 250 µg/ml ethidium bromide (Roth, Germany) was added to 50 ml Agarose gel for DNA visualization. Appropriate amounts of 6x loading dye (B7025; NEB, USA) were added to the samples. For separation a current of 90 V was applied to the gel for approximately 40 min.

2.3.4 Generation of mutations in *Synechocystis*

To generate mutations in *Synechocystis*, the GOI was amplified by PCR together with 500 bp up- and downstream of the gene sequence of GOI. The amplified product was eluted from an agarose gel and ligated into a cloning vector i.e., pGEMT or pJET1.2/blunt for propagation. The reading frame of the GOI was disrupted by the insertion of an antibiotic resistance cassette. Cloning strategies, applied to generate the mutants studied in this thesis, can be found in the Appendix Figure 1, 2 and 4. For the insertion, naturally occurring restriction enzyme cutting sides in the gene sequence were utilized to open the GOI. Cutting sides were

chosen close to the transcription offset point and to remove as much genetic information as possible. The generated plasmid containing the mutated GOI was verified by sequencing and concomitantly used to transform *Synechocystis*. To transform *Synechocystis*, 5 µl of plasmid DNA was added to 400 µl dark green cells and consequently incubated in the dark shaking ON at 30 °C. The suspension was evenly spread across 30 ml solid BG11 plates. Cultures were incubated at 30 °C under a light intensity of 100 µmol photons m^{-2} s^{-1} for up to 3 d and then layered with full antibiotic concentration applied underneath, dispensed in 500 µl fresh BG11 medium. *Synechocystis* was grown at 30 °C and 100 µmol photons m^{-2} s^{-1} until transformed colonies appeared. Colonies were picked and singled out on a new BG11 plate containing the full antibiotic concentration. gDNA was isolated from singled out colonies and used as a template for genotyping PCR.

2.3.5 Vectors

The vector systems pGEM-T (Promega, USA) and pJET1.2/blunt (Thermofisher Scientific, USA) were used as entry vectors for cloning and gene propagation. Antibiotic resistance gene cassettes were retrieved from pUC4K (kanamycin; Amersham, USA) and the lab generated derivatives pUK4S (spectinomycin) and pUK4G (gentamycin). The autonomous replicating plasmid pVZ322 (Zinchenko et al., 1999) was used for generating complementation constructs.

2.3.6 DNA digestion and ligation

Restriction endonucleases were used to cut plasmid DNA at endonuclease specific recognition sides to mutate the GOI and to retrieve antibiotic resistance cassettes. Table 5 shows a standard set up for a single digest. Incubation of the digest set up was performed accordingly to the manufacturer's instructions. Digested DNA fragments were separated by fragment size by performing an agarose gel electrophoresis. The desired DNA fragments were eluted from the agarose gel using the EasyPure kit (Macherey-Nagel, Germany). DNA fragments were eluted in a small volume for high concentration. To create blunt ends on DNA fragments the Klenow fragment (Thermofisher Scientific, USA) was applied. The Klenow fragments exhibit a polymerase activity from 5'-3' strand direction and an exonuclease activity in 3'-5' strand direction and can therefore fill in in 3' strand overhangs and cut off 5' strand overhangs. The blunting set up (Table 5) was incubated for 10 min at 37 °C. The reaction was stopped by heat inactivation at 75 °C for 10 min. Blunted DNA fragments were used for DNA ligation. The antibiotic resistance cassette genes were ligated into the backbone of the GOI

using the CloneJET kit (Thermofisher Scientific, USA) (Table 5). Ligations were carried out for 20 min at RT.

Table 5: Reaction set up for a single DNA restriction digest, ligation and blunting reaction.

Restriction digest (Σ 20 µl)	Ligation (Σ 20 µl)	Blunting reaction mix (Σ 20 µl)
x µl Buffer (enzyme specific)	10 µl ligation buffer	x µl (0.1-0.4 µg) DNA
x µl (1 µg) plasmid DNA	1 µl vector (DNA backbone)	2 µl 10x reaction buffer
1 µl enzyme (each)	5 µl eluate (DNA insert)	0.1 µl 10 mM dNTPs
x µl ddH_2O	1 µl T4 ligase	0.5 µl Klenow fragment
	x µl ddH_2O	x µl ddH_2O

2.4 Microbiological Methods

2.4.1 Heat shock transformation of *E. coli*

Chemically competent DH5α or C2925 cells were transformed using a heat shock method. A 100 µl aliquot of deep-frozen competent cells was thawed on ice. Plasmid DNA was added to the cells, and subsequently incubated on ice for 30 min. The cells were then subjected to a heat shock at 42 °C for 100 s, followed by 5 min incubation on ice. Subsequently, 1 ml of LB medium was added, and the transformed cells were allowed to recover for 1 h at 37 °C shaking at 200 rpm. After recovery, transformed cells were streaked onto LB agar plates containing antibiotics appropriate for the transformed vector. The plates were incubated ON at 37 °C.

2.4.2 Plasmid isolation

Plasmid DNA was isolated from 5 ml ON culture Using the NucleoSpin Plasmid Kit (Macherey Nagel, Germany). Plasmids were eluted in 30 µl ddH_2O. DNA concentrations were measured using a Nanodrop spectrophotometer (Thermofisher Scientific, USA). For verification, the plasmids were sequenced (Microsynth AG, Switzerland).

2.4.3 Photoautotrophic growth in ambient air

WT and mutant strains were pre-cultivated in glass tubes with 5% CO_2 (HC) at 30°C under an illumination of 120 µmol photons m^{-2} s^{-1} in BG11 TES buffer (pH 8.0) (Rippka et al, 1979) for 3 d. Subsequently, the *Synechocystis* suspension was adjusted to an OD_{720} of 0.2 using BG 11 TES buffer (pH 7.0) and grown under ambient air. Growth was monitored using the Multi-Cultivator MC-1000-OD system (Photon Systems Instruments; Czech Republic). The OD_{720} was continuously recorded at 30°C under an illumination of 100 µmol photons m^{-2} s^{-1} for 4 d.

Samples from both HC and LC acclimated cells were used to record absorption spectra from 400-750 nm and were applied for pigment quantification. Raw growth data were normalized to their respective initial OD_{720} ($OD720_N$= $OD720_n$/$OD720_0$) and consequently normalized to the WT from 0 to 1 ($OD720_{NMut}$=($OD720_{Mut}$-$OD720_{NWTmin}$)/($OD720_{NWTmax}$-$OD720_{NWTmin}$).

2.4.4 Pigment quantification

For Pigment quantification a spectrum from 400-750 nm using a plate reader (Synergy HTX, BioTek, USA) was recorded for *Synechocystis* cells acclimated to either HC or LC. Cells were diluted 1:1 with fresh BG11 medium, and 250 µl of the diluted cell suspension was transferred to a 96-well microtiter plate. Pigment quantities were calculated according to Sigalat & Kouchkovsky (1975).

2.4.5 Cultivation and sampling for proteomics and phospho-proteomics

WT and kinase deficient mutants were pre-cultivated in batch cultures under HC in buffered BG-11 medium (TES pH 8.0) at 30°C with an illumination of 120 µmol photons m^{-2} s^{-1}. Cultures were grown in glass tubes until the cell suspension reached the OD_{750} of 1–1.2. *Synechocystis* cultures were transferred daily into fresh BG-11 medium. Two days before the shift experiment, the pre-cultures were adjusted to an OD_{750} of 1.0 and split into three individual cultures maintained under HC conditions. After 24 h of growth, the cell suspensions were readjusted to an OD_{750} of 0.8 - 1.0. Cells were harvested by centrifugation and resuspended in fresh BG-11 medium, then split into six individual cultures of 120 ml each, with an OD_{750} of 1. To allow recovery and acclimation, cells were agitated with HC in the light for 2 h before HC samples were taken. From each culture, two 20 ml aliquots were withdrawn into 50 ml tubes filled with ice to rapidly cool the suspension to below 4 °C, ensuring rapid inhibition of enzyme activities. The cells were immediately harvested by centrifugation (6000 rpm; 7 min; 4°C). Cell pellets were washed with 7 ml ice-cold PBS buffer (137 mM NaCl, 2.7 mM KCl, 10 mM Na_2HPO_4, and 1.8 mM KH_2PO_4), snap-frozen in liquid nitrogen, and stored at -80°C until further processing. For the shift to LC conditions, the medium of the remaining culture was removed by centrifugation, and the cells were resuspended in the same volume of BG-11 medium (TES pH 7.0) and further cultivated under LC. Samples from LC-shifted cultures were taken after 3 h and 24 h. Three independent cultivations were conducted for phospho-proteome analysis.

2.4.6 Photo-mixotrophic growth in ambient air

Synechocystis WT and kinase deficient mutants were inoculated from cultures grown on solid medium into 100 ml BG11 medium in Erlenmeyer flasks. The strains were pre-cultivated shaking (140 rpm) for 7 d under LC, with an illumination of 35 µmol photons m^{-2} s^{-1} and 30 °C. Before the growth experiment, cultures were adjusted to an OD_{750} of 0.5 with BG11 (TES pH 8.0) and consequently split into two separate cultures: one treated with 10 mM Gluc and the other served as a control. *Synechocystis* strains were grown under LC with 35 µmol photons m^{-2} s^{-1} and 30°C. Growth was monitored by measuring the OD_{750} every 24 h until the cultures reached the stationary growth phase. Raw growth data were normalized to their initial OD_{720} and subsequently normalized to the WT values, ranging from 0 to 1 ($OD720_{NMut}$=($OD720_{Mut}$-$OD720_{WTmin}$)/($OD720_{WTmax}$-$OD720_{WTmin}$).

2.4.7 HCO_3^- dependent photosynthetic O_2 evolution rates

HCO_3^- dependent photosynthetic O_2 evolution rates were quantified using an S1 Oxygraph (Hansatech Instruments, King's Lynn, UK). Suspensions of HC and LC acclimated cells were adjusted to Chl*a* 10 µg/ml with CO_2 free BG-11. 3 ml of the adjusted suspension were used to quantify O_2 evolution rates at 30°C and a saturating light intensity of 300 µmol photons $m^{-2}s^{-1}$ in the presence of increasing HCO_3^- concentrations (0,33.3, 66.7, 133.3, 266.7, 400, 533.3, 666.7, 1000, 1333.3, 2000 and 2666.7 µM). Photosynthetic rates at each HCO_3^- concentration was recorded in 30 s intervals. Data were used to calculate K_m.

2.4.8 State transition measurements

For low temperature (77K) fluorescence measurements, WT (M) and Δ*spkB* were precultivated under LC conditions in BG11 TES medium (pH 7.0) at 30 °C and a light intensity of 120 µmol photons m^{-2} s^{-1} in batch culture until the desired biomass was reached. Samples were kept in glass Pasteur capillaries and were rapidly frozen in liquid nitrogen after different light treatments. Cells were acclimated to darkness for 30 min and concomitantly exposed to either far-red light (100 µmol photons m^{-2} s^{-1}, wavelength 730 nm) and orange light (100 µmol photons m^{-2} s^{-1}, wavelength 600-630 nm). Emission spectra were recorded with a Hitachi F4010 (Hitachi Inc., Japan). Excitation wavelengths was set at 600 nm with a band pass of 10 nm, allowing direct measurements without the use of cut-off filters. Spectra were normalized to the emission peak at ~ 722 nm.

2.4.9 Drop dilution assays

Kinase deficient mutants and their respective WT were cultivated in shaking flasks containing BG11 medium (TES pH 8.0) at 30 °C and a light intensity of 100 µmol m^{-2} s^{-1} in an LC environment until they reached the desired OD_{750}. For the drop dilution assay, *Synechocystis* was adjusted to the OD_{750} of 0.2 with BG11 medium (TES pH 8.0). A serial dilution to 1:10, 1:100 and 1:1000 of the suspension was prepared. 2 µl of the dilution series were spotted onto solid BG11 plates (TES pH 8.0; 1.5 % bacto agar) containing different supplements. For photo-mixotrophic and diurnal conditions 10 mM Gluc and, 500 mM NaCl for a high salinity environment were added to the medium. BG11 plates without supplementation served as control references. Plates were incubated at 30 °C under constant light (100 µmol m^{-2} s^{-1}) for photo-mixotrophic and high salinity conditions. For diurnal conditions, plates were incubated at fluctuating light (12 h light/ 12 h darkness) at 30 °C with a light intensity of 75 µmol m^{-2} s^{-1} for 4 d. Photos were taken of the plates alongside their respective control plate.

2.4.10 Tolerance towards externally supplied ROS

To test the sensitivity of the mutant strains towards externally supplied ROS, cells were probed with increasing amount of H_2O_2. Strains were pre-cultivated in shaking flasks in BG11 (TES pH 8.0) at 30°C and a light intensity of 100 µmol photons m^{-2} s^{-1} in an LC environment until they reached the desired OD_{750}. Cell suspensions were then adjusted to an OD_{750} of 0.4 and probed with either 3 mM or 4 mM of H_2O_2 followed by an incubation under growth light conditions for 1 h. After H_2O_2 incubation, a serial dilution of 1:10, 1:100, or 1:1000 of the suspension was performed. 2 µl of the dilution series were spotted onto solid BG11 plates (TES pH 8.0; 1.5 % bacto agar). Surviving cells recovered for 4 d at 30°C and 100 µmol photons m^{-2} s^{-1} at constant light. Pictures were taken alongside with their respective control plate.

2.4.11 Glycogen quantification

For cellular glycogen quantification, *Synechocystis* was precultivated in a batch culture under either HC (BG11 TES pH 8.0) or LC (BG11 TES pH 7.0) conditions at 30 °C and 100 µmol photons m^{-2} s^{-1} continuous light until desired OD_{750} of 1 was reached. Cells were shifted to either LC or HC. Upon shift, cells were spun down (5 min; 4000 rpm) and resuspended in either BG11 TES pH 7.0 or BG11 TES pH 8.0. *Synechocystis* was further cultivated under LC condition for 24 h. Samples for glycogen quantification were taken either at a HC or LC acclimated state and 3 h and 24 h after shifting to either a LC or HC environment. Cellular

glycogen content was determined by applying the method described by Gründel et al. (2012). Glycogen was quantified as Gluc in the supernatant using the o-toluidine reagent (Roth, Germany). Gluc levels were calculated using a Gluc standard curve.

2.4.12 Metabolite quantification

For metabolite quantification under fluctuating Ci conditions, *Synechocystis* was precultivated in a batch culture under either HC (BG11 TES pH 8.0) or LC (BG11 TES pH 7.0) conditions at 30°C and 100 µmol photons m^{-2} s^{-1} continuous light until desired OD_{750} of 1 was reached. Cells were shifted either to a LC or HC. Upon shift cells were spun down (5 min; 4000 rpm) and resuspended in either BG11 TES pH 7.0 or BG11 TES pH 8.0. *Synechocystis* was further cultivated under LC condition for 24 h. 4 ml samples were taken on nitrocellulose filters (25 mm, Porafil, Macherey-Nagel) at a either HC or LC acclimated state after 1, 3, 6 and 24 h after shifting to either a LC or HC environment. For metabolite quantification under NO_3^- deprivation *Synechocystis* was pre-grown in LC (BG11 TES pH 7.0) until the culture reached OD_{750} of 1. Upon the shift cells were spun down (5 min; 4000 rpm) and resuspended in NO_3^- free BG11 medium. 5 ml samples were taken at a LC acclimated state and 20, 40, 60 and 120 min after the shift to a NO_3 free atmosphere on nitrocellulose filters (25 mm, Porafil, Macherey-Nagel). Metabolites were extracted and analyzed according to Lucius et al. (2021).

2.5 Protein biochemistry

2.5.1 Quantitative proteomics and phosphoproteomics

Sample preparation, quantitative proteomics and phospho-proteomics were performed by Dr. Philipp Spät and Prof. Dr. Boris Macek at the institute of quantitative proteomics at the University of Tübingen. Details of the applied methods can be found in Spät & Barske et al. (2021) and Barske & Spät et al. (2023).

2.5.2 Protein extraction and quantification

20 ml of *Synechocystis* was spun down (5 min; 4000 rpm). Cells were resuspended in 300 µl protein extraction buffer (20 mM TRIS-HCl pH 7.5, 100 mM NaCl) and consequently broken down by sonicating six times, 15 bursts at a duty cycle of 20 and an output of 75 % (Bandelin Sonoplus HD70, Germany) with intermittent cooling on ICE for 10 s. The disrupted cell suspension was then spun down for 20 min at 3000 rpm and 4 °C. The crude extract was used for quantifying total protein content applying the ROTI Nanoquant kit (Roth, Germany) according to the manufacturer's instruction. Protein extracts were kept cool at any time point.

2.5.3 SDS-PAGE

Sodium dodecylsulfate polyacrylamide gel electrophoresis (SDS-PAGE) was performed to separate proteins isolated by their molecular mass by applying an electric field (Laemmli, 1970). Protein samples were adjusted in 3x SDS loading buffer (3.9 ml 500 mM Tris/HCl pH 8.0 (v/v), 1.5 mg bromophenol blue (w/v), 600 mg SDS (w/v), 3 ml glycerol (v/v), 1.5 ml 2-mercaptoethanol (v/v), filled up to 10 ml with ddH_2O) and denaturated for 10 min at 95 °C under shaking. Total protein extracts were loaded onto a 12 % separating gel (Table 6). SDS-PAGE was covered with running buffer (30 g Tris base pH 8.3 (w/v), 144g glycine (w/v), and 10 g SDS (w/v), filled up to 1 l with ddH_2O). The electrophoresis was run at a current of 15 mA per gel.

2.5.4 Native-PAGE

Crude protein extracts were probed with Native-PAGE sample buffer (187.5 mM TRIS-HCl pH 6.8, 30 % (v/v) glycerol, 0.0015 % (v/v) bromophenol blue, filled up to 16 ml with ddH_2O) in a 3:1 ratio. 10 µg of total protein cell extract were loaded onto a Native-PAGE (Table 6) and separated for approximately 3 h at 170 V, layered by 1x Native-PAGE running buffer (5x; 0.124 M TRIS pH 8.3, 0.960 M glycine, fill up to 2 l with ddH_2O).

Table 6: PAGE separation and stacking gels.

SDS-PAGE*		**Native-PAGE***	
Separating Gel (12%)	Stacking Gel (4%)	Separating Gel (15%)	Stacking Gel (4%)
3.35 ml H_2O	2.725 ml H_2O	3.4 ml H_2O	5.5 ml H_2O
3.35 l Rotiphorese 40 (29:1)	0.975 ml Rotiphorse 40 (29:1)	7.5 ml Rotiphorese 40 (29:1)	1.3 ml Rotiphorse 40 (29:1)
2.5 ml Tris-HCl pH 8.8	1.25 ml Tris-HCl pH 6.8	3.8 ml Tris-HCl pH 8.8	1 ml Tris-HCl pH 6.8
100 µl 10 % (w/v) SDS	50 µl 10 % (w/v) SDS	150 µl 10 % APS	80 µl 10 % APS
150 µl 10 % APS	80 µl 10 % APS	10 µl TEMED	5 µl TEMED
5 µl TEMED	5 µl TEMED		* 2 small gels

2.5.5 Western blot and immunodetection

Proteins were transferred to a PVDF membrane (Thermofisher Scientific, USA) using a semidry blot system (Thermofisher Scientific, USA). Running gels were incubated together with two Whatmann paper in transfer buffer (25 mM Tris pH 8.3, 192 mM glycine, 0.1 % (w/v)

SDS, 20 % (v/v) methanol). After activation in methanol, the PVDF membrane was also placed in transfer buffer. The assembly involved sandwiching, where the running gel was placed on top of a piece of Whatmann paper, followed by the PVDF membrane, and then covered with an additional layer of Whatmann paper (sandwich assembled from cathode to anode). Proteins were transferred applying a constant current of 6 V for 90 min. Subsequently, the membrane was blocked in milk powder (MP, 5 % w/v in TBS) for 40 min at RT. Afterwards, the membrane was rinsed once in TBS (20 mM Tris pH 7.6, 150 mM NaCl) to remove MP residues. The immunoblot was probed with either a primary antibody against the PII protein (Forchhammer & Tandeau De Marsac, 1994; 1:1000) or against CmpA (Omata et al., 1999) 1:500) ON at 4 °C shaking. Following, the membrane was washed 3 times with TBS-T Buffer (1xTBS, 0.1% (v/v) Tween 20). Anti-Rabbit-HRP conjugated secondary antibody was incubated for 1 h under shaking at RT. The PVDF membrane was washed twice in TBS-T and two times in TBS. Subsequently, 1.5 ml of chemiluminescence solution (SuperBright, Agrisera, Sweden) was added to the membrane according to the manufacturer's instruction to facilitate the western blot development. The Intas Chemostar camera system (Intas, Germany) was used for blot visualization.

3 Results

To elucidate the importance of PTM, particularly p-phosphorylation on Ser and Thr residues in acclimation processes of the primary C metabolism towards fluctuating Ci availability, a comprehensive investigation of its respective role was conducted with the cyanobacterium *Synechocystis*. This involved a global proteome and phospho-proteome study in *Synechocystis* WT (F) subjected to a Ci shift. Furthermore, *Synechocystis* mutants deficient in the twelve Ser/Thr protein kinases (SpkA-L) were generated and their physiological responses towards changing environmental conditions were recorded. Mutant strains severely affected by the tested conditions were used in a Ci limiting proteome and phospho-proteome approach to unravel potential kinase/substrate relationships.

3.1 Cellular acclimation processes of WT (F) towards Ci limitation

To grow under fluctuating Ci availability, *Synechocystis* needs to undergo several cellular acclimation processes to adjust to changing environmental conditions. Ci related alterations in protein abundancies and p-events were documented in a global Ci dependent proteome and phospho-proteome study conducted with *Synechocystis* WT (F) in three independent replicates. Proteome, phospho-proteome and correlation analysis data presented in this thesis were previously published in Spät & Barske et al. (2021).

3.1.1 Ci dependent changes in protein abundancies in WT (F)

A shift experiment was performed with *Synechocystis* WT (F) cultivated under HC and subsequently put in LC. Samples were taken before the shift and after 3 h and 24 h of acclimation to LC. WT (F) was analyzed for changes in protein abundancies as a response to a change in Ci availability. The 3 h and 24 h LC acclimated cells were quantitively compared to HC grown cells in an LC-MS approach. Three independent biological replicates were studied. Quantitative changes in the proteome were put in correlation with transcriptome data from a study under Ci limiting conditions by Klähn et al. (2015) (Table 7, Figure 12). Overall, 2284 individual protein were detected in at least two replicates, among them 37 proteins were found in significantly elevated and 50 proteins in diminished levels after 3 h in LC, whereas 109 proteins were quantified in higher and 119 proteins in lower amounts after 24 h in LC. Up to 50% of the detected proteins with significantly changed amounts were hypothetical proteins or proteins with no assigned functions. The generated dataset reports a strong correlation

between mRNA levels and increased protein abundancies (Figure 12). For most proteins found in higher amounts under LC, mRNA levels correspondingly increased. A few exceptions were found i.e., the upregulation of proteins was matched with unchanged or even decreased mRNA levels in cases of ManR, PsbY and PsaJ.

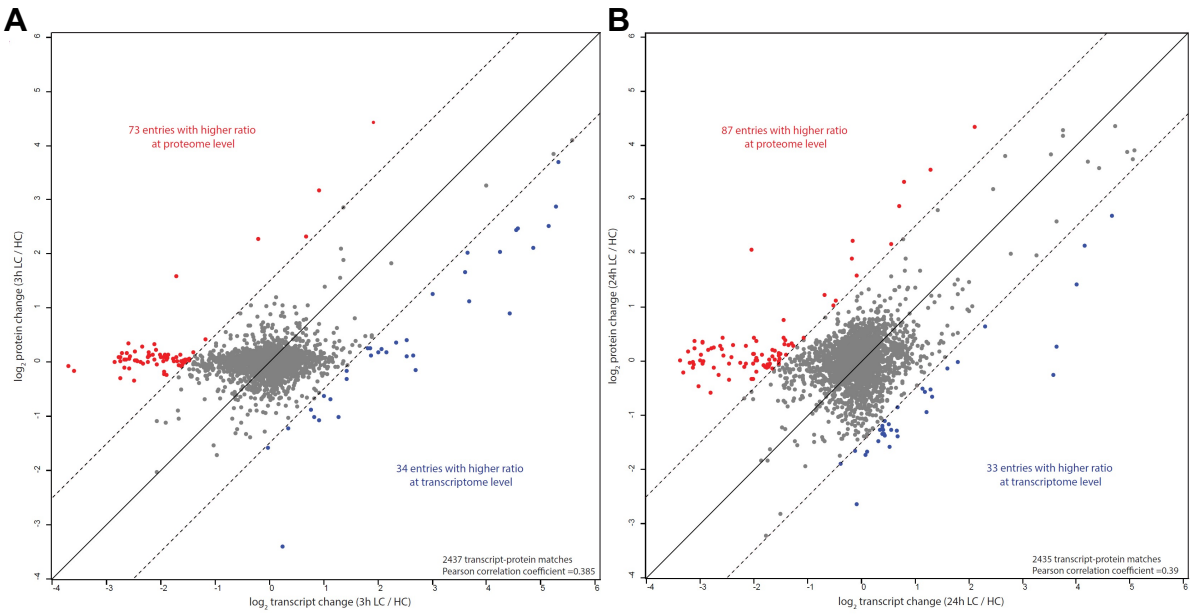

Figure 12: Correlation analysis between transcriptome and proteome changes under Ci limitation: Transcriptome data from Klähn et al. (2015) were correlated to proteome data after 3 h (**A**) and 24 h (**B**) of acclimation to LC. Overall, 2544 transcripts and proteins could be matched after 3 h (**A**) and 2555 transcripts and proteins after 24 h in LC (**B**). 95.8% (**A**) and 95.3% (**B**) show a close expression correlation falling within a 1.5-fold (Log_2) difference respectively. (Figure taken from Spät & Barske et al. 2021)

Many proteins with proven functions in CCM were found to be induced under LC (Table 7). Including all units involved in assembling of the ABC-type HCO_3^- transporter BCT1 encoded by the operon *cmpA-D* were among the proteins which showed the strongest accumulation when shifted to LC reaching an up to 18-fold increase after 24 h in LC. The HCO_3^- transporter SbtA together with its regulator SbtB accumulated significantly after 24 h in LC. Additionally, NdhF3, NdhD3, CupA and CupS, forming the NDH1-3 CO_2 hydrating complex, were significantly increased in LC cells. Other proteins associated with NDH1 complex such as NdhG, NdhH, NdhI, NdhJ, NdhK and NdhN also showed a significant accumulation under LC conditions. Matching to the induced HCO_3^- transporter BCT1 and NHD1 complex, the responsible transcriptional regulators CmpR (*cmp* operon) and NdhR (NHD1 complex and many others) showed a significant increase in protein levels. A putative cellular carbonic anhydrase EcaB was also found in higher quantities. Apart from proteins directly involved in Ci uptake, other proteins functionally related to LC acclimation were detected in higher quantities. Flavoprotein Flv2 and Flv4 showed strong induction in an Ci limited atmosphere with an up to 17-fold increase in protein levels.

Table 7: Proteins significantly accumulated in WT (F) in LC. Shown are fold changes (FC) in relation to the HC acclimated state. Abundancy changes were compared to Ci related transcript level according to Klähn et al., (2015). Significant alterations are highlighted in bold letters. Values marked with * were quantified in less than 3 replicates. Boxes indicate an operon structure. Transcript levels in grey shading indicate unchanged or decreased mRNA levels. Entire proteome data can be found in Spät & Barske et al. (2021). (FC= fold changes; n=3 (biological), student's *t*-test, two-tailed, * p<0.05)

		Protein [FC]		mRNA [Log_2 FC]	
Gene	**Protein description**	**LC3h/ HC**	**LC24h/ HC**	**LC3h/ HC**	**LC24h/ HC**
sll0030	CmpR, *cmp* operon transcriptional regulator	1.24	**2.32**	0.891	0.332
sll0217	Flv2, flavoprotein	**17.15**	**14.59**	5.584	4.948
sll0218	Hypothetical protein	12.92*	14.97*	5.325	5.077
sll0219	Flv4, flavoprotein	**14.40**	**13.38**	5.228	5.051
sll0520	NdhI, NADH dehydrogenase subunit	1.40	**2.77**	1.762	2.009
sll0521	NdhG, NADH dehydrogenase subunit 6	1.31	**2.86**	1.586	1.795
sll1262	NdhN, subunit of NDH1-like complex	**1.28**	**2.61**	1.204	0.699
sll1515	Glutamine synthetase inactivating factor IF17	**4.26**	**6.97**	1.254	1.103
sll1594	NdhR, *ndhF3* operon transcriptional regulator	1.56	**3.19**	1.254	1.103
sll1732	NdhF3, NADH dehydrogenase subunit 5 (Ndh1-3)	4.33*	11.97*	4.858	4.428
sll1733	NdhD3, NADH dehydrogenase subunit 4 (Ndh1-3)	1.88*	4.40*	4.419	4.158
sll1734	CupA, involved in low CO_2-inducible, high affinity CO_2 uptake	**4.06**	**14.27**	3.652	3.528
sll1735	CupS, involved in low CO_2-inducible, high affinity CO_2 uptake	**2.39**	**9.07**	3.008	2.446
slr0006	Unknown low CO_2-induced protein	**2.19**	**3.90**	3.684	3.255
slr0007	probable sugar-phosphate nucleotidyltransferase	1.33	**1.91**	2.527	2.003
slr0040	CmpA, bicarbonate transport substrate-binding protein	**7.31**	**20.33**	5.276	4.734
slr0041	CmpB, bicarbonate transport permease protein	**5.68**	**6.49**	5.136	4.658
slr0042	Probable porin; major outer membrane protein	**5.44**	**12.95**	4.538	**7**4.208
slr0043	CmpC, bicarbonate transport ATP-binding protein	**4.08**	**5.99**	4.237	3.642
slr0044	CmpD, bicarbonate transport ATP-binding protein	**9.55**	**17.98**	3.987	3.755
Slr0051	EcaB, periplasmic beta-type carbonic anhydrase	1.21	**1.59**	0.351	0.395
slr0261	NdhH, NADH dehydrogenase subunit 7	1.19	**2.33**	1.371	1.308
Slr0370	GapD, succinate-semialdehyde dehydrogenase	1.12	**1.52**	0.285	0.336
slr1280	NdhK, NADH dehydrogenase subunit NdhK	1.41	**2.68**	1.885	1.731
slr1281	NdhJ, NADH dehydrogenase subunit I	1.38	**2.52**	1.877	1.883
slr1406	Periplasmic protein, function unknown	1.24	**2.57**	1.656	1.012
slr1407	Unknown protein	1.19	**2.50**	1.247	0.617
slr1409	Periplasmic WD-repeat protein	1.10	**2.07**	0.824	0.718
slr1410	Periplasmic WD-repeat protein	1.12	**2.23**	0.803	0.830
slr1512	SbtA, sodium-dependent bicarbonate transporter	**5.56**	**19.44**	4.578	3.753
slr1513	SbtB, c-AMP-binding regulator of SbtA	**3.17**	**13.98**	3.602	2.678
slr1562	GrxC, glutaredoxin	1.26	**1.60**	-0.267	-0.080
slr1623	Hypothetical protein	**1.48**	**2.53**	0.877	0.139
slr1837	ManR, Rre16, two-component response regulator	1.19	**2.18**	0.476	0.436
slr2032	Hypothetical protein YCF23	**2.07**	**4.71**	0.255	-0.164
sml0007	PsbY, photosystem II protein Y	0.88	**1.27**	0.041	-0.028
sml0008	PsaJ, photosystem I subunit IX	1.07	**3.73**	0.215	0.823
ssl0352	Hypothetical protein	**1.32**	**2.57**	1.035	0.873
ssl1633	HliC, High light-inducible CAB/ELIP/HLIP family	**7.24**	**7.35**	1.365	0.710
ssl1690	Hypothetical protein	**1.33**	**2.50**	0.498	0.634
ssl1911	Glutamine synthetase inactivating factor IF7	**21.57**	**20.30**	1.912	2.115
ssr1789	HliB, High light-inducible CAB/ELIP/HLIP family	1.11	**1.89**	-0.202	-0.229

Proteins associated with ROS scavenging such as HliB, HliC and GrxC presented increased levels under LC. Photosystem subunits PsbY and PsaJ were found in higher quantities under

ambient air. Among proteins related to primary C and N metabolism, only the glutamine synthase regulators IF7 and IF17 showed to be strongly upregulated with an almost 7-fold elevation under LC, whereas enzymes taking part in the primary C metabolism did not show any LC related changes in their quantities. The only exception was GapD (succinate-semialdehyde dehydrogenase) that displayed a significantly higher amount after 24 h in LC.

3.1.2 Ci dependent changes in protein phosphorylation in WT(F)

Protein extracts from LC shifted cells were used in a global phospho-proteome study. Phospho-peptides were enriched by TiO_2 metal-oxide affinity chromatography. Quantitative side specific changes in p-phosphorylation were analyzed in relation to HC acclimated samples. Overall, 105 p-proteins were detected in this study with a total of 200 p-events. Out of 200 identified p-events, 35 p-events on 24 proteins showed significant alteration when acclimating to LC (Table 8). Amongst, 13 p-events after 3 h LC and 12 p-events after 24 h LC were highlighted by elevated phosphorylation levels whereas, 12 p-events after 3 h LC and 6 p-events after 24h of LC showed to be significantly less phosphorylated on specific sides. Phycobilisome proteins presented the highest phosphorylation frequency with a total of 13 p-events on CpcA. T45, Y60 and Y65 of CpcA revealed a strong phosphorylation after 24 h acclimation to ambient air. After 3 h LC, phosphorylation levels on the DNA-polymerase DnaX presented a 22-fold increase on S1012 which again declined after 24 h of LC. The p-event on S1012 marked the overall highest observed change in a side specific phosphorylation pattern. Other proteins linked to the cell cycle such as SbcC, NusG and IleS were also highlighted by an 8-fold increased phosphorylation on T107 and S109 of SbcC after 3h in LC as well as 10-fold intensified p-event on S2 of NusG and a 5-fold higher p-occupancy on Y83 of Iles after 24 h LC respectively. It can be speculated that these increases in phosphorylation of cell cycle proteins might be related to the growth arrest of *Synechocystis* after the shift from HC to LC. The unknown protein coded by *slr0377* was emphasized by a 15-fold increase in p-occupancy after 3 h and a 13-fold increase after 24 h LC on Y97 and Y100 . The regulatory P_{II} (GlnB) protein presented a significantly reduced phosphorylation on S49 and T52 after 3 h in an LC environment. In LC shifted cells phosphorylation on S54 and S55 of the CBB regulator CP12 was diminished. Interestingly, the substrate binding subunit CmpA and the permease CmpB of the HCO_3^- transporter BCT1 showed a significant decrease in phosphorylation at T129 and S110 (CmpA) and T3 (CmpB). It needs to be stated, that the decreased p-event at T3 of CmpB was accompanied by a 2-fold higher p-occupancy after 24 h under LC. Furthermore, the protein kinase SpkC displayed a significant increase in phosphorylation at T304 and T312 after short term acclimation to ambient air. Among other proteins with altered p-events were the functionally annotated Fed5, PsaD, and GroES.

Table 8: Significantly changed p-events in WT (F) in LC. Recorded altered p-events of HC-LC shifted *Synechocystis* WT (F). Significant alterations are highlighted in bold letters. p-sides marked with + were already known previously. Entire phospho-proteome data can be in Spät & Barske et al. (2021). (n=3 (biological), student's *t*-test, two-tailed, * p<0.05)

Gene	Protein description	p-site	$LC_{3\ h}$/HC phosphorylation ratio	$LC_{24\ h}$/HC phosphorylation ratio
sll1360	DnaX, DNA polymerase III subunit gamma/tau	S1012	**22.20**	**2.20**
slr0377	Unknown protein	Y97	**15.58**	**13.04**
		Y100	**15.58**	**13.04**
slr1048	Exonuclease subunit SbcC	T107	**8.33**	n.d.
		S109	**8.33**	n.d.
slr0322	CheA-like 2-component hybrid sensor/regulator	T358	**5.79**	1.56
		T357	**4.83**	1.64
slr0737	PsaD, photosystem I subunit II	T2+	**4.93**	**2.70**
slr0599	SpkC, serine/threonine kinase	T304+	**3.32**	1.58
		T312+	**2.84**	1.14
sll0497	Hypothetical protein	Y119	**2.04**	n.d.
slr0148	Fed5, ferredoxin-like protein	T18+	**1.97**	1.42
		T72+	**1.83**	1.76
sll1578	CpcA, phycocyanin alpha subunit	T45+	1.25	**1.91**
		Y60+	1.14	**2.97**
		Y65	1.14	**2.97**
sll0103	Hypothetical protein	S407	1.11	**2.30**
sll1742	NusG, transcription antitermination protein	S2+	0.95	**9.98**
sll1362	IleS, isoleucyl-tRNA synthetase	Y83	0.93	**5.36**
sll0108	Amt, ammonium/methylammonium permease	T504	0.45	**2.06**
sll1821	RplM, 50S ribosomal protein L13	T121	0.79	**0.05**
sll0982	Unknown protein, thylakoid associated	T88	0.55	**0.11**
sll0947	LrtA, light repressed protein A homolog	T11	0.44	**0.06**
slr0041	CmpB, bicarbonate transporter permease	T3	**0.26**	**2.08**
slr1735	ATP-bind. subunit, basic amino acid transporter	T2	**0.24**	n.d.
slr0040	CmpA, bicarbonate transport substrate-binding	T129	**0.23**	0.25
		S110+	**0.23**	0.15
ssl3364	CP12 polypeptide	T54+	**0.22**	n.d.
		T55	**0.13**	0.16
slr0426	FolE, GTP cyclohydrolase I	S24	**0.18**	**0.02**
		T30+	**0.14**	**0.09**
slr6040	CopR, 2-component regulator, pSYSX copy	T228	**0.18**	**0.09**
slr2075	GroES, 10 kDa chaperonin	T29+	**0.12**	0.58
ssl0707	GlnB, nitrogen regulatory protein P_{II}	T52+	**0.19**	0.36
		S49+	**0.08**	0.15

3.2 Generation of *spk* deficient mutants

To understand the physiological importance of Ser/Thr protein kinases (Spks) in acclimation processes to changing environmental conditions, gene-disruptive mutations were established for the kinase encoding genes (*spkA-L*) annotated in *Synechocystis* by interrupting the reading frame of the GOI through the insertion of an antibiotic resistance cassette gene (Appendix Figure 1, 2). *Synechocystis* has twelve genes that are annotated to encode for Ser/Thr protein kinases (Cyanobase; http://genome.microbedb.jp/cyanobase/GCA_000009725.1, C.-C. Zhang et al., 1998; Leonard et al., 1998; Shi et al., 1998). The annotated protein kinases are

classified as either resembling Hanks-type or ABC1-type of protein kinases (Table 9) (C.-C. Zhang et al., 1998; Leonard et al., 1998; Shi et al., 1998). Their organization according to Kopf et al., (2014) in transcription units (TU) and operons can be found in Table 9.

Table 9: Overview of annoated Ser/Thr protein kinase and their organization and classification in the genome of *Synechocystis*. (http://genome.microbedb.jp/cyanobase/GCA_000009725.1; C.-C. Zhang et al., 1998; Leonard et al., 1998; Shi et al., 1998; Kopf et al., 2014; TU= transcriptive unit)

Gene	Name	Size [bp]	TU	Operon	Kinase Type
sll1574/1575	*spkA*	1567	TU730	Yes	Hanks
slr1697	*spkB*	1725	TU2066	No	Hanks
slr0599	*spkC*	1608	TU3703	Yes	Hanks
sll0776	*spkD*	1524	TU3253	Yes	Hanks
slr1443	*spkE*	1845	TU1108	Yes	Hanks
slr1225	*spkF*	1448	TU1051	No	Hanks
slr0152	*spkG*	1896	TU2267	No	Hanks
sll0005	*spkH*	2046	TU2606	No	ABC1
sll1770	*spkI*	1758	TU1249	Yes	ABC1
slr0889	*spkJ*	1227	TU1196	Yes	ABC1
slr1919	*spkK*	1701	TU622	No	ABC1
sll0095	*spkL*	1596	TU3154	No	ABC1

Based on protein sequence alignments, the protein kinases SpkA-G share a strong similarity to Hanks-type protein kinases, whereas the kinases SpkH-L are closely related to the ABC1-type of protein kinases (C.-C. Zhang et al., 1998; Leonard et al., 1998; Shi et al., 1998). Genes encoding for SpkA, SpkC, SpkD, SpkE, SpkI and SpkJ are transcribed in large TU in an operon structure (Kopf et al., 2014). Interestingly, protein kinase SpkA is annotated to be transcribed by two genes (*sll1574*/*sll1575*), which resulted from a frameshift mutation inside the *spkA* gene found in the original *Synechocystis* strain used for genome sequencing in the first published genome data by Kaneko et al. (1996) (C.-C. Zhang et al., 1998). In this study, out of the annotated twelve kinases, eleven were successfully knocked out. WT copies of the kinases encoding genes were completely absent for the mutated gene constructs. Eight mutation constructs (pTB1Km, pTB2Km, pTB3Km, pTB4Km, pTB5Gm, pTB6Km, pTB8Km, pTB12Km) for modifying the protein kinase genes were newly established and used to transform *Synechocystis* WT (F) (Appendix Table 2). The protein kinase mutants Δ*spkA,* Δ*spkB,* Δ*spkE* and Δ*spkG* were obtained from Dr. Sylvie Bédu (Aix-Marseille Université, France).

3.2.1 Genotyping of Δ*spkA,* Δ*spkB,* Δ*spkE* and Δ*spkG*

Segregation status of protein kinase mutants Δ*spkA,* Δ*spkB,* Δ*spkE* and Δ*spkG* was confirmed. For this purpose, DNA was extracted from the protein kinase deficient strains and

used in a genotyping PCR (Figure 13). Gene specific primer pairs were used to amplify the mutated *spk* genes (Figure 13, Appendix Table 1). The insertion of an antibiotic resistance gene led to an enlarged amplified DNA fragment compared to WT (Table 9). This resulted in a 2130 bp fragment for Δ*spkA*, a 2977 bp fragment for Δ*spkB*, a 2888 bp fragment for Δ*spkE* and 3956 bp fragment for Δ*spkG*. Additional bands were seen in the genotyping PCR for Δ*spkE*. Though not present in the WT control, extra bands appear to be due to unspecific binding of the chosen primer pair for Δ*spkE*. WT-like bands were absent in every mutant.

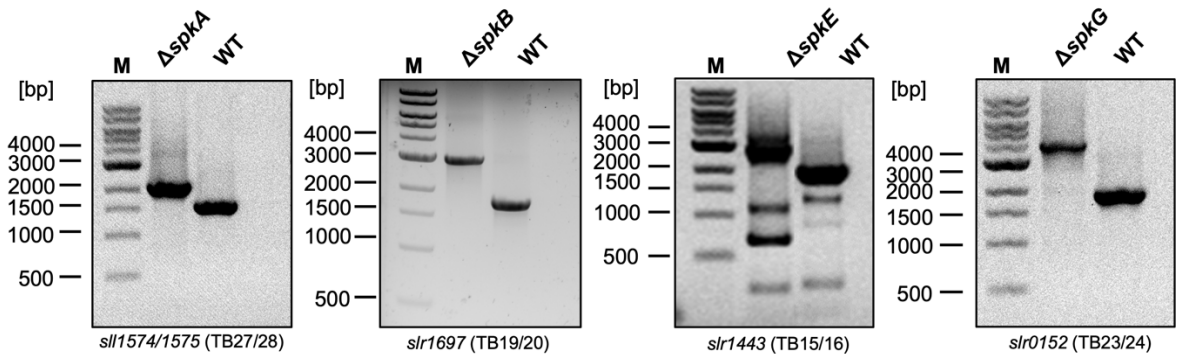

Figure 13: Genotyping of protein kinase mutants. Segregation status was confirmed. gDNA was isolated from kinase mutants Δ*spkA*, Δ*spkB*, Δ*spkE* and Δ*spkG*. Extracted gDNA was used in a genotyping PCR with gene specific primers (Appendix Table 1). Mutated kinase genes were enlarged by the introduction of an antibiotic resistance gene. WT served as control. DNA was separated on a 1% (w/v) agarose gel.

To elucidate the cloning strategy of the mutants, the *spk* coding regions together with 500 bp up and downstream of the GOI from gDNA isolated from the deficient mutant strains were amplified by PCR and subsequently subcloned in pJET1.2/blunt. The generated plasmids pTB15Km, pTB16Km, pTB17Km and pTB18Sm (Appendix Table 2) were send for sequencing. Sequencing results revealed that *sll1575 (*spkA, Appendix Figure 1 A*)* was interrupted by adding a kanamycin resistance (Km^R) between the cutting sides of *EcoR*V. The SpkB encoding gene *slr1697* (*spkB*, Appendix Figure 1 B) was enlarged by introducing a Km^R at the position of *Stu*I. *Slr1443* (*spkE*, Appendix Figure 1 C) was as well altered by inserting of Km^R between the cutting sides of *Hinc*II and *slr0152* (*spkG*, Appendix Figure 1 C) was expanded by the introduction of a spectinomycin resistance (Sp^R) at position of *Nhe*I.

3.2.2 Generation and genotyping of Δ*spk*

To newly established mutations in the genes coding for SpkC, SpkD, SpkF, SpkH, SpkI, SpkJ, SpkK and SpkL mutation constructs needed to be created. Protein kinase genes were amplified from WT gDNA and ligated into either pJET1.2/blunt or pGEMT. Cutting sides were chosen to remove as much coding sequence as possible. Removed gene sequences were

replaced by antibiotic resistance genes (Appendix Figure 2 A-H). The created plasmids pTB1Km, pTB2Km, pTB3Km, pTB4Km, pTB5Gm, pTB6Km, pTB8Km and pTB12Km (Appendix Table 2) were used to transform *Synechocystis* WT (F) and WT (M). gDNA was isolated form the mutated strains and used as DNA template in a genotyping PCR to verify their segregation status for the mutated genes with gene specific primer pairs (Appendix Table 1; Figure 14).

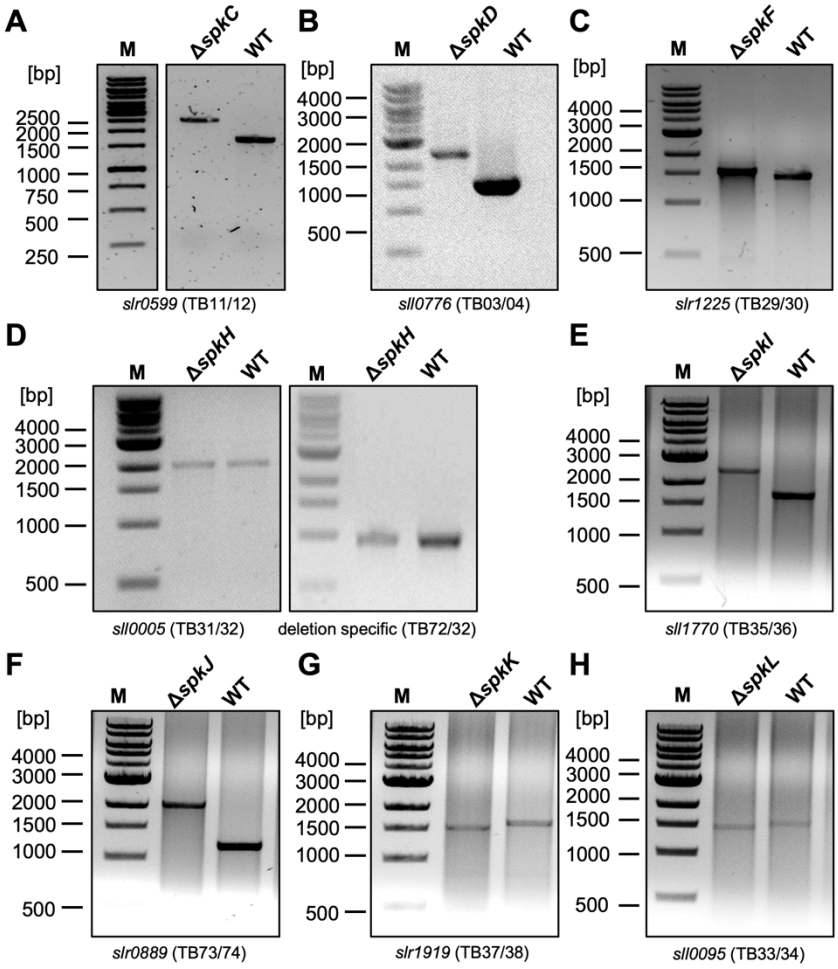

Figure 14: Genotyping of newly established protein kinase mutants. Segregation status was evaluated of WT transformed with the mutation constructs (Appendix Table 2) for *spkC* (**A**), *spkD* (**B**), *spkF* (**C**), *spkH* (**D**), *spkI* (**E**), *spkJ* (**F**), *spkK* (**G**) and *spkL* (**H**). Isolated gDNA of transformed WT was used in a genotyping PCR with gene specific primers (Appendix Table 1). Kinase genes were enlarged and reduced in size by sequence deletion and subsequent introduction of an antibiotic resistance gene. WT served as control. DNA was separated on an 1% (w/v) agarose gel.

WT gene copies were completely segregated for the mutation constructs indicated either by larger amplified DNA fragments of 2369 bp for *spkC*, a 2300 bp fragment for *spkD*, a 1602 bp fragment for *spkF*, a 2515 bp fragment for *spkI* and a 1699 bp fragment for *spkJ* or smaller found DNA fragments of 1598 bp for *spkK* and a 1497 bp fragment for *spkL* compared to their respective WT gene sizes (Table 9, Figure 14 A-C; E-H, Appendix Table 1). Only the gene

spkH (*sll0005*) could not be fully segregated for the mutation construct pTB8Km (Figure 14 D). The deletion of the coding sequence of *spkH* and subsequent insertion of a Km^R led to a mutation construct of equal size to the WT gene. Therefore, primers binding in the erased region of the WT gene were used to check segregation. For the transformed WT strain and the WT, a 1000 bp PCR product could be amplified indicating that *spkH* could not be segregated for the mutation construct (Table 9, Figure 14 D, Appendix Table 1). Different segregation conditions were tested such as HC, low HPO_4 and low light (20 µmol photons m^{-2} s^{-1}) without success. Hence, *spkH* was deemed essential under our laboratory condition.

3.3 Physiological characterization of Δ*spk* mutants

To unravel the role of Spks in *Synechocystis* in acclimation processes towards changing environmental conditions, all members of the newly established Δ*spk* mutant collection were checked for their fitness under various conditions. Moreover, Δ*spk*s with evidence of a Ci related phenotype were chosen to perform in a global proteomic and phospho-proteomic study. Changes in protein abundancies and alteration in p-phosphorylation pattern gave insights to possible protein kinase/substrate interaction cascades. Results were already partially published in Barske & Spät et al. (2023).

3.3.1 Comparative transcriptome data on various environmental conditions

Global RNA-Seq data of *Synechocystis* WT (F) were utilized from the database CyanoExpress (http://cyanoexpress.sysbiolab.eu/) originating from the work of Kopf et al. (2014) to evaluate possible alterations in gene expression of the *spk* genes upon changes in their environment. Given data were filtered for the twelve annotated protein kinases (Table 9). In the applied study, WT (F) cells were put under various environmental perturbations i.e., temperature stress, light stress and the limitation of Fe, Ci, PO_4^{3-} and NO_3^- as well as variations in gene expression in non-logarithmic growth were observed (Figure 15). Changes in the transcript are indicated by log_2-fold changes in regards to non-treated WT (F).

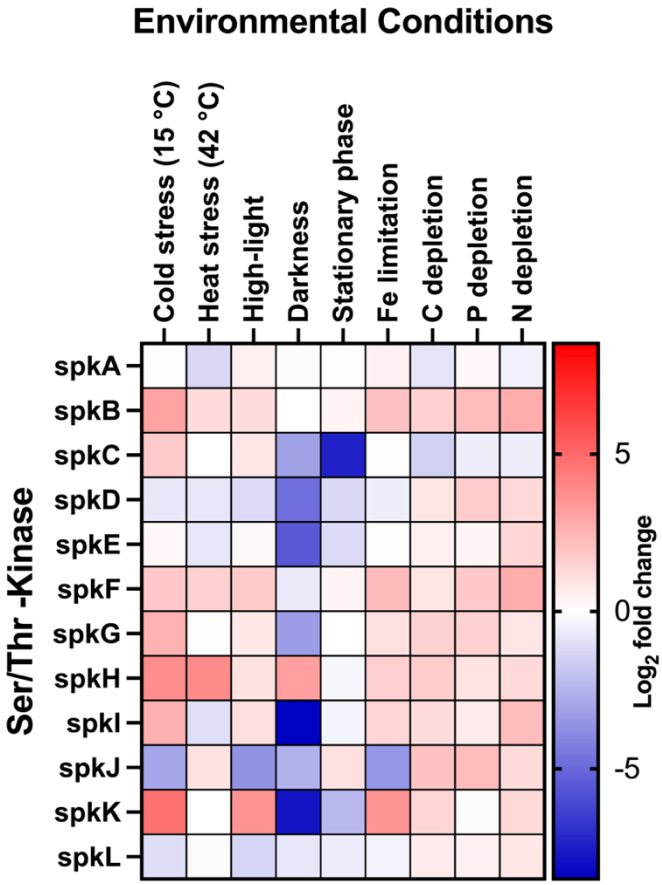

Figure 15: RNA-Seq expression data under varying enviornmental conditios. Global RNA-Seq expression data of *Synecocystis* WT (F) exposed to changing growth conditions. Data were colected from the database CyanoExpress (http://cyanoexpress.sysbiolab.eu/) and orginate from the work around Kopf et al. (2014). Changes in gene expression are indicated by log_2 fold changes, with shades of red highlighting an increase in gene expression and shades of blue a decrease in expression levels compared to untreated WT (F).

Generally, the retrieved RNA-Seq data revealed that the twelve protein kinases are likely constitutively expressed. The tested environmental condition did not strongly alter the expression levels for most of the *spks*. Overall, darkness proved to have the greatest impact on expression levels on several protein kinase genes, which resulted in reduced detected transcripts for *spkC*, *spkD*, *spkE*, *spkG*, *spkJ* and strongly lowered levels for *spkI* and *spkK* transcripts. On the contrary *spkH* was the only protein kinase with increased transcript levels in darkness. Reduced mRNA levels for *spkJ* were additionally reported for cold stress, high light and under an Fe limited environment. The direct opposite could be found for *spkK* with an increase of mRNA levels under cold stress, high light and under an Fe limitation. Strikingly, *spkC* expression levels were strongly reduced under stationary growth.

3.3.2 Acclimation to ambient air

The Δ*spk* collection was screened for their ability to acclimate to ambient air. For this purpose, HC pre-cultivated kinase mutants were shifted to LC and the growth was monitored for 4 d. Growth data were standardized to their starting OD720 and subsequently normalized to their respective WT. Photos of LC acclimated *Synechocystis* were taken at the end of the growth experiment (Figure 16). Protein kinase mutants Δ*spkA*, Δ*spkD*, Δ*spkE* and Δ*spkF* showed no, or only minor differences in growth compared to their respective WT (Figure 16 A, D, E, F). Even though Δ*spkD* depicted a WT-like growth it was accompanied by yellowish pigmentation (Figure 16 D). Δ*spkJ*s and Δ*spkL*s growth was only slowed down at an advanced stage of the recording interval, resulting in an overall significantly reduced suspension density at the end of the grow phase (Figure 16 I, K). Δ*spkL* displayed a light pigmentation phenotype when acclimated to LC (Figure 16 K). Protein kinase mutants Δ*spkB*, Δ*spkC,* Δ*spkG*, Δ*spkI* and Δ*spkK* presented to be significantly affected by the HC LC shift, with Δ*spkB*, Δ*spkC,* Δ*spkG* and Δ*spkK* only reaching about 75 % of relative growth levels in comparison to their respective WT (Figure 16 B, C, G, H, J). Accompanied were these changes with a yellow pigmentation phenotype for Δ*spkB* and Δ*spkG* (Figure 16 B, G). A dark pigmentation phenotype was observed for Δ*spkK* (Figure 16 J). Overall, Δ*spkI* growth was highlighted by the strongest reduction in relative growth levels by reaching only 50 % of WT level (Figure 16 H).

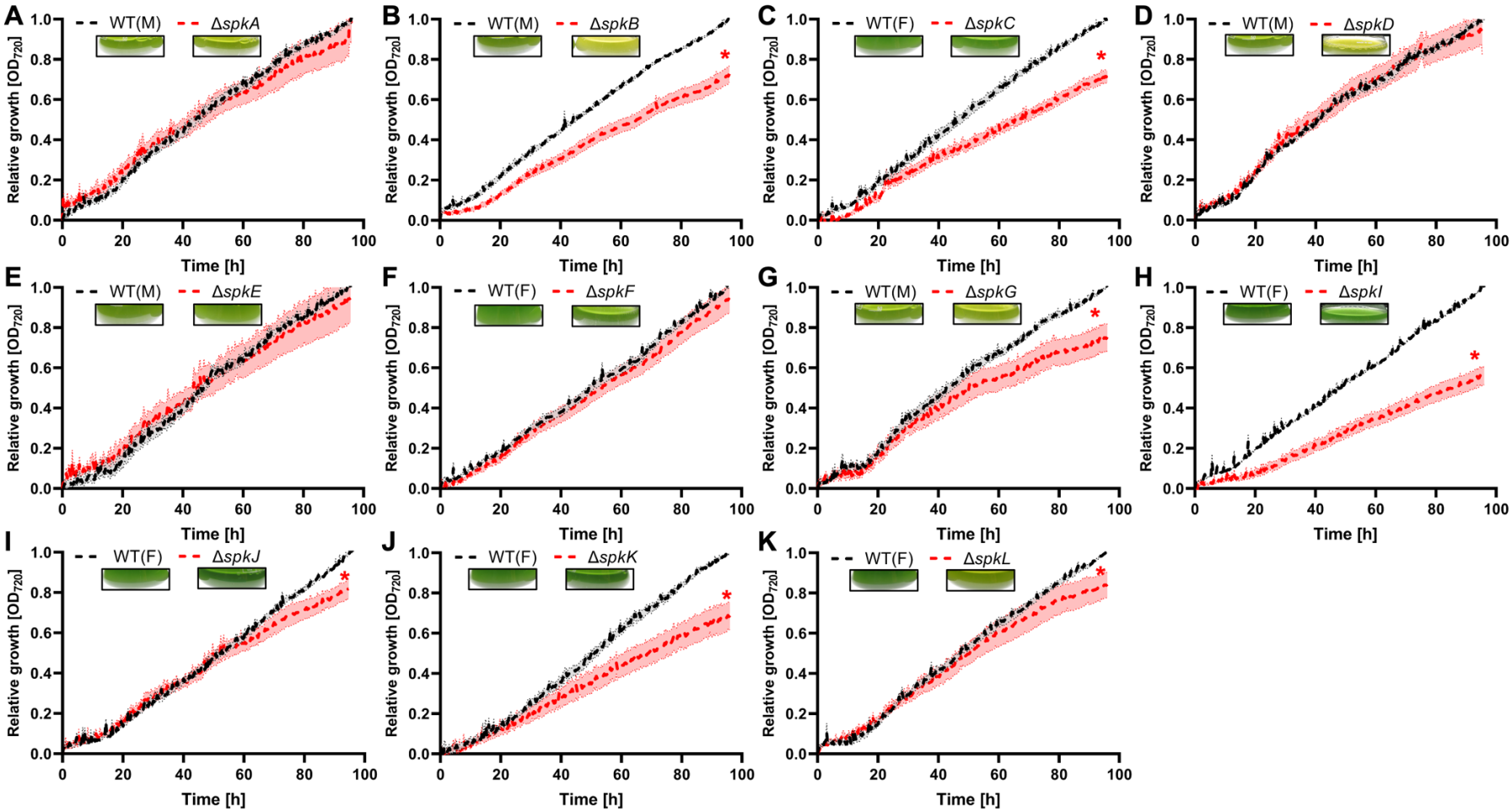

Figure 16: Acclimation of Δ*spk*s to ambient air: The collection of eleven Δ*spks* (**A**-**K**) were screened for their ability to acclimate to ambient air. Protein kinase mutants were pre-cultivated in a HC environment together with their corresponding WT. *Synechocystis* suspensions were subsequently adjusted to the same starting OD720 of 0.2. Growth was monitored for 4 d at LC in a bioreactor system (Multi-Cultivator MC-1000-OD system, Photon Systems Instruments; Czech Republic). Growth data were standardized to their starting OD720 and subsequently normalized to their respective WT. Growth data are visualized with their respective standard errors. Inlets represent documented phenotypes of LC acclimated cells. (n=8 (biological), data are shown as mean values and standard error; student's *t*-test, two-tailed, * p<0.05)

3.3.3 Pigmentation levels of HC and LC acclimated Δ*spk*s

A spectrum from 350-750 nm was recorded from Δ*spk*s while performing the LC acclimation experiment. Spectrum data of HC and LC grown cells were used to quantify chlorophyll *a* (Chl*a*), phycocyanin (PC) and carotenoid (Car) levels (Table 10). When cultivated under HC, Chl*a* levels of Δ*spkD* and Δ*spkI* were significantly higher, PC levels of Δ*spkF*, Δ*spkJ* and Δ*spkL* were significantly reduced and Car quantities of Δ*spkD* and Δ*spkI* were found to be significantly increased compared to their respective WT. After long-term LC acclimation Δ*spkB* depicted a significant reduction in Chl*a* level whereas all Δ*spks* in the WT (F) background showed an overall significantly higher amount of Chl*a*. PC levels were significantly reduced in Δ*spkG* and Δ*spkI*. Elevated levels of PC could be found in Δ*spkK* and Δ*spkL*. Δ*spkA*, Δ*spkD*, Δ*spkK* and Δ*spkL* were characterized by significantly higher levels of Car when being adapted to LC.

Table 10: Pigment levels of Δ*spk*s acclimated to HC and LC. HC and LC acclimated cells of Δ*spk*s were used to record a spectrum from 350-750 nm. Spectrum data were utilized to quantify Chlorophyll *a* (**Chl*a***), Phycocyanin (**PC**) and Carotenoid (**Car**) levels according to Sigalat & Kouchkovsky (1975). (WT n=8, data are shown as mean values, Δ*spk* n=4 (biological); student's *t*-test, two-tailed, * p<0.05)

	HC			LC		
Strain	**Chl*a***	**PC**	**Car**	**Chl*a***	**PC**	**Car**
WT (M)	7.52	3.12	9.45	6.22	2.33	9.58
Δ*spkA*	7.76	3.01	8.84	6.67	2.59	11.02*
Δ*spkB*	8.09	2.52	10.04	3.71*	2.12	9.30
Δ*spkD*	10.72*	3.61	12.17*	6.23	2.52	10.55*
Δ*spkE*	6.82	2.31	8.16	6.41	2.43	9.96
Δ*spkG*	7.47	2.91	8.14	5.22	1.94*	9.26
WT (F)	8.43	3.59	8.94	5.41	2.90	9.65
Δ*spkC*	7.22	2.68	7.80	7.43*	2.55	9.53
Δ*spkF*	6.54	2.19*	7.98	8.30*	2.64	9.07
Δ*spkI*	11.93*	4.34	10.97*	6.35*	2.54*	8.77*
Δ*spkJ*	5.82*	1.94*	6.84	8.68*	2.86	9.27
Δ*spkK*	7.70	2.83	7.48	9.01*	3.53*	12.08*
Δ*spkL*	6.30	1.93*	7.65	9.51*	3.24*	12.08*

c [µmol/l $OD750^{-1}$]

3.3.4 Acclimation of Δ*spk*s to photo-mixotrophic conditions

The ability of Δ*spk*s in liquid culture to acclimate to photo-mixotrophic conditions was investigated by adding 10 mM Gluc to the growth medium in the presence of light. Growth was documented for up to 5 d. Growth data of Δ*spk*s were normalized to the maximum of their respective WT (Figure 17).

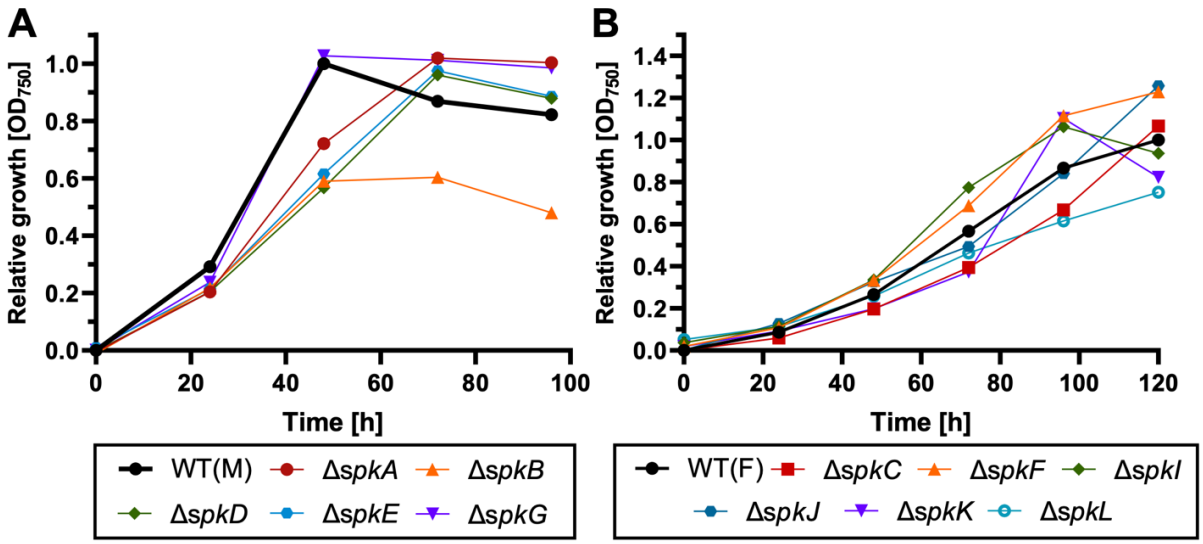

Figure 17: Acclimation of Δ*spk*s to photo-mixotrophic conditions. Δ*spk*s were pre-cultivated shaking (140 rpm) for 7 d in ambient air with 35 µmol photons m^{-2} s^{-1} and 30°C together with their corresponding WT in BG11 pH 8.0 filled Erlenmeyer flasks. Prior, cultures were adjusted to OD750 of 0.5 with BG11 (TES pH 8.0). Cultures were treated with 10 mM Gluc. *Synechocystis* mutants were grown under ambient air with 35 µmol photons m^{-2} s^{-1} and 30 °C until the stationary growth phase was reached. OD750 was measured every 24 h. Growth data of Δ*spk*s were normalized to maximum OD750 of their respective WT (**A**, **B**). (n=3 (biological), data are shown as mean values)

Protein kinase mutants in WT (M) background (Figure 17 A) exhibited rapid growth after the addition of 10 mM Gluc. WT (M) and kinase mutants reached the stationary growth phase after 40 h, except for Δ*spkB*. Like WT (M), Δ*spkB* entered stationary growth after 40 h but overall growth level was only 60 % respectively to WT (M) (Figure 17 A). WT (F) and its *spk* mutants showed a delayed ability to utilize the supplemented Gluc compared to WT (M) and its respective Δ*spk* mutants, which was indicated by a prolonged growth phase (Figure 17 A, B). Δ*spk*s with WT (F) background (Figure 17 B) entered the stationary phase after 120 h. Interestingly, Δ*spkF* and Δ*spkJ* could be characterized with an enhanced growth under photo-mixotrophic condition compared to WT (F) (Figure 17 B), while Δ*spkL* did not reach WT (F)-like growth levels after 120 h (Figure 17 B).

3.3.5 Drop dilution assays

Drop dilution assays were performed to test effects of other environmental conditions on the growth of Δ*spks*. For this purpose, LC acclimated *Synechocystis* was diluted in a serial manner and dropped on solid BG11 agar plates supplemented with either 10 mM Gluc (photo-mixotrophic, diurnal; Figure 18 A, B) or 500 mM of NaCl (Figure 18 C). Subsequently, plates were incubated under different light conditions at LC (Figure 18). WT (M), WT (F) and the Δ*spk*s tolerated elevated Gluc levels (Figure 18 A, B). Under continuous light in the presence of Gluc, Δ*spk*s in the WT (M) background revealed overall WT-like growth except for Δ*spkD* (Figure 18 A). Δ*spkD* was highlighted by denser colonies compared to WT (M) in the dilution steps of 10^{-1}. WT (F) and Δ*spk*s with the WT (F) background were characterized by a higher tolerance towards externally supplied Gluc in contrast to WT (M) and its protein kinase mutants indicated by denser appearing colonies in the 10^{-1} dilution step. Only Δ*spkJ* presented WT (F)-like growth. Furthermore, diurnal growth (12 h light/12 h dark cycles) was studied without and in the presence of 10 mM Gluc (Figure 18 B). Δ*spk*s, WT (M) and WT (F) were able to grow in a light and dark rhythm (Figure 18 B). Δ*spkB* and Δ*spkE* revealed a light-yellow phenotype. When 10 mM Gluc was present in the medium, Δ*spkB* and Δ*spkE* expressed strongly reduced growth phenotypes (Figure 18 B). Osmotic stress was applied to the Δ*spk*s collection by the addition of 500 mM of NaCl to the growth medium (Figure 18 C). WT (M), WT (F) and all protein kinase deficient mutants grew under raised salt concentrations, with all displaying a light-yellow pigmentation phenotype. Interestingly, growth of Δ*spkI* was affected in all tested environmental condition (Figure 18 A, B, C). In fact, Δ*spkI* displayed already under control condition a strongly retarded growth phenotype (Figure 18 A, B, C). This phenotype became even more pronounced when 10 mM Gluc was added to the medium (Figure 18 A) and additionally put under diurnal light rhythmic (Figure 18 B). Elevated NaCl led to an almost complete arrest of growth (Figure 18 C).

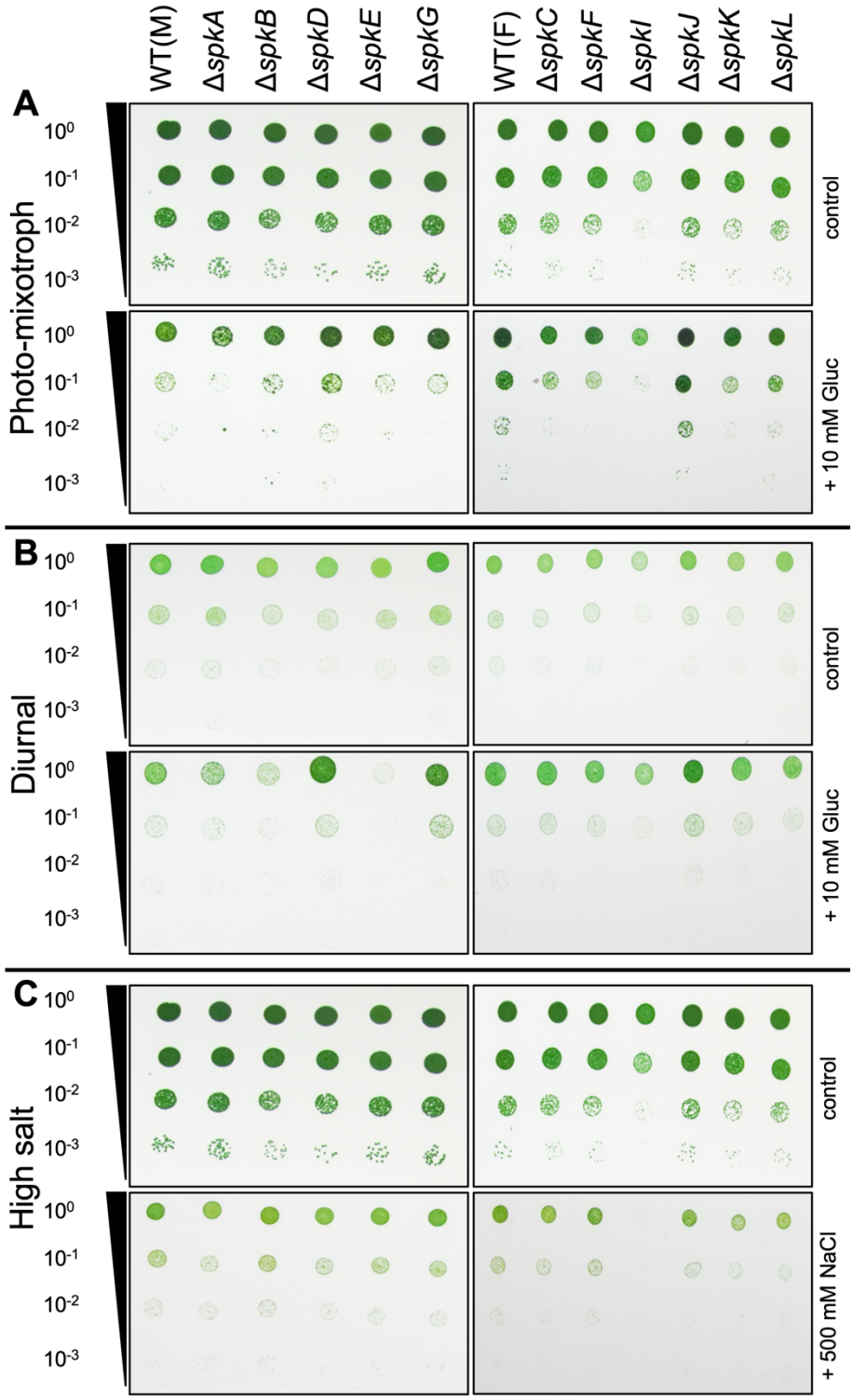

Figure 18: Drop dilution assay to test effects of different environmental conditions on Δ*spk* growth. Δ*spk*s were pre-cultivated under LC condition in shaking flasks under 100 µmol photons m^{-2} s^{-1} and 30 °C. Cultures were adjusted with BG11 to OD750 of 0.2 and susbsequently diluted in a serial manner (10^{-1}, 10^{-2}, 10^{-3}). 2 µl were dropped on BG11 agar plates. (**A)** photo-mixotrophic conditions were tested by adding 10 mM Gluc to the growth medium. (**C**) The tolerance toward elevated salinity was analyzed by placing 500 mM NaCl in the grwoth medium. (**A**, **C**) Plates were incubated at 100 µmol photons m^{-2} s^{-1} and 30 °C for 4 d. (**B**) Diurnal rhytmic (12 h light/ 12 h dark) was studied on plates without and with the addition of 10 mM Gluc. Plates incubated in 75 µmol m^{-2} s^{-1} and 30 °C. (**A**, **B**, **C**) Pictures were taken after 4 d of incubation together with their respective control. (n=3 (biological))

3.3.6 Tolerance of Δ*spk*s towards externally supplied ROS

In a survival experiment, the tolerance of Δ*spk*s towards externally supplied H_2O_2 was tested (Figure 19). In a preliminary experiment, lethal H_2O_2 concentration for WT (M) and WT (F) were determined (Appendix Figure 3). Cultures were adjusted to OD750 of 0.4 and probed with 3 mM and 4 mM H_2O_2 and exposed to light for 1 h. Serially diluted, H_2O_2 treated *Synechocystis* suspensions recovered for 4 d under constant light on BG11 agar plates (Figure 19). When exposed to 3 mM H_2O_2, most protein kinase mutants were able tolerate the ROS stress except for Δ*spkF and* Δ*spkI*. Δ*spkF* showed only minor growth whereas Δ*spkI* could not recover from the treatment indicated by a completely abolished growth. Most Δ*spk*s were unable to recover from a 4 mM H_2O_2 treatment. Only Δ*spkB*, Δ*spkG*, Δ*spkK* and Δ*spkL* resumed growth after the handling, with Δ*spkB* and Δ*spkG* even depicting a stronger tolerance towards externally supplied ROS than their respective WT (M). WT (M) and WT (F) were highlighted by different H_2O_2 tolerance levels with WT (F) recovering from higher concentrations.

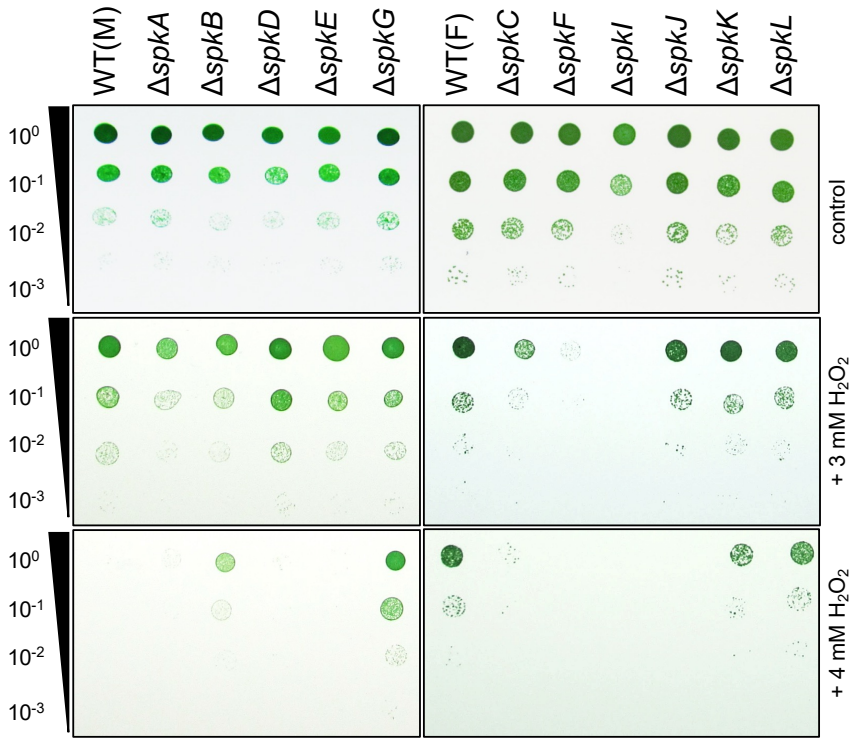

Figure 19*:* Tolerance of Δ*spk*s towards externally supplied ROS. Externally supplied H_2O_2 was used to study the ROS tolerance of Δ*spk*s. Cultures were pre-cultivated in shaking flasks under LC and constant light (100 µmol photons m^{-2} s^{-1}) and 30 °C. Prior to the survival experiment, the suspensions were adjusted to OD750 of 0.4 and probed with 3 mM and 4 mM H_2O_2 and exposed to light for 1 h (100 µmol photons m^{-2} s^{-}). Further, cultures were diluted in a serial manner (10^{-1}, 10^{-2}, 10^{-3}) and 2 µl of diluted *Synechocystis* was dropped on BG11 agar plates. Cultures were allowed to recover for 4 d at 100 µmol photons m^{-2} s^{-1} and 30 °C. Photos were taken with their respective control after 4 d. (n=3, (biological))

3.4 Studies on selected Δ*spks*

The Δ*spk* collection was physiologically characterized under various environmental conditions (Figure 16, 17, 18, 19). Occurring phenotypes were collected and summarized in Table 11. Out of the eleven protein kinase mutants analyzed, growth of all mutans was affected under at least one tested condition. The extent of the physiological alterations varied among the kinases, from mild to severely impaired. Out of the given data, Δ*spkB,* Δ*spkC,* Δ*spkI* and Δ*spkK* seemed to be very promising candidates to analyze in detail. Concomitantly, HC acclimated Δ*spkB,* Δ*spkC,* Δ*spkI* and Δ*spkK* presented severely diminished growth when acclimating to a LC atmosphere (Figure 16 B, C, H, J). Δ*spkK* showed to be only severely affected in LC (Figure 16 J), other tested condition affected it only mildly (Figure 17, 18, 19). Hence, Δ*spkK* was not considered to be analyzed in detail. Through the observed LC impaired growth of Δ*spkB* (Figure 16 B) together with its negatively impacted vitality under photo-mixotrophic conditions (Figure 17 A; 18 A, B) it could be suggested that the recorded phenotypes are C related. Moreover, Δ*spkC* displayed significantly reduced growth under LC (Figure 16 C) and its phosphorylation status was found altered in the global phospho-proteome study with WT (F) (Table 8). These results imply SpkC as a potential regulator of Ci related acclimation processes and that it could play a vital role in controlling HCO_3^- uptake. Overall, growth of Δ*spkI* was highlighted by reduced growth under any tested condition (Figure 16, 17, 18, 19). Thus, a clear indicator of which specific physiological role SpkI might possess remains elusive.

Table 11: Summary of collected Δ*spk* phenotypes. Collection or recorded phenotypes (Figure 16-19) of Δ*spk*s empirically ranked in comparison to their respective WT. (diurnal^G= with Gluc; Green to red scale: +++ WT -like; + severely changed from WT; blue scale: + WT -like, +++ outperformed WT)

ΔKinase	HC-LC	Pigmentation	Gluc	diurnal	diurnal^G	salt	ROS
Δ*spkA*	+++	+++	++	+++	+++	++	+
Δ*spkB*	+	++	+	+++	+	+++	++
Δ*spkC*	+	+++	+++	+++	+++	+++	+
Δ*spkD*	+++	++	+++	+++	+++	++	+
Δ*spkE*	+++	+++	+++	+	+	+++	+
Δ*spkF*	+++	+++	++	+++	+++	+++	+
Δ*spkG*	++	+++	++	+++	+++	+++	+++
Δ*spkI*	+	+	++	++	++	+	+
Δ*spkJ*	++	+++	+++	+++	+++	+++	+
Δ*spkK*	+	++	++	+++	+++	+++	++
Δ*spkL*	++	++	++	+++	+++	+++	++

3.4.1 Detailed analyses of Δ*spkB* acclimation to different Ci conditions

The protein kinase deficient mutant Δ*spkB* presented itself to be strongly affected when grown under LC condition accompanied by significantly reduced Chl*a* levels (Figure 16 B, Table 10). Additionally, a negatively impacted growth phenotype under photo-mixotrophic conditions in the presence of 10 mM Gluc on either solid medium or in liquid culture was observed in continues and diurnal light (Figure 17 A; Figure 18 A, B). Interestingly, Δ*spkB* was characterized by an increased tolerance towards externally supplied ROS stress in from of H_2O_2 (Figure 19). Collectively, the observed Δ*spkB* phenotypes could potentially be related to Ci allocation issues in the mutant. Therefore, the kinase deficient mutant was selected to be analyzed in detail. Glycogen levels and metabolome data were generated under fluctuating Ci conditions. A global proteome and phospho-proteome study was conducted with Δ*spkB* and WT (M) under Ci limitation. Information gained from the phospho-proteome was applied to examine the physiological relevance of the detected altered p-events in Δ*spkB* by performing state transition fluorescence measurements, studying photosynthetic activity and by immunoblots. A complementation of Δ*spkB* was introduced and preliminarily characterized for the compensation of the recorded growth phenotype. Results were already partially published in Barske & Spät et al. (2023).

3.4.2 Ci dependent cellular glycogen levels of Δ*spkB*

Cellular glycogen levels of Δ*spkB* were quantified from HC to LC shifted cells (Figure 20). Samples were taken at the HC pre-acclimated state and after 3 h and 24 h in LC. Glycogen levels were quantified as Gluc monomers. When acclimated to a HC environment, Δ*spkB* showed significantly increased glycogen levels compared to WT (M) (Figure 20). When shifted to LC for 3 h, stored glycogen depleted significantly faster in the mutant than in WT (M). Cellular glycogen levels were equal after 24 h of LC acclimation in the mutant and in WT (M).

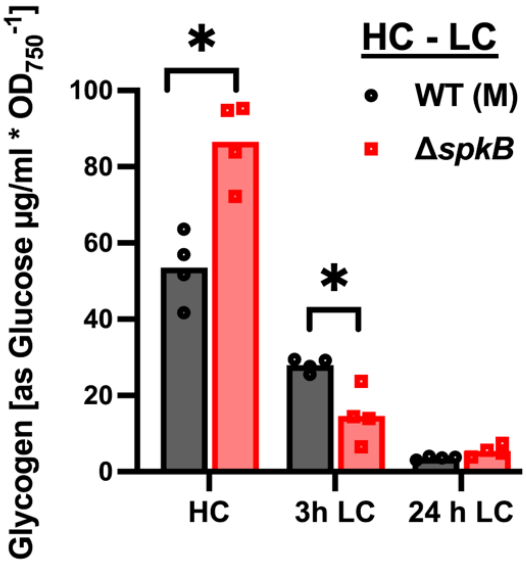

Figure 20: Cellular glycogen levels in Δ*spkB* under Ci limitation. Δ*spkB* and WT (M) were shifted from HC to LC. Samples were taken at HC acclimated state and after 3 h and 24 h in LC. Glycogen levels were quantified as Gluc monomers. (n=4 (biological), data are shown as single values with mean average; student's *t*-test, two-tailed, * p<0.05)

3.4.3 Ci dependent changes in the metabolome of Δ*spkB*

Ci dependent metabolome changes in Δ*spkB* were studied. Metabolites associated with the TCA cycle, N assimilation and photosynthesis together with cellular AA levels were quantified in an LC-MS approach. Prior, Δ*spkB* and WT (M) were shifted from HC to LC and samples were taken after 1, 3, 6, and 24 h after the shift to LC. Selected metabolome data are presented as a heatmap in $\log_2$ fold changes in relation to WT (M) at a HC acclimated state (Figure 21). Statistical deviations from Δ*spkB* and WT (M) were calculated in relation to corresponding WT (M) sampling timepoints. Metabolites associated with the TCA cycle, such as aconitic acid, citric/isocitric acid, fumaric acid and succinic acid were found in significantly higher quantities in Δ*spkB* under HC. Likewise, AA such as Arg, Asp, Met and Tyr showed higher levels in the mutant at HC compared to WT (M). When shifted to LC for 1 h, AA directly linked to N assimilation showed strong deviation from WT (M). Significantly lowered levels of Arg, Gln and Glu were found in Δ*spkB* which all remained in reduced levels throughout the shift experiment. TCA metabolite succinic acid remained in higher quantities after 1 h of LC in Δ*spkB*. During the shift experiment AA such as Ala, Asp, Gly, Lys, Phe, Pro, Trp and Tyr showed reduced levels at any given sampling point after the shift to LC in contrast to WT (M). Only Met levels were significantly increased under LC in Δ*spkB*. Overall changes after 24 h LC in metabolite quantities remained minor with only Arg and Pro displaying significantly reduced levels.

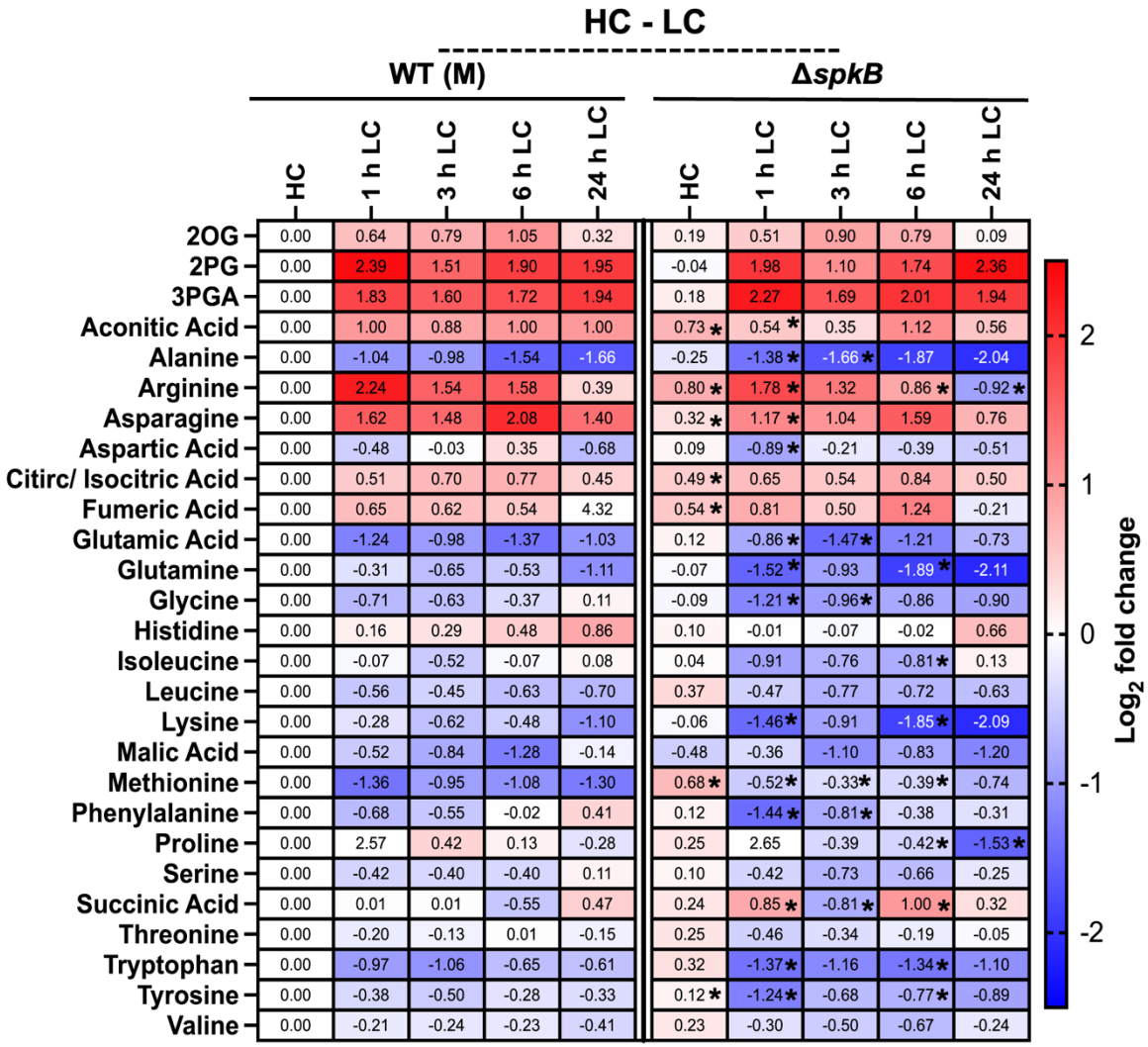

Figure 21: Metabolites of HC-LC shifted Δ*spkB*. Δ*spkB* and WT (M) were shifted from HC to LC conditions. Samples were taken at a HC acclimated state and 1, 3, 6 and 24 h after the initial shift to LC. Samples were analyzed in a LC-MS approach. Data are shown as $\log_2$ fold changes in a heat map displaying metabolic changes during the shift in relation to WT (M) in HC. Significant deviations were calculated in relation to corresponding WT (M) sampling points. (red = increased quantities, blue lowered quantities; n=4 (biological), student's *t*-test, two-tailed, * $p<0.05$)

3.4.4 Ci dependent changes in protein abundancies in Δ*spkB*

To gain insight on how Δ*spkB* is acclimating to an LC atmosphere, a global proteome study was conducted in which Δ*spkB* together with WT (M) were pre-acclimated under HC and subsequently put for 3 and 24 h in LC. Cell extracts were then used in an LC-MS-based proteomic approach, which quantified 2200 proteins in three biological replicates. Data are shown as $\log_2$ fold changes of Δ*spkB* in comparison to the same timepoint of WT (M). The overall deviations between Δ*spkB* and WT (M) were minor (Table 12). In HC pre-grown Δ*spkB* nine proteins were found in higher and five proteins in lower quantities whereas seven proteins were quantified in increased and three in reduced amounts after 3 h as well as eight proteins

in a greater and three proteins to a lower extend after 24 h in LC. The greatest changes in protein abundancies were reported for the unknown protein Sll1009, which showed to be 7-fold increased after 3 h in LC in the mutant. Further, most changes were seen for proteins with a variety of different cellular functions. The surface layer protein Sll1951 presented significantly higher levels at a HC acclimated state in the mutant. The pili-forming proteins encoded by the *pilA*-operon (Slr2017, Slr2018) accumulated in Δ*spkB* under HC. In contrast Slr1929, another pilin-like protein, presented reduced quantities after 3 h in LC. Osmo-regulatory proteins such as GgpS and GlpD showed a significantly higher amount under LC in Δ*spkB*, with GgpS being enriched under any given timepoint. The phosphate-binding protein PstS was found in higher concentrations after 24 h in LC in the mutant. The Hik Sll0094 and the hydrogenase subunit Sll1226 were among the proteins with lowered quantities in Δ*spkB* throughout the experiment.

Table 12: Proteins with significantly altered abundancies in Δ*spkB* in LC. Shown are log_2 fold changes (FC) of Δ*spkB* in relation to WT (M). Significant alterations are highlighted in bold letters. Entire proteome data can be found in Barske & Spät et al. (2023). (FC= fold changes; n=3 (biological), student's *t*-test, two-tailed, p<0.05)

		Protein [FC]		
Gene	**Protein description**	**Δ*spkB*$_{HC}$/ WT$_{HC}$**	**Δ*spkB*$_{3hLC}$/ WT$_{3hLC}$**	**Δ*spkB*$_{24hLC}$/ WT$_{24hLC}$**
sll0094	two-component sensor histidine kinase	**-1.282**	-0.786	-0.885
sll0680	PstS, phosphate-binding periplasmic protein precursor (PBP)	3.699	3.751	**3.772**
sll0721	unknown protein	**2.200**	**2.173**	**2.359**
sll1009	Funknown protein	4.623	**7.251**	5.092
sll1085	GlpD, glycerol-3-phosphate dehydrogenase	2.230	**2.296**	1.872
sll1220	putative diaphorase subunit of the bidirectional hydrogenase		-1.497	**-2.335**
sll1226	hydrogenase subunit of the bidirectional hydrogenase	**-1.674**	**-1.690**	-1.855
sll1241	unknown protein	**0.976**	0.548	0.845
sll1483	periplasmic protein, similar to transforming growth factor induced protein	-0.463	0.538	**1.365**
sll1566	GgpS, glucosylglycerolphosphate synthase	**2.555**	**2.764**	**2.425**
sll1951	surface layer protein Sll1951	**4.603**	4.446	1.904
slr0168	unknown protein	1.602	1.205	**1.411**
slr0226	unknown protein	**-2.012**	-1.346	**-1.546**
slr0355	bioU, biotin synthesis factor	-1.512	**-1.899**	**-1.861**
slr0408	unknown protein	**2.101**	**1.928**	2.015
slr0657	aspartate kinase	0.355	**0.784**	0.654
slr1100	hypothetical protein	**-1.536**	-1.072	-0.955
slr1167	GldA, glycerol dehydrogenase	**-2.968**	-3.103	-3.069
slr1929	type 4 pilin-like protein	-2.916	**-2.938**	-2.830
slr1983	two-component hybrid sensor and regulator	1.378	1.406	**1.376**
slr2017	type 4 pilin-like protein, essential for motility operon	**2.048**	1.892	1.884
slr2018	unknown protein	**1.873**	1.534	1.797
slr5005	hypothetical protein	3.460	3.700	**2.067**
slr9201	hypothetical protein	**3.580**	**3.313**	**3.836**
ssr3304	hypothetical protein	**0.466**	0.437	0.366

3.4.5 Ci dependent changes in protein phosphorylation of Δ*spkB*

Phospho-peptides of Δ*spkB* and WT (M) were enriched by TiO_2 metal-oxide affinity chromatography and used in an LC-MS phospho-proteome approach. The dataset was screened for p-events exclusively quantified in WT (M) and absent in Δ*spkB*. T266 of the glutathione S-transferase (Gst1, Sll1545) and T34 or T35 of the hypothetical protein Slr0483 were exclusively detected in at least one replicate in WT throughout the experiment but never in the mutant. In this study 235 individual p-events were quantified on 119 different proteins. Out of the identified p-proteins only six proteins showed alterations in their phosphorylation pattern in Δ*spkB* compared to WT (Table 13). The hypothetical protein Sll0103 was highlighted by eight p-events from which six p-sides were significantly changed in the mutant. T361, T344 and T58 were considerably less phosphorylated in Δ*spkB* in a HC state compared to WT (M). Upon shift to LC conditions, T58, T344, T349, T361 and T403 of Sll0103 were distinctively less phosphorylated in Δ*spkB*. The carboxysome structural protein CcmM displayed a clearly reduced p-occupancy at T358 at any given timepoint in the mutant, whereas other p-events S352, T585, T609 and the unspecified p-event S454-459 in CcmM did not change in the mutant. Interestingly, the regulatory protein PII (GlnB) was significantly less phosphorylated at S49 after 3 h of incubation at LC. The PSI subunit PsaE displayed a substantially reduced phosphorylation at S31 when shifted to LC. Moreover, the protein kinase SpkF revealed a less pronounced (auto)phosphorylation at T24 after 24 h in LC in Δ*spkB*. The only protein with a detected increased phosphorylation in Δ*spkB* was the allophycocyanin subunit ApcA at T31.

Table 13: Significantly changed p-events in Δ*spkB* in LC. Recorded altered p-events of HC LC shifted Δ*spkB* compared to WT (M). Significant alterations are highlighted in bold letters. Phosphorylation sides marked with + were already known previously. Entire phospho-proteome data can be found in Barske & Spät et al. (2023). (n=3 (biological), student's *t*-test, two-tailed, p<0.05)

			Phosphorylation ratio		
Protein ID	**Protein description**	**p-site**	**Δ*spkB*$_{HC}$/ WT$_{HC}$**	**Δ*spkB*$_{3hLC}$/ WT$_{3hLC}$**	**Δ*spkB*$_{24hLC}$/W T$_{24hLC}$**
sll0103	hypothetical protein	T58+	**-0.381**	**-1.614**	**-0.375**
		T344+	**-3.223**	-1.946	**-2.554**
		T349+	-2.723	-1.367	**-2.598**
		T361+	**-1.738**	**-1.313**	**-1.854**
		T380+	-1.278	**-1.399**	-1.597
		T403+	-1.951	**-1.173**	**-1.655**
sll1031	CcmM, putative carboxysome structural protein	T358+	**-2.549**	**-2.602**	**-2.162**
slr1225	SpkF, serine/threonine kinase	T24+	-0.680	0.201	**-1.004**
slr2067	ApcA, allophycocyanin alpha subunit	T31+	1.721	**1.663**	1.283
ssl0707	GlnB, nitrogen regulatory protein PII	S49+	-1.793	**-5.529**	-1.073
ssr2831	PsaE, photosystem I subunit IV	S31+	-1.782	**-1.280**	**-1.724**

3.4.5.1 Low temperature 77K fluorescence measurements

ApcA was shown to be the only p-event with a significantly increased p-occupancy at T31 in Δ*spkB* when shifted to LC conditions (Table 13). To investigate the effects of the altered phosphorylation status of the allophycocyanin subunit on photosynthetic energy transfer, low temperature 77K fluorescence measurements were performed with LC acclimated Δ*spkB* (Figure 22). Prior to fluorescence measurements, cells were dark incubated and either snap frozen or concomitantly exposed to orange or far-red light. Emission spectra were recorded when cells were excited at the level of PBS (EX570 nm, Figure 22 A) or the chlorophylls (EX440 nm, Figure 22 B). Selected emission spectra ratios from certain wavelength were applied to understand the photosynthetic energy transfer within mutant and the WT (M). The energy transfer between PSI/CP43 (PSI/686 nm), PSI/CP47 (PSI/696 nm), CP47/CP43 (696 nm/686 nm) and PSI/allophycocyanin (PSI/662 nm) was evaluated. Samples of WT (M) and the mutant were treated identically and statistically compared.

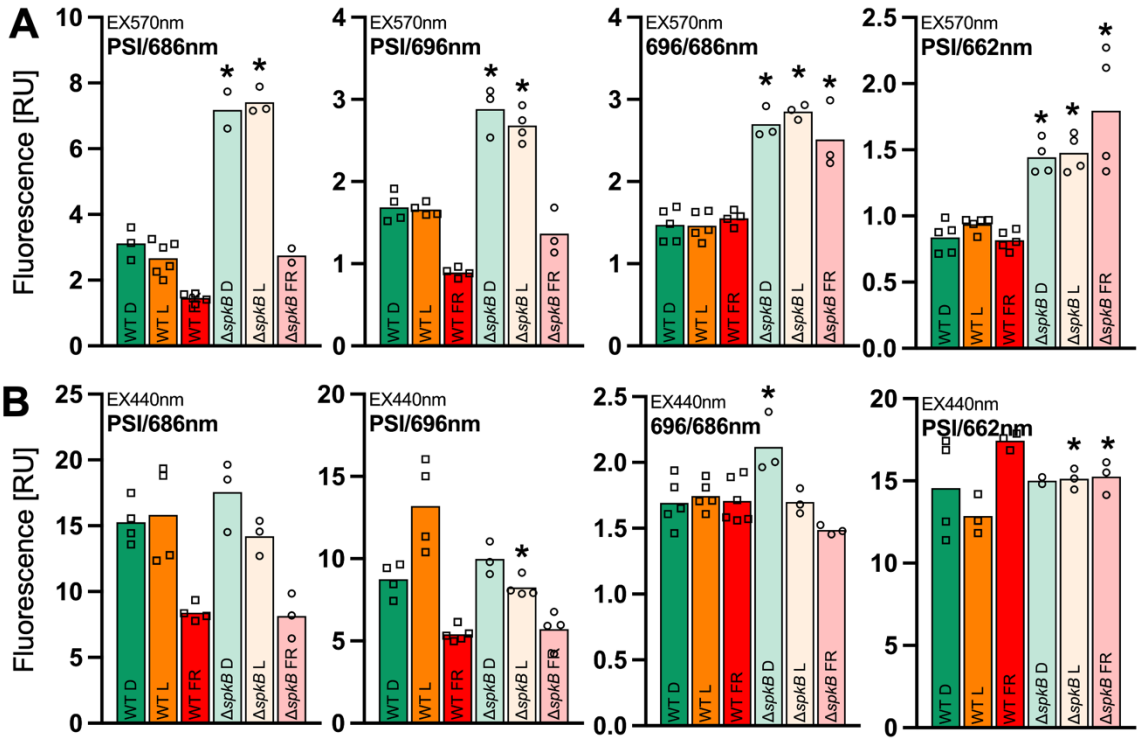

Figure 22: Energy transfer between different photosynthetic complexes by low temperature 77K fluorescence measurements. For low temperature (77K) fluorescence measurements, WT (M) and Δ*spkB* were cultivated under LC condition. Cells were acclimated to darkness for 30 min and concomitantly exposed to either far-red light (100 µmol photons m^{-2} s^{-1}, wavelength 730 nm) or orange light (100 µmol photons m^{-2} s^{-1}, wavelength 600-630 nm). Fluorescence emission ratios between different photosynthetic complexes of the deep-frozen samples were analyzed after excitation at either 570 nm (**A**) or 440 nm (**B**). (RU= relative fluorescence; n=3 (biological); student's *t*-test, two-tailed, $p<0.05$)

When PBS were excited at 570 nm in Δ*spkB* in a LC acclimated state (Figure 22 A), cells incubated in the dark and illuminated under orange light were showing an increased PSI/686 nm, PSI/696 nm, 696/686 nm and PSI/662 nm relative fluorescence (RU) compared to the WT (M) control. Far-red treated Δ*spkB* showed WT (M)-like PSI/686 nm and PSI/686 nm fluorescence ratios but were again strongly elevated for 696/686 nm and PSI/662 nm in the mutant. Many of the recorded effects seen after PBS excitation at 550 nm (Figure 22 A) were not observed when chlorophylls of Δ*spkB* were excited at 440 nm (Figure 22 B).

3.4.5.2 HCO_3^- dependent photosynthetic activity of Δ*spkB*

It was shown in the Δ*spkB* phospho-proteome dataset that the carboxysome structural protein CcmM was phosphorylated at S352, T358, T585, T609 and at the unspecified p-event S454-459. T358 showed a significantly lowered p-occupancy at any sampling timepoint in the mutant compared to WT (M). To elucidate if altered phosphorylation state of T358 influences the CCM and the photosynthetic activity of Δ*spkB*, O_2 evolution measurements were performed with HC and LC acclimated Δ*spkB* and WT (M) against increasing HCO_3^- concentrations under saturating light conditions (Figure 23). HC acclimated Δ*spkB* did not differ from WT (M) in HCO_3^- affinity represented by similar K_m -values and V_{max} (Figure 23 A). The same was found for LC acclimated Δ*spkB* (Figure 23 B). Hence, the changed p-event on T358 did not influence the overall CCM and photosynthetic activity of Δ*spkB*.

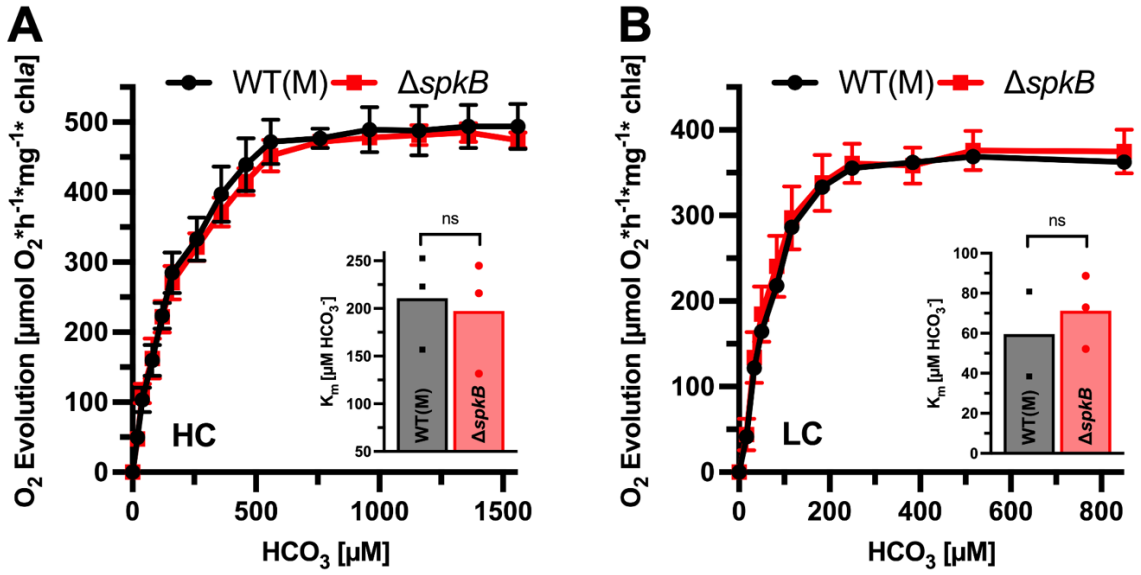

Figure 23: Photosynthetic activity of HC and LC acclimated Δ*spkB*. Photosynthetic activity of Δ*spkB* under increasing HCO_3^- concentrations and saturating light conditions. Δ*spkB* and WT (M) were either acclimated to HC (**A**) or LC (**B**). Inlets represent calculated K_m -values. (n=3 (biological), data are shown as mean values and standard errors; student's *t*-test, two-tailed, * p<0.05)

3.4.5.3 Altered P_{II} phosphorylation in Δ*spkB* under NO_3^- depletion

The canonical P_{II} protein was among the proteins which showed to be significantly dephosphorylated at position S49 after 3 h of LC acclimation in Δ*spkB* (Table 13). P_{II} phosphorylation can be easily studied in a Native-PAGE approach because each of the three identical P_{II} subunits can be phosphorylated on its S49 leading to a stepwise increase in mobility due to the increased protein charge (Forchhammer & Tandeau De Marsac, 1994). The P_{II} phosphorylation pattern was visualized with a P_{II}-specific antibody in an immunoblot assay. For this purpose, a shift experiment was performed where Δ*spkB* and WT (M) were pre-grown at LC conditions in NO_3^- containing BG11 medium, which results in the lowest P_{II} phosphorylation level (Forchhammer & Tandeau De Marsac, 1994; Schwarz et al., 2014). Subsequently, Δ*spkB* and WT (M) were deprived of NO_3^- for 2 h. Samples were taken after 20, 40, 60, and 120 min after the initial shift. The Western-blot analysis revealed that when Δ*spkB* and WT (M) are acclimated to LC conditions the P_{II} -trimer is in a non-phosphorylated state indicated by the highest single band (Figure 24). When WT (M) was deprived from its N source rapidly, each P_{II} -subunit was being phosphorylated on S49 denoted by multiple faster migrating bands. After 120 min in a N limiting environment each P_{II} unit in WT (M) is phosphorylated with only low amounts of unphosphorylated P_{II} remaining. Contrary to WT (M), Δ*spkB* showed a delayed response to NO_3^- deprivation. Like WT (M), the P_{II} trimer of Δ*spkB* started to phosphorylate after 20 min of N limitation, but even after 60 min Δ*spkB* showed only one of the P_{II} subunits to be phosphorylated compared to WT (M). Interestingly, most of P_{II} remained unphosphorylated in Δ*spkB* throughout the experiment. Strikingly, even after 120 min in a NO_3^- free environment P_{II} did not reach its fully phosphorylated state in Δ*spkB*. Hence, these experiments verified the lowered P_{II} phosphorylation in the mutant compared to WT seen in the phospho-proteome (Table 13) however, the PII protein is still phosphorylated pointing at the action of several kinases.

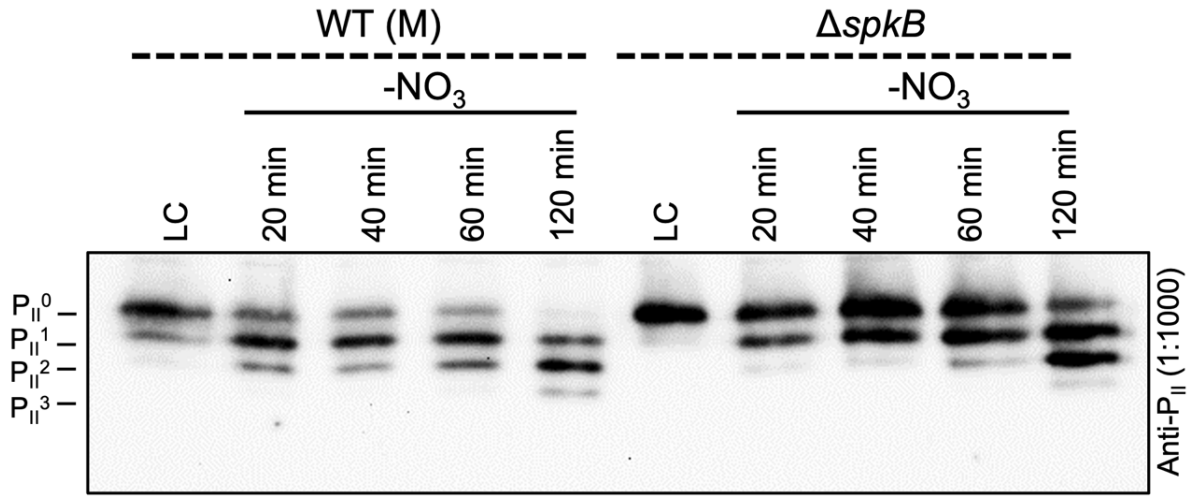

Figure 24: Analysis of P_{II} phosphorylation dynamics under NO3$^-$ depletion in Δ*spkB*. A shift experiment was performed were LC acclimated Δ*spkB* and WT (M) were deprived of NO_3^-. Samples were taken at the LC acclimated state and after 20, 40, 60 and 120 min of acclimation in a NO_3^- deprived environment. 10 µg of crude cell extract in its native state was loaded onto a 15 % Native-PAGE. Proteins were transferred to a PVDF membrane and visualized with a P_{II} antibody (1:1000). P_{II} phosphorylation status is indicated by P_{II}^0 to P_{II}^3.

3.4.5.4 NO_3^- dependent metabolic changes in Δ*spkB*

To further investigate the effects of altered P_{II} phosphorylation in LC acclimated Δ*spkB* under NO_3^- limitation, metabolome data were generated from Δ*spkB* deprived from NO_3^- for 20, 40, 60 and 120 min and subjected to LC-MS analyses. Selected metabolome data are presented as a heatmap in log_2 fold changes in relation to the WT (M) at a LC acclimated state (Figure 25). Statistical deviations from Δ*spkB* were calculated in relation to corresponding WT (M) at the same sampling timepoints. No differences in the amounts of 2OG were detected. At LC, Δ*spkB* showed significantly higher levels of 3PGA and succinic acid as well as increased quantities of Arg, Asp, Gln, His, Leu, Lys and Thr compared to WT (M). When shifted to NO_3^- free medium, significantly higher amounts of Asp, Glu as well as for the TCA cycle metabolites aconitic acid, citric/isocitric acid were recorded for Δ*spkB* for the first 40 min of deprivation. 20 min after the initial shift, reduced levels of Phe and Pro were reported for Δ*spkB*. Over the course of the entire experiment, significantly raised levels of Ala, Gln and Leu together with enriched quantities of malic acid and succinic acid were seen in the mutant at any given timepoint in NO_3^- free atmosphere. 120 min in an NO_3^- free environment was highlighted by raised concentrations of Arg, Met, Pro and Thr accompanied with an accumulation of 2PG in the mutant. Interestingly, considerably reduced amounts of pyruvic acid were seen 40 and 120 min after the shift in Δ*spkB*.

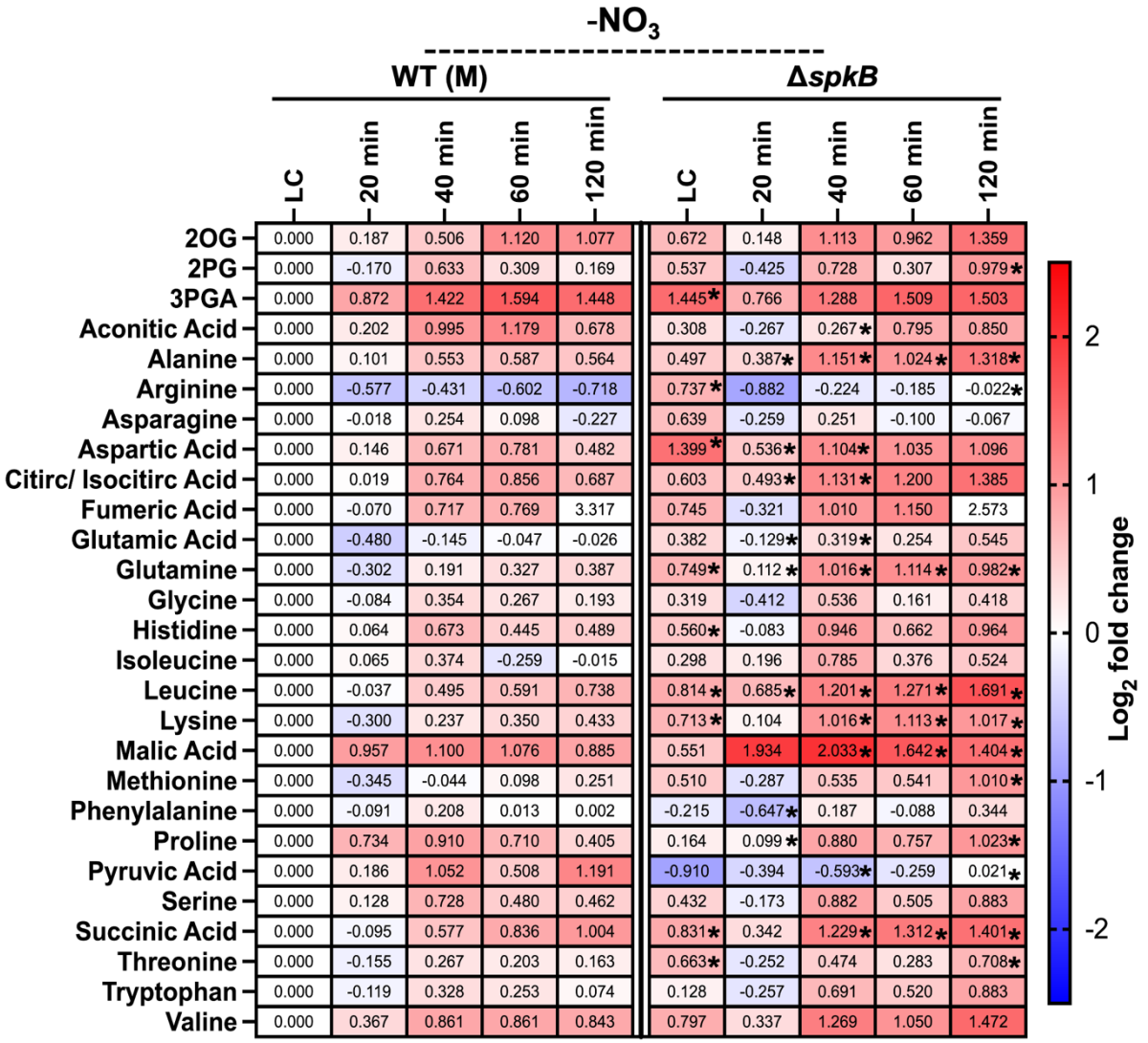

Figure 25: Metabolites of Δ*spkB* shifted to NO_3^- free environment. LC acclimated Δ*spkB* and WT (M) were shifted to NO_3^- free medium. Samples were taken at a LC acclimated state and 20, 40, 60 and 120 min after the initial shift to an NO_3^- free atmosphere. Samples were analyzed in a LC-MS approach. Data are shown as log_2 fold changes in a heat map displaying metabolic changes during the shift in relation to WT (M) in LC. Significant deviations were calculated in relation to corresponding WT (M) sampling points. (red = increased quantities, blue lowered quantities; n=4 (biological), student's *t*-test, two-tailed, * p<0.05)

3.4.5.5 Generation and genotyping of Δ*spkB* complementation

A complementation line with native *spkB* in the background of Δ*spkB* has been established to prove that the observed LC growth phenotype is based on the disruption of *slr1697* in Δ*spkB*. Therefore, native *slr1697* together with 300 bp upstream sequence, coding for the native promotor of *slr1697*, was cloned into the autonomous plasmid pVZ322 (Appendix Figure 4). The generated plasmid pTB29 (Appendix Table 2) was used to transform Δ*spkB*. gDNA was extracted from complemented Δ*spkB* (Δ*spkB*^{C}) and used for genotyping (Figure 26 A). In the first step of genotyping primers were chosen which bind within the construct and

the pVZ322 backbone resulting in an expected fragment of 2910 bp (Figure 26 A) with pTB29 serving as positive control. Further, the Δ*spkB* mutant background was confirmed by *slr1697* specific primers (Appendix Table 1) resulting in an enlarged fragment of 2900 bp in the Δ*spkB*^{c} and Δ*spkB* (Figure 26 B).

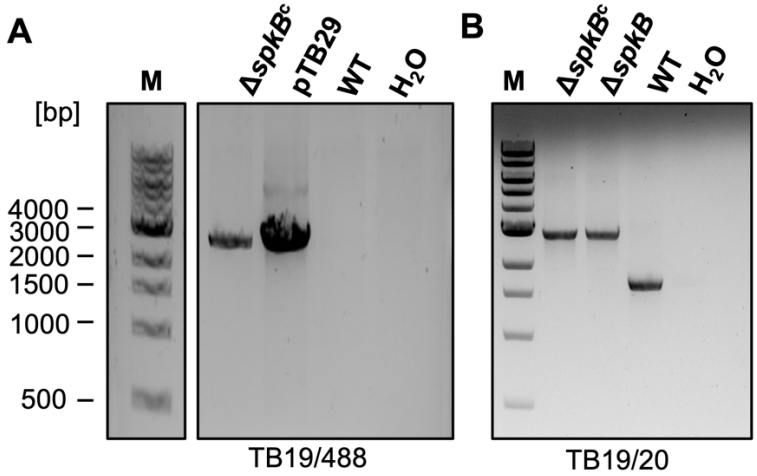

Figure 26: Genotyping of Δ*spkB*^{c}: Δ*spkB* was transformed with pTB29. Mutant colonies were picked and singled out and extracted gDNA was used for genotyping complemented Δ*spkB* (Δ*spkB*^{C}). A successful complementation was tested by performing a PCR with a combination of gene specific and pVZ322 primer resulting in a 2910 bp fragment (**A**). Further, the Δ*spkB* background of Δ*spkB*^{C} was confirmed by PCR with *slr1697* specific primer causing the amplification of a 2900 bp fragment in the mutant compared to 1725 bp in the WT (**B**).

3.4.5.6 Acclimation of Δ*spkB*^{C} to LC

HC pre-grown Δs*pkB*^{C} was shifted to LC for 4 d together with WT (M) and Δ*spkB* (Figure 27). Δs*pkB*^{C} and Δs*pkB* growth data were normalized to WT (M). The growth data indicated that Δs*pkB*^{C} restored WT (M)-like growth under LC. Further, Δs*pkB*s bleaching phenotype (Figure 16 B) was rebuilt in the complementation (Figure 27).

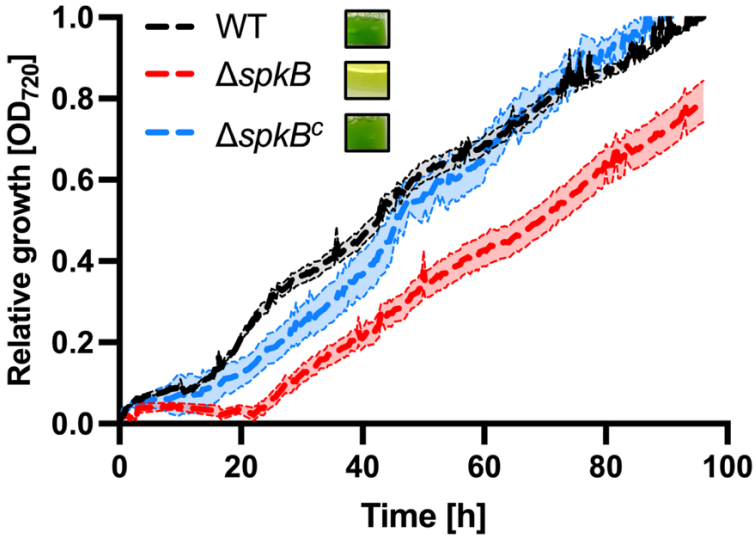

Figure 27: Acclimation of Δ*spkB*^{C} to ambient air. Δ*spkB*^{C} together with Δ*spkB* and WT (M) was pre-grown at HC and subsequently adjusted to the same starting OD720 of 0.2. Growth was monitored for 4 d at LC in a bioreactor system (Multi-Cultivator MC-1000-OD system, Photon Systems Instruments; Czech Republic). Growth data were standardized to their starting OD720 and subsequently normalized to their respective WT. Mean average growth data are visualized with their respective standard errors. Inlets represent documented pigmentation phenotypes of LC acclimated cells. (n=3 (biological))

3.4.6 Detailed analyses of Δ*spkC* acclimation to different Ci conditions

The protein kinase SpkC was found altered in its p-occupancy at T304 and T312 after a short-term LC acclimation (Table 8). Additionally, the Δ*spkC* revealed a severely affected growth when exposed to changing Ci conditions (Figure 16 C). Therefore, the *spkC* deficient mutant was selected to be analyzed in detail. Concomitantly to the global proteome and phospho-proteome study with WT (F), an analog study was conducted with Δ*spkC*. Applying the information of the Ci related proteome and phospho-proteome of Δ*spkC*, cellular glycogen levels, HCO_3^- affinity and an immunoblot analysis were conducted. Results were already partially published in Spät & Barske et al. (2021).

3.4.7 Ci dependent changes in protein abundancies in Δ*spkC*

To understand the effect of the loss of the protein kinase SpkC on a proteome level, a shift experiment was conducted with HC pre-grown Δ*spkC* shifted to LC for 3 h. Ci dependent proteome data of Δ*spkC* were analyzed in respect to WT (F) in a HC adapted state. In three replicates, 2690 proteins could be assigned. Overall abundancy changes in Δ*spkC* remained minor (Table 14). Comparing the HC acclimated states of Δ*spkC* and WT (F), it became apparent that several proteins involved with CCM are more abundant in the mutant than in the

WT i.e., SbtA, its regulator SbtB and the ROS scavenging associated protein HliC. Contrary to this, CmpB as part of the BCT1 transporter showed significantly reduced levels compared to WT (F) at the same state. Other proteins with reduced quantities under HC were the PSI subunit PsaJ and the formerly undetected Prk. After short acclimation to LC the differences between Δ*spkC* and WT (F) became more pronounced. Several proteins involved in CCM showed altered abundancies in the mutant in relation to the WT (F). Proteins assembling the BCT1 transporter such as CmpA and Slr0042 were on the one hand present in higher levels than in the WT (F) after 3 h in LC, but on the other hand CmpB and CmpC levels were reduced in Δ*spkC*. Interestingly, proteins of the NDH1-3 CO_2 hydrating complex NdhF3 and CupS were also less abundant in Δ*spkC* at 3 h of LC compared to WT (F). Flv2 levels were strongly reduced in the mutant after 3 h of LC. Glutamine synthase inactivating factors IF17 and IF7 were also altered in their quantities. HliC levels were strongly increased in Δ*spkC* kinase mutant after 3 h in LC.

Table 14: Proteins with significantly altered abundancies in Δ*spkC* in LC. Shown are fold changes (FC) of Δ*spkC* in relation to WT (F) in a HC acclimated state. Significant alterations are highlighted in bold letters. Values marked with * were quantified in less than 3 replicates. Boxes indicate an operon structure. Entire proteome data can be found in Spät & Barske et al. (2021). (FC= fold changes; n=3 (biological), student's *t*-test, two-tailed, * p<0.05)

		WT (F) [FC]	**Δ*spkC* [FC]**	
Gene	**Protein description**	**WT_{3hLC}/ WT_{HC}**	**Δ*spkC*$_{HC}$ / WT_{HC}**	**Δ*spkC*$_{3hLC}$ / WT_{HC}**
sll0217	Flv2, flavoprotein	**17.15**	1.090	**7.549**
sll0218	Hypothetical protein	12.92*	0.938	**2.732**
sll0219	Flv4, flavoprotein	**14.40**	0.804	**15.101**
sll1515	Glutamine synthetase inactivating factor IF17	**4.26**	1.523	**3.200**
sll1525	Phosphoribulokinase (Prk)	n.d.	**0.557**	**0.575**
sll1732	NdhF3, NADH dehydrogenase subunit 5 (Ndh1-3)	4.33*	2.180	**3.200**
sll1733	NdhD3, NADH dehydrogenase subunit 4 (Ndh1-3)	1.88*	0.851	1.300
sll1734	CupA, involved in low CO_2-inducible, high affinity CO_2 uptake	**4.06**	1.585	**3.190**
sll1735	CupS, involved in low CO_2-inducible, high affinity CO_2 uptake	**2.39**	1.427	**2.265**
slr0006	Unknown low CO_2-induced protein	**2.19**	0.974	**2.095**
slr0040	CmpA, bicarbonate transport substrate-binding protein	**7.31**	1.310	**11.723**
slr0041	CmpB, bicarbonate transport permease protein	**5.68**	**0.456**	**2.560**
slr0042	Probable porin; major outer membrane protein	**5.44**	1.206	**7.699**
slr0043	CmpC, bicarbonate transport ATP-binding protein	**4.08**	1.097	**2.780**
slr0044	CmpD, bicarbonate transport ATP-binding protein	**9.55**	0.931	**9.846**
slr1512	SbtA, sodium-dependent bicarbonate transporter	**5.56**	**2.935**	**4.378**
slr1513	SbtB, c-AMP-binding regulator of SbtA	**3.17**	**2.190**	**3.579**
slr2032	Hypothetical protein YCF23	**2.07**	**2.033**	**2.458**
sml0008	PsaJ, photosystem I subunit IX	1.07	**0.455**	**0.328**
ssl1633	HliC, High light-inducible CAB/ELIP/HLIP family	**7.24**	**2.924**	**14.368**
ssl1690	Hypothetical protein	**1.33**	1.309	**1.772**
ssl1911	Glutamine synthetase inactivating factor IF7	**21.57**	1.070	**23.413**

3.4.8 Ci dependent changes of protein phosphorylation in Δ*spkC*

Phospho-peptides of Δ*spkC* and WT (M) were enriched by TiO_2 metal-oxide affinity chromatography and used in an LC-MS phospho-proteome approach. Changes in p-phosphorylation was analyzed in relation to a HC acclimated WT (F). In the three biological replicates, 110 p-events could be quantified after 3 h in LC (Table 15).

Table 15: **Significantly changed p-events in Δ*spkC* in LC.** Recorded altered p-events of HC-LC shifted Δ*spkC* compared to WT (F). Significant alterations are highlighted in bold letters. p-sides marked with + were already published previously. Not detected p-events were marked with n.d. Entire phospho-proteome data can be found in Spät & Barske et al. (2021). (n=3, student's *t*-test, two-tailed, * p<0.05)

			WT (F)	**Δ*spkC***
Protein ID	**Protein description**	**p-site**	**WT_{3hLC}/WT_{HC}** phosphorylation ratio	**Δ*spkC*$_{3hLC}/WT_{HC}$** phosphorylation ratio
sll1360	DnaX, DNA polymerase III subunit gamma/tau	S1012	**22.20**	n.d.
slr0377	Unknown protein	Y97	**15.58**	n.d.
		Y100	**15.58**	n.d.
slr1048	Exonuclease subunit SbcC	T107	**8.33**	n.d.
		S109	**8.33**	n.d.
slr0322	Hik43 2-component hybrid sensor/regulator	T358	**5.79**	0.36
		T357	**4.83**	0.65
slr0737	PsaD, photosystem I subunit II	T2+	**4.93**	**5.36**
slr0599	SpkC, serine/threonine kinase	T304+	**3.32**	n.d.
		T312+	**2.84**	n.d.
sll0497	Hypothetical protein	Y119	**2.04**	n.d.
slr0148	Fed5, ferredoxin-like protein	T18+	**1.97**	0.92
		T72+	**1.83**	1.73
sll1578	CpcA, phycocyanin alpha subunit	T45+	1.25	n.d.
		Y60+	1.14	n.d.
		Y65	1.14	n.d.
sll0103	Hypothetical protein	S407	1.11	1.38
sll1742	NusG, transcription antitermination protein	S2+	0.95	0.73
sll1362	IleS, isoleucyl-tRNA synthetase	Y83	0.93	n.d.
sll0108	Amt, ammonium/methylammonium permease	T504	0.45	0.57
sll1821	RplM, 50S ribosomal protein L13	T121	0.79	n.d.
sll0982	Unknown protein, thylakoid associated	T88	0.55	0.54
sll0947	LrtA, light repressed protein A homolog	T11	0.44	1.37
slr0041	CmpB, bicarbonate transporter permease	T3	**0.26**	n.d.
slr1735	ATP-bind. subunit, basic amino acid transporter	T2	**0.24**	n.d.
slr0040	CmpA, bicarbonate transport substrate-binding	T129	**0.23**	**n.d.**
		S110+	**0.23**	**n.d.**
ssl3364	CP12 polypeptide	T54+	**0.22**	0.77
		T55	**0.13**	0.79
slr0426	FolE, GTP cyclohydrolase I	S24	**0.18**	n.d.
		T30+	**0.14**	0.32
slr6040	CopR, 2-component regulator, pSYSX copy	T228	**0.18**	n.d.
slr2075	GroES, 10 kDa chaperonin	T29+	**0.12**	0.66
ssl0707	GlnB, nitrogen regulatory protein P_{II}	T52+	**0.19**	n.d.
		S49+	**0.08**	**0.08**

Like Δ*spkC* proteome data, phosphorylation data were predominantly in line with WT (F) data (Table 15). A few p-events formerly detected in WT (F) could not be identified in Δ*spkC* after 3 h in LC. Interestingly, among the proteins with abolished p-events were the substrate binding

subunit CmpA and the permease CmpB of the BCT1 transporter as well as the DNA polymerase III subunit DnaX, which were always detected as phosphorylated proteins in each WT (F) replicate. Strongly phosphorylated Hik43 at T357 and T358 in WT (F) showed reduced p-events in the *spkC* mutant. A Similar trend could be observed for Fed5 at T18. PSI subunit PsaD showed a higher p-occupancy at T2 after 3 h of LC compared to WT (F).

3.4.8.1 HCO_3^- dependent photosynthetic activity of Δ*spkC*

The reported reduced growth of Δ*spkC* under LC condition (Figure 16 C) and the missing p-events on HCO_3^- transporter BCT1 units CmpA and CmpB (Table 15) when acclimated to LC led to the investigation of possible effects on CCM activity in the kinase mutant. For this purpose, O_2 evolution measurements with increasing HCO_3^- concentrations under saturating light conditions were performed (Figure 28). Δ*spkC* and WT (F) were cultivated under HC and subsequently put under LC for 24 h. When acclimated to HC, Δ*spkC* and WT (F) showed no significant differences in HCO_3^- affinity represented by similar K_m -values, albeit V_{max} of Δ*spkC* was lowered compared to WT (F) (Figure 28 A). When acclimated to LC for 24 h, Δ*spkC* displayed a strongly reduced V_{max} which was accompanied by a significantly higher K_m value presenting a lowered affinity towards HCO_3^- compared to WT (F) (Figure 28 B).

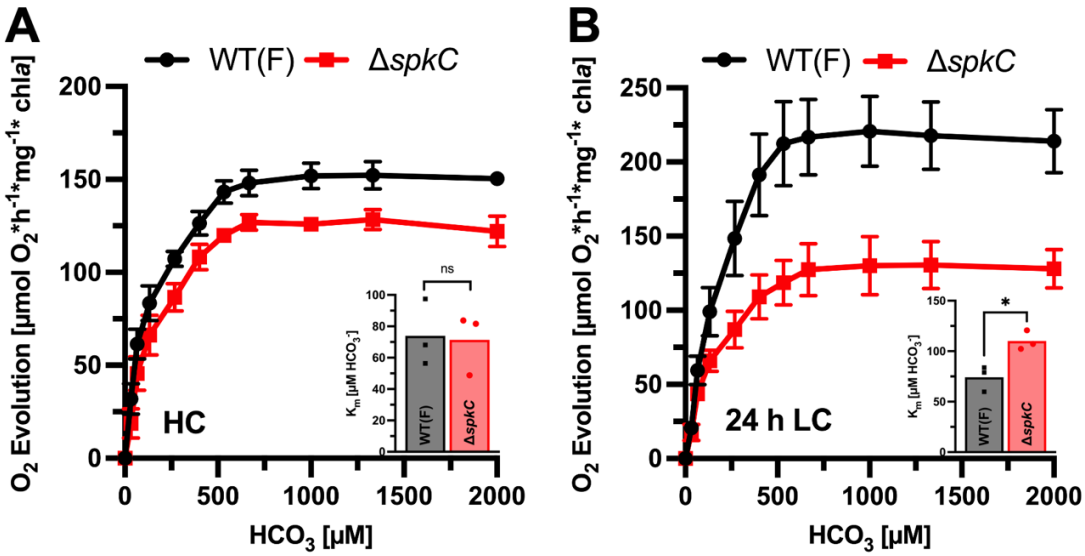

Figure 28: Photosynthetic activity of HC and LC acclimated Δ*spkC*. Photosynthetic activity of Δ*spkC* was analyzed against increasing HCO_3^- concentrations under saturating light conditions. Δ*spkC* and WT (F) were acclimated to HC (**A**) and subsequently shifted to LC (**B**) for 24 h. Inlets represent calculated K_m values. (n=3 (biological), data are shown as mean values and standard errors; student's *t*-test, two-tailed, * p<0.05)

3.4.8.2 Ci dependent cellular glycogen levels of Δ*spkC*

The documented reduced growth of Δ*spkC* when acclimating to LC (Figure 16 C) was coupled with a lowered photosynthetic activity and affinity to Ci (Figure 28 B). To see if the decreased photosynthetic activity had an influence on cellular glycogen levels, glycogen was quantified as Gluc subunits in cells shifted from HC to LC (Figure 29). Glycogen levels of Δ*spkC* did not show any significant differences to WT (F) under HC. When shifted to LC for 3 h it became apparent that Δ*spkC*s glycogen levels remained in a significantly higher quantity than in WT (F). However, after 24 h in LC, Δ*spkC* and WT (F) showed again no distinctive differences from one another.

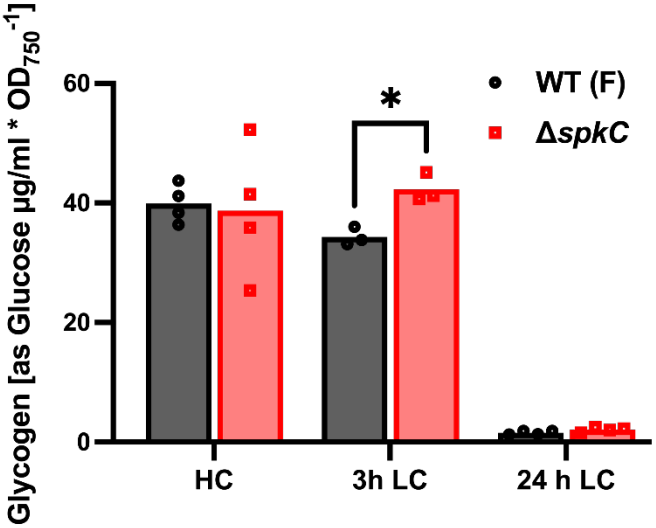

Figure 29: Cellular glycogen levels in Δ*spkC* under Ci limitation. Δ*spkC* and WT (F) were shifted from HC to LC conditions. Samples were taken at the HC acclimated state and after 3 h and 24 h of LC acclimation. Glycogen levels were quantified as Gluc monomers. (n=4 (biological), data are shown as single values with mean average; student's *t*-test, two-tailed, * p<0.05)

3.4.8.3 Quantification of cellular CmpA levels in Δ*spkC*

Seen in the proteome data (Table 14), CmpA levels were significantly increased in Δ*spkC* after 3 h in LC compared to WT (F). Total protein extracts of Δ*spkC* and WT (F) shifted from HC to LC were trialed to verify this finding by Western-blot experiments (Figure 30). Samples were taken in short intervals of 0.5, 1, 2, and 3 h of LC acclimation. Separated proteins were transferred onto a PVDF membrane and probed with an CmpA-specific antibody. The expected size of CmpA was 49.5 kDa. Strongly increased levels of CmpA, which were found in the proteome data of Δ*spkC* (Table 14), could not be verified *in vivo* in protein extracts. At any given sampling timepoint, signal intensities for CmpA did not differ from WT (F) (Figure 30).

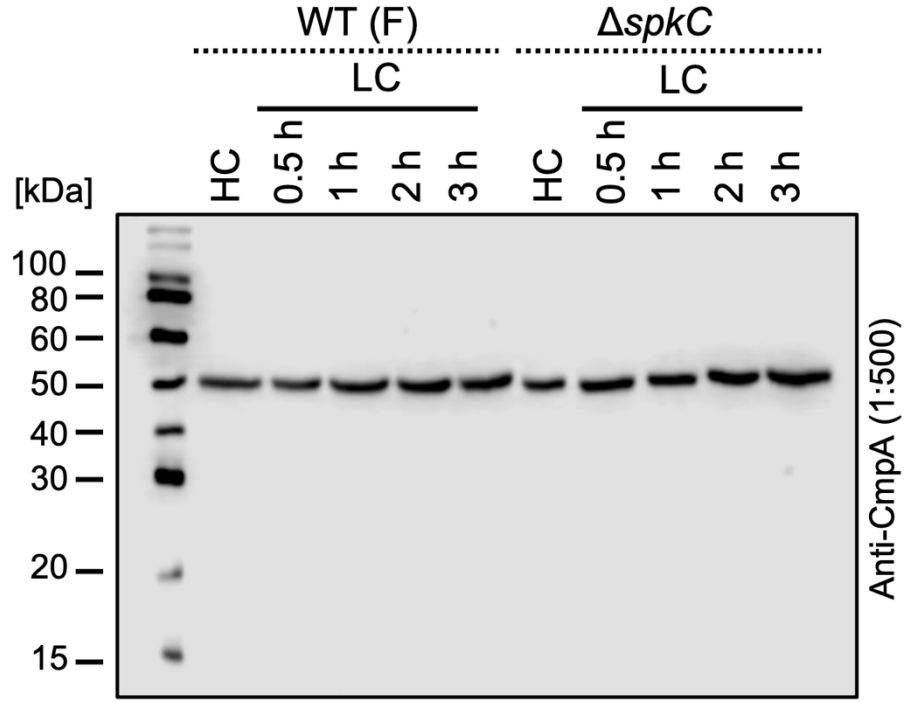

Figure 30: CmpA levels in HC LC shifted Δ*spkC*. Δ*spkC* and WT (F) were shifted from HC to LC. Samples were taken in short intervals of 0.5, 1, 2 and 3 h after the initial shift. 10 µg of total protein extracts were loaded for each sampling timepoint onto a 12 % SDS-PAGE. Separated protein were transferred to a PVDF membrane and probed with a CmpA specific antibody (1:500). Expected protein size of CmpA was 49.5 kDa. Detected proteins are visualized by black bands.

4 Discussion

This thesis aimed to elucidate the overall importance of PTM i.e., p-phosphorylation in physiological acclimation processes particularly related to changes in Ci availability in *Synechocystis*. Ci related effects on protein abundancies and p-events were documented in a global proteome and phospho-proteome study with *Synechocystis* WT (F) shifted from HC to LC conditions. Moreover, *Synechocystis* mutants for the twelve Ser/Thr protein kinases (SpkA-L) were physiologically characterized under various growth conditions. Kinase mutants Δ*spkB* and Δ*spkC* were studied in detail after displaying phenotypes with a probable relationship to Ci.

4.1 Physiological acclimation of *Synechocystis* WT to Ci limitation

A global proteome and phospho-proteome study was conducted with *Synechocystis* WT (F) shifted from HC to LC conditions. Samples were taken after short-term (3 h) and long-term (24 h) acclimation to ambient air. Documented proteome data (Table 7) were corelated with transcriptome data (Klähn et al., 2015) generated under similar growth condition and sampling timepoints. More than 2400 transcript/protein pairs could be correlated (Figure 12) confirming a meaningful relationship between transcriptome and proteome. This finding agreed with similar studies conducted under varying conditions e.g., high salinity (Klähn et al., 2021), N limitation (S. Huang et al., 2013) and fluctuating light (Mustila et al., 2021) but was in sharp contrast to analyses under phototrophic, mixotrophic and heterotrophic conditions reporting a low correlation (Toyoshima et al., 2020). Overall, quantified proteins with altered abundancies were lower than changed transcripts (Table 7, Figure 12). These discrepancies are attributed to cellular processes additional to transcript concentration in establishing expression levels of a protein i.e., translation rates, translation rate modulation, protein half-life, protein transport and increased translation of existing transcripts on demand to quickly synthesize the required proteins and, targeted degradation to speed up the removal of unneeded proteins (Y. Liu et al., 2016). Differences in the overall coverage between transcriptome and proteome could have a meaningful impact on correlating these two datasets. However, it appears critical that only datasets from similar cultivation methods and preferably the same experiments should be pulled for correlation studies due to natural deviations even under replicated cultivation conditions. Employing transcriptome and proteome data for correlation analysis from separate experiments could cause a low correlation as described in Toyoshima et al. (2020).

In this study a total number of 2577 proteins was detected in all replicates which were equivalent to about two third of the theoretical proteome

(https://www.uniprot.org/proteomes?query=synechocystis%20sp%206803). Out of this, 2284 proteins were ubiquitously identified in at least two replicates. Overall, high reproducibility and coverage was reached for all the conducted proteome analysis with WT (F) (Figure 31 A) and the mutant studies with Δ*spkB* (Figure 31 B) and Δ*spkC* (Figure 31 C) sharing more than 84% of detected peptides within their individual replicates.

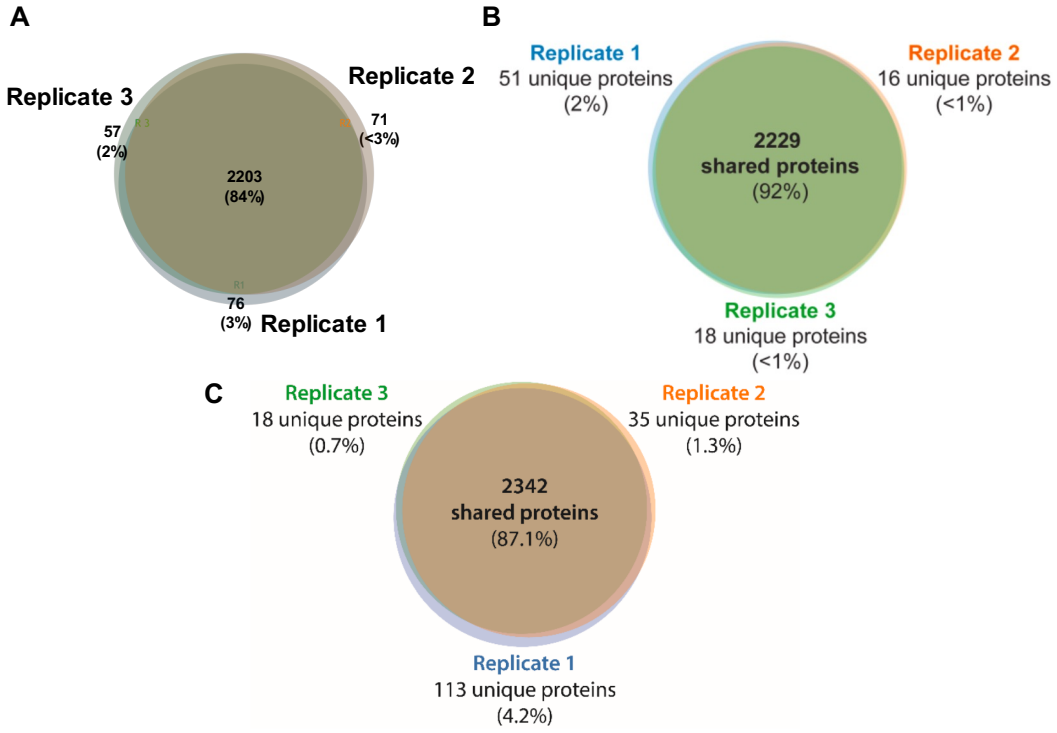

Figure 31: Proteome reproducibility within the individual proteome studies. Shared identified proteins within the individual proteome studies and respective replicates for (**A**) WT (F), (**B**) Δ*spkB*/WT (M) at HC and (**C**) Δ*spkC*/WT (F). Illustrated are the total numbers of shared proteins found in each of the experiments as percentages. (n=3 (biological); Figure **A, C** taken from Spät & Barske et al., (2021), Figure **B** taken from Barske & Spät et al., (2023).

Roughly 10% of all quantified proteins responded to changes in Ci levels. The dataset was dissected for significantly altered protein quantities in response to LC with respect to HC levels (Table 7). Many proteins significantly responding to short-term (3 h) LC conditions were proven to take part in the CCM. *Synechocystis* showed a rapid response upon sensing LC conditions highlighted by an immediate raise in low CO_2 induced transporter system levels (Figure 2) such as all subunits of the HCO_3^- ABC-type transporter BCT1 (CmpA-D, Omata et al., 1999), the Na^+ dependent HCO_3^- transporter SbtA together with its regulator SbtB (Shibata et al., 2002; Selim et al., 2018) and the components of the high affinity CO_2 hydrating complex NDH1-3 (Shibata et al., 2001) i.e., NdhF3, NdhD3, CupA and CupS to compensate for the change in the Ci atmosphere after 3 h in LC. Highest accumulations of the Ci uptake systems were reached after 24 h in LC with reaching an up to 20-fold increase in case of CmpA (BCT1)

compared to HC levels (Figure 7). It has been previously shown that the expression of these Ci uptake systems is strongly regulated by transcriptional control involving at least three transcriptional factors (Hagemann et al., 2021). This proteome data set detected four transcription factors with proven function in controlling CCM: (i) CmpR, the transcriptional regulator of the *cmp*-operon (BCT1) (Omata et al., 2001), (ii) NdhR regulating the expression of the *ndhF3* and the *sbtAB*-operon (Figge et al., 2001; H. L. Wang et al., 2004) were found in significantly higher quantities after 24 h of LC whereas, (iii) CyAbrB2 (Shalev-Malul et al., 2008; Orf, Schwarz, et al., 2016) and (iv) RbcR (Bolay et al., 2022) were found unaltered throughout the experiment. It was demonstrated that CyAbrB2 is influencing both C and N uptake in *Synechocystis* by having the capability to interact with the transcription factors NdhR and CmpR as well as NtcA, which is controlling the N uptake systems and thus, is considered to act as a supplementary factor in Ci mediated responses (Orf, Schwarz, et al., 2016). The transcription factor RbcR, which plays not only a role in the expression and regulation of RuBisCO genes, was also shown to influence transcript levels of *sbtA*, *ccmK* and the *ndhF3* operon (Bolay et al., 2022). Concluding from the proteome data increased levels of CyAbrB2 and RbcR are not needed for rapid responses in acclimation to low Ci, whereas the increased amounts of NdhR and CmpR are well contributing to the Ci dependent upregulation of the CCM particularly, Ci uptake activities.

Additional subunits associated in NDH1-3 complex assembly and stability i.e., NdhG, NdhH, NdhI, NdhJ, NdhK and NdhN (Schuller et al., 2020) were significantly enriched only after 24 h in LC, suggesting a long-term Ci triggered change in NDH1-3 complex formation (e.g., He & Mi, 2016) compared to the rapid increase of other components of the CO_2 uptake system. The remaining subunits of NDH1-3 complex (Schuller et al., 2020) were either significantly unchanged in their abundancies or were not detected. The detected subunits were mostly part of the hydrophilic arm of the NDH1-3 complex which resulted in a better overall protein extraction (He & Mi, 2016). The constitutively expressed HCO_3^- transporter BicA could not be recovered in the dataset, which is probably due to the strong membrane integration and the therefore caused insolubility (Price et al., 2004). Interestingly, no alterations were recorded for proteins assembling carboxysomes, nor subunits of RubisCO or the carboxysomal CA, even though LC grown *Synechocystis* possess a higher number of carboxysomes than HC grown (Hackenberg et al., 2012). Only the extracellular CA EcaB known to be a regulator of CCM by interacting with the NDH1-3 complex (N. Sun et al., 2019) presented elevated levels after 24 h in LC.

About 50 % of all detected proteins with significantly changed quantities under LC conditions were either proteins of unknown function or hypothetical proteins (Table 7, Spät & Barske et

al., 2021). This clarifies that the underlying mechanism of acclimation to Ci involves more than just upregulation of Ci uptake mechanisms, it demonstrates the importance of several yet to be functional described proteins and their physiological role in acclimation processes. Interestingly, many of those proteins showed a changed expression in a mutant defective in SbtB (Mantovani et al., 2022), the carbon regulator protein modulating SbtA function, and many more features related to LC acclimation (Mantovani et al., 2023). Apart from proteins assigned to the CCM, other functionally annotated proteins responded significantly to low Ci. Among these were the photoprotective flavoproteins Flv2 and Flv4 that increased their abundancies to a high extent. The unchanged Flv1 and Flv3 are known to act in a Mehler-like reaction in draining electrons from PSI and reducing O_2 to H_2O in a photoprotective manner (Helman et al., 2003; Allahverdiyeva et al., 2013). Flv2 and Flv4 show photoprotective traits at the side of PSII under LC conditions (Bersanini et al., 2014). At ambient air levels, photosynthetic electron flow is limited by its terminal acceptors due to limited CBB activities and thus, making PSII prone for photodamage that can exceed the repair capacity (Aro et al., 1993). Flv2 and Flv4 form a heterodimer that is believed to act in proper energy transfer from phycobiliproteins (PB) to PSII under LC conditions by serving as an electron sink for PSII and thereby keeping the PQ pool in an oxidized state and repressing the formation of singlet oxygen (P. Zhang et al., 2012; Bersanini et al., 2014). Recent evidence suggested that Flv2/Flv4 can also act in a Mehler-like reaction (Santana-Sanchez et al., 2019). The Flv2/Flv4 regulon is co-transcribed with the small protein Slr0218 which is thought to function as a chaperon to stabilize the PSII dimer in low Ci (P. Zhang et al., 2012). Additional photoprotective proteins were found in elevated amounts i.e., GrxC, HliB and HliC. Glutaredoxins such as GrxC are small proteins operating in scavenging of ROS (Marteyn et al., 2009; Sánchez-Riego et al., 2013). Interestingly, previous studies reported constitutively expression of GrxC under various growth conditions (Sánchez-Riego et al., 2013) giving the speculation that GrxC could have an important role under LC conditions. Here, raised protein levels for GrxC were reported after 24 h in LC albeit, correlated mRNA levels revealed a reduction in transcript (Table 7; Figure 12). The high light induced CAB/ELIP/HLIP-like proteins HliB and HliC are single-helix membrane proteins which accumulate under stress condition and are mostly associated with PSII (Sinha et al., 2012). Although their exact function remains elusive, evidence reports that CAB/ELIP/HLIP-like proteins might play a role in chlorophyll biosynthesis and could possess protective traits against oxidative damage for PSII (Havaux et al., 2003; Sinha et al., 2012). Overall, these changes strongly suggest that the transfer from HC into LC is accompanied by an oxidative stress situation, which is most likely induced due to acceptor limitation in the photosynthetic electron transport chain leading to the production of ROS. In contrast to proteins involved in redox regulation, only few changes in proteins associated with the core PSII and PSI were detected. Increased protein quantities were only documented for the PSII

and PSI subunits PsbY and PsaJ after 24 h in Ci limitation which could indicate a possible role in restructuring the PSII/I to accommodate for the changed conditions (Meetam et al., 1992; Xu et al., 1994; Kruip et al., 1997). However, their respective role in the PSII/I remains unknown. The non-catalytically active WD-repeat proteins Slr1409 and Slr1410 accumulated after 24 h in ambient air. WD-repeat proteins are a diverse group of proteins which are unified by a strictly conserved structural organization but are nevertheless mostly with undefined functions although, metabolic regulation has been suggested for this family of proteins by protein-protein interactions (Hisbergues, 2001). The WD-repeat protein Hat has been shown to be involved in the control of high affinity Ci transport under Ci limiting conditions, giving rise to the idea that Slr1409 and Slr1410 could be further player in that adjustment processes.

In agreement with previous transcriptomic studies under low Ci (Klähn et al., 2015; Orf et al., 2015) almost no changes in the abundancy of catalytic enzymes inside the primary C and N metabolism were found, except for the succinate-semialdehyde dehydrogenase GapD which was highlighted by increased levels after 24 h in LC. GapD is part of the γ-aminobutyric acid shunts which closes the TCA cycle (Figure 4) (Xiong et al., 2014). Together with the GS inactivating factors IF7 and IF17, which were among the strongest accumulated proteins in ambient air, indicated that adjustment of N assimilation is necessary in LC. IF7 and IF17 decrease the activity of the ammonia assimilating enzyme GS (Garci´a et al., 1999). The increased levels of GapD, IF7 and IF17 contribute to the overall adjustment of C/N balance in Ci deprived cells by inactivating GS and bypassing GS-GOGAT cycle and closing the TCA cycle through the γ-aminobutyric acid shunts (Garci´a et al., 1999; Xiong et al., 2014).

4.1.1 Changes in phosphorylation events in *Synechocystis* WT under Ci limitation

Ci related changes in p-events were analyzed in a global phospho-proteomics approach with *Synechocystis* WT (F) (Table 8, Spät & Barske et al., 2021). In this study a total of 200 p-events was characterized on 105 proteins. Across all conducted phospho-proteome studies under various conditions (Mikkat et al., 2014; Spät et al., 2015; Z. Chen et al., 2015; Angeleri et al., 2016; Toyoshima et al., 2020) a total number of approx. 500 p-proteins (Appendix Table 3) has been identified in *Synechocystis*, which is in sharp contrast to the only twelve annotated Ser/Thr protein kinases (SpkA-L) (C.-C. Zhang et al., 1998; Leonard et al., 1998; Shi et al., 1998). However, this occurrence is also true for other bacteria e.g., *E. coli* (Macek et al., 2008), *B. subtilis* (Macek et al., 2007) or the marine cyanobacterium *Synechococcus* sp. PCC7002 (Yang et al., 2013). This discrepancy indicates that besides kinase mediated phosphorylation, adjuvant forms of phosphorylation are occurring. Non-enzymatic p-phosphorylation has been shown for the metabolic enzymes PGM1 (Sll0726) and PGM2 (Slr1334) which acquire their

phosphate group from their substrates i.e., phosphorylated sugars such as glucose-1,6-bisphosphate and fructose1,6-bisphiosphate respectively (Doello et al., 2022; Neumann et al., 2022). This mode of non-enzymatic phosphorylation is also plausible for other metabolic enzymes. Additionally, the importance of non-enzymatic acetyl phosphate dependent phosphorylation was highlighted in the bacteria *Streptococcus pneumoniae* (Kaiser et al., 2020) and *B. subtilis* (Cairns et al., 2015) and could potentially contribute to overall p-events in *Synechocystis*, because a homologue to the acetyl phosphate forming enzyme AckA, Sll1299 (https://www.uniprot.org/uniprotkb/P73162/entry), was also found in *Synechocystis*. Strict protein kinase substrate specificity is a matter of debate. It was proposed that bacterial protein kinases have a rather relaxed substrate specificity (Kobir et al., 2011), which is further supported by the observation of multiple kinases involved in the phosphorylation of GroES (A. Zorina et al., 2011). Typically, protein kinase recognition sides consist of only one to three residues critical for efficient phosphorylation, therefore potential matching motifs are widespread in the proteome (Kobe et al., 2005; Miller & Turk, 2018). In the phospho-proteome analysis conducted in this thesis (Table 8, Spät & Barske et al., 2021; Barske & Spät et al., 2023) and in previously published studies (e.g., Spät et al., 2015, 2018) protein kinases were among the proteins with altered p-events under fluctuating conditions, which in turn could impact their specificity. It also needs to be considered, if we have a complete picture of Ser/Thr protein kinases in *Synechocystis*. Many bacterial Ser/Thr protein kinases resemble Hanks-type kinases which is also true for *Synechocystis* (C.-C. Zhang et al., 1998; Leonard et al., 1998; Shi et al., 1998) however, there is a chance of evolutionary unrelated protein kinases such as the isocitrate dehydrogenase kinase/phosphatase found in *E. coli* (Zheng & Jia, 2010).

Out of the 200 p-events charactered in *Synechocystis*, amongst 74 novel p-event (Spät & Barske et. al., 2021), 35 p-events on 24 proteins showed a significant alteration in p-occupancy in response to LC conditions (Table 8). 13 p-events after 3 h and 24 p-events after 24 h of growth under ambient air were highlighted by a significant increase in p-phosphorylation whereas 12 p-events after 3 h and 6 p-events after 24 h in LC displayed a significant decrease in phosphorylation levels. Among the found p-proteins, many p-sides were previously unidentified. Yet, the overall reproducibility of p-events remained low throughout the experiment with only 13 % of detected p-events were shared across the replicates (Figure 32 A). Low reproducibility was observed also for phospho-proteome studies conducted with the kinase mutants Δ*spkB* (Figure 32 B) and Δ*spkC* (Figure 32 C), showing only 50 % and 23.8 % overlap of p-events between their replicates, respectively.

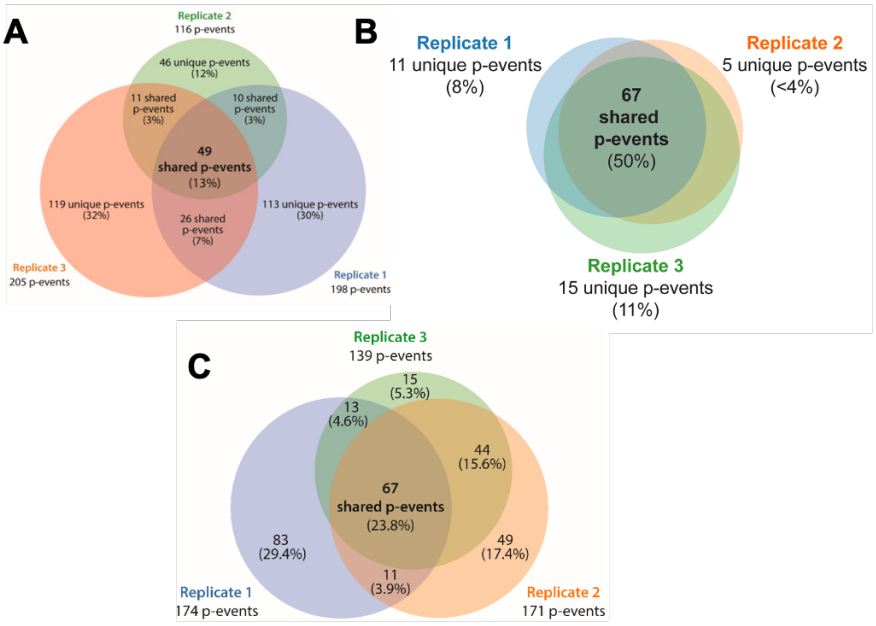

Figure 32: Reproducibility of identified p-events between independent replicates. Identified p-events shared across individual replicates, illustrated for the total number of p-events found in the experiment with WT (F) (**A**) and the kinase mutant Δ*spkC* (**C**). p-events characterized in Δ*spkB* at 3 h LC were compared (**B**). Percentages are relative to the overall identified p-events. (n=3 (biological); Figure **A, C** were taken from Spät & Barske et al. (2021), Figure **B** was taken from Barske & Spät et al. (2023).

Even though, phospho-proteomic analyzes are carried out on a routine basis, technical limitations are still faced i.e., the analysis of low abundant proteins, low stoichiometry of the p-event, potentially impaired digestion efficiency, phosphorylated peptides lost during preparation and enrichment by chromatography, impaired ionization of phosphorylated peptides, peculiar behavior of unstable phosphate groups upon collision induced dissociation and the correct localization of a p-event on a peptide impacts the reproducibility of p-events (Solari et al., 2015). Additionally, the experimental set up and sample preparation steps prior to LC-MS can drastically influence the phospho-proteome outcome e.g., Mertins et al. (2014) reported a relative high stability of the general proteome after sampling however, up to 24% of the phospho-proteome showed rapid changes in p-events. Given the fact of the analyses of three biological replicates and the hereto related natural biological and technical variances, a low reproducibility is not beyond the expected.

The highest overall phosphorylation frequency was observed for PB with 13 p-events alone for CpcA. Among these T45, Y60 and T65 of CpcA presented an increase in p-occupancy after 24 h in LC. Extensive phosphorylation of PB has been previously reported in earlier phospho-proteome studies under N starvation and under different Ci acclimation states (Spät

et al., 2015; Angeleri et al., 2016), however their potential role in light absorption and photosynthetic energy transfer remains to be defined, albeit the evidence of p-phosphorylation in structural and functional processes in PB (Mann, 1994; Z. Chen et al., 2015). But due to the frequent occurrence of p-events on PB an important regulatory function is indicated. The hypothetical protein Sll0103 presented an additional protein to be strongly phosphorylated at nine different sides, among S407 which revealed increased phosphorylation level after 24 h in LC. Protein sequence alignment of Sll0103 recognized a strong similarity to a 'van Willebrand' factor type A domain (vWF; Edwards & Perkins, 1995), which are known to be involved in protein/protein interactions and complex formations (e.g., Peetermans et al., 2020). Rising phosphorylation levels on T349 and T361 of Sll0103 were additionally observed under N starvation (Spät et al., 2015). The demonstrated altered p-events of Sll0103 under Ci and N limitation could indicate a distinctive role of Sll0103 in regulating C and N metabolism in *Synechocystis* but with specific interaction partners yet to be discovered.

Serval proteins with altered phosphorylation levels in response to changed Ci levels can be functionally grouped to DNA replication, transcription and translation processes. A 22-fold increase in p-occupancy was recorded for S1020 of the major DNA polymerase in bacteria, DNA polymerase III subunit DnaX after 3 h in LC which is thought to be important for the fidelity and speed of the entire polymerase complex (Fijalkowska et al., 2012). The DnaX gene codes for two different protein isoforms, the C-terminally truncated γ-subunit and the full-length isoform subunit τ, which is harboring the recorded altered p-side S1020 (Fijalkowska et al., 2012). This indicated a possible role of the phosphorylated DnaX protein in overall control of the fidelity of DNA replication in response to changes in Ci levels. SbcC, required for the completion of DNA replication (Wendel et al., 2017), showed significantly enhanced phosphorylation at T107 and S109 after 3 h in ambient air. Thus, the need of adjustment of DNA replication fidelity under LC conditions seems reasonable due the reported stall of growth in LC-shifted *Synechocystis* highlighted by reduced DNA contents and cell diameters compared to HC adapted cells (Gärtner et al., 2019). Additionally, several proteins involved in protein biosynthesis processes responded to changed Ci conditions. NusG, acting as anti-termination factor for modulating the RNA polymerase activity (Mandell et al., 2021) could be characterized with a 9-fold increase in phosphorylation at S2 after 24 h in LC. Likewise, the isoleucyl t-RNA synthase Iles catalyzing aminoacylation of t-RNA by their cognate amino acid (Kermgard et al., 2017) was recorded with an elevated p-event at Y83 24 h after the shift to ambient air. On the contrary, the phosphorylation at T121 of 50s ribosomal protein L13 RpmlM (Aseev et al., 2016) was reduced after 24 h LC. Moreover, the CheA-like RR involved in cell motility (Yoshihara et al., 2002) presented increased p-levels at T357 and T358 after short acclimation of 3 h in LC whereas the CopR RR of the CopRS TCS involved in copper

resistance (Giner-Lamia et al., 2020) showed significantly reduced p-events at T228 at any timepoint in LC. Combined, this data suggest that p-phosphorylation may be a crucial checkpoint in regulating protein biosynthesis related proteins and thereby, playing a vital role in acclimating protein quantities in reaction to changing environmental conditions such as altered Ci availability.

Among other p-proteins which showed altered p-events under changing Ci conditions was the regulatory P_{II} protein. Besides the canonical S49 (Forchhammer & Selim, 2019), T52 showed significantly lowered p-occupancy after 3 h in LC. S49 is located at the tip of the large flexible T-loop that promotes interaction with several P_{II} interactors (Forchhammer & Selim, 2019). Loss of the S49 p-event is accompanied with altered regulatory functions of P_{II}, whereas no physiological function has yet been associated to the recently observed T52 p-event. Various experiments already confirmed P_{II} dephosphorylation in ambient air and increased p-levels under N-starvation by detecting the different P_{II} proteo-forms in an immunoblotting approach under native condition (e.g., Schwarz et al., 2014; Spät et al., 2015; Figure 24). By binding 2OG, ATP and ADP, P_{II} can integrate information about the C/N balance and the energy state of the cell and adjust C and N fluxes accordingly (Forchhammer & Selim, 2019). Furthermore, it could recently be revealed that P_{II} regulates phosphoenolpyruvate carboxylase (PEPC) activity in *Synechocystis* (Scholl et al., 2020), which catalyzes the formation of oxaloacetate (OAA) by incorporating HCO_3^- and therefore acting as an additional Ci fixing enzyme. The P_{II} target protein Amt1 was characterized with an increased p-event at T504 after 24 h in LC. Amt1 is mainly responsible for ammonium uptake (Montesinos et al., 1998), but ammonium uptake needs to be adjusted accordingly to avoid toxic accumulation (Watzer et al., 2019). Moreover, P_{II} regulates the flux out of the CBB through its interaction with the small protein PirC (Orthwein et al., 2021).

Another important small regulatory protein, the intrinsically disordered protein CP12 was detected as a p-protein. Interestingly, CP12 was found to be significantly less phosphorylated at T54 and T55 after 3 h in ambient air. Under oxidative conditions such as diurnal light/dark cycles, CP12 binds phosphoglyceraldehyde dehydrogenase 2 (GapDH2) and phosphoribulokinase (PRK) and thereby inactivating the CBB cycle, again releasing GapDH2 and PRK under reductive conditions in the light (Wedel & Soll, 1998; McFarlane et al., 2019). This view was recently expanded by CP12 also being involved in fine-tuning the CBB cycle activity under different light and concomitant redox conditions in *Synechocystis* (Lucius et al., 2022). However, T54 and the neighboring T52 were in addition found to be stronger phosphorylated under conditions of resuscitation form N starvation (Spät et al., 2018), a condition that also has a strong impact on the C/N ratio. Though, the detected p-events are

located in the central part of CP12, between the N-terminal PRK-binding and C-terminal GapDH2-binding domain, they remain accessible for kinase activity (McFarlane et al., 2019). Though, the physiological relevance of the phosphorylation sides is not known, one could speculate about their potential significance in responding towards changing Ci and N levels and accompanied redox changes in *Synechocystis*.

One of the initial hypotheses was that enzymes involved in the primary C and N metabolism are regulated in their activities due to differential p-phosphorylation. The phospho-proteome datasets of WT (F), Δ*spkB* and Δ*spkC* (Table 8, 13; 15) revealed the phosphorylation of the following metabolic enzymes i.e., FbaA (Sll0018), Pgm1 (Slr1945), Gnd (Sll0329), GapDH 2 (Sll1342) and FbpI (Slr2094) (Spät & Barske et. al., 2021, Barske & Spät et al., 2023), but none of them showed significant changed p-events during the HC to LC shift. Further, additional metabolic enzymes such as PgmII (Slr1334), PgI (Slr1349), FbpII (Slr0952) and Eno (Slr0752) were described to be p-proteins (Mikkat et al., 2014) but were not detected throughout the conducted studies. Low protein abundancy of metabolic enzymes and low stoichiometry of those respective p-events could be a plausible reason that p-events and alterations on p-events could not be detected on catalytic proteins inside the central metabolism.

Strikingly, two subunits of the low CO_2 induced HCO_3 transporter BCT1 were characterized with altered p-events in a Ci limited atmosphere i.e., reduced p-occupancy at T129 and S110 of the HCO_3^- binding subunit CmpA and lowered p-levels of the permease subunit CmpB at T3 after 3 h which in turn increased again after 24 h of LC acclimation (Table 8). Though, all subunits of BCT1 presented strongly increasing abundancies after the shift to ambient air (Table 7), the reduced phosphorylation frequencies can be attributed to the *de novo* synthesis and the yet to be modified proteins. The phosphorylation abundance of CmpA and CmpB p-sides are increasing after 24 h in LC suggesting kinase activity on these residues. Reports revealed that HCO_3^- uptake was stimulated after short-term exposure to LC and that rapid induction could be inhibited by protein kinase inhibitors (Sültemeyer et al., 1998; Amoroso et al., 2003). Hence, these data suggest that the rapid change in p-occupancy in the detected p-events on CmpA and CmpB could have a regulatory function in BCT1 transport activity and could impact the overall change in the metabolic signature in LC-shifted cells.

Protein kinases usually show autophosphorylation at their activation domains therefore, phosphorylated kinases are expected. Interestingly, among the low Ci responding proteins the p-sides T304 and T312 of the protein kinase SpkC reported a higher phosphorylation frequency after 3 h in LC, which may be correlating with observed reduced growth of Δ*spkC*

in LC (Figure 16 C). SpkC has been previously characterized with four reduced p-events under N limitation, amongst was low Ci responding phosphorylation side T312 (Spät et al., 2015). SpkC was categorized as an integral protein in the plasma membrane (Liberton et al., 2016) but a specific target is yet to be assigned. Reports suggested that SpkC could likely phosphorylate chaperonin GroES in a cascade together with SpkF and SpkK (A. Zorina et al., 2011). However, our data rather suggest that SpkC could be involved in the phosphorylation of the BCT1 transporter (see below). SpkF was also found to be phosphorylated in the generated dataset but with unaltered p-events under fluctuating Ci levels. Interestingly, GroES was found to a lesser extent phosphorylated at T29 after 24 h LC. If SpkC is indeed phosphorylating GroES, the results imply that the increased phosphorylation of SpkC would reduce its activity which is in turn indicated by reduced phosphorylation levels of GroES under LC, albeit the potential roles of SpkF and SpkK in GroES phosphorylation cannot be rules out. The ferredoxin like protein Fed5 was additionally found with enhanced p-events at T18 and T72 after 3 h in LC. Reports showed that the protein kinase SpkG, which is situated in the same operon *slr0142-slr0152* as Fed5, is involved in the phosphorylation of Fed5 (Angeleri et al., 2018). SpkG was found amongst the characterized p-proteins but with unchanged p-events after the shift to LC conditions.

4.2 The role of Ser/Thr protein kinases in acclimation processes

Twelve Ser/Thr protein kinases are annotated in the genome of *Synechocystis* (Cyanobase; http://genome.microbedb.jp/cyanobase/GCA_000009725.1). According to protein sequence alignments, the protein kinase SpkA-G share a strong resemblance to Hanks-type protein kinases whereas SpkH-L are classified as atypical protein kinases of the ABC1-type (Table 9) (C.-C. Zhang et al., 1998; Leonard et al., 1998; Shi et al., 1998). To understand their relevance in acclimatation responses towards changing environmental conditions, knockout mutants for the kinase encoding genes were generated (Table 1). The kinase deficient mutants (Δ*spkA-L*) were physiologically characterized.

4.2.1 Establishing of a Δ*spk* mutant collection

The kinase mutants Δ*spkA,* Δ*spkB,* Δ*spkE* and Δ*spkG* were generated in WT (M) (Table 1) by the group of Prof. Dr. Sylvie Bédu at the Aix-Marseille Université. Prior to the analysis of those Δ*spk*s, the cloning strategy and their segregation status was confirmed by PCR and DNA sequencing (Appendix Figure 1; Figure 13). Sequencing results indicated that the mutations *spkA, spkB, spkE* and *spkG* were initiated by employing naturally occurring exonuclease cutting sides (Appendix Figure 1) and thereby disrupting the DNA coding

sequence of *spkA* and *spkE* and by enlarging the sequence of *spkB* through the insertion of a Km^R and a Sp^R into *spkG*. Successful segregation of Δ*spkA,* Δ*spkB,* Δ*spkE* and Δ*spkG* was confirmed in a PCR approach with gene specific primer (Figure 13).

Mutation constructs for *spkC-D* and *spkH-L* were newly generated (Appendix Table 2). *In silico* sequence analysis of the GOI exposed suitable naturally existing exonuclease cutting sides. Cutting sides were chosen to remove as much coding sequence as possible from the targeted GOI (Appendix Figure 2). Fully segregated genes were found for Δ*spkC-D* and Δ*spkI-L* (Figure 14). However, even after multiple attempts Δ*spkH* could not be segregated for the mutated gene construct (Figure 14 D). Thus, unable to segregate Δ*spkH* the idea arose that SpkH might be essential for the applied growth conditions. Nevertheless, earlier studies reported successful segregation for Δ*spkH* under similar growth conditions (A. Zorina et al., 2011). Evaluating the mutation strategy of the successfully segregated Δ*spkH*, it became apparent that the reading frame of *sll0005* was interrupted by the insertion of a Sp^R between the naturally occurring cutting sides of *Nco*I. The mutation disrupted a third of the putative kinase catalytic domain (https://genome.microbedb.jp/cyanobase/GCA_000009725.1/genes/sll0005) compared to complete deletion of the kinase domain in the mutation attempted in this study (Appendix Figure 2; Figure 14 D). Hence, it might be possible that a Sll0005 protein with residual kinase activity was still be translated and allowed for a successful segregation as seen in A. Zorina et al. (2011). Interestingly *spkH* is not transcribed in an operon manner (Table 9; Kopf et al., 2014). This further underlined the idea that SpkH could be essential for photoautotrophic growth under LC and HC conditions, because polar effects on neighboring genes in an operon structure could be ruled out. SpkH remains an attractive candidate for future studies. For further experiments new approaches in analyzing this kinase should be followed e.g., instead of disrupting *spkH*, an overexpression construct could be used that potentially enhances the physiological impact of SpkH in *Synechocystis*. Alternatively, a gene knock-out of *spkH* could be attempted by either using a CRISPR/Cas silencing approach or by employing a rhamnose-inducible expression system (Kelly et al., 2018).

4.2.2 Physiological characterization of Δ*spk* mutants

Prior to physiological experiments, RNA-Seq data generated under different growth condition were examined for expression changes of *spk* genes (Figure 15; Kopf et al., (2014); http://cyanoexpress.sysbiolab.eu/). The overall documented transcript levels remained almost unaltered under most tested condition. However, the protein kinases *spkC, spkD, spkE, spkG, spkI, spkJ* and *spkK* responded with reduced transcript levels to darkness. The shift from light to darkness is concomitantly followed by drastic changes in glycolytic routes in the primary C

metabolism, switching from a photoautotrophic to a heterotrophic lifestyle (Pelroy & Bassham, 1972; Takahashi et al., 2008). This finding could indicate a yet to be defined role in photoautotrophic growth for the responding protein kinases. Further, *spkC* presented reduced transcript levels in the stationary growth phase (Figure 15). In the presented data, stationary growth phase was reached by growing a high-density culture (Kopf et al., 2014). A high-density culture is commonly accompanied with a low light transmittance through the *Synechocystis* suspension, which in turn can impose similar effects like darkness. However, *spkC* is the only protein kinase transcript strongly impacted by this condition. This finding underlines a potential role of *spkC* in the primary metabolism. Further, several protein kinase genes were found in higher quantities after a cold-shock treatment. Among them were *spkC*, *spkF* and *spkK* which were shown to be involved in the phosphorylation of the heat-shock protein GroES (A. Zorina et al., 2011). Interestingly, no drastic changes in transcript amounts were reported under Ci limitation. This result agrees with other transcriptome studies under shift condition from HC to LC (e.g., Klähn et al., 2015; Orf et al., 2015). Furthermore, Spk protein level remained unaffected when acclimating to ambient air (Table 7; Spät & Barske et al., 2021). Collectively, the protein kinase genes *spkA-L* are likely constitutively expressed in the majority of evaluated environmental conditions.

The generated protein kinase deficient mutants Δ*spkA-L* were physiologically characterized under various environmental conditions (Figure 16, 17, 18, 19). Initially, we focused on their ability to acclimate to changing Ci levels. Alongside growth (Figure 16), pigment composition (Table 10) was documented. Out of the eleven examined protein kinase mutants, Δ*spkB,* Δ*spkC,* Δ*spkG,* Δ*spkI,* Δ*spkJ,* Δ*spkK and* Δ*spkL* showed significantly reduced overall growth at the end of the monitored period in relation to their respective WT when acclimating to ambient air levels (Figure 16 B, C, G, H, I, J, K). While the growth deviation remained minor for Δ*spkJ* and Δ*spkL* (Figure 16 I, K), reduction for Δ*spkB,* Δ*spkC,* Δ*spkG,* Δ*spkI* and Δ*spkK* (Figure 16 B, C, G, H, J) were more pronounced with reaching only roughly 75% of the relative final culture density of their respective WT. The greatest impact on photoautotrophic growth was presented by Δ*spkI* with a reported reduction of 50% respectively to its WT in LC (Figure 16 H). In case of Δ*spkB*, Δ*spkG* and Δ*spkD* the LC acclimation period was accompanied with a yellowish pigmentation phenotype (Figure 16 B, G, D). The bleaching phenotype of Δ*spkB* (Figure 16 B) was caused by significantly reduced Chl*a* levels (Table 10) in LC. Glu is the precursor molecule for Chl*a* synthesis (Cornah et al., 2003; Vavilin & Vermaas, 2007). Combined with the general growth reduction in LC, a C allocation defect could be caused by the mutation of *spkB.* Deviations in Glu levels were documented for Δ*spkB* under HC-LC shifting conditions (Figure 21) however, LC steady-state Glu amounts (Figure 21) were only slightly reduced. Similar, Δ*spkG* presented lowered phycocyanin levels when acclimating to

ambient air (Table 10). Phycobilin and chlorophyll synthesis is branching out from Glu (Mills et al., 2020). *spkG* is part of the PSII assembly protein (Pap) operon, which is not essential for photosynthetic growth but expresses proteins with putative bilin binding domains (Wegener et al., 2008). Thus, polar effects on the Pap operon expression caused by the mutation of *spkG* cannot be ruled out. An earlier study reported a high sensitivity of Δ*spkD* towards low Ci (Laurent et al., 2008) however, this phenotype could not be confirmed in this study. Nevertheless, the proposed role in adjusting the TCA metabolite is still open for debate as indicated by altered pigment composition under HC (Table 10). Δ*spkI* presented the strongest growth reduction in low Ci acclimation (Figure 16 H), without a visually noticeable change in pigmentation (Table 10). However, pigment quantification revealed significantly increased level of Chl*a*, phycocyanin and carotenoids under HC as well as significantly reduced amounts of the former in LC (Table 10). *spkI* is found in the same TU with *pphA*, upstream of the P_{II} phosphatase (Irmler & Forchhammer, 2001). Modifying *spkI* could have posed polar effects on *pphA*, even though it was indicated that *pphA* is independently transcribed from *spkI* (Irmler & Forchhammer, 2001; Kopf et al., 2014). The Δ*pphA* mutant did not exhibit growth reduction under laboratory conditions (Irmler & Forchhammer, 2001), yet an effect on P_{II} phosphorylation levels and subsequent influence on C/N homeostasis needs to be considered. The other gene products co-transcribed with *spkI* (*sll1769, ssl3383, ssl3383;* Kopf et al., 2014) are classified as hypothetical proteins. Future studies need to investigate, if the reported growth phenotype (Figure 16 H) is solely based on the loss of *spkI* or related to the disruption of the TU (Table 9).

Further, protein kinase mutants Δ*spkA-L* were evaluated under photo-mixotrophic growth in continuous light condition (Figure 17; 18 A), where 10 mM Gluc was supplemented. In liquid culture all Δ*spk* were able to utilize the supplied Gluc (Figure 17). However, growth of Δ*spkB* plateaued already after 48 h (Figure 17 A). The WT (M)-like growth of Δ*spkB* in the beginning of the experiments, indicated that Gluc uptake was not impaired in the mutant, but effects could be likely the results of a time related metabolite accumulation. It was demonstrated that the ED pathway is the favored glycolytic route under photo-mixotrophic condition because it not sharing enzymes participating in the CBB cycle (X. Chen et al., 2016). However, recent metabolite flux studies under photo-mixotrophic conditions showed an increased mobilization of Gluc through the PGI (glucose-6-phosphate isomerase) and OPP shunt to replenish the CBB cycle, while no flux through the ED pathway was measured (Muth-Pawlak et al., 2022; Schulze et al., 2022). Moreover, PGI was characterized as a phospho-protein (Mikkat et al., 2014). Taken together, this result further indicated a potential regulatory role of SpkB in coordinating C allocation in *Synechocystis*. Surprisingly, results of similar experiments on solid BG11 medium supplemented with 10 mM Gluc differed from the ones in liquid culture

(Comparison Figure 17 and 18 A). Instead of enhanced growth, all *Synechocystis* strains presented reduced growth in comparison to control conditions (Figure 18 A). The experimental setup differed in the applied light quantity with 35 µmol photons m^{-2} s^{-1} (Figure 17) used in liquid culture compared to normal light condition of 100 µmol photons m^{-2} s^{-1} on solid media plates (Figure 18 A). Reports indicated that photosynthetic rates drop under prolonged photo-mixotrophic conditions with only residual PSII activity remaining (Solymosi et al., 2020), which could have causes an overreduction of the photosynthetic chain under 100 µmol photons m^{-2} s^{-1}. If the NADPH sink capacity of the CBB is saturated, the photosynthetic electron transfer chain may became overly reduced and could in turn promoted the formation of ROS, which severely damaged *Synechocystis* and could be a possible explanation of the observed growth reduction (Figure 18 A; Nikkanen et al., 2021). Furthermore, growth was monitored under fluctuating light settings in a 12 h/ 12h day and night cycle (Figure 18 B), which revealed that Δ*spkA-L* were tolerating diurnal conditions. With the addition of 10 mM Gluc, Δ*spkB* presented again reduced growth in comparison to the controls, further underlying the idea that SpkB is acting in C allocation. Intriguingly, Δ*spkE* was characterized with strongly diminished growing under diurnal condition in the presence of Gluc (Figure 18 B). Though, Δ*spkE* depicting a WT (M)-like phenotype under control condition in diurnal cycles (Figure 18 B) and under continues light in the presence of Gluc (Figure Figure 17; 18 A), issues in C mobilization can be ruled out. During the night the OPP cycle becomes the primary glycolytic route (Pelroy & Bassham, 1972; Takahashi et al., 2008). An overly active OPP cycle during the day could have created futile effects on Δ*spkE* growth by running CBB and OPP in parallel. Thus, one could suggest a probable role of SpkE in directing glycolytic fluxes in a light/dark transition phase. To further investigate the Δ*spkE* phenotype, metabolic profiling during the day, night and at the transition phases of day/night and night/day should be performed under diurnal photo-mixotrophic conditions to trace C fluxes in the cell. Furthermore, it would be worth investigating if the diminished growth in light/dark cycles in Δ*spkE* is also present under LC condition without the addition of Gluc. A *spkE* overexpression mutant could moreover help to elucidate prospective targets by enhanced p-events in a phospho-proteomic approach.

The mutant strains were tested for their capability to adjust to osmotic changes in their environment. Therefore, osmotic pressure in form of 500 mM NaCl was added to BG11 growth medium (Figure 18 C). Except for Δ*spkI* (Figure 18 C), all Δ*spk* were able to sustain growth under elevated salt levels. Recently, it was proposed that SpkI might be important to sustain normal photosynthetic activity under elevated salt conditions (X. Wang et al., 2022). Δ*spkI* mutant used by X. Wang et al. (2022) depicted a lower non photochemical quenching (NPQ), lower PSII and PSI levels and strongly reduced PQ pool when exposed to 600 mM NaCl in the growth medium which was subsequently followed by retarted growth. Those results agreed

with the phenotype found in this study (Figure 18 C). Earlier studies predicted an increased salt sensitivity for Δ*spkG* (C. Liang et al., 2011), which could not be confirmed in this thesis (Figure 18 C). Liang et al. (2011) reported strongly diminished growth of Δ*spkG* when NaCl concentration exceeded 855 mM. In contrast, NaCl concentrations higher than 500 mM turned out to be lethal for WT (M) and WT (F) and Δ*spkA-L* (data not shown) in this study. Differences in light quantity, 30 µmol photons m^{-2} s^{-1} (C. Liang et al., 2011) compared to 100 µmol photons m^{-2} s^{-1} used in this study, could have caused the overall deviations in NaCl resistance.

Additionally, the capacity of Δ*spkA-L* in tolerating externally supplemented ROS in form of H_2O_2 was examined (Figure 19). Prior to the experiment, H_2O_2 tolerance of WT (M) and WT (F) was determined (Appendix Figure 3). High levels of H_2O_2 in continuous illumination causes severe harm to PSII with damages exceeding the repair capacities and, leading to potential photoinhibition (Hakkila et al., 2013). WT-like tolerance after the 3 mM of H_2O_2 treatment was observed for all Δ*spk*, except for Δ*spkF* and Δ*spkI* showing only a marginal recovery (Figure 19). Critical concertation of H_2O_2 were reached with 4 mM, indicated by abolished WT (M) growth and only marginal growth of WT (F) (Figure 19). Surprisingly, Δ*spkB* and Δ*spkG* presented a higher recovery capacity than their respective WT (M) (Figure 19). Contrasting to these results, a previous study illustrated a decreased ROS tolerance of Δ*spkB* when treated with methyl-viologen (Mata-Cabana et al., 2012). Deviating observations could be explained through the differences in applied ROS stress scenarios. Externally supplemented H_2O_2 first needs to diffuse into the cells to potentially cause harm, compared to the internally generated ROS at side of PSI caused by methyl-viologen treatment. However, changed cell wall properties were found for Δ*spkB* in the proteome study under LC (Table 12), which could potentially decrease the H_2O_2 inward diffusion and therefore, increasing the resistance of Δ*spkB* towards external ROS. Flow cytometry-based ROS measurements could elucidate cellular levels of H_2O_2 in Δ*spkB* and the rates of detoxification (Mondal & Singh, 2022).

4.3 Physiological role of SpkB

Δ*spkB* was selected to be studied in detail, because physiological characterization revealed significantly reduced growth under fluctuating Ci conditions and a lowered ability to metabolize Gluc (Figure 16 B; Figure 17 A; 18 A, B). Hence, the recoded phenotypes (Table 11) of Δ*spkB* suggested difficulties in the metabolism in form of C allocation under fluctuating C conditions. To trace the specific role(s) of SpkB, a HC-LC shift was performed for glycogen quantification and metabolome analysis (Figure 20; 21). At a HC pre-grown state Δ*spkB* accumulated significantly more glycogen than WT (M) (Figure 20), implying that Δ*spkB* favors anabolic glycolytic routes under HC by storing excessive amounts of Ci as glycogen. The stored C gets

significantly faster mobilized in Δ*spkB* when cells were shifted to LC (Figure 20). Contradictory, increased glycogen amounts at HC were met with an enrichment of TCA metabolites i.e., citric/isocitric acid, aconitic acid and fumaric acid at steady state levels (Figure 21). Further, Arg quantities were significantly raised at HC in the mutant (Figure 21). Together, these data imply an increased flux through the GS-GOGAT cycle and enhanced formation of Arg. N assimilation is controlled by the P_{II} protein, sensing 2OG levels (Forchhammer et al., 2022). In a HC atmosphere C/N balance is altered by increased availability of Ci, which results in raised 2OG levels. Phosphorylated P_{II} integrates the high Ci energy state of the cell by binding 2OG and preventing N assimilation through the GS-GOGAT cycle and in turn stopping the Arg synthesis by negative feedback inhibitions of the N-acetyl-L-glutamate (NAG)-kinase by Arg (Forchhammer & Selim, 2019). However, 2OG levels were not significantly different in the mutant compared to WT (Figure 21). Therefore, 2OG signaling through P_{II} is most likely not the major explanation for the changes in C/N-ratio related metabolites. In addition to 2OG, the activity of P_{II} is significantly altered by measuring the energy state i.e., cellular ATP and ADP levels (Forchhammer & Selim, 2019), which is likely altered upon HC to LC shifts. Lastly, P_{II} phosphorylation is different in the mutant (discussed below), which certainly influences the interaction of P_{II} with its target proteins.

When Δ*spkB* was shifted to LC, metabolites linked to N assimilation i.e., Glu and Gln were significantly altered in their abundancies together with depleting Arg levels (Figure 21), caused by increasing dephosphorylation of P_{II} and rising activity of the NAG-K (Schwarz et al., 2014; Forchhammer & Selim, 2019). Although, steady-state levels of Glu and Gln and 2OG remained unchanged after 24 h LC in relation to WT (M) (Figure 21). Observation of altered Tyr, Phe, Tryp, Gly and Ala levels (Figure 21) could be due to their biosynthesis interconnection with Glu (Mills et al., 2020). Altered levels of TCA and N assimilation metabolites in Δ*spkB* in a HC acclimated state further underlined the hypothesis of SpkBs role in C allocation and moreover, gave rise to the idea that it marks a control point in C/N balance.

To further elucidate potential target proteins of SpkB, a comparative global proteome and phospho-proteome study under limiting Ci conditions was performed with Δ*spkB* (Table 12; 13). The loss of *spkB* had an overall minor impact on the proteome of Δ*spkB* (Table 12; Barske & Spät et al., 2023). Many significantly altered events were found for unknown or hypothetical proteins. Several proteins for cell motility i.e., Slr2017, Slr2018 and Slr1929 were among proteins with altered quantities, which is in agreements with a previous study which suggested an essential role of SpkB in *Synechocystis* gliding movement (Kamei et al., 2003). The surface (s) -layer protein Sll1951 was significantly enriched at HC in the mutant. A potentially thicker s-layer of Δ*spkB* could explain the reported increased tolerance towards externally supplied

H_2O_2 (Figure 19). Studies showed the importance of Sll1951 in protecting the cell against heavy metals, antibiotics, and osmotic stress and could pose further protective functions (Sakiyama et al., 2011; Trautner & Vermaas, 2013). Interestingly, the glucosylglycerolphosphate synthase (GgpS) was found highly enriched at any given sampling timepoint. GgpS is involved in catalyzing the NaCl dependent formation of the compatible solute glucosylglycerol (GG) from ADP-glucose and glyceraldehyde 3-phosphate (G3P) (Pade & Hagemann, 2015). Accumulating GgpS in Δ*spkB,* could eventually led to a NaCl independent formation of GG and could portray a possible C sink in the proposed impaired C allocation in the mutant (Díaz-Troya et al., 2020). Though all analyzed protein kinase deficient mutants tolerated elevated NaCl concentration, Δ*spkB* presented a slightly fitter growth at higher dilutions compared to WT (M) (Figure 18 C). In future experiments GG levels of Δ*spkB* should be quantified to further investigate this hypothesis.

The overall impact of missing *spkB* on the Ci dependent global phospho-proteome remained again minor (Table 13). No protein could be identified which was exclusively phosphorylated in WT (M) but not in the mutant that would qualify it as potential SpkB target (see Barske & Spät et al., 2023). The most quantitative deviation for a p-event was recorded for the hypothetical protein Sll0103 with six altered p-sides. A Ci related increased p-event of Sll0103 was previously detected in WT (F) after 24 h in ambient air (Table 8). Similarly, p-sides T349 and T361 of Sll0103 were additionally recorded to have a higher p-occupancy under N-starvation in WT (Spät et al., 2015). In Δ*spkB*, all six p-sides of Sll0103 were significantly reduced throughout the Ci stepdown (Table 13). With p-events significantly responding to differences in Ci and N availability, Sll0103 could be involved in maintaining C/N balance. Structural alignments of Sll0103 highlighted a ‘van Willebrand’ factor type A domain similarity and a protein/protein interaction possibility (Edwards & Perkins, 1995; Peetermans et al., 2020). Hence, SpkB could be vital for the phosphorylation of Sll0103 by direct or indirect involvement in its signal cascade. In addition, five p-events on the carboxysome structural protein CcmM which recruits RuBisCO and CA to form pro-carboxysome, were detected (Hagemann et al., 2021) however, T358 was found to be the only p-side significantly less phosphorylated in Δ*spkB* (Table 13). Potential physiological effects on photosynthetic activity in the mutant was examined with HC and LC pre-grown Δ*spkB* (Figure 23). O_2 evolution rates and HCO_3^- affinity did not differ from WT (M) (Figure 23 A, B). Concluding from those results, it seems unlikely that CcmM p-event T358 is vital for the condensate formation with RuBisCO during carboxysome assembly (H. Wang et al., 2019). This assumption is supported, when the CcmM protein sequence is aligned with CcmMs from other model cyanobacteria e.g., *Synechococcus elongatus* PCC 7942 (Syc0133) and *Anabaena* sp. PCC 7120 (All0865). Their

CcmM proteins share conservation in distinct parts, but the phosphorylation side(s) identified in *Synechocystis* CcmM were not conserved (Figure 33).

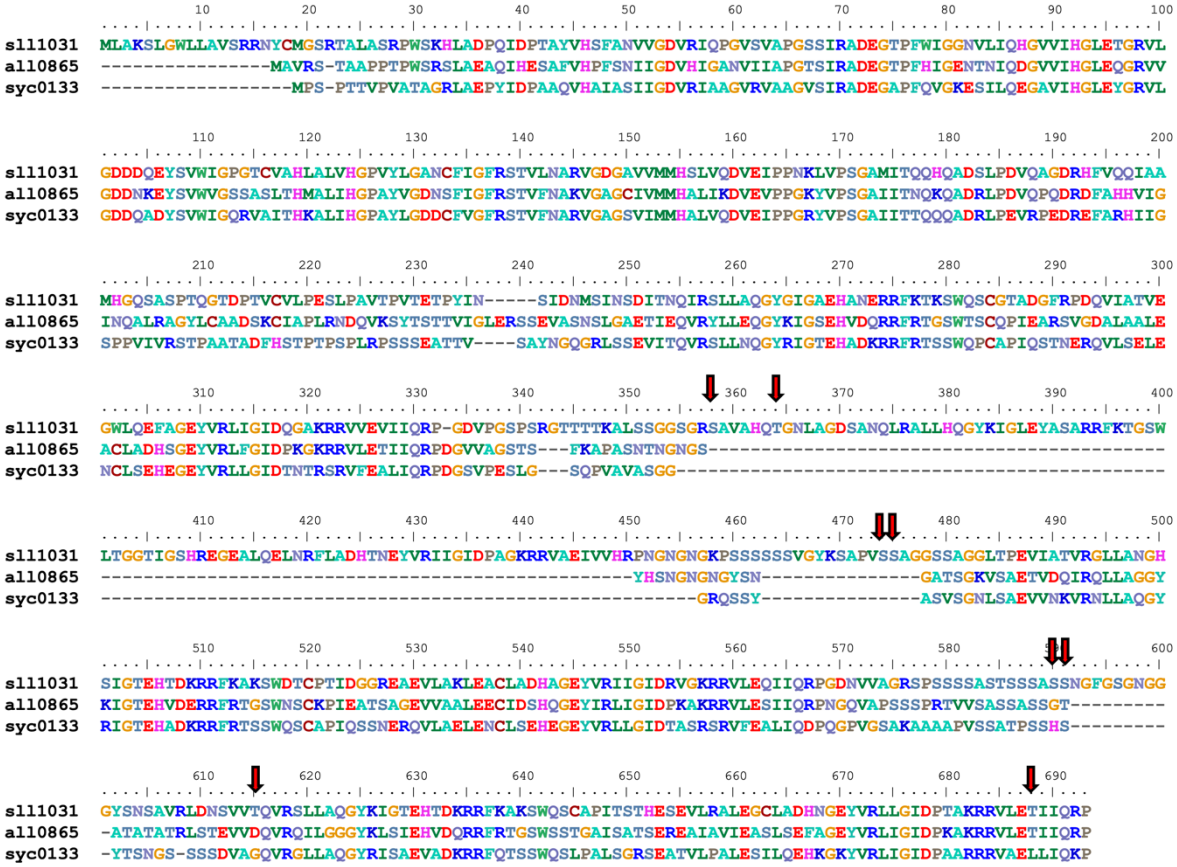

Figure 33: Sequence alignment of *Synechocystis* CcmM with homologs from different cyanobacteria: Multiple AA sequence alignment with CcmM from *Synechocystis* (Sll1031), *Anabaena* sp. PCC 7120 (All0865) and *Synechococcus elongatus* PCC 7942 (Syc0133). Detected p-events in CcmM from *Synechocystis* (Table 13; Barske & Spät et al., 2023) are marked with red arrows.

As seen in global phospho-proteome studies on WT (F) (Table 8; Spät et al., 2015, 2018; Z. Chen et al., 2015) PB are heavily phosphorylated proteins. State transition alters the energy distribution between PBS and PSII or PSI upon changes in the redox state of the PQ pool under fluctuating light or Ci conditions (Calzadilla & Kirilovsky, 2020). The phospho-proteome of Δ*spkB* found allophycocyanin alpha subunit (ApcA) significantly stronger phosphorylated on T31 at LC compared to WT (M) (Table 13). ApcA is a terminal emitter of light energy from the PBS to chlorophyll (MacColl, 2004). To study a potential impact of the altered p-event on the photosynthetic energy transfer in Δ*spkB*, low temperature 77K fluorescence measurements with LC acclimated Δ*spkB* was conducted (Figure 22). Mutant cells excited on Chl*a* (Figure 22 B) did not differ from WT (M) and proved that the general energy transfer between PSII and PSI was not impaired. This was also true for the additionally found deviated p-event on PSI subunit PsaE (Table 13, Figure 22 B; 23). Remarkably, a stronger coupling of PBS and PSI could be observed for Δ*spkB* which was indicated by a generally higher recorded

PSI fluorescence when PB were excited (Figure 22 A).Those findings hinted that the mutant was in a State II -like conformation under LC (Calzadilla & Kirilovsky, 2020). Especially increased energy transfer was documented from allophycocyanin to PSI (Figure 22A). These data suggest that the changed p-event at T31 on ApcA could indeed have had an impact on light absorption and energy transfer in the mutant. Previously PBS phosphorylation has been implicated as a possible regulator of photosynthetic light absorption among cyanobacteria (Z. Chen et al., 2015). Future experiments with ApcA phosphorylation mutants in WT and Δ*spkB* background could help understanding the role of ApcA phosphorylation in photosynthetic energy transfer. However, since ApcA p-event at T31 became increased in the kinase deficient mutant, this alteration is most likely an indirect effect. But a lowered p-event at T24 was demonstrated on the protein kinase SpkF under ambient air in Δ*spkB* (Table 13). SpkF holds 3 transmembrane domains (X. Zhang et al., 2007; A. Zorina, 2013) and could potentially be involved in ApcA phosphorylation. Δ*spkF* growth was WT-like in HC-LC conditions (Figure 16 F), though phycocyanin levels were significantly reduced in HC (Table 10). Therefore, a potential role of SpkF in ApcA phosphorylation cannot be ruled out.

Remarkably, in Δ*spkB* significantly lowered p-occupancy at S49 of the P_{II} protein was detected in LC (Table 13). The recorded reduced growth under various C conditions (Figure 16 B; 17 A; 18 A, B) and the observed metabolome pattern (Figure 21) in Δ*spkB* could be in fact the consequence of reduced P_{II} p-levels at S49. The complementation strain Δ*spkB*^{C} showed to complement the growth phenotype of Δ*spkB* in a HC-LC shift (Figure 27). S49 is located on the tip of the flexible T-loop at each of the three P_{II} monomers and promotes contact with P_{II} interactors (Forchhammer & Selim, 2019). There are four distinct phosphorylation states of the P_{II} trimer, which are influenced in NO_3^- grown *Synechocystis* cells by CO_2 supply (Schwarz et al., 2014). High Ci leads to considerably stronger phosphorylated P_{II} compared to low Ci, while N starvation leads to the strongest observed P_{II} phosphorylation (Forchhammer & Selim, 2019). To verify the *in vivo* P_{II} phosphorylation pattern in Δ*spkB*, whole protein extracts of NO_3^- deprived *Synechocystis* cells were run on a Native-PAGE to follow the P_{II} phosphorylation dynamics (Figure 24). Remarkably, the P_{II} phosphorylation response differed in the mutant from WT (M). P_{II} phosphorylation in Δ*spkB* was delayed and did not reach a fully phosphorylated state with a majority of the P_{II} protein staying non-phosphorylated after 120 min in a NO_3^- free atmosphere (Figure 24). This was principally in consent with the reduced P_{II} phosphorylation found in the phospho-proteome (Table 13). The metabolic profile of NO_3^- deprived Δ*spkB* revealed an increase in TCA related metabolites such as citric acid, succinic acid and malic acid and, N assimilation associated metabolites like Arg, Gln and Glu but unaltered 2OG levels (Figure 25). Interestingly, pyruvic acid amounts were significantly lowered in the mutant (Figure 25). Despite the long known P_{II} phosphorylation in cyanobacteria

(Forchhammer & Tandeau De Marsac, 1994), a P_{II} specific protein kinase remains to be found, though the P_{II} phosphatase was successfully identified as PphA (Irmler & Forchhammer, 2001). Collectively, the presented data suggest that SpkB could be potentially a P_{II} specific kinase. Altered P_{II} S49 phosphorylation in Δ*spkB* is influencing the protein complex formation with its respective interaction partners and therewith, distorting responses regulating the C/N balance (Radchenko & Merrick, 2011; Forchhammer & Lüddecke, 2016). This is of special relevance with P_{II} interaction partners PirC and PEPC regulating the C flux into lower glycolysis and TCA, depending on the P_{II} conformation status (Scholl et al., 2020; Orthwein et al., 2021). Deviating interactions with PirC and PEPC could serve as plausible explanation for the observed enhanced glycogen accumulation and breakdown (Figure 20), reduced pyruvate levels (Figure 21) and different TCA metabolites and AA levels (Figure 21; 25) in Δ*spkB* under changing C conditions. Recently, P_{II} hyper-phosphorylation combined with significantly reduced glycogen levels was reported for Δ*hik8* (C. Huang et al., 2023). Hik8 is known to play a regulatory role in the C metabolism. (A. K. Singh & Sherman, 2005; Osanai et al., 2015). These novel finding agree with our documented decreased P_{II} phosphorylation at S49 (Table 13) and accumulation of glycogen under HC (Figure 20). Nevertheless, residual P_{II} phosphorylation was still observed in Δ*spkB* under NO_3^- limitation (Figure 24) directing the idea that SpkB could be part of a kinase network. Nevertheless, it cannot be ruled out that SpkB is also involved in the inactivation of PphA. An overly active phosphatase PphA could explain the elevated dephosphorylation of P_{II} in Δ*spkB*. Clearly, SpkB is involved in maintaining the C/N balance in *Synechocystis*. This notion is further amplified by the recorded lowered P_{II} phosphorylation (Table 13, Figure 24) in Δ*spkB*. Therefore, future experiments should be focused on *in vitro* phosphorylation assays with recombinant SpkB and P_{II} in the presence of and without PphA.

4.4 Physiological role of SpkC

Significant enhanced p-events at T305 and T312 on SpkC were found in WT (F) phospho-proteome in response to changing Ci conditions (Table 8). Before, T312 has already been identified as significantly less phosphorylated in N Starvation (Spät et al., 2015). Concomitantly, Δ*spkC* presented a significantly reduced growth when shifted from HC to LC (Figure 16 C). Taken together, these results indicated a possible role of SpkC in acclimation responses towards changing Ci availability. The comparative proteome study with Δ*spkC* under Ci limitation (Table 14) revealed that the overall impact of missing SpkC was minor. However, many LC induced proteins involved in CCM related HCO_3^- and CO_2 uptake such as SbtA, CupA, subunits CmpB and CmpC of the high affinity HCO_3^- transporter BCT1 as well as the photoprotective flavoprotein Flv2 were found in lower quantities in Δ*spkC*. Contrasting,

HliC and the HCO_3^- binding subunit CmpA of BCT1 were strongly enriched in LC in the mutant. Flv2 and HliC are believed to have photoprotective traits at the side of PSII (Havaux et al., 2003; P. Zhang et al., 2012; Sinha et al., 2012; Bersanini et al., 2014; Santana-Sanchez et al., 2019). All subunits of the low Ci induced ABC-type transporter BCT1 are co-transcribed within the *cmpA*-operon (Omata et al., 1999). Deviating amounts of individual BCT1 subunits in Δ*spkC* i.e, CmpA and CmpB (Table 14) indicate either differential mRNA processing and/or PTM influencing either mRNA maturation or protein stability. It is known that differential gene expression of gene operons is an important regulatory mechanism for gene expression and which can be influenced by fluctuating environmental conditions e.g., temperature fluctuations (Albert et al., 2020; Vargas-Blanco & Shell, 2020). Increased amounts of CmpA in Δ*spkC* suggests a change in stoichiometries in BCT1 composition which could be a response towards optimizing efficient Ci uptake under LC. Enrichment of CmpA in Δ*spkC* in response to low Ci was evaluated by immunoblot analysis (Figure 30) however, differences in CmpA abundancies could not be confirmed. Overall, the proteome changes in Δ*spkC* often effected proteins with known functions (Table 14; Spät & Barske et al., 2021), which supports the hypothesis that SpkC may play an important role in this acclimation process.

The comparative phospho-proteome analysis between Δ*spkC* and WT (F) under low Ci (Table 15) revealed that several of the characterized p-events in WT (F) could not be detected in the mutant. DNA polymerase III subunit DnaX, which was always detected as p-protein in each WT replicate (Table 8) was not found as such in Δ*spkC*. However, DnaX p-events were neither detected in the phospho-proteome of WT (M) and Δ*spkB* (Table 13; Barske & Spät et al., 2023), which makes it an unlikely substrate for SpkC. Strikingly, the phosphorylation at T129 and T110 of CmpA and T3 of CmpB were among the unrecognized p-events in Δ*spkC* (Table 15). This suggested a putative role of CmpA and CmpB as substrates of SpkC and thereby, defining a role of SpkC in Ci uptake. Further affirming was that CmpA and CmpB p-events were again recovered in the Ci related phospho-proteome study conducted with Δ*spkB* (Barske & Spät et al., 2023). A role in regulating C allocation inside the primary C metabolism could be ruled out due to no characterized phenotypes under mixotrophic, diurnal conditions (Figure 17 B; 18 A, B) and WT (F)-like glycogen accumulation and degradation (Figure 29), as well as unchanged abundances and p-events of enzymes in the primary metabolism (Spät & Barske et al., 2021). To further explore this hypothesis, HCO_3^- dependent O_2 evolution measurements were conducted with HC and LC pre-grown Δ*spkC* (Figure 28). Km values of HC acclimated Δ*spkC* did not differ from WT (F) (Figure 28 A) even though, O_2 production rates were slightly lower in the mutant. However, significantly reduced HCO_3^- affinity was found for Δ*spkC* in a LC acclimated state (Figure 28 B) with O_2 production rates comparable to a HC acclimated state (Figure 28). A role of SpkC in rapid activation of a high affinity HCO_3^-

transporter seemed plausible. The precise mechanism of the activation/ inactivation of HCO_3^- transporters is not known, but activation by protein kinase mediated phosphorylation has already been discussed in earlier reports (Bloye et al., 1992; Sültemeyer et al., 1998; Price et al., 2013). Sültemeyer et al. (1998) presented conclusive evidence that rapid LC induced HCO_3^- uptake could be experimentally repressed by common kinase inhibitors. The global WT (F) phospho-proteome did not identify the constitutively expressed HCO_3^- transporters BicA and low Ci induced SbtA to be phosphorylated under altering Ci conditions (Table 8). However, phosphorylation of SbtA has been reported in N starved cells (Spät et al., 2015). Reduced p-events of CmpA and CmpB found in WT (F) (Table 8) were attributed to the strongly occurring *de novo* synthesis of BCT1 under ambient air and awaiting kinase mediated phosphorylation (Table 7, 8). Missing in Δ*spkC* proposed that SpkC could be involved in the phosphorylation of T129 and T110 of CmpA and T3 of CmpB and thereby, eventually modulating the rapid low C_i induced HCO_3^- transport through BCT1. Furthermore, reduced cellular HCO_3^- levels could have caused the strong accumulation of HliC (Table 14). HCO_3^- is essential for linear electron flow at PSII (Shevela et al., 2012). Changes in cellular HCO_3^- levels could promote the formation of ROS and the increased need of photoprotective proteins such as HliC (Havaux et al., 2003; Sinha et al., 2012). The chaperonin GroES was suspected to be a target of SpkC/F/K in a kinase cascade (A. Zorina et al., 2011). However, Δ*spkC* did not show significantly altered p-events for GroES (Table 15). Nonetheless, it cannot be ruled out that SpkF and SpkK kinase activity are responsible for GroES phosphorylation.

Following up on this hypothesis, a Δ*spkC* complementation strain needs to be established to rule out polar effect on neighboring genes in its TU (Table 9; Kopf et al., 2014). Moreover, *in vitro* phosphorylation assays with recombinant SpkC, CmpA and CmpB need to be performed. Phosphorylation variant mutants for SpkC at T305 and T312 should be generated to determine their importance in kinase activity. Additionally, phosphorylation variant mutants of CmpA and CmpB altered at p-sides T129, T110 and T3 could help in elucidating their respective role in BCT1 activity.

4.5 Concluding remarks on protein phosphorylation under changing Ci conditions in *Synechocystis*

Cyanobacteria such as *Synechocystis* present a remarkable capability in acclimating to fluctuating environmental conditions and were therefore able to inhabit all kinds of diverse habitats (Houmard, 1995). Their diversity in responding to rapidly fluctuating environmental conditions is highlighted by their complexity in signal perception systems (A. Zorina, 2013).

Rapid signal transmission through PTM, particularly through p-phosphorylation, is essential for adequate cellular responses (Macek & Mijakovic, 2011). In this thesis the physiological importance of p-phosphorylation in *Synechocystis* under fluctuating Ci conditions was studied. In our initial hypothesis we postulated that the switch from C anabolism towards C catabolism in constant light can be mainly regulated by modifications on enzyme activities due to differential phosphorylation states. The presented experimental data with *Synechocystis* WT (F) documented 200 p-events on 105 proteins with an extensive number of alternating p-events under changing Ci conditions in a HC-LC shift (Table 8). Among the identified p-events are proteins associated with CCM (i.e., CmpA, CmpB), photosynthesis (i.e., PsaD, CpcA), DNA replication (i.e., DnaX, SbcC, NusG) and regulatory proteins (e.g., CP12, P_{II}). These results confirmed the hypothesis that *Synechocystis* relies on p-phosphorylation to acclimate towards fluctuating Ci availability. Although metabolic enzymes acting in the primary C metabolism could be characterized in the global phospho-proteome studies (e.g., FbaA (Sll0018), Pgm1 (Slr1945), Gnd (Sll0329), GapDH2 (Sll1342) and FbpI (Slr2094)) (Spät & Barske et al., 2021; Barske & Spät et al., 2023), alterations on their p-occupancy were not reported. The general physiological relevance of the characterized p-events on protein activity under the investigated Ci conditions remains mostly elusive and needs to be further studied.

The phospho-proteome studies conducted for this thesis (Table 8, 13, 15) revealed the technical limitation of this method highlighted by the overall observed low reproducibility among the replicates within each individual experiment (Figure 32). Even though, phospho-proteomic analysis are carried out routinely, technical limitations are still faced i.e., the analysis of low abundant proteins, low stoichiometry of the p-event, potentially impaired digestion efficiency, phosphorylated peptides lost during preparation and enrichment by chromatography, impaired ionization of phosphorylated peptides, peculiar behavior of unstable p-groups upon collision induced dissociation and the correct localization of a p-event on a peptide impacts the reproducibility of p-events (Solari et al., 2015). Advances in sensitivity of future LC-MS devices and phospho-peptide enrichment independent analyses methods could help further expanding the number of detected p-proteins and broaden the scope of p-events in acclimation processes in cyanobacteria such as *Synechocystis*.

Further, the role of Ser/Thr specific protein kinases (SpkA-L; Table 9, 11) and their role in acclimation processes was investigated (Figure 16, 17, 18, 19). Albeit reversible protein modification on Ser/Thr residues are extensively employed to acclimate to ambient air (Table 8), knowledge about protein kinases carrying out the modification is scarce. *Synechocystis* genome holds twelve Ser/Thr protein kinases (C.-C. Zhang et al., 1998; Leonard et al., 1998; Shi et al., 1998). Their specific role in acclimation processes under fluctuating environmental

conditions was studied in eleven *Synechocystis* mutant strains (Δ*spkA-L*, Table 1). Collectively, our results strongly support the hypothesis that p-phosphorylation via Spks play an important role in stress acclimation for *Synechocystis* seen in the diverse phenotypes documented in this work (Table 11). Particularly, the phenotypes of Δ*spkB,* Δ*spkC* and Δ*spkE* (Table 11) highlighted that SpkB, SpkC and SpkE are promising candidates in regulating C allocation. Δ*spkB* and Δ*spkC* showed significantly reduced growth in HC-LC shift growth experiments (Figure 16 B, C) with Δ*spkB* presenting an additional impairment in Gluc utilization (Figure 17 A; 18 A) whereas decreased growth was observed under diurnal conditions for Δ*spkE* (Figure 18 B). The global phospho-proteome of Δ*spkB* (Table 13) revealed significantly lowered P_{II} phosphorylation in Δ*spkB*. Altered P_{II} phosphorylation in Δ*spkB* could further be verified in an immunoblot assay (Figure 24), concluding in regulatory role of SpkB in C/N homeostasis. This notion was further affirmed by deviating TCA and N assimilation related metabolites (Figure 21, 25) and cellular glycogen levels in the mutants (Figure 20). Moreover, SpkC was found to be differentially phosphorylated in WT (F) in response to LC (Table 8). Δ*spkC* was significantly impacted under HC-LC shift condition (Figure 16 C). Δ*spkC*s global phospho-proteome presented abolished p-events on CmpA and CmpB of the high affinity HCO_3^- transporter BCT1 (Table 15) followed by significantly lowered affinity to HCO_3^- in LC acclimated Δ*spkC* (Figure 28). These observations concluded in a suggested role of SpkC in modulating rapid low C_i induced HCO_3^- transport.

Nevertheless, the proposed functions of the studied protein kinases are only evidence based. *In vitro* assays proofing the direct interaction with their claimed targets remains to be conducted in future experiments with recombinant SpkB and SpkC and their potential substrates. However, it is generally assumed that bacterial Spks have a rather relaxed substrate specificity (Kobir et al., 2011). This idea was further supported by the data in this thesis. 200 p-events were detected in the presented studies and the overall more than 500 p-events reported throughout all major phospho-proteome analysis in *Synechocystis* (Appendix Table 3; Mikkat et al., 2014; Spät et al., 2015; Z. Chen et al., 2015; Angeleri et al., 2016; Toyoshima et al., 2020; Spät & Barske et al., 2021; Barske & Spät et al., 2023) which is in sharp contrast to the only twelve annotated Ser/Thr protein kinases found in *Synechocystis* (C.-C. Zhang et al., 1998; Leonard et al., 1998; Shi et al., 1998). This discrepancy indicates that besides kinase mediated p-events, kinase independent p-events are occurring to a high extent e.g., the phosphorylation of PGM1 and PGM2 (Doello et al., 2022; Neumann et al., 2022). Those events could vastly increase the total number of p-events. Furthermore, the complete picture of Ser/Thr protein kinases in *Synechocystis* should be re-evaluated. Many bacterial Ser/Thr protein kinases resemble Hanks-type kinases which is also true for *Synechocystis* (C.-C. Zhang et al., 1998; Leonard et al., 1998; Shi et al., 1998) nevertheless,

there is a chance of evolutionary unrelated protein kinases such as the isocitrate dehydrogenase kinase/phosphatase found in *E. coli* (Zheng & Jia, 2010) or the non-enzymatic acetyl phosphate dependent phosphorylation which was reported in the bacteria *Streptococcus pneumoniae* (Kaiser et al., 2020) and *B. subtilis* (Cairns et al., 2015). Moreover, p-phosphorylation represents only one layer of possible PTM. Carbamylation of Lys residues has been recently identified as a wide-spread modification in *Synechocystis*, which can modulate the protein activities of proteins such as RuBisCO and the P_{II} protein in a Ci related manner (King et al., 2022). On a single peptide sequence, different PTM can occur simultaneously on multiple residues or in a tandem cascade (Steen et al., 2003; Walsh et al., 2005; Macek et al., 2019). Kinase cascades with upstream kinases activating specific downstream kinases have been suspected in the phosphorylation of GroES (A. Zorina et al., 2011; Miller & Turk, 2018). To fully understand the role of p-phosphorylation in acclimation to changing Ci conditions, the full spectrum of protein modifications and its impact on enzyme activity needs to be included to understand the entire scope of action.

In future experiments an expanding variety of environmental conditions having a direct impact of C allocation in *Synechocystis* i.e., photo-mixotrophic, diurnal and heterotrophic modes of lifestyles should be studied in a dynamic phospho-proteomic approach. As it was seen in the data presented in this thesis, serval identified p-proteins were characterized as either hypothetical or unknown such as Sll0103. Sll0103 was found to be heavily phosphorylated under tested Ci conditions (Table 8, 13, 15) with S407 responding significantly to LC (Table 8, 13). Interestingly, Sll0103 p-events were also found with altered p-occupancy under N starvation (Spät et al., 2015). Cross-checking phospho-proteome dataset for proteins responding to more than one fluctuating condition could help to identify novel putative regulatory proteins and assign functional roles to yet undescribed proteins. Similar, identical p-sides of already described proteins such as CP12 and SpkC were found to be not only responding to Ci fluctuation but also to changes in N availability (Table 8; Spät et al., 2015, 2018). Side-specific phosphorylation mutants could assist in elucidating putative roles of p-events in acclimation processes and could contribute in broaden the physiological relevance of such proteins. Continuing work on Ser/Thr protein kinases should focus on the protein kinases SpkE, SpkH, SpkI, SpkJ and SpkK. Δ*spkE* was shown to be impacted by diurnal growth condition (Figure 18 B) and could potentially have a central role in adjusting C fluxes in a day and night transition. The metabolomic profile of Δ*spkE* at the end of the light and dark phase should be analyzed in detail and be checked for alteration to WT patterns. Another interesting candidate is SpkH which was shown to be indispensable under our laboratory conditions (Figure 14 D) and could potentially pose a central role in the metabolisms. An SpkH overexpression or CRISPR/Cas silencing approach could help by either enhancing a Δ*spkH*

phenotype or by creating a gene knock-out. Δ*spkI* was shown to be severely affected by every tested environmental condition (Figure 16, 17, 18, 19). However, *spkI* is found in an operon structure together with the P_{II} phosphatase PphA (Irmler & Forchhammer, 2001). To rule out polar effects on downstream genes inside the TU caused by the mutation, a *spkI* complementation strain should be generated and checked for similar phenotypes like Δ*spkI*. Lastly *spkJ* and *spkK* were found inversely regulated in the global RNA-Seq study (Figure 15; Kopf et al., 2014). Phenotypes of Δ*spkJ* and Δ*spkK* under cold stress, high light and Fe-limitations (Figure 15) should be evaluated to elucidate if these kinases could act in a cascade manner.

5 Bibliography

Alagesan, S., Sandeep, Gaudana, B., Sinha, A., Pramod, Wangikar, P., Alagesan, S., Gaudana, Á. S. B., Sinha, Á. A., & Wangikar, Á. P. P. (2013). Metabolic flux analysis of *Cyanothece* sp. ATCC 51142 under mixotrophic conditions. *Photosynthesis research,* ***118***, 191-198.

Albert, X., Rosana, R. R., Whitford, D. S., Migur, A., Steglich, C., Kujat-Choy, S. L., Hess, W. R., George, X., & Owttrim, W. (2020). RNA helicase-regulated processing of the *Synechocystis* rimO-crhR operon results in differential cistron expression and accumulation of two sRNAs. *Journal of Biological Chemistry*, ***295***(19), 6372–6386.

Allahverdiyeva, Y., Mustila, H., Ermakova, M., Bersanini, L., Richaud, P., Ajlani, G., Battchikova, N., Cournac, L., & Aro, E. M. (2013). Flavodiiron proteins Flv1 and Flv3 enable cyanobacterial growth and photosynthesis under fluctuating light. *PNAS*, ***110***(10), 4111–4116.

Allakhverdiev, S. I., Nishiyama, Y., Miyairi, S., Yamamoto, H., Inagaki, N., Kanesaki, Y., & Murata, N. (2002). Salt stress inhibits the repair of photodamaged photosystem II by suppressing the transcription and translation of psbA genes in *Synechocystis*. *Plant Physiology*, ***130***(3), 1443–1453.

Allen, J. F., & Holmes, N. G. (1986). A general model for regulation of photosynthetic unit function by protein phosphorylation. *FEBS Letters*, ***202***(2), 175–181.

Allen, J. F., Sanders, C. E., & Holmes, N. G. (1985). Correlation of membrane protein phosphorylation with excitation energy distribution in the cyanobacterium *Synechococcus* 6301. *FEBS letters*, ***193***(2), 271-275.

Amoroso, G., Seimetz, N., & Sültemeyer, D. (2003). The dc13 gene upstream of ictB is involved in rapid induction of the high affinity Na+ dependent HCO3- transporter in cyanobacteria. *Photosynthesis Research*, ***77***, 127–138.

Anderson, S. L., & McIntosh, L. (1991). Light-activated heterotrophic growth of the cyanobacterium *Synechocystis* sp. strain PCC 6803: A blue-light-requiring process. *Journal of Bacteriology*, ***173***(9), 2761–2767.

Angeleri, M., Muth-Pawlak, D., Aro, E. M., & Battchikova, N. (2016). Study of O-Phosphorylation Sites in Proteins Involved in Photosynthesis-Related Processes in *Synechocystis* sp. Strain PCC 6803: Application of the SRM Approach. *Journal of Proteome Research*, ***15***(12), 4638–4652.

Angeleri, M., Zorina, A., Aro, E. M., & Battchikova, N. (2018). Interplay of SpkG kinase and the Slr0151 protein in the phosphorylation of ferredoxin 5 in *Synechocystis* sp. strain PCC 6803. *FEBS Letters*, ***592***(3), 411–421.

Angermayr, S. A., Hellingwerf, K. J., Lindblad, P., & Teixeira de Mattos, M. J. (2009). Energy biotechnology with cyanobacteria. *Current Opinion in Biotechnology*, ***20***(3), 257–263.

Aro, E.-M., Virgin, I., & Andersson, B. (1993). Photoinhibition of Photosystem II. Inactivation, protein damage and turnover. *BBA,* ***1143***(2), 113–134.

Aseev, L. V., Koledinskaya, L. S., & Boni, I. V. (2016). Regulation of Ribosomal Protein Operons rplM-rpsI, rpmB-rpmG, and rplU-rpmA at the Transcriptional and Translational Levels. *Journal of Bacteriology*, ***198***(18), 2494.

Atsumi, S., Higashide, W., & Liao, J. C. (2009). Direct photosynthetic recycling of carbon dioxide to isobutyraldehyde. *Nature Biotechnology,* ***27***(12), 1177–1180.

Bachhar, A., & Jablonsky, J. (2020). A new insight into role of phosphoketolase pathway in *Synechocystis* sp. PCC 6803. *Scientific Reports*, ***10***(1), 22018.

Baers, L. L., Breckels, L. M., Mills, L. A., Gatto, L., Deery, M. J., Stevens, T. J., Howe, C. J., Lilley, K. S., & Lea-Smith, D. J. (2019). Proteome Mapping of a Cyanobacterium Reveals Distinct Compartment Organization and Cell-Dispersed Metabolism. *Plant Physiology*, ***181***(4), 1721-1738.

Barske, T., Spät, P., Schubert, H., Walke, P., Maček, B., & Hagemann, M. (2023). The Role of Serine/Threonine-Specific Protein Kinases in Cyanobacteria - SpkB Is Involved in Acclimation to Fluctuating Conditions in *Synechocystis* sp. PCC 6803. *Molecular & Cellular Proteomics*, ***22***(11).

Bassham, J. A., Benson, A. A., Kay, L. D., Harris, A. Z., Wilson, A. T., & Calvin, M. (1954). The Path of Carbon in Photosynthesis. XXI. The Cyclic Regeneration of Carbon Dioxide Acceptor. *Journal of the American Chemical Society*, ***76***(7), 1760–1770.

Bateman, A., Murzin,' And, A. G., & Teichmann', S. A. (1998). Structure and distribution of pentapeptide repeats in bacteria. *Protein Science*, ***7***(6), 1477–1480.

Beenstock, J., Mooshayef, N., & Engelberg, D. (2016). How Do Protein Kinases Take a Selfie (Autophosphorylate)?. *Trends in Biochemical Sciences*, ***41***(11), 938–953.

Bersanini, L., Battchikova, N., Jokel, M., Rehman, A., Vass, I., Allahverdiyeva, Y., & Aro, E.-M. (2014). Flavodiiron Protein Flv2/Flv4-Related Photoprotective Mechanism Dissipates Excitation Pressure of PSII in Cooperation with Phycobilisomes in Cyanobacteria. *Plant Physiology*, ***164***(4), 805–818.

Bertran-Vicente, J., Serwa, R. A., Schümann, M., Schmieder, P., Krause, E., & Hackenberger, C. P. R. (2014). Site-specifically phosphorylated lysine peptides. *Journal of the American Chemical Society*, ***136***(39), 13622–13628.

Bhatti, A. F., Choubeh, R. R., Kirilovsky, D., Wientjes, E., & van Amerongen, H. (2020). State transitions in cyanobacteria studied with picosecond fluorescence at room temperature. *BBA*, ***1861***(10), 148255.

Blankenship, R. E. (2002). Molecular Mechanisms of Photosynthesis. *John Wiley & Sons.*

Bloye, S. A., Silman, N. J., Mann, N. H., & Carr, N. G. (1992). Bicarbonate concentration by *Synechocystis* PCC6803: Modulation of protein phosphorylation and inorganic carbon transport by glucose. *Plant Physiology*, ***99***(2), 601–606.

Bolay, P., Schlüter, S., Grimm, S., Riediger, M., Hess, W. R., & Klähn, S. (2022). The transcriptional regulator RbcR controls ribulose-1,5-bisphosphate carboxylase/oxygenase (RuBisCO) genes in the cyanobacterium *Synechocystis* sp. PCC 6803. *New Phytologist*, ***235***(2), 432–445.

Bousquet, I., Dujardin, G., & Slonimski, P. P. (1991). ABC1, a novel yeast nuclear gene has a dual function in mitochondria: it suppresses a cytochrome b mRNA translation defect and is essential for the electron transfer in the bc 1 complex. *The EMBO Journal*, ***10***(8), 2023–2031.

Brasseur, G., Tron, P., Dujardin, G., Slonimski, P. P., & Brivet-Chevillotte, P. (1997). The nuclear ABC1 gene is essential for the correct conformation and functioning of the cytochrome bc1 complex and the neighboring complexes II and IV in the mitochondrial respiratory chain. *European Journal of Biochemistry*, ***246***(1), 103–111.

Bryant, D. A., & Frigaard, N. U. (2006). Prokaryotic photosynthesis and phototrophy illuminated. *Trends in microbiology*, ***14***(11), 488–496.

Burnap, R. L., Hagemann, M., & Kaplan, A. (2015). Regulation of CO 2 Concentrating Mechanism in Cyanobacteria. *Life*, ***5***(1), 348–371.

Cain, J. A., Solis, N., & Cordwell, S. J. (2014). Beyond gene expression: The impact of protein post-translational modifications in bacteria. *Journal of proteomics*, ***97***, 265–286.

Cairns, L. S., Martyn, J. E., Bromley, K., & Stanley-Wall, N. R. (2015). An alternate route to phosphorylating DegU of *Bacillus subtilis* using acetyl phosphate. *BMC Microbiology*, ***15***(1), 1–12.

Calzadilla, P. I., & Kirilovsky, D. (2020). Revisiting cyanobacterial state transitions. *Photochemical and Photobiological Sciences*, ***19***(5), 585–603.

Cavalier-Smith, T. (2000). Membrane heredity and early chloroplast evolution. *Trends in Plant Science*, ***5***(4), 174–182.

Chan, C. X., & Bhattacharya, D. (2010). The origin of plastids. In *Nature Education, **3***(9), 84–1.

Cheek, S., Zhang, H., & Grishin, N. V. (2002). Sequence and Structure Classification of Kinases. *Journal of Molecular Biology*, ***320***(4), 855–881.

Chen, G., Cao, Y., Zhong, H., Wang, X., Li, Y., Cui, X., Lu, X., Bi, X., & Dai, M. (2021). Serine/threonine Kinases Play Important Roles in Regulating Polyunsaturated Fatty Acid Biosynthesis in *Synechocystis* sp. PCC6803. *Frontiers in Bioengineering and Biotechnology*, ***9***, 618969.

Chen, X., Schreiber, K., Appel, J., Makowka, A., Fähnrich, B., Roettger, M., Hajirezaei, M. R., Sönnichsen, F. D., Schönheit, P., Martin, W. F., & Gutekunst, K. (2016). The Entner-Doudoroff pathway is an overlooked glycolytic route in cyanobacteria and plants. *PNAS*, ***113***(19), 5441–5446.

Chen, Z., Zhan, J., Chen, Y., Yang, M., He, C., Ge, F., & Wang, Q. (2015). Effects of Phosphorylation of β Subunits of Phycocyanins on State Transition in the Model Cyanobacterium *Synechocystis* sp. PCC 6803. *Plant and Cell Physiology*, ***56***(10), 1997–2013.

Cornah, J. E., Terry, M. J., & Smith, A. G. (2003). Green or red: What stops the traffic in the tetrapyrrole pathway?. *Trends in plant science*, ***8***(5), 224-230.

Cortay, J. -C, Rieul, C., Duclos, B., & Cozzone, A. J. (1986). Characterization of the phosphoproteins of *Escherichia coli* cells by electrophoretic analysis. *European Journal of Biochemistry*, ***159***(2), 227–237.

Cozzone, A. J. (1993). ATP-dependent protein kinases in bacteria. *Journal of Cellular Biochemistry*, ***51***(1), 7–13.

Deng, M. De, & Coleman, J. R. (1999). Ethanol synthesis by genetic engineering in cyanobacteria. *Applied and Environmental Microbiology*, ***65***(2), 523–528.

Díaz-Troya, S., Roldán, M., Mallén-Ponce, M. J., Ortega-Martínez, P., & Florencio, F. J. (2020). Lethality caused by ADP-glucose accumulation is suppressed by salt-induced carbon flux redirection in cyanobacteria. *Journal of Experimental Botany*, ***71***(6), 2005–2017.

Do, T. Q., Hsu, A. Y., Jonassen, T., Lee, P. T., & Clarke, C. F. (2001). A Defect in Coenzyme Q Biosynthesis is Responsible for the Respiratory Deficiency in *Saccharomyces cerevisiae* abc1 Mutants. *Journal of Biological Chemistry*, ***276***(21), 18161–18168.

Doello, S., Neumann, N., & Forchhammer, K. (2022). Regulatory phosphorylation event of Phosphoglucomutase 1 tunes its activity to regulate glycogen metabolism. *The FEBS Journal,* ***289***(19), 6005-6020.

Ducat, D. C., Avelar-Rivas, J. A., Way, J. C., & Silvera, P. A. (2012). Rerouting carbon flux to enhance photosynthetic productivity. *Applied and Environmental Microbiology*, ***78***(8), 2660–2668.

Ducat, D. C., Way, J. C., & Silver, P. A. (2011). Engineering cyanobacteria to generate high-value products. *Trends in Biotechnology*, ***29***(2), 95–103.

Dufresne, A., Salanoubat, M., Dé, F., Partensky, R., Artiguenave, F., Axmann, I. M., Rie Barbe, V., Duprat, S., Galperin, M. Y., Koonin, E. V, Le Gall, F., Makarova, K. S., Ostrowski, M., Oztas, S., Robert, C., Rogozin, I. B., Scanlan, D. J., Tandeau De Marsac, N., Weissenbach, J., … Hess, W. R. (2003). Genome sequence of the cyanobacterium *Prochlorococcus marinus* SS120, a nearly minimal oxyphototrophic genome. *PNAS*, ***100***(17), 10020–10025.

Durall, C., & Lindblad, P. (2015). Mechanisms of carbon fixation and engineering for increased carbon fixation in cyanobacteria. *Algal Research*, ***11***, 263-270.

Edwards, Y. J. K., & Perkins, S. J. (1995). The protein fold of the von Willebrand factor type A domain is predicted to be similar to the open twisted β-sheet flanked by α-helices found in human ras-p21. *FEBS Letters*, ***358***(3), 283–286.

Eisenhut, M., Ruth, W., Haimovich, M., Bauwe, H., Kaplan, A., & Hagemann, M. (2008). The photorespiratory glycolate metabolism is essential for cyanobacteria and might have been conveyed endosymbiontically to plants. *PNAS,* ***105***(44), 17199–17204.

Eisenhut, M., Von Wobeser, E. A., Jonas, L., Schubert, H., Ibelings, B. W., Bauwe, H., Matthijs, H. C. P., & Hagemann, M. (2007). Long-term response toward inorganic carbon limitation in wild type and glycolate turnover mutants of the cyanobacterium *Synechocystis* sp. strain PCC 6803. *Plant Physiology*, ***144***(4), 1946–1959.

Elsholz, A. K. W., Turgay, K., Michalik, S., Hessling, B., Gronau, K., Oertel, D., Mäder, U., Bernhardt, J., Becher, D., Hecker, M., & Gerth, U. (2012). Global impact of protein arginine phosphorylation on the physiology of *Bacillus subtilis*. *PNAS*, ***109***(19), 7451–7456.

Enami, M., & Ishihama, A. (1984). Protein Phosphorylation in *Escherichia coli* and Purification of a Protein Kinase. *The Journal of Biological Chemistry*, ***259*****(**1), 526–533.

Figge, R. M., Cassier-Chauvat, C., Chauvat, F., & Cerff, R. (2001). Characterization and analysis of an NAD(P)H dehydrogenase transcriptional regulator critical for the survival of cyanobacteria facing inorganic carbon starvation and osmotic stress. *Molecular Microbiology*, ***39***(2), 455–469.

Fijalkowska, I. J., Schaaper, R. M., & Jonczyk, P. (2012). DNA replication fidelity in *Escherichia coli*: a multi-DNA polymerase affair. *FEMS Microbiology Reviews*, ***36***(6), 1105–1121.

Flügel, F., Timm, S., Arrivault, S., Florian, A., Stitt, M., Fernie, A. R., & Bauwe, H. (2017). The Photorespiratory Metabolite 2-Phosphoglycolate Regulates Photosynthesis and Starch Accumulation in Arabidopsis. *The Plant Cell*, ***29***(10), 2537–2551.

Forchhammer, K., & Lüddecke, J. (2016). Sensory properties of the PII signalling protein family. *FEBS Journal*, ***283***(3), 425–437.

Forchhammer, K., & Selim, K. A. (2019). Carbon/nitrogen homeostasis control in cyanobacteria. *FEMS Microbiology Reviews*, ***44***(1), 33-53.

Forchhammer, K., Selim, K. A., & Huergo, L. F. (2022). New views on PII signaling: from nitrogen sensing to global metabolic control. *Trends in Microbiology*, **2053**.

Forchhammer, K., & Tandeau De Marsac, N. (1994). The PII Protein in the Cyanobacterium *Synechococcus* sp. Strain PCC 7942 Is Modified by Serine Phosphorylation and Signals the Cellular N-Status. *Journal of Bacteriology*, ***176***(1), 84–91.

Fuhrmann, J., Schmidt, A., Spiess, S., Lehner, A., Turgay, K., Mechtler, K., Charpentier, E., & Clausen, T. (2009). McsB Is a protein arginine kinase that phosphorylates and inhibits the heat-shock regulator CtsR. *Science*, ***324***(5932), 1323–1327.

Fuhrmann, J., Subramanian, V., Kojetin, D. J., & Thompson, P. R. (2016). Activity-Based Profiling Reveals a Regulatory Link between Oxidative Stress and Protein Arginine Phosphorylation. *Cell Chemical Biology*, ***23***(8), 967–977.

Fuhrmann, J., Subramanian, V., & Thompson, P. R. (2013). Targeting the arginine phosphatase YwlE with a catalytic redox-based inhibitor. *ACS Chemical Biology*, ***8***(9), 2024–2032.

Galkin, A. N., Mikheeva, L. E., & Shestakov, S. V. (2003). The insertional inactivation of genes encoding eukaryotic-type serine/threonine protein kinases in the cyanobacterium *Synechocystis* sp. PCC 6803. *Microbiology*, ***72***, 52–57.

Gao, L., Shen, C., Liao, L., Huang, X., Liu, K., Wang, W., Guo, L., Jin, W., Huang, F., Xu, W., & Wang, Y. (2014). Functional proteomic discovery of Slr0110 as a central regulator of carbohydrate metabolism in *Synechocystis* species PCC6803. *Molecular and Cellular Proteomics*, ***13***(1), 204–219.

Gao, Z., Zhao, H., Li, Z., Tan, X., & Lu, X. (2012). Photosynthetic production of ethanol from carbon dioxide in genetically engineered cyanobacteria. *Energy and Environmental Science*, ***5***(12), 9857–9865.

Garci´a, M., Domi´nguez, G.-D., Reyes, J. C., & Florencio, F. J. (1999). Glutamine synthetase inactivation by protein–protein interaction. *PNAS,* ***96***(13), 7161–7166.

Gärtner, K., Klähn, S., Watanabe, S., Mikkat, S., Scholz, I., Hess, W. R., & Hagemann, M. (2019). Cytosine N4-Methylation via M. Ssp6803II Is Involved in the Regulation of Transcription, Fine-Tuning of DNA Replication and DNA Repair in the Cyanobacterium *Synechocystis* sp. PCC 6803. *Frontiers in Microbiology*, *10*, 1233.

Giner-Lamia, J., López-Maury, L., Reyes, J. C., & Florencio, F. J. (2020). The CopRS Two-Component System Is Responsible for Resistance to Copper in the Cyanobacterium *Synechocystis* sp. PCC 6803. *Plant physiology*, ***159***(4), 1806–1818.

Grangeasse, C., Nessler, S., & Mijakovic, I. (2012). Bacterial tyrosine kinases: Evolution, biological function and structural insights. In *Philosophical Transactions of the Royal Society B: Biological Sciences,* ***367***(1602), 2640–2655.

Grigorieva, G., & Shestakov, S. (1982). Transformation in the cyanobacterium *Synechocystis* sp. 6803. *FEMS Microbiology Letters*, ***13***(4), 367–370.

Gross, R., Aricò, B., & Rappuoli, R. (1989). Families of bacterial signal-transducing proteins. In *Molecular Microbiology,* ***3***(11), 1661–1667.

Gründel, M., Scheunemann, R., Lockau, W., & Zilliges, Y. (2012). Impaired glycogen synthesis causes metabolic overflow reactions and affects stress responses in the cyanobacterium *Synechocystis* sp. PCC 6803. *Microbiology,* ***158***(12), 3032–3043.

Gurrieri, L., Fermani, S., Zaffagnini, M., Sparla, F., & Trost, P. (2021). Calvin–Benson cycle regulation is getting complex. *Trends in Plant Science*, ***26***(9), 898–912.

Hackenberg, C., Huege, J., Engelhardt, A., Wittink, F., Laue, M., Matthijs, H. C. P., Kopka, J., Bauwe, H., & Hagemann, M. (2012). Low-carbon acclimation in carboxysome-less and photorespiratory mutants of the cyanobacterium *Synechocystis* sp. strain PCC 6803. *Microbiology*, ***158***(2), 398–413.

Hagemann, M., Golldack, D., Biggins, J., & Erdmann, N. (1993). Salt-dependent protein phosphorylation in the cyanobacterium *Synechocystis* PCC 6803. *FEMS Microbiology Letters*, ***113***(2), 205–209.

Hagemann, M., & Hess, W. R. (2018). Systems and synthetic biology for the biotechnological application of cyanobacteria. *Current Opinion in Biotechnology*, ***49***, 94–99.

Hagemann, M., Song, S., & Brouwer, E.-M. (2021). Inorganic Carbon Assimilation in Cyanobacteria: Mechanisms, Regulation, and Engineering. *Cyanobacteria Biotechnology,* 1–31.

Hakkila, K., Antal, T., Rehman, A. U., Kurkela, J., Wada, H., Vass, I., Tyystjärvi, E., & Tyystjärvi, T. (2013). Oxidative stress and photoinhibition can be separated in the cyanobacterium *Synechocystis* sp. PCC 6803. *BBA,* ***1837***(2), 217–225.

Hanks, S. K. (2003). Genomic analysis of the eukaryotic protein kinase superfamily: A perspective. *Genome biology*, ***4***, 1–7.

Hanks, S. K., & Hunter, T. (1995). The eukaryotic protein kinase superfamily: kinase (catalytic) domain structure and classification. *The FASEB Journal*, ***9***(8), 576–596.

Hanks, S. K., Quinn, A. M., & Hunter, T. (1988). The protein kinase family: Conserved features and deduced phylogeny of the catalytic domains. *Science*, ***241***(4861), 42–52.

Havaux, M., Guedeney, G., He, Q., & Grossman, A. R. (2003). Elimination of high-light-inducible polypeptides related to eukaryotic chlorophyll a/b-binding proteins results in aberrant photoacclimation in *Synechocystis* PCC6803. *BBA*, ***1557***, 21–33.

He, Z., & Mi, H. (2016). Functional Characterization of the Subunits N, H, J, and O of the NAD(P)H Dehydrogenase Complexes in *Synechocystis* sp. Strain PCC 6803. *Plant Physiology*, ***171***(2), 1320–1332.

Helman, Y., Tchernov, D., Reinhold, L., Shibata, M., Ogawa, T., Schwarz, R., Ohad, I., & Kaplan, A. (2003). Genes encoding A-type flavoproteins are essential for photoreduction of O2 in cyanobacteria. *Current Biology*, ***13***(3), 230–235.

Hernández-Prieto, M. A., Schön, V., Georg, J., Barreira, L., Varela, J., Hess, W. R., & Futschik, M. E. (2012). Iron Deprivation in *Synechocystis*: Inference of Pathways, Non-coding RNAs, and Regulatory Elements from Comprehensive Expression Profiling. *G3: Genes| Genomes| Genetics*, ***2***(12), 1475–1495.

Herva Ä, M. S., Ä Navarro, J. A., & De La Rosa, M. A. (2003). Electron Transfer between Membrane Complexes and Soluble Proteins in Photosynthesis. *Accounts of Chemical Research*, ***36***(10), 798–805.

Hihara, Y., Sonoike, K., Kanehisa, M., & Ikeuchi, M. (2003). DNA microarray analysis of redox-responsive genes in the genome of the cyanobacterium *Synechocystis* sp. strain PCC 6803. *Journal of Bacteriology*, ***185***(5), 1719–1725.

Hill, R., & Bendall, F. (1960). Function of the two cytochrome components in chloroplasts: a working hypothesis. *Nature*, ***186***(4719), 136–137.

Hirakawa, H., Kurushima, J., Hashimoto, Y., & Tomita, H. (2020). Progress overview of bacterial two-component regulatory systems as potential targets for antimicrobial chemotherapy. *Antibiotics*, ***9***(10), 635.

Hisbergues, M. (2001). A noncanonical WD-repeat protein from the cyanobacterium *Synechocystis* PCC6803: Structural and functional study. *Protein Science*, ***10***(2), 293–300.

Hohmann-Marriott, M. F., & Blankenship, R. E. (2011). Evolution of Photosynthesis. *Annual Review of Plant Biology*, ***62***, 515–548.

Houmard, J. (1995). How Do Cyanobacteria Perceive and Adjust to Their Environment?. *Molecular Ecology of Aquatic Microbes*, 153-170, Springer Berlin Heidelberg.

Huang, C., Duan, X., Ge, H., Xiao, Z., Zheng, L., Wang, G., Dong, J., Wang, Y., Zhang, Y., Huang, X., An, H., Xu, W., & Wang, Y. (2023). Parallel proteomic comparison of mutants with altered carbon metabolism reveals Hik8 regulation of PII phosphorylation and glycogen accumulation in a cyanobacterium. *Molecular & Cellular Proteomics*, **100582**.

Huang, L., McCluskey, M. P., Ni, H., & LaRossa, R. A. (2002). Global gene expression profiles of the cyanobacterium *Synechocystis* sp. strain PCC 6803 in response to irradiation with UV-B and white light. *Journal of Bacteriology*, ***184***(24), 6845–6858.

Huang, S., Chen, L., Te, R., Qiao, J., Wang, J., & Zhang, W. (2013). Complementary iTRAQ proteomics and RNA-seq transcriptomics reveal multiple levels of regulation in response to nitrogen starvation in *Synechocystis* sp. PCC 6803. *Molecular BioSystems*, ***9***(10), 2565–2574.

Hunter, T. (1991). [1] Protein kinase classification. *Methods in enzymology*, ***200***, 3–37.

Hunter, T. (2012). Why nature chose phosphate to modify proteins. *Philosophical Transactions of the Royal Society B: Biological Sciences*, ***367***(1602), 2513–2516.

Huse, M., & Kuriyan, J. (2002). The conformational plasticity of protein kinases. *Cell*, ***109***(3), 275–282.

Iijima, H., Shirai, T., Okamoto, M., Kondo, A., Yokota Hirai, M., & Osanai, T. (2015). Changes in primary metabolism under light and dark conditions in response to overproduction of a response regulator RpaA in the unicellular cyanobacterium *Synechocystis* sp. PCC 6803. *Frontiers in Microbiology*, ***6***, 888.

Ikeuchi, M., & Satoshi Tabata, &. (2001). *Synechocystis* sp. PCC 6803–a useful tool in the study of the genetics of cyanobacteria. *Photosynthesis Research*, ***70***, 73–83.

Irmler, A., & Forchhammer, K. (2001). A PP2C-type phosphatase dephosphorylates the PII signaling protein in the cyanobacterium *Synechocystis* PCC 6803. *PNAS*, ***98***(23), 12978–12983.

Jablonsky, J., Papacek, S., & Hagemann, M. (2016). Different strategies of metabolic regulation in cyanobacteria: From transcriptional to biochemical control. *Scientific Reports*, ***6***(1), 33024.

Janczarek, M., Vinardell, J. M., Lipa, P., & Karaś, M. (2018). Hanks-type serine/threonine protein kinases and phosphatases in bacteria: Roles in signaling and adaptation to various environments. *International journal of molecular sciences*, ***19***(10), 2872.

Junker, S., Maa, S., Otto, A., Michalik, S., Morgenroth, F., Gerth, U., Hecker, M., & Becher, D. (2018). Spectral Library Based Analysis of Arginine Phosphorylations in *Staphylococcus aureus*. *Molecular and Cellular Proteomics*, ***17***(2), 335–348.

Kaiser, S., Hoppstädter, L. M., Bilici, K., Heieck, K., Brückner, R., & Siemens Chair, W. (2020). Control of acetyl phosphate-dependent phosphorylation of the response regulator CiaR by acetate kinase in *Streptococcus pneumoniae*. *Microbiology*, ***166***(4), 411–421.

Kamei, A., Yoshihara, S., Yuasa, T., Geng, X., & Ikeuchi, M. (2003). Biochemical and functional characterization of a eukaryotic-type protein kinase, SpkB, in the cyanobacterium *Synechocystis* sp. PCC 6803. *Current Microbiology*, ***46***(4), 296–301.

Kamei, A., Yuasa, T., Geng, X., & Ikeuchi, M. (2002). Biochemical Examination of the Potential Eukaryotic-type Protein Kinase Genes in the Complete Genome of the Unicellular Cyanobacterium *Synechocystis* sp. PCC 6803. *DNA research*, ***9***(3), 71–78.

Kamei, A., Yuasa, T., Orikawa, K., Geng, X. X., & Ikeuchi, M. (2001). A eukaryotic-type protein kinase, SpkA, is required for normal motility of the unicellular Cyanobacterium *Synechocystis* sp. strain PCC 6803. *Journal of Bacteriology*, ***183***(5), 1505–1510.

Kaneko, T., Sato, S., Kotani, H., Tanaka, A., Asamizu, E., Nakamura, Y., Yasuda, M., Miyajima, N., Hirosawa, M., Hosouchi, T., Wada, T., Shimpo, S., Nakazaki, N., Kimura, T., Sugiura, M., Takeuchi, C., Sasamoto, S., Naruo, K., Watanabe, A., … Tabata, S. (1996). Sequence Analysis of the Genome of the Unicellular Cyanobacterium *Synechocystis* sp. Strain PCC6803. II. Sequence Determination of the Entire Genome and Assignment of Potential Protein-coding Regions. *DNA Research*, ***3***(3), 109–136.

Kaneko, T., & Tabata, S. (1997). Complete genome structure of the unicellular cyanobacterium *Synechocystis* sp. PCC6803. *Plant and Cell Physiology*, ***38***(11), 1171–1176.

Kannan, N., Taylor, S. S., Zhai, Y., Venter, J. C., & Manning, G. (2007). Structural and Functional Diversity of the Microbial Kinome. *PLoS biology*, ***5***(3), e17.

Kasting, J. F., & Siefert, J. L. (2002). Life and the evolution of Earth's atmosphere. *Science*, ***296***(5570), 1066–1068.

Kelly, C. L., Taylor, G. M., Hitchcock, A., Torres-Méndez, A., & Heap, J. T. (2018). A Rhamnose-Inducible System for Precise and Temporal Control of Gene Expression in Cyanobacteria. *ACS Synthetic Biology*, ***7***(4), 1056–1066.

Kennelly, P. J. (2002). Protein kinases and protein phosphatases in prokaryotes: a genomic perspective. *FEMS Microbiology Letters*, ***206***(1), 1–8.

Kermgard, E., Yang, Z., Michel, A.-M., Simari, R., Wong, J., Ibba, M., & Lazazzera, B. A. (2017). Quality Control by Isoleucyl-tRNA Synthetase of *Bacillus subtilis* Is Required for Efficient Sporulation. *Scientific Reports*, ***7***(1), 41763.

Kim, Y. H., Park, Y. M., Kim, S. J., Park, Y. Il, Choi, J. S., & Chung, Y. H. (2004). The role of Slr1443 in pilus biogenesis in *Synechocystis* sp. PCC 6803: Involvement in post-translational modification of pilins. *Biochemical and Biophysical Research Communications*, ***315***(1), 179–186.

King, D. T., Zhu, S., Hardie, D. B., Serrano-Negrón, J. E., Madden, Z., Kolappan, S., & Vocadlo, D. J. (2022). Chemoproteomic identification of CO2-dependent lysine carboxylation in proteins. *Nature Chemical Biology*, ***18***(7), 782–791.

Kizawa, A., Kawahara, A., Takimura, Y., Nishiyama, Y., & Hihara, Y. (2016). RNA-seq Profiling Reveals Novel Target Genes of LexA in the Cyanobacterium *Synechocystis* sp. PCC 6803. *Frontiers in Microbiology, **7**, 193.*

Klähn, S., Mikkat, S., Riediger, M., Georg, J., Hess, W. R., & Hagemann, M. (2021). Integrative analysis of the salt stress response in cyanobacteria. *Biology Direct*, ***16***(1), 26.

Klähn, S., Orf, I., Schwarz, D., Matthiessen, J. K. F., Kopka, J., Hess, W. R., & Hagemann, M. (2015). Integrated transcriptomic and metabolomic characterization of the low-carbon response using an ndhR mutant of *Synechocystis* sp. PCC 6803. *Plant Physiology*, ***169***(3), 1540–1556.

Kobe, B., Kampmann, T., Forwood, J. K., Listwan, P., & Brinkworth, R. I. (2005). Substrate specificity of protein kinases and computational prediction of substrates. *BBA*, ***1754***(1–2), 200–209.

Kobir, A., Shi, L., Boskovic, A., Grangeasse, C., Franjevic, D., & Mijakovic, I. (2011). Protein phosphorylation in bacterial signal transduction. *BBA*, ***1810***(10), 989-994.

Köbler, C., Schultz, S. J., Kopp, D., Voigt, K., & Wilde, A. (2018). The role of the *Synechocystis* sp. PCC 6803 homolog of the circadian clock output regulator RpaA in day–night transitions. *Molecular Microbiology*, ***110***(5), 847–861.

Koch, M., Doello, S., Gutekunst, K., & Forchhammer, K. (2019). PHB is produced from Glycogen turn-over during nitrogen starvation in *Synechocystis* sp. PCC 6803. *International Journal of Molecular Sciences*, ***20***(8), 1942.

Kopf, M., Klähn, S., Scholz, I., Matthiessen, J. K. F., Hess, W. R., & Voß, B. (2014). Comparative analysis of the primary transcriptome of *Synechocystis* sp. PCC 6803. *DNA Research*, ***21***(5), 527–539.

Kornev, A. P., & Taylor, S. S. (2010). Defining the Conserved Internal Architecture of a Protein Kinase. *BBA*, ***1804***(3), 440–444.

Koyano, F., Okatsu, K., Kosako, H., Tamura, Y., Go, E., Kimura, M., Kimura, Y., Tsuchiya, H., Yoshihara, H., Hirokawa, T., Endo, T., Fon, E. A., Trempe, J.-F., Saeki, Y., Tanaka, K., & Matsuda, N. (2014). Ubiquitin is phosphorylated by PINK1 to activate parkin. *Nature*, ***510***(7503), 162–166.

Krebs, H. A. (1970). The History of the Tricarboxylic Acid Cycle. *Perspectives in biology and medicine, **14***(1), 154–172.

Kruip, J., Chitnis, P. R., Lagoutte, B., Rögner, M., & Boekema, E. J. (1997). Structural Organization of the Major Subunits in Cyanobacterial Photosystem 1. *Journal of Biological Chemistry*, ***272***(27), 17061–17069.

Krupa, A., & Srinivasan, N. (2005). Diversity in domain architectures of Ser/Thr kinases and their homologues in prokaryotes. *BMC genomics*, ***6***, 1–20.

Laemmli, U. K. (1970). Cleavage of Structural Proteins during the Assembly of the Head of Bacteriophage T4. *Nature*, ***227***, 680–685.

Laurent, S., Jang, J., Janicki, A., Zhang, C. C., & Bédu, S. (2008). Inactivation of spkD, encoding a Ser/Thr kinase affects the pool of the TCA cycle metabolites in *Synechocystis* sp. strain PCC 6803. *Microbiology*, ***154***(7), 2161–2167.

Lea-Smith, D. J., Bombelli, P., Vasudevan, R., & Howe, C. J. (2016). Photosynthetic, respiratory and extracellular electron transport pathways in cyanobacteria. *BBA*, ***1857***(3), 247–255.

Leonard, C. J., Aravind, L., & Koonin, E. v. (1998). Novel families of putative protein kinases in bacteria and archaea: Evolution of the “eukaryotic” protein kinase superfamily. *Genome Research*, ***8***(10), 1038–1047.

Lévine, A., Vannier, F., Absalon, C., Kuhn, L., Jackson, P., Scrivener, E., Labas, V., Vinh, J., Courtney, P., Garin, J., & Séror, S. J. (2006). Analysis of the dynamic **Bacillus subtilis** Ser/Thr/Tyr phosphoproteome implicated in a wide variety of cellular processes. *Proteomics*, ***6***(7), 2157–2173.

Li, H., Singh, A. K., McIntyre, L. M., & Sherman, L. A. (2004). Differential gene expression in response to hydrogen peroxide and the putative PerR regulon of *Synechocystis* sp. strain PCC 6803. *Journal of Bacteriology*, ***186***(11), 3331–3345.

Liang, C., Zhang, X., Chi, X., Guan, X., Li, Y., Qin, S., & Shao, H. B. (2011). Serine/threonine protein kinase SpkG is a candidate for high salt resistance in the unicellular cyanobacterium *Synechocystis* sp. PCC 6803. *PLoS One*, ***6***(5), e18718.

Liang, W., Yan, F., Wang, M., Li, X., Zhang, Z., Ma, X., Hu, J., Wang, J., & Wang, L. (2021). Comprehensive Phosphoproteomic Analysis of *Nostoc flagelliforme* in Response to Dehydration Provides Insights into Plant ROS Signaling Transduction. *ACS Omega*, ***6***(21), 13554–13566.

Liberton, M., Saha, R., Jacobs, J. M., Nguyen, A. Y., Gritsenko, M. A., Smith, R. D., Koppenaal, D. W., & Pakrasi, H. B. (2016). Global proteomic analysis reveals an exclusive role of thylakoid membranes in bioenergetics of a model cyanobacterium. *Molecular and Cellular Proteomics*, ***15***(6), 2021–2032.

Lindberg, P., Park, S., & Melis, A. (2010). Engineering a platform for photosynthetic isoprene production in cyanobacteria, using *Synechocystis* as the model organism. *Metabolic Engineering*, *12*(1), 70–79.

Liu, J., Chen, L., Wang, J., Qiao, J., & Zhang, W. (2012). Proteomic analysis reveals resistance mechanism against biofuel hexane in *Synechocystis* sp. PCC 6803. *Biotechnology for biofuels*, ***5***(1), 1–17.

Liu, X., Sheng, J., & Curtiss, R. (2011). Fatty acid production in genetically modified cyanobacteria. *PNAS*, ***108***(17), 6899–6904.

Liu, Y., Beyer, A., & Aebersold, R. (2016). On the Dependency of Cellular Protein Levels on mRNA Abundance. *Cell*, ***165***(3), 535–550.

Liu, Z. X., Li, H. C., Wei, Y. P., Chu, W. Y., Chong, Y. L., Long, X. H., Liu, Z. P., Qin, S., & Shao, H. B. (2015). Signal transduction pathways in *Synechocystis* sp. PCC 6803 and biotechnological implications under abiotic stress. *Critical reviews in biotechnology*, ***35***(2), 269–280.

Los, D. A., Zorina, A., Sinetova, M., Kryazhov, S., Mironov, K., & Zinchenko, V. V. (2010). Stress sensors and signal transducers in cyanobacteria. *Sensors*, ***10***(3), 2386–2415.

Lucius, S., Makowka, A., Michl, K., Gutekunst, K., & Hagemann, M. (2021). The Entner-Doudoroff Pathway Contributes to Glycogen Breakdown During High to Low CO2 Shifts in the Cyanobacterium *Synechocystis* sp. PCC 6803. *Frontiers in Plant Science*, ***12***, 787943.

Lucius, S., Theune, M., Arrivault, S., Hildebrandt, S., Mullineaux, C. W., Gutekunst, K., & Hagemann, M. (2022). CP12 fine-tunes the Calvin-Benson cycle and carbohydrate metabolism in cyanobacteria. *Frontiers in Plant Science*, ***13***, 1028794.

Lundquist, P. K., Davis, J. I., & van Wijk, K. J. (2012). ABC1K atypical kinases in plants: Filling the organellar kinase void. *Trends in plant science*, ***17***(9), 546–555.

MacColl, R. (2004). Allophycocyanin and energy transfer. *BBA* ***657***(2-3), 73–81.

Macek, B., Forchhammer, K., Hardouin, J., Weber-Ban, E., Grangeasse, C., & Mijakovic, I. (2019). Protein post-translational modifications in bacteria. *Nature Reviews,* ***17***(11), 651-664.

Macek, B., Gnad, F., Soufi, B., Kumar, C., Olsen, J. V, Mijakovic, I., & Mann, M. (2008). Phosphoproteome Analysis of *E. coli* Reveals Evolutionary Conservation of Bacterial Ser/Thr/Tyr Phosphorylation. *Molecular & Cellular Proteomics*, ***7***(2), 299–307.

Macek, B., & Mijakovic, I. (2011). Site-specific analysis of bacterial phosphoproteomes. *Proteomics*, ***11***(15), 3002–3011.

Macek, B., Mijakovic, I., Olsen, J. V., Gnad, F., Kumar, C., Jensen, P. R., & Mann, M. (2007). The serine/threonine/tyrosine phosphoproteome of the model bacterium *Bacillus subtilis*. *Molecular and Cellular Proteomics*, ***6***(4), 697–707.

Makowka, A., Nichelmann, L., Schulze, D., Spengler, K., Wittmann, C., Forchhammer, K., & Gutekunst, K. (2020). Glycolytic Shunts Replenish the Calvin-Benson-Bassham Cycle as Anaplerotic Reactions in Cyanobacteria. *Molecular Plant*, ***13***(3), 471–482.

Mandell, Z. F., Oshiro, R. T., Yakhnin, A. V., Vishwakarma, R., Kashlev, M., Kearns, D. B., & Babitzke, P. (2021). NusG is an intrinsic transcription termination factor that stimulates motility and coordinates gene expression with NusA. *Elife,* ***10,*** e61880.

Mann, N. H. (1994). Protein phosphorylation in cyanobacteria. *Microbiology*, *140*(12), 3207–3321.

Mann, N. H., Rippka, R., & Herdman, M. (1991). Regulation of protein phosphorylation in the cyanobacterium *Anabaena* strain PCC 7120. *Microbiology,* ***137***(2), 331-339.

Mantovani, O., Haffner, M., Selim, K. A., Hagemann, M., & Forchhammer, K. (2023). Roles of second messengers in the regulation of cyanobacterial physiology: the carbon-concentrating mechanism and beyond. *Microlife*, ***4***, uqad008.

Mantovani, O., Reimann, V., Haffner, M., Herrmann, F. P., Selim, K. A., Forchhammer, K., Hess, W. R., & Hagemann, M. (2022). The impact of the cyanobacterial carbon-regulator protein SbtB and of the second messengers cAMP and c-di-AMP on CO2-dependent gene expression. *New Phytologist*, ***234***(5), 1801–1816.

Marteyn, B., Domain, F., Legrain, P., Chauvat, F., & Cassier-Chauvat, C. (2009). The thioredoxin reductase-glutaredoxins-ferredoxin crossroad pathway for selenate tolerance in *Synechocystis* PCC6803. *Molecular Microbiology*, ***71***(2), 520–532.

Mata-Cabana, A., García-Domínguez, M., Florencio, F. J., & Lindahl, M. (2012). Thiol-based redox modulation of a cyanobacterial eukaryotic-type serine/threonine kinase required for oxidative stress tolerance. *Antioxidants and Redox Signaling*, ***17***(4), 521–533.

McFarlane, C. R., Shah, N. R., Kabasakal, B. V., Echeverria, B., Cotton, C. A. R., Bubeck, D., & Murray, J. W. (2019). Structural basis of light-induced redox regulation in the Calvin–Benson cycle in cyanobacteria. *PNAS*, ***116***(42), 20984–20990.

Meeks, J. C., Wolk, $ C Peter, Thomas, J., Lockau, W., Shaffer, P. W., Austin, S. M., Chien, W.-S., & Galonsky, A. (1977). The pathways of assimilation of 13NH4+ by the cyanobacterium *Anabaena cylindrica*. *Journal of Biological Chemistry*, *252*(21), 7894.

Meetam, M., Keren, N., Ohad, I., & Pakrasi, H. B. (1992). The PsbY Protein Is Not Essential for Oxygenic Photosynthesis in the Cyanobacterium *Synechocystis* sp. PCC 6803. *Plant Physiology*, ***121***(4), 1267–1272.

Mertins, P., Yang, F., Liu, T., Mani, D. R., Petyuk, V. A., Gillette, M. A., Clauser, K. R., Qiao, J. W., Gritsenko, M. A., Moore, R. J., Levine, D. A., Townsend, R., Erdmann-Gilmore, P., Snider, J. E., Davies, S. R., Ruggles, K. V., Fenyo, D., Kitchens, R. T., Li, S., … Carr, S. A. (2014). Ischemia in tumors induces early and sustained phosphorylation changes in stress kinase pathways but does not affect global protein levels. *Molecular and Cellular Proteomics*, ***13***(7), 1690–1704.

Mijakovic, I., Grangeasse, C., & Urs¸adurs¸ad Turgay, K. (2016). Exploring the diversity of protein modifications: special bacterial phosphorylation systems. *FEMS Microbiology Reviews*, ***40***(3), 398–417.

Mijakovic, I., & Macek, B. (2012). Impact of phosphoproteomics on studies of bacterial physiology. *FEMS microbiology reviews, **36***(4), 877–892.

Mikkat, S., Fulda, S., & Hagemann, M. (2014). A 2D gel electrophoresis-based snapshot of the phosphoproteome in the cyanobacterium *Synechocystis* sp. strain PCC 6803. *Microbiology, **160***(2), 296–306.

Miller, C. J., & Turk, B. E. (2018). Homing in: mechanisms of substrate targeting by protein kinases HHS Public Access. *Trends in biochemical sciences*, ***43***(5), 380–394.

Mills, L. A., McCormick, A. J., & Lea-Smith, D. J. (2020). Current knowledge and recent advances in understanding metabolism of the model cyanobacterium *Synechocystis* sp. PCC 6803. *Bioscience Reports*, ***40***(4), BSR20193325.

Minguez, P., Parca, L., Diella, F., Mende, D. R., Kumar, R., Helmer-Citterich, M., Gavin, A.-C., van Noort, V., & Bork, P. (2012). Deciphering a global network of functionally associated post-translational modifications. *Molecular Systems Biology*, *8*, 599.

Mitchell, P. (1961). Coupling of phosphorylation to electron and hydrogen transfer by a chemi-osmotic type of mechanism. *Nature*, ***191***(4784), 144–148.

Mondal, S., & Singh, S. P. (2022). Flow Cytometry-based Measurement of Reactive Oxygen Species in Cyanobacteria. *Bio-protocol*, ***12***(10), e4417-e4417.

Montesinos, M. L., Muro-Pastor, A. M., Herrero, A., & Flores, E. (1998). Ammonium/Methylammonium Permeases of a Cyanobacterium. *Journal of Biological Chemistry*, ***273***(47), 31463–31470.

Morrison, S. S., Mullineaux, C. W., & Ashby, M. K. (2005). The influence of acetyl phosphate on DspA signalling in the cyanobacterium *Synechocystis* sp. PCC6803. *BMC microbiology*, ***5***(1), 1–8.

Mullineaux, C. W., & Allen, J. F. (1988). Fluorescence induction transients indicate dissociation of Photosystem II from the phycobilisome during the State-2 transition in the cyanobacterium *Synechococcus* 6301. *BBA*, ***934***(1), 96–107.

Mullineaux, C. W., Tobin, M. J., & Jones, G. R. (1997). Mobility of photosynthetic complexes in thylakoid membranes. *Nature*, ***390***(6658), 421–424.

Muñoz-Dorado, J., Inouye, S., & Inouye, M. (1991). A gene encoding a protein serine/threonine kinase is required for normal development of *M. xanthus*, a gram-negative bacterium. *Cell*, ***67***(5), 995–1006.

Mustila, H., Muth-Pawlak, D., Aro, E. M., & Allahverdiyeva, Y. (2021). Global proteomic response of unicellular cyanobacterium *Synechocystis* sp. PCC 6803 to fluctuating light upon CO2 step-down. *Physiologia Plantarum*, ***173***(1), 305–320.

Muth-Pawlak, D., Kreula, S., Gollan, P. J., Huokko, T., Allahverdiyeva, Y., & Aro, E. M. (2022). Patterning of the Autotrophic, Mixotrophic, and Heterotrophic Proteomes of Oxygen-Evolving Cyanobacterium *Synechocystis* sp. PCC 6803. *Frontiers in Microbiology*, ***13***, 891-895.

Nakajima, M., Imai, K., Ito, H., Nishiwaki, T., Murayama, Y., Iwasaki, H., Oyama, T., & Kondo, T. (2005). Reconstitution of circadian oscillation of cyanobacterial KaiC phosphorylation in vitro. *Science*, ***308***(5720), 414–415.

Neumann, N., Friz, S., & Forchhammer, K. (2022). Glucose-1,6-Bisphosphate, a Key Metabolic Regulator, Is Synthesized by a Distinct Family of α-Phosphohexomutases Widely Distributed in Prokaryotes. *MBio*, ***13***(4), e01469-22.

Nikkanen, L., Solymosi, D., Jokel, M., & Allahverdiyeva, Y. (2021). Regulatory electron transport pathways of photosynthesis in cyanobacteria and microalgae: Recent advances and biotechnological prospects. *Physiologia Plantarum*, ***173***(2), 514–525.

Ohashi, Y., Shi, W., Takatani, N., Aichi, M., Maeda, S.-I., Watanabe, S., Yoshikawa, H., & Omata, T. (2011). Regulation of nitrate assimilation in cyanobacteria. *Journal of Experimental Botany*, ***62***(4), 1411–1424.

Olsen, J. v., & Mann, M. (2013). Status of large-scale analysis of posttranslational modifications by mass spectrometry. *Molecular & cellular proteomics*, ***12***(12), 3444-3452.

Omata, T., Gohta, S., Takahashi, Y., Harano, Y., & Maeda, S. I. (2001). Involvement of a CbbR homolog in low CO2-induced activation of the bicarbonate transporter operon in cyanobacteria. *Journal of Bacteriology*, ***183***(6), 1891–1898.

Omata, T., Price, G. D., Badger, M. R., Okamura, M., Gohta, S., & Ogawa, T. (1999). Identification of an ATP-binding cassette transporter involved in bicarbonate uptake in the cyanobacterium *Synechococcus* sp. strain PCC 7942. *PNAS*, ***96***(23), 13571–13576.

Orf, I., Klähn, S., Schwarz, D., Frank, M., Hess, W. R., Hagemann, M., & Kopka, J. (2015). Integrated Analysis of Engineered Carbon Limitation in a Quadruple CO 2 /HCO 3 2 Uptake Mutant of *Synechocystis* sp. PCC 6803. *Plant Physiology*, ***169***(3), 1787–1806.

Orf, I., Schwarz, D., Kaplan, A., Kopka, J., Hess, W. R., Hagemann, M., & Klähn, S. (2016). CyAbrB2 contributes to the transcriptional regulation of low CO2 acclimation in *Synechocystis* sp. PCC 6803. *Plant and Cell Physiology*, ***57***(10), 2232–2243.

Orf, I., Timm, S., Bauwe, H., Fernie, A. R., Hagemann, M., Kopka, J., & Nikoloski, Z. (2016). Can cyanobacteria serve as a model of plant photorespiration? - A comparative meta-analysis of metabolite profiles. *Journal of experimental botany*, ***67***(10), 2941–2952.

Orthwein, T., Scholl, J., Spät, P., Lucius, S., Koch, M., Macek, B., Hagemann, M., & Forchhammer, K. (2021). The novel P II-interactor PirC identifies phosphoglycerate mutase as key control point of carbon storage metabolism in cyanobacteria. *PNAS*, ***118***(6), e2019988118.

Osanai, T., Imashimizu, M., Seki, A., Sato, S., Tabata, S., Imamura, S., Asayama, M., Ikeuchi, M., & Tanaka, K. (2009). ChlH, the H subunit of the Mg-chelatase, is an anti-sigma factor for SigE in *Synechocystis* sp. PCC 6803. *PNAS*, ***106***(16), 6860–6865.

Osanai, T., Kanesaki, Y., Nakano, T., Takahashi, H., Asayama, M., Shirai, M., Kanehisa, M., Suzuki, I., Murata, N., & Tanaka, K. (2005). Positive regulation of sugar catabolic pathways in the cyanobacterium *Synechocystis* sp. PCC 6803 by the group 2 σ factor SigE. *Journal of Biological Chemistry*, ***280***(35), 30653–30659.

Osanai, T., Oikawa, A., Azuma, M., Tanaka, K., Saito, K., Hirai, M. Y., & Ikeuchi, M. (2011). Genetic engineering of group 2 σ factor SigE widely activates expressions of sugar catabolic genes in *Synechocystis* species PCC 6803. *Journal of Biological Chemistry*, ***286***(35), 30962–30971.

Osanai, T., Oikawa, A., Numata, K., Kuwahara, A., Iijima, H., Doi, Y., Saito, K., & Hirai, M. Y. (2014). Pathway-level acceleration of glycogen catabolism by a response regulator in the cyanobacterium *Synechocystis* species PCC 6803. *Plant Physiology*, ***164***(4), 1831–1841.

Osanai, T., Shirai, T., Iijima, H., Kuwahara, A., Suzuki, I., Kondo, A., & Hirai, M. Y. (2015). Alteration of cyanobacterial sugar and amino acid metabolism by overexpression hik8, encoding a KaiC-associated histidine kinase. *Environmental Microbiology*, ***17***(7), 2430–2440.

Pade, N., Erdmann, S., Enke, H., Dethloff, F., Dühring, U., Georg, J., Wambutt, J., Kopka, J., Hess, W. R., Zimmermann, R., Kramer, D., & Hagemann, M. (2016). Insights into isoprene production using the cyanobacterium *Synechocystis* sp. PCC 6803. *Biotechnology for Biofuels*, ***9***, 1–16.

Pade, N., & Hagemann, M. (2015). Salt acclimation of cyanobacteria and their application in biotechnology. *Life*, ***5***(1), 25–49.

Paithoonrangsarid, K., Shoumskaya, M. A., Kanesaki, Y., Satoh, S., Tabata, S., Los, D. A., Zinchenko, V. V., Hayashi, H., Tanticharoen, M., Suzuki, I., & Murata, N. (2004). Five histidine kinases perceive osmotic stress and regulate distinct sets of genes in *Synechocystis. Journal of Biological Chemistry*, ***279***(51), 53078–53086.

Panichkin, V. B., Arakawa-Kobayashi, S., Kanaseki, T., Suzuki, I., Los, D. A., Shestakov, S. V., & Murata, N. (2006). Serine/threonine protein kinase SpkA in *Synechocystis* sp. strain PCC 6803 is a regulator of expression of three putative pilA operons, formation of thick pili, and cell motility. *Journal of Bacteriology*, ***188***(21), 7696–7699.

Pattanayak, G. K., Korbinian, R., Osanai, T., Iijima, H., Nakaya, Y., Kuwahara, A., & Hirai, M. Y. (2015). Seawater cultivation of freshwater cyanobacterium *Synechocystis* sp. PCC 6803 drastically alters amino acid composition and glycogen metabolism. *Frontiers in Microbiology*, ***6***, 326.

Pearce, M. J., Mintseris, J., Ferreyra, J., Gygi, S. P., & Darwin, K. H. (2008). Ubiquitin-Like Protein Involved in the Proteasome Pathway of *Mycobacterium tuberculosis*. *Science*, ***322***(5904), 1101–1104.

Peetermans, M., Meyers, S., Liesenborghs, L., Vanhoorelbeke, K., De Meyer, S. F., Vandenbriele, C., Lox, M., Hoylaerts, M. F., Martinod, K., Jacquemin, M., Vanassche, T., & Verhamme, P. (2020). Von Willebrand factor and ADAMTS13 impact on the outcome of *Staphylococcus aureus* sepsis. *Journal of Thrombosis and Haemostasis*, ***18***(3), 722–731.

Pelroy, R. A., & Bassham, J. A. (1972). Photosynthetic and dark carbon metabolism in unicellular blue-green algae. *Archiv Für Mikrobiologie*, ***86***, 25–38.

Pereira, S. F. F., Goss, L., & Dworkin, J. (2011). Eukaryote-Like Serine/Threonine Kinases and Phosphatases in Bacteria. *Microbiology and Molecular Biology Reviews*, ***75***(1), 192–212.

Pérez, J., Castañeda-García, A., Jenke-Kodama, H., Müller, R., & Muñoz-Dorado, J. (2008). Eukaryotic-like protein kinases in the prokaryotes and the myxobacterial kinome. *PNAS*, ***105***(41), 15950–15955.

Phalip, V., & Zhang, C.-C. (2001). HstK, a cyanobacterial protein with both a serine/threonine kinase domain and a histidine kinase domain: implication for the mechanism of signal transduction. *Biochemical Journal*, ***360***(3), 639-644.

Poon, W. W., Davis, D. E., Ha, H. T., Jonassen, T., Rather, P. N., & Clarke, C. F. (2000). Identification of *Escherichia coli* ubiB, a Gene Required for the First Monooxygenase Step in Ubiquinone Biosynthesis. *Journal of bacteriology*, ***182***(18), 5139-5146.

Potel, C. M., Lin, M.-H., Heck, A. J. R., & Lemeer, S. (2018). Widespread bacterial protein histidine phosphorylation revealed by mass spectrometry-based proteomics. *Nature methods,* ***15***(3), 187-190.

Prabakaran, S., Lippens, G., Steen, H., & Gunawardena, J. (2012). Post-translational modification: nature's escape from genetic imprisonment and the basis for dynamic information encoding Reversible phosphorylation as information processing. *Wiley Interdisciplinary Reviews: Systems Biology and Medicine*, ***4***(6), 1–29.

Price, G. D., Pengelly, J. J. L., Forster, B., Du, J., Whitney, S. M., von Caemmerer, S., Badger, M. R., Howitt, S. M., & Evans, J. R. (2013). The cyanobacterial CCM as a source of genes for improving photosynthetic CO2 fixation in crop species. *Journal of Experimental Botany*, ***64***(3), 753–768.

Price, G. D., Woodger, F. J., Badger, M. R., Howitt, S. M., & Tucker, L. (2004). Identification of a SulP-type bicarbonate transporter in marine cyanobacteria. *PNAS*, ***101***(52), 18228–18233.

Radchenko, M., & Merrick, M. (2011). The role of effector molecules in signal transduction by PII proteins. *Biochemical Society Transactions*, ***39***(1), 189–194.

Rae, B. D., Long, B. M., Badger, M. R., & Price, G. D. (2013). Functions, Compositions, and Evolution of the Two Types of Carboxysomes: Polyhedral Microcompartments That Facilitate CO 2 Fixation in Cyanobacteria and Some Proteobacteria. *Microbiology and Molecular Biology Reviews*, ***77***(3), 357–379.

Ramazi, S., & Zahiri, J. (2021). Post-translational modifications in proteins: Resources, tools and prediction methods. *Database*, ***2021***, baab012.

Raven, J. A., Beardall, J., & Sánchez-Baracaldo, P. (2017). The possible evolution and future of CO2-concentrating mechanisms. *Journal of Experimental Botany*, ***68***(14), 3701–3716.

Reed, R. H., & Stewart, W. D. P. (1985). Osmotic adjustment and organic solute accumulation in unicellular cyanobacteria from freshwater and marine habitats. *Marine Biology*, ***88***, 1–9.

Rippka, R., Deruelles, J., Herdman, M., Waterbury, J. B., & Stanier, R. Y. (1979). Generic Assignments, Strain Histories and Properties of Pure Cultures of Cyanobacteria. *Journal of General Microbiology*, ***111***(1), 1–61.

Saha, R., Liu, D., Hoynes-O, A., Liberton, M., Yu, J., Bhattacharyya-Pakrasi, M., Balassy, A., Zhang, F., Seok Moon, T., Maranas, C. D., Pakrasi, H. B., Saha, C. R., & James Tiedje, E. M. (2016). Diurnal Regulation of Cellular Processes in the Cyanobacterium *Synechocystis* sp. Strain PCC 6803: Insights from Transcriptomic, Fluxomic, and Physiological Analyses. *MBio*, ***7***(3), 10-1128.

Sakiyama, T., Araie, H., Suzuki, I., & Shiraiwa, Y. (2011). Functions of a hemolysin-like protein in the cyanobacterium *Synechocystis* sp. PCC 6803. *Archives of Microbiology*, ***193***(8), 565–571.

Sánchez-Riego, A. M., López-Maury, L., Florencio, F. J., & Rouhier, N. (2013). Glutaredoxins are essential for stress adaptation in the cyanobacterium *Synechocystis* sp. PCC 6803. *Frontiers in plant science*, ***4***, 428.

Santana-Sanchez, A., Solymosi, D., Mustila, H., Bersanini, L., Aro, E. M., & Allahverdiyeva, Y. (2019). Flavodiiron proteins 1–to-4 function in versatile combinations in O2 photoreduction in cyanobacteria. *ELife*, ***8***, e45766.

Scheeff, E. D., & Bourne, P. E. (2005). Structural Evolution of the Protein Kinase-Like Superfamily. *PLoS Computational Biology*, ***1***(5), e49.

Scheurer, N. M., Rajarathinam, Y., Timm, S., Köbler, C., Kopka, J., Hagemann, M., & Wilde, A. (2021). Homologs of Circadian Clock Proteins Impact the Metabolic Switch Between Light and Dark Growth in the Cyanobacterium *Synechocystis* sp. PCC 6803. *Frontiers in Plant Science*, ***12,*** 675227.

Schlebusch, M., & Forchhammer, K. (2010). Requirement of the Nitrogen Starvation-Induced Protein Sll0783 for Polyhydroxybutyrate Accumulation in **Synechocystis** sp. Strain PCC 6803. *Applied and Environmental Microbiology*, ***76***(18), 6101.

Schmidt, A., Trentini, D. B., Spiess, S., Fuhrmann, J., Ammerer, G., Mechtler, K., & Clausen, T. (2014). Quantitative phosphoproteomics reveals the role of protein arginine phosphorylation in the bacterial stress response. *Molecular and Cellular Proteomics*, ***13***(2), 537–550.

Scholl, J., Dengler, L., Bader, L., & Forchhammer, K. (2020). Phosphoenolpyruvate carboxylase from the cyanobacterium *Synechocystis* sp. PCC 6803 is under global metabolic control by PII signaling. *Molecular Microbiology*, ***114***(2), 292–307.

Schuller, J. M., Saura, P., Thiemann, J., Schuller, S. K., Gamiz-Hernandez, A. P., Kurisu, G., Nowaczyk, M. M., & Kaila, V. R. I. (2020). Redox-coupled proton pumping drives carbon concentration in the photosynthetic complex I. *Nature Communications*, ***11***(1), 494.

Schulze, D., Kohlstedt, M., Becker, J., Cahoreau, E., Peyriga, L., Makowka, A., Hildebrandt, S., Gutekunst, K., Portais, J. C., & Wittmann, C. (2022). GC/MS-based 13C metabolic flux analysis resolves the parallel and cyclic photomixotrophic metabolism of *Synechocystis* sp. PCC 6803 and selected deletion mutants including the Entner-Doudoroff and phosphoketolase pathways. *Microbial Cell Factories*, ***21***(1),69.

Schuster, G., Owens, G. C., Cohen, Y., & Ohad, I. (1984). Thylakoid polypeptide composition and light-independent phosphorylation of the chlorophyll a, b-protein in Prochloron, a prokaryote exhibiting oxygenic photosynthesis. *BBA*, ***767***(3), 596-605.

Schwarz, D., Orf, I., Kopka, J., & Hagemann, M. (2014). Effects of Inorganic Carbon Limitation on the Metabolome of the *Synechocystis* sp. PCC 6803 Mutant Defective in glnB Encoding the Central Regulator PII of Cyanobacterial C/N Acclimation. *Metabolites*, ***4***(2), 232–247.

Selim, K. A., Haase, F., Hartmann, M. D., Hagemann, M., & Forchhammer, K. (2018). PII-like signaling protein SbtB links cAMP sensing with cyanobacterial inorganic carbon response. *PNAS*, ***115***(21), E4861–E4869.

Shalev-Malul, G., Lieman-Hurwitz, J., Viner-Mozzini, Y., Sukenik, A., Gaathon, A., Lebendiker, M., & Kaplan, A. (2008). An AbrB-like protein might be involved in the regulation of cylindrospermopsin production by *Aphanizomenon ovalisporum*. *Environmental Microbiology*, ***10***(4), 988–999.

Shevela, D., Eaton-Rye, J. J., Shen, J.-R., & Govindjee. (2012). Photosystem II and the unique role of bicarbonate: A historical perspective. *BBA*, ***1817***(8), 1134–1151.

Shi, L., Potts, M., & Kennelly, P. J. (1998). The serine, threonine, and/or tyrosine-specific protein kinases and protein phosphatases of prokaryotic organisms: a family portrait. *FEMS Microbiology Reviews*, ***22***(4), 229–253.

Shibata, M., Katoh, H., Sonoda, M., Ohkawa, H., Shimoyama, M., Fukuzawa, H., Kaplan, A., & Ogawa, T. (2002). Genes essential to sodium-dependent bicarbonate transport in cyanobacteria: Function and phylogenetic analysis. *Journal of Biological Chemistry*, ***277***(21), 18658–18664.

Shibata, M., Ohkawa, H., Kaneko, T., Fukuzawa, H., Tabata, S., Kaplan, A., & Ogawa, T. (2001). Distinct constitutive and low-CO2-induced CO2 uptake systems in cyanobacteria: Genes involved and their phylogenetic relationship with homologous genes in other organisms. *PNAS*, ***98***(20), 11789–11794.

Sigalat, C., & Kouchkovsky, Y. (1975). Fractionnement et caractérisation de l'appareil photosynthétique de l'Algue bleue unicellulaire Anacystis nidulans: I. Obtention de fractions membranaires par "lyse osmotique" et analyse pigmentaire. *Physiologie Végétale*, ***13***(2), 243–258.

Singh, A. K., Li, H., & Sherman, L. A. (2004). Microarray analysis and redox control of gene expression in the cyanobacterium *Synechocystis* sp. PCC 6803. *Physiologia Plantarum*, ***120***(1), 27–35.

Singh, A. K., & Sherman, L. A. (2005). Pleiotropic Effect of a Histidine Kinase on Carbohydrate Metabolism in *Synechocystis* sp. Strain PCC 6803 and Its Requirement for Heterotrophic Growth. *Journal of bacteriology,* ***187***(7), 2368-2376.

Singh, N. K., Sonani, R. R., Rastogi, R. P., Madamwar, D., & Patel, S. A. N. (2015). The phycobilisomes: an early requisite for efficient photosynthesis in cyanobacteria. *EXCLI journal*, ***14***, 268.

Sinha, R. K., Komenda, J., Knoppová, J., Sedlářová, M., & Pospíšil, P. (2012). Small CAB-like proteins prevent formation of singlet oxygen in the damaged photosystem II complex of the cyanobacterium *Synechocystis* sp. PCC 6803. *Plant, Cell and Environment*, ***35***(4), 806–818.

Solari, F. A., Dell'Aica, M., Sickmann, A., & Zahedi, R. P. (2015). Why phosphoproteomics is still a challenge. *Molecular BioSystems*, ***11***(6), 1487–1493.

Solymosi, D., Nikkanen, L., Muth-Pawlak, D., Fitzpatrick, D., Vasudevan, R., Howe, C. J., Lea-Smith, D. J., & Allahverdiyeva, Y. (2020). Cytochrome c M Decreases Photosynthesis under Photomixotrophy in *Synechocystis* sp. PCC 6803. *Plant Physiology*, ***183***(2), 700–716.

Spät, P., Barske, T., Maček, B., & Hagemann, M. (2021). Alterations in the CO2 availability induce alterations in the phosphoproteome of the cyanobacterium *Synechocystis* sp. PCC 6803. *The New Phytologist*, ***231***(3), 1123–1137.

Spät, P., Klotz, A., Rexroth, S., Maček, B., & Forchhammer, K. (2018). Chlorosis as a developmental program in cyanobacteria: The proteomic fundament for survival and awakening. *Molecular and Cellular Proteomics*, ***17***(9), 1650–1669.

Spät, P., Krauspe, V., Hess, W. R., Maček, B., & Nalpas, N. (2023). Deep Proteogenomics of a Photosynthetic Cyanobacterium. *Journal of Proteome Research*, ***22***(6), 1969–1983.

Spät, P., Macek, B., & Forchhammer, K. (2015). Phosphoproteome of the cyanobacterium *Synechocystis* sp. PCC 6803 and its dynamics during nitrogen starvation. *Frontiers in Microbiology*, ***6***, 248.

Stancik, I. A., Šestak, M. S., Ji, B., Axelson-Fisk, M., Franjevic, D., Jers, C., Domazet-Lošo, T., & Mijakovic, I. (2018). Serine/Threonine Protein Kinases from Bacteria, Archaea and Eukarya Share a Common Evolutionary Origin Deeply Rooted in the Tree of Life. *Journal of Molecular Biology*, ***430***(1), 27–32.

Steen, H., Fernandez, M., Ghaffari, S., Pandey, A., & Mann, M. (2003). Phosphotyrosine Mapping in Bcr/Abl Oncoprotein Using Phosphotyrosine-specific Immonium Ion Scanning. *Molecular and Cellular Proteomics*, *2*, 138–145.

Steinhauser, D., Fernie, A. R., & Araújo, W. L. (2012). Unusual cyanobacterial TCA cycles: Not broken just different. *Trends in plant science*, ***17***(9), 503–509.

Stock, A. M., Robinson, V. L., & Goudreau, P. N. (2000). Two-component signal transduction. *Annual review of biochemistry*, ***69***(1), 183–215.

Sültemeyer, D., Klughammer, B., Badger, M. R., & Price, G. D. (1998). Fast Induction of High-Affinity HCO3 Transport in Cyanobacteria. *Plant Physiology*, ***116***(1), 183–192.

Sun, F., Ding, Y., Ji, Q., Liang, Z., Deng, X., Wong, C. C. L., Yi, C., Zhang, L., Xie, S., Alvarez, S., Hicks, L. M., Luo, C., Jiang, H., Lan, L., & He, C. (2012). Protein cysteine phosphorylation of SarA/MgrA family transcriptional regulators mediates bacterial virulence and antibiotic resistance. *PNAS*, ***109***(38), 15461–15466.

Sun, N., Han, X., Xu, M., Kaplan, A., Espie, G. S., & Mi, H. (2019). A thylakoid-located carbonic anhydrase regulates CO 2 uptake in the cyanobacterium *Synechocystis* sp. PCC 6803. *New Phytologist*, ***222***(1), 206–217.

Szymanski, C. M., Burr, D. H., & Guerry, P. (2002). Campylobacter Protein Glycosylation Affects Host Cell Interactions. *Infection and Immunity*, ***70***(4), 2242–2244.

Takahashi, H., Uchimiya, H., & Hihara, Y. (2008). Difference in metabolite levels between photoautotrophic and photomixotrophic cultures of *Synechocystis* sp. PCC 6803 examined by capillary electrophoresis electrospray ionization mass spectrometry. *Journal of Experimental Botany*, ***59***(11), 3009–3018.

Tcherkez, G. G. B., Farquhar, G. D., & Andrews, T. J. (2006). Despite slow catalysis and confused substrate specificity, all ribulose bisphosphate carboxylases may be nearly perfectly optimized. *PNAS*, ***103***(19), 7246–7251.

Toth, M., Chow, J. W., Mobashery, S., & Vakulenko, S. B. (2009). Source of Phosphate in the Enzymic Reaction as a Point of Distinction among Aminoglycoside 2”-Phosphotransferases. *Journal of Biological Chemistry*, ***284***(11), 6690-6696.

Toyoshima, M., Tokumaru, Y., Matsuda, F., & Shimizu, H. (2020). Assessment of Protein Content and Phosphorylation Level in *Synechocystis* sp. PCC 6803 under Various Growth Conditions Using Quantitative Phosphoproteomic Analysis. *Molecules, **25**(16), 3582.*

T**rautmann, D., Voß, B., Wilde, A., Al-Babili, S., & Hess, W. R.** (2012). Microevolution in Cyanobacteria: Re-sequencing a Motile Substrain of *Synechocystis* sp. PCC 6803. *DNA Research*, ***19***(6), 435–448.

Trautner, C., & Vermaas, W. F. J. (2013). The *sll1951* Gene encodes the surface layer protein of *Synechocystis* sp. strain PCC 6803. *Journal of Bacteriology*, ***195***(23), 5370–5380.

Udo, H., Munoz-Dorado, J., Inouye, M., & Inouye, S. (1995). *Myxococcus xanthus*, a gram-negative bacterium, contains a transmembrane protein serine/threonine kinase that blocks the secretion of β-lactamase by phosphorylation. *Genes and Development*, ***9***(8), 972–983.

van Heerden, J. H., Bruggeman, F. J., & Teusink, B. (2015). Multi-tasking of biosynthetic and energetic functions of glycolysis explained by supply and demand logic. *BioEssays*, ***37***(1), 34–45.

Vargas-Blanco, D. A., & Shell, S. S. (2020). Regulation of mRNA Stability During Bacterial Stress Responses. *Frontiers in Microbiology*, ***11***, 2111.

Vavilin, D., & Vermaas, W. (2007). Continuous chlorophyll degradation accompanied by chlorophyllide and phytol reutilization for chlorophyll synthesis in *Synechocystis* sp. PCC 6803. *BBA*, ***1767***(7), 920–929.

Vermaas, W. F. (2001). Photosynthesis and respiration in cyanobacteria. *e LS*.

Walsh, C. T., Garneau-Tsodikova, S., & Gatto, G. J. (2005). Protein posttranslational modifications: The chemistry of proteome diversifications. *Angewandte Chemie International Edition*, ***44***(45), 7342–7372.

Wang, H. L., Postier, B. L., & Burnap, R. L. (2004). Alterations in Global Patterns of Gene Expression in *Synechocystis* sp. PCC 6803 in Response to Inorganic Carbon Limitation and the Inactivation of ndhR, a LysR Family Regulator. *Journal of Biological Chemistry*, ***279***(7), 5739–5751.

Wang, H., Yan, X., Aigner, H., Bracher, A., Nguyen, N. D., Hee, W. Y., Long, B. M., Price, G. D., Hartl, F. U., & Hayer-Hartl, M. (2019). Rubisco condensate formation by CcmM in β-carboxysome biogenesis. *Nature*, ***566***(7742), 131–135.

Wang, J., Chen, L., Huang, S., Liu, J., Ren, X., Tian, X., Qiao, J., & Zhang, W. (2012). RNA-seq based identification and mutant validation of gene targets related to ethanol resistance in cyanobacterial *Synechocystis* sp. PCC 6803. *Biotechnology for biofuels*, ***5***(1), 1–18.

Wang, L., Sun, Y.-P., Chen, W.-L., Li, J.-H., & Zhang, C.-C. (2002). Genomic analysis of protein kinases, protein phosphatases and two-component regulatory systems of the cyanobacterium *Anabaena* sp. strain PCC 7120. *FEMS microbiology letters,* ***217***(2), 155–165.

Wang, X., Ge, H., Zhang, Y., Wang, Y., & Zhang, P. (2022). Ser/Thr Protein Kinase SpkI Affects Photosynthetic Efficiency in *Synechocystis* sp. PCC 6803 upon Salt Stress. *Life*, ***12***(5), 713.

Wang, Y., Sun, T., Gao, X., Shi, M., Wu, L., Chen, L., & Zhang, W. (2016). Biosynthesis of platform chemical 3-hydroxypropionic acid (3-HP) directly from CO2 in cyanobacterium *Synechocystis* sp. PCC 6803. *Metabolic Engineering*, ***34***, 60–70.

Watzer, B., Spät, P., Neumann, N., Koch, M., Sobotka, R., Macek, B., ... & Forchhammer, K. (2019). The signal transduction protein PII controls ammonium, nitrate and urea uptake in cyanobacteria. *Frontiers in microbiology*, ***10***, 1428

Watzer, B., Engelbrecht, A., Hauf, W., Stahl, M., Maldener, I., & Forchhammer, K. (2015). Metabolic pathway engineering using the central signal processor PII. *Microbial Cell Factories*, ***14***(1), 1–12.

Weber, A. P. M., Linka, M., & Bhattacharya, D. (2006). Single, ancient origin of a plastid metabolite translocator family in *Plantae* from an endomembrane-derived ancestor. *Eukaryotic Cell*, ***5***(3), 609–612.

Wedel, N., & Soll, J. (1998). Evolutionary conserved light regulation of Calvin cycle activity by NADPH-mediated reversible phosphoribulokinase/CP12/ glyceraldehyde-3-phosphate dehydrogenase complex dissociation. ***PNAS***, *95*(16), 9699–9704.

Wegener, K. M., Welsh, E. A., Thornton, L. E., Keren, N., Jacobs, J. M., Hixson, K. K., Monroe, M. E., Camp, D. G., Smith, R. D., & Pakrasi, H. B. (2008). High sensitivity proteomics assisted discovery of a novel operon involved in the assembly of photosystem II, a membrane protein complex. *Journal of Biological Chemistry*, ***283***(41), 27829–27837.

Wendel, B. M., Cole, J. M., Courcelle, C. T., & Courcelle, J. (2017). SbcC-SbcD and ExoI process convergent forks to complete chromosome replication. *PNAS*, ***115***(2), 349–354.

Xiong, W., Brune, D., & Vermaas, W. F. J. (2014). The γ-aminobutyric acid shunt contributes to closing the tricarboxylic acid cycle in *Synechocystis* sp. PCC 6803. *Molecular Microbiology*, ***93***(4), 786–796.

Xiong, W., Lee, T. C., Rommelfanger, S., Gjersing, E., Cano, M., Maness, P. C., Ghirardi, M., & Yu, J. (2015). Phosphoketolase pathway contributes to carbon metabolism in cyanobacteria. *Nature plants, **2***(1), 1–8.

Xu, Q., Yuo, L., Chitniss, V. P., & Chitnisa, P. R. (1994). Function and Organization of Photosystem I in a Cyanobacterial Mutant Strain That Lacks PsaF and PsaJ Subunits. *Journal of Biological Chemistry*, ***269***(5), 3205–3211.

Yang, M. K., Qiao, Z. X., Zhang, W. Y., Xiong, Q., Zhang, J., Li, T., Ge, F., & Zhao, J. D. (2013). Global phosphoproteomic analysis reveals diverse functions of serine/threonine/tyrosine phosphorylation in the model cyanobacterium *Synechococcus* sp. strain PCC 7002. *Journal of Proteome Research*, ***12***(4), 1909–1923.

Yoshihara, S., Geng, X., & Ikeuchi, M. (2002). pilG Gene Cluster and Split pilL Genes Involved in Pilus Biogenesis, Motility and Genetic Transformation in the Cyanobacterium *Synechocystis* sp. PCC 6803. *Plant and cell physiology, **43***(5), 513–521.

Zaffagnini, M., Fermani, S., Costa, A., Lemaire, S. D., Trost, P., & Lindermayr, C. (2013). Plant cytoplasmic GAPDH: redox post-translational modifications and moonlighting properties. *Frontiers in Plant Science*, ***4***, 450.

Zavřel, T., Očenášová, P., & Červeny, J. (2017). Phenotypic characterization of *Synechocystis* sp. PCC 6803 substrains reveals differences in sensitivity to abiotic stress. *PLoS One, **12***(12), e0189130.

Zhang, C. C. (1996). Bacterial signalling involving eukaryotic-type protein kinases. *Molecular microbiology*, ***20***(1), 9–15.

Zhang, C.-C. (1993). A gene encoding a protein related to eukaryotic protein kinases from the filamentous heterocystous cyanobacterium *Anabaena* PCC 7120. *PNAS*, ***90***(24), 11840–11844.

Zhang, C.-C., Gonzalez, L., & Phalip, V. (1998). Survey, analysis and genetic organization of genes encoding eukaryotic-like signaling proteins on a cyanobacterial genome. *Nucleic acids research*, ***26***(16), 3619–3625.

Zhang, C.-C., Jang, J., Sakr, S., & Wang, L. (2005). Protein phosphorylation on Ser, Thr and Tyr residues in cyanobacteria. *Journal of molecular microbiology and biotechnology*, ***9***(3–4), 154–166.

Zhang, P., Eisenhut, M., Brandt, A.-M., Carmel, D., Silén, H. M., Vass, I., Allahverdiyeva, Y., Salminen, T. A., & Aro, E.-M. (2012). Operon flv4-flv2 Provides Cyanobacterial Photosystem II with Flexibility of Electron Transfer C W. *The Plant Cell*, ***24***(5), 1952–1971.

Zhang, S., & Bryant, D. A. (2011). The tricarboxylic acid cycle in cyanobacteria. *Science*, ***334***(6062), 1551–1553.

Zhang, X., Zhao, F., Guan, X., Yang, Y., Liang, C., & Qin, S. (2007). Genome-wide survey of putative serine/threonine protein kinases in cyanobacteria. *BMC genomics, **8***(1), 1–16.

Zheng, J., & Jia, Z. (2010). Structure of the bifunctional isocitrate dehydrogenase kinase/phosphatase. *Nature*, ***465***(17), 961–965.

Zinchenko, V., Zinchenko, У. V, Piven, V., Melnik, V. A., & Shestakov, S. V. (1999). Vectors for the Complementation Analysis of Cyanobacterial Mutants. *Russian Journal of Genetics*, ***35***, 228–232.

Zorina, A. (2013). Eukaryotic protein kinases in cyanobacteria. *Russian Journal of Plant Physiology*, ***60***(5), 589–596.

Zorina, A. A., Bedbenov, V. S., Novikova, G. V., Panichkin, V. B., & Los', D. A. (2014). Involvement of serine/threonine protein kinases in the cold stress response in the cyanobacterium *Synechocystis* sp. PCC 6803: Functional characterization of SpkE protein kinase. *Molecular Biology*, ***48***, 390–398.

Zorina, A. A., Novikova, G. V., Gusev, N. B., Leusenko, A. V., Los, D. A., & Klychnikov, O. I. (2023). SpkH (Sll0005) from *Synechocystis* sp. PCC 6803 is an active Mn2+-dependent Ser kinase. *Biochimie*, ***213***, 114–122.

Zorina, A., Stepanchenko, N., Novikova, G. V., Sinetova, M., Panichkin, V. B., Moshkov, I.E., Zinchenko, V. V., Shestakov, S. V., Suzuki, I., Murata, N., & Los, D. A. (2011). Eukaryotic-like Ser/Thr protein kinases SpkC/F/K are involved in phosphorylation of GroES in the cyanobacterium *Synechocystis*. *DNA Research*, ***18***(3), 137–151.

Appendix

Appendix Table 1: Primer and primer combinations used throughout this study.

Name	Sequence	Purpose
TB3	CTAAAAGTTTACTAATTGACTGGCAATCC	gen specific; amplification of *sll0776* (spkD)
TB4	ATGAATGTCCAAGTACTCGACC	
TB11	ATGGTTACCCCACTCAAACTACTCA	gen specific; amplification of *sll0599* (spkC)
TB12	CTAATTTTGCTCGGGGTCGAT	
TB15	ATGACCCCATCCTTGTCCCTG	gen specific; amplification of *slr1443* (spkE)
TB16	TCAAAATGGTTGAGCACTGGC	
TB19	ATGAGTTTTTGCGTTAATCCCAATTGTC	gen specific; amplification of *slr1697*(spkB)
TB20	CTATCTCCGCCGACCAGA	
TB23	ATGGAATCACTCCCCGTCCT	gen specific; amplification of *slr0152* (spkG)
TB24	TTAGCGTTTTTCCTGGCGTT	
TB27	TCACAATCCTGAAACCTCCTTGTTAAAG	gen specific; amplification of *sll1574/1575* (spkA)
TB28	ATGACCCCTGACTCCCG	
TB29	ATGGATCTGCTCTGCACCCG	gen specific; amplification of *slr1225* (spkF)
TB30	TCAAACCCTGGTTAAAACTGCA	
TB31	CTAGGCTGCATTGCGGATTTTGAT	gen specific; amplification of *sll0005* (spkH)
TB32	ATGTCTCCAGCCCCCAT	
TB33	CTACCTTTTTTGCACCAGTCG	gen specific; amplification of *sll0095* (spkL)
TB34	GTGTTCTTTTTGTCGTGGGACCG	
TB35	TTAAAACATCCGGTCCTGTCTTT	gen specific; amplification of *sll1770* (spkI)
TB36	GTGTCTGCCCTATCCACTAAGCTT	
TB37	GTGCCTAACCCCAAACCCC	gen specific; amplification of *slr1919* (spkK)
TB38	TTATCGTTGCGGCAGAATGG	
TB39	AGCTTGCATCTTTTTAAAAGCAGTG	amplification of *sll0776* (spkD); +/-500 bp up-/downstream
TB40	GGTAATATTCCTATAAGTTTGTCTGTATGAGGCAAC	
TB41	CCTCTGTCCCAATATCCACCACG	amplification of *slr1697* (spkB); +/-500 bp up-/downstream
TB42	AAGAAACAGTATTGGCCGCC	
TB43	ACGCCGAAGCCTATTACCAA	amplification of *slr0152* (spkG); +/-500 bp up-/downstream
TB44	CGGCAAAAGGGGGATGGCA	
TB45	TTGACGACCTGGCTCATGGC	amplification of *sll0599* (spkC); +/-500 bp up-/downstream
TB46	GATAATGCCCGTGGCGG	
TB49	GGGGATGCGTGGGTTTCCC	amplification of *slr1443* (spkE); +/-500 bp up-/downstream
TB50	GTTCCGATGTTGGTAAATGGGG	
TB51	CCGGATAGGAGGGAGTCGGC	amplification of *sll0005* (spkH); +/-500 bp up-/downstream
TB52	CCCTAGGAGGAGATTCCAAACTG	

TB53	ACGGTCTACTCCGGTTAAATCC	amplification of *sll1574/1575* (spkA); +/-500 bp up-/downstream
TB54	ATTGGAGCCAGGCCGATGG	
TB55	GAGCCCTTGGTAATACTTTTCCCGTT	amplification of *sll0095* (spkL); +/-500 bp up-/downstream
TB56	AAATACTTGCGGCAAATTTTCCAAG	
TB57	GCCCTGGCCACCCAGGTA	amplification of *sll1770* (spkI); +/-500 bp up-/downstream
TB58	GATCGCCACGGTGGATGG	
TB59	ACCATAGACCAAATCCCTGGTGGC	amplification of *slr1919* (spkK); +/-500 bp up-/downstream
TB60	ACTTACCAAATTCATCAATGACAAACTG	
TB61	TATCGGCTCTCCTCCCATG	amplification of *slr1225* (spkF); +/-500 bp up-/downstream
TB62	CTGGTGGCCCTGGAAACCCT	
TB69	GCCATGGTGGATTGGCCCC	amplification of *slr0889*; +/-500 bp up-/downstream
TB70	CCATTTTTTAACCTCAAGGTAAACTGTAATAT	
TB72	GGAAAAAGCCATGTTCCAACAAT	genotyping Δ*spkH*
TB73	ATGTTTGCCTTACCTCAAGCCG	gene specific; amplification of *slr0889* (spkJ)
TB74	TCATCCAGCGCCTTCTAAATTG	
TB79	CTGCAGTTGACAGAGATGCGCATGGGTTTCCTTTTCTA	amplification of $P_{slr1697}$*::slr1697*::flag for Δ*slr1697* (Δ*spkB*) complementation
TB80	CTCGAGCTATTTATCATCATCATCTTTATAATCAATATCATGATCTTTATAATCGCCATCATGATCTTTATAATCTCTCCGCCGACCAGAACCGGGCATAACCGT	

Appendix Table 2: Plasmids generated in this study.

Name	Feature
pTB1Km	Δ*slr0599*::Km in pGEM-T
pTB2Km	Δ*slr1919*::Km in pGEM-T
pTB3Km	Δ*slr1225*::Km in pGEM-T
pTB4Km	Δ*sll1770*::Km in pJet1.2/Blunt
pTB5Gm	Δ*sll0776*::Gm in pGEM-T
pTB6Km	Δ*sll0095*::Km in pGEM-T
pTB8Km	Δ*sll0005*::Km in pJET1.2/Blunt
pTB12Km	Δ*slr0889*::Km in pJet1.2/Blunt
pTB15Km	Δ*spkA*::Km in pJET1.2/Blunt
pTB16Km	Δ*spkB*::Km in pJET1.2/Blunt
pTB17Km	Δ*spkE*::Km in pJET1.2/Blunt
pTB18Km	Δ*spkG*::Sp in pJET1.2/Blunt
pTB29	$P_{slr1697}$::slr1697::flag in pVZ322

Appendix Table 3: Curated list of identified p-protein based on all published global phospho-proteome studies (Mikkat et al., 2014; Spät et al., 2015, Z. Chen et al., 2015; Angeleri et al., 2016; Toyoshima et al., 2020; Spät & Barske et al., 2021; Barske & Spät et al., 2023)

Cyanobase ID	Protein Name	Protein Function	Cyanobase ID	Protein Name	Protein Function
sll0017	HemL	glutamate-1-semialdehyde aminomutase	*slr0171*	Ycf37	photosystem I assembly related protein Ycf37
sll0018	FbaA	fructose-bisphosphate aldolase, class II	*slr0185*	PyrE	orotate phosphoribosyltransferase
sll0019	Dxr	1-deoxy-d-xylulose 5-phosphate reductoisomerase	*slr0186*	LeuA	2-isopropylmalate synthase
sll0039	PixH	positive phototaxis protein, two-component response regulator CheY subfamily	*slr0192*	Slr0192	hypothetical protein
sll0040	PixI	positive phototaxis protein, homologous to chemotaxis protein CheW	*slr0193*	Rbp31	RNA-binding protein
sll0041	PixJ	phytochrome-like photoreceptor protein for positive phototaxis;homologous to methyl-accepting chemotaxis protein	*slr0213*	GuaA	GMP synthetase
sll0042	PixJ2; Tar	methyl-accepting chemotaxis protein for positive phototaxis	*slr0228*	FtsH2	cell division protein FtsH
sll0043	PixL	positive phototaxis protein, homologous to chemotaxis protein CheA, two-component hybrid histidine kinase	*slr0242*	Bcp	bacterioferritin comigratory protein homolog
sll0057	GrpE	heat shock protein GrpE	*slr0261*	NdhH	NADH dehydrogenase subunit 7
sll0068	Sll0068	unknown protein	*slr0288*	GlnN	glutamate--ammonia ligase
sll0094	Hik37	two-component sensor histidine kinase	*slr0301*	PpsA	phosphoenolpyruvate synthase
sll0103	Sll0103	hypothetical protein	*slr0322*	Hik43	two-component hybrid sensor and regulator

sll0108	Amt1	ammonium/methylammonium permease	*slr0335*	ApcE	phycobilisome core-membrane linker polypeptide LCM
sll0135	MtnP	putative 5'-methylthioadenosine phosphorylase	*slr0342*	PetB	cytochrome b6
sll0142	Sll0142	probable cation efflux system protein	*slr0363*	Slr0363	hypothetical protein
sll0144	PyrH	uridine monophosphate kinase	*slr0374*	Slr0374	hypothetical protein
sll0163	Sll0163	WD-repeat protein	*slr0377*	Slr0377	unknown protein
sll0172	Sll0172	periplasmic protein, function unknown	*slr0384*	SqdX	sulfoquinovosyldiacylglycerol biosynthesis protein SqdX
sll0173	Vgb	virginiamycin B hydrolase, periplasmic protein	*slr0393*	#N/A	#N/A
sll0182	Sll0182	ABC transporter ATP-binding protein	*slr0394*	Pgk	phosphoglycerate kinase
sll0185	Sll0185	hypothetical protein	*slr0397*	Slr0397	hypothetical protein
sll0199	PetE	plastocyanin	*slr0404*	Slr0404	hypothetical protein
sll0205	Sll0205	hypothetical protein	*slr0426*	FolE	GTP cyclohydrolase I
sll0207	RfbA	glucose-1-phosphate thymidylyltransferase	*slr0434*	Efp	elongation factor P
sll0217	Flv4	flavoprotein Flv4	*slr0447*	UrtA	periplasmic protein, ABC-type urea transport system substrate-binding protein
sll0225	Sll0225	unknown protein	*slr0452*	IlvD	dihydroxyacid dehydratase
sll0236	Sll0236	unknown protein	*slr0453*	Slr0453	hypothetical protein
sll0245	Sll0245	probable GTP binding protein	*slr0455*	Slr0455	hypothetical protein
sll0258	PsbV	cytochrome c550	*slr0459*	Slr0459	hypothetical protein
sll0260	Sll0260	hypothetical protein	*slr0476*	Slr0476	unknown protein
sll0271	NusB	N utilization substance protein B homolog	*slr0483*	Slr0483	hypothetical protein
sll0301	Sll0301	hypothetical protein	*slr0503*	Ycf66	hypothetical protein YCF66
sll0320	Rnd	probable ribonuclease D	*slr0536*	HemE	uroporphyrinogen decarboxylase

sll0329	Gnd	6-phosphogluconate dehydrogenase	*slr0543*	TrpB	tryptophan synthase beta subunit
sll0359	CyAbrB	CyAbrB, putative regulatory protein	*slr0546*	TrpC	indole-3-glycerol phosphate synthase
sll0370	CarB	carbamoyl-phosphate synthase, pyrimidine-specific, large chain	*slr0549*	Asd	aspartate beta-semialdehyde dehydrogenase
sll0377	Mfd	transcription-repair coupling factor	*slr0551*	Slr0551	hypothetical protein
sll0379	LpxA	acyl-[acyl-carrier-protein]-UDP-N-acetylglucosamine o-acyltransferase	*slr0552*	Slr0552	hypothetical protein
sll0408	Sll0408	peptidyl-prolyl cis-trans isomerase	*slr0557*	ValS	valyl-tRNA synthetase
sll0416	GroL2	60 kDa chaperonin 2, GroEL2, molecular chaperone	*slr0559*	NatB	periplasmic binding protein of ABC transporter for natural amino acids
sll0430	HtpG	HtpG, heat shock protein 90, molecular chaperone	*slr0585*	ArgG	argininosuccinate synthetase
sll0446	Sll0446	unknown protein	*slr0599*	SpkC	serine/threonine kinase SpkC
sll0469	PrsA	ribose-phosphate pyrophosphokinase	*slr0601*	Slr0601	unknown protein
sll0497	Sll0497	hypothetical protein	*slr0609*	Slr0609	hypothetical protein
sll0505	Sll0505	hypothetical protein	*slr0617*	Slr0617	unknown protein
sll0508	Sll0508	unknown protein	*slr0623*	TrxA	thioredoxin
sll0513	Sll0513	hypothetical protein	*slr0637*	Slr0637	hypothetical protein
sll0517	RbpA	putative RNA binding protein	*slr0645*	Slr0645	hypothetical protein
sll0518	Sll0518	unknown protein	*slr0649*	MetS	methionyl-tRNA synthetase
sll0529	Sll0529	hypothetical protein	*slr0654*	Slr0654	unknown protein
sll0541	DesC (des9)	acyl-lipid desaturase (delta 9)	*slr0661*	ProC	pyrroline-5-carboxylate reductase
sll0542	AcsA	acetyl-coenzyme A synthetase	*slr0670*	Slr0670	hypothetical protein
sll0550	Flv3	flavoprotein Flv3	*slr0676*	CysC	adenylylsulfate kinase
sll0563	Sll0563	unknown protein	*slr0686*	Slr0686	hypothetical protein
sll0567	Fur	ferric uptake regulation protein	*slr0700*	Slr0700	probable amino acid permease

sll0569	RecA	RecA gene product	*slr0708*	Slr0708	periplasmic protein, function unknown
sll0576	HrEpiB	putative sugar-nucleotide epimerase/dehydratease	*slr0721*	Me	malic enzyme
sll0585	Sll0585	hypothetical protein	*slr0729*	Slr0729	hypothetical protein
sll0602	Sll0602	hypothetical protein	*slr0730*	Slr0730	hypothetical protein
sll0617	Vipp1	plasma membrane protein essential for thylakoid formation	*slr0737*	PsaD	photosystem I subunit II
sll0634	BtpA	photosystem I biogenesis protein BtpA	*slr0744*	InfB	translation initiation factor IF-2
sll0635	ThiE	probable thiamine-phosphate pyrophosphorylase	*slr0752*	Eno	enolase
sll0654	Sll0654	alkaline phosphatase	*slr0755*	Slr0755	hypothetical protein
sll0660	PdxA	pyridoxal phosphate biosynthetic protein PdxA	*slr0758*	KaiC	circadian clock protein KaiC homolog
sll0680	PstS	phosphate-binding periplasmic protein precursor (PBP)	*slr0772*	ChlB	light-independent protochlorophyllide reductase subunit ChlB
sll0726	Pgm	phosphoglucomutase	*slr0820*	#N/A	#N/A
sll0744	Sll0744	hypothetical protein	*slr0833*	DnaB	replicative DNA helicase [Contains: Ssp dnaB intein]
sll0756	Sll0756	unknown protein	*slr0875*	MscL	large-conductance mechanosensitive channel
sll0764	UrtD	urea transport system ATP-binding protein	*slr0882*	Ycf84	hypothetical protein YCF84
sll0776	SpkD	serine/threonine kinase SpkD	*slr0884*	Gap1	glyceraldehyde 3-phosphate dehydrogenase 1 (NAD+)
sll0778	#N/A	#N/A	*slr0891*	AmiA	N-acetylmuramoyl-L-alanine amidase
sll0788	#N/A	#N/A	*slr0906*	PsbB	photosystem II core light harvesting protein
sll0813	CtaC	cytochrome c oxidase subunit II	*slr0925*	Ssb	single-stranded DNA-binding protein
sll0819	PsaF	photosystem I reaction center subunit III precursor (PSI-F), plastocyanin (cyt c553) docking protein	*slr0929*	Slr0929	chromosome partitioning protein, ParA family

sll0822	CalB	hypothetical protein	*slr0942*	Slr0942	alcohol dehydrogenase [NADP+]
sll0851	PsbC	photosystem II CP43 protein	*slr0943*	Fda	fructose-bisphosphate aldolase, class I
sll0854	Sll0854	hypothetical protein	*slr0947*	RpaB	response regulator for energy transfer from phycobilisomes to photosystems
sll0863	#N/A	#N/A	*slr0952*	Fbp	fructose-1,6-bisphosphatase
sll0865	#N/A	#N/A	*slr0963*	Sir	ferredoxin-sulfite reductase
sll0877	Sll0877	hypothetical protein	*slr0982*	RfbB	probable polysaccharide ABC transporter ATP binding subunit
sll0897	#N/A	DnaJ protein, heat shock protein 40, molecular chaperone	*slr1044*	McpA	methyl-accepting chemotaxis protein, required for the biogenesis of thick pilli
sll0899	GlmU	UDP-N-acetylglucosamine pyrophosphorylase	*slr1046*	TatA	putative TatA protein
sll0901	PurE	phosphoribosylaminoimidazole carboxylase	*slr1048*	Slr1048	hypothetical protein
sll0915	PqqE	periplasmic protease	*slr1055*	ChlH	magnesium protoporphyrin IX chelatase subunit H
sll0920	Ppc	phosphoenolpyruvate carboxylase	*slr1063*	Slr1063	probable glycosyltransferase
sll0922	#N/A	#N/A	*slr1067*	GalE	UDP-glucose 4-epimerase
sll0923	EpsB	unknown protein	*slr1096*	LpdA	dihydrolipoamide dehydrogenase
sll0927	MetX	S-adenosylmethionine synthetase	*slr1102*	Slr1102	hypothetical protein
sll0928	ApcD	allophycocyanin-B	*slr1103*	Slr1103	hypothetical protein
sll0934	CcmA	carboxysome formation protein CcmA	*slr1104*	Slr1104	hypothetical protein
sll0947	LrtA	light repressed protein A homolog	*slr1123*	Gmk	guanylate kinase
sll0981	Sll0981	unknown protein	*slr1129*	Rne	ribonuclease E
sll0982	Sll0982	unknown protein	*slr1130*	RnhB	ribonuclease HII
sll0996	MiaB	hypothetical protein	*slr1133*	ArgH	L-argininosuccinate lyase
sll0998	RbcR	LysR family transcriptional regulator	*slr1137*	CtaD	cytochrome c oxidase subunit I
sll1020	Sll1020	probable glycosyltransferase	*slr1160*	Slr1160	periplasmic protein, function unknown

sll1028	CcmK2	carbon dioxide concentrating mechanism protein CcmK	*slr1161*	Slr1161	hypothetical protein
sll1028;sll1029	#N/A	#N/A	*slr1163*	Slr1163	unknown protein
sll1029	CcmK1	carbon dioxide concentrating mechanism protein CcmK	*slr1166*	Slr1166	UDP-glucose:tetrahydrobiopterin glucosyltransferase
sll1031	CcmM	carbon dioxide concentrating mechanism protein CcmM, putative carboxysome structural protein	*slr1176*	GlgC	glucose-1-phosphate adenylyltransferase
sll1033	Sll1033	probable protein phosphatase	*slr1184*	#N/A	#N/A
sll1039	Sll1039	hypothetical protein	*slr1225*	SpkF	serine/threonine kinase SpkF
sll1043	Pnp	polyribonucleotide nucleotidyltransferase	*slr1237*	#N/A	#N/A
sll1059	Adk2	adenylate kinase	*slr1261*	Slr1261	hypothetical protein
sll1070	TktA	transketolase	*slr1270*	Slr1270	periplasmic protein, function unknown
sll1074	LeuS	leucyl-tRNA synthetase	*slr1272*	Slr1272	probable porin;major outer membrane protein
sll1076	ZiaA	cation-transporting ATPase PacL	*slr1274*	PilM	probable fimbrial assembly protein PilM, required for motility
sll1089	Sll1089	periplasmic protein, function unknown	*slr1280*	NdhK1	NADH dehydrogenase subunit NdhK
sll1096	RpsL	30S ribosomal protein S12	*slr1281*	NdhJ	NADH dehydrogenase subunit I
sll1097	RpsG	30S ribosomal protein S7	*slr1282*	#N/A	#N/A
sll1099	Tuf	elongation factor Tu	*slr1289*	Icd	isocitrate dehydrogenase (NADP+)
sll1101	RpsJ	30S ribosomal protein S10	*slr1295*	FutA1	iron transport system substrate-binding protein
sll1106	Sll1106	hypothetical protein	*slr1300*	Slr1300	similar to 2-octaprenyl-6-methoxyphenol hydroxylase
sll1130	Sll1130	unknown protein	*slr1311*	#N/A	#N/A
sll1184	#N/A	heme oxygenase	*sll1867*	#N/A	#N/A

sll1185	HemF	coproporphyrinogen III oxidase, aerobic (oxygen-dependent)	*slr1325*	SpoT	GTP pyrophosphokinase
sll1188	Sll1188	hypothetical protein	*slr1329*	AtpB	ATP synthase beta subunit
sll1194	PsbU	photosystem II 12 kDa extrinsic protein	*slr1334*	ManB	phosphoglucomutase/phosphomannomutase
sll1213	Sll1213	GDP-fucose synthetase	*slr1338*	Slr1338	hypothetical protein
sll1214	#N/A	hypothetical protein YCF59	*slr1349*	Pgi	glucose-6-phosphate isomerase
sll1217	Sll1217	unknown protein	*slr1356*	Rps1A	30S ribosomal protein S1
sll1242	Sll1242	hypothetical protein	*slr1390*	FtsH1	cell division protein FtsH
sll1244	RplI	50S ribosomal protein L9	*slr1435*	PmbA	PmbA protein homolog
sll1247	Sll1247	hypothetical protein	*slr1459*	ApcF	phycobilisome core component
sll1260	RpsB	30S ribosomal protein S2	*slr1463*	FusA	elongation factor EF-G
sll1275	Pyk2	pyruvate kinase 2	*slr1476*	PyrB	aspartate carbamoyltransferase
sll1283	SpoIID	similar to stage II sporulation protein D	*slr1505*	Slr1505	unknown protein
sll1292	Sll1292	two-component response regulator CheY subfamily	*slr1512*	SbtA	sodium-dependent bicarbonate transporter
sll1294	PilJ	methyl-accepting chemotaxis protein	*slr1513*	SbtB	periplasmic protein, function unknown
sll1306	Sll1306	periplasmic protein, function unknown	*slr1516*	SodB	superoxide dismutase
sll1307	Sll1307	periplasmic protein, function unknown	*slr1517*	LeuB	3-isopropylmalate dehydrogenase
sll1314	DctP	putative C4-dicarboxylase binding protein, periplasmic protein	*slr1529*	Slr1529	nitrogen assimilation regulatory protein
sll1316	PetC2	cytochrome b6-f complex iron-sulfur subunit (Rieske iron sulfur protein)	*slr1531*	Ffh	signal recognition particle protein
sll1324	AtpF	ATP synthase B chain (subunit I) of CF(0)	*slr1536*	RecQ	ATP-dependent DNA helicase RecQ

sll1325	AtpD	ATP synthase delta chain of CF(1);ATP synthase delta chain of CF(1)	*slr1588*	Slr1588	two-component transcription regulator
sll1326	AtpA	ATP synthase alpha chain	*slr1603*	Slr1603	hypothetical protein
sll1330	Sll1330	two-component system response regulator OmpR subfamily	*slr1619*	Slr1619	hypothetical protein
sll1334	Sll1334	two-component sensor histidine kinase	*slr1622*	Ppa	soluble inorganic pyrophosphatase
sll1338	Sll1338	unknown protein	*slr1624*	Slr1624	hypothetical protein
sll1341	Bfr	bacterioferritin	*slr1634*	Slr1634	hypothetical protein
sll1342	Gap2	NAD(P)-dependent glyceraldehyde-3-phosphate dehydrogenase	*slr1641*	ClpB1	ClpB protein
sll1350	Sll1350	hypothetical protein	*slr1643*	PetH	ferredoxin-NADP oxidoreductase (FNR)
sll1360	DnaX	DNA polymerase III subunit gamma/tau [Contains: Ssp dnaX intein]	*slr1655*	PsaL	photosystem I subunit XI
sll1362	IleS	isoleucyl-tRNA synthetase	*slr1657*	Slr1657	hypothetical protein
sll1363	IlvC	ketol-acid reductoisomerase	*slr1659*	Slr1659	hypothetical protein
sll1367	Sll1367	hypothetical protein	*slr1665*	DapF	diaminopimelate epimerase
sll1384	Sll1384	similar to DnaJ protein	*slr1686*	Slr1686	hypothetical protein
sll1396	Sll1396	unknown protein	*slr1693*	Slr1693	two-component response regulator PatA subfamily
sll1398	Psb28	photosystem II reaction center 13 kDa protein	*slr1697*	SpkB	serine/threonine kinase SpkB
sll1426	Sll1426	unknown protein	*slr1704*	Slr1704	hypothetical protein
sll1434	MrcA	penicillin-binding protein	*slr1710*	MrcB	penicillin-binding protein
sll1450	NrtA	nitrate/nitrite transport system substrate-binding protein	*slr1718*	ComB	hypothetical protein
sll1451	NrtB	nitrate/nitrite transport system permease protein	*slr1729*	KdpB	potassium-transporting P-type ATPase B chain

sll1464	Sll1464	hypothetical protein	*slr1735*	BgtA	ATP-binding subunit of the ABC-type Bgt permease for basic amino acids and glutamine
sll1469	Sll1469	hypothetical protein	*slr1744*	AmiA	N-acetylmuramoyl-L-alanine amidase, periplasmic protein
sll1479	Pgl	6-phosphogluconolactonase	*slr1751*	Prc	periplasmic carboxyl-terminal protease
sll1499	GlsF	ferredoxin-dependent glutamate synthase	*slr1756*	GlnA	glutamate--ammonia ligase
sll1503	#N/A	#N/A	*slr1763*	Slr1763	probable methyltransferase
sll1525	Prk	phosphoribulokinase	*slr1783*	Ycf29	two-component response regulator NarL subfamily
sll1526	Sll1526	hypothetical protein	*slr1788*	Slr1788	unknown protein
sll1536	MoeB	molybdopterin biosynthesis MoeB protein	*slr1789*	Slr1789	unknown protein
sll1541	Sll1541	hypothetical protein	*slr1793*	TalB	transaldolase
sll1542	Sll1542	hypothetical protein	*slr1796*	Slr1796	hypothetical protein
sll1545	Gst1	glutathione S-transferase	*slr1816*	Slr1816	hypothetical protein
sll1547	Sll1547	hypothetical protein	*slr1834*	PsaA	P700 apoprotein subunit Ia
sll1553	PheT	phenylalanyl-tRNA synthetase	*slr1835*	PsaB	P700 apoprotein subunit Ib
sll1559	Sll1559	soluble hydrogenase 42 kD subunit	*slr1841*	Slr1841	probable porin;major outer membrane protein
sll1573	Sll1573	hypothetical protein	*slr1843*	Zwf	glucose 6-phosphate dehydrogenase
sll1577	CpcB	phycocyanin beta subunit	*slr1844*	UvrA	excinuclease ABC subunit A
sll1578	CpcA	phycocyanin alpha subunit	*slr1856*	Slr1856	anti-sigma factor antagonist Slr1856; phosphoprotein substrate of icfG gene cluster
sll1579	CpcC2	phycobilisome rod linker polypeptide LR30	*slr1859*	Slr1859	anti-sigma f factor antagonist Slr1859; phosphoprotein substrate of icfG gene cluster
sll1580	CpcC1	phycobilisome rod linker polypeptide	*slr1870*	Slr1870	hypothetical protein

sll1595	KaiC2	circadian clock protein KaiC homolog	*slr1874*	Ddl	D-alanine--D-alanine ligase
sll1600	#N/A	#N/A	*slr1894*	Slr1894	probable DNA-binding stress protein
sll1621	AhpC	AhpC/TSA family protein	*slr1920*	Slr1920	unknown protein
sll1626	LexA	LexA repressor	*slr1924*	Slr1924	D-alanyl-D-alanine carboxypeptidase, periplasmic protein
sll1656	Sll1656	hypothetical protein	*slr1939*	HtpX	unknown protein
sll1665	Sll1665	unknown protein	*slr1942*	KaiC3	circadian clock protein KaiC homolog
sll1672	Hik12	two-component hybrid sensor and regulator	*slr1945*	PGAM	2,3-bisphosphoglycerate-independent phosphoglycerate mutase
sll1692	Sll1692	hypothetical protein	*slr1950*	CtaA	copper-transporting P-type ATPase CtaA
sll1693	Sll1693	hypothetical protein	*slr1963*	OCP	water-soluble carotenoid protein OCP
sll1694	HofG	pilin polypeptide PilA1	*slr1983*	Slr1983	two-component hybrid sensor and regulator
sll1712	Hup	DNA binding protein HU	*slr1984*	Rps1b	nucleic acid-binding protein, 30S ribosomal protein S1 homolog
sll1734	CupA	protein involved in low CO2-inducible, high affinity CO2 uptake	*slr1986*	ApcB	allophycocyanin beta subunit
sll1742	NusG	transcription antitermination protein NusG	*slr1991*	CyaA	adenylate cyclase
sll1746	RplL	50S ribosomal protein L12	*slr1992*	Gpx2	glutathione peroxidase-like NADPH peroxidase
sll1747	AroC	chorismate synthase	*slr1994*	FabG2	PHA-specific acetoacetyl-CoA reductase
sll1757	Sll1757	hypothetical protein	*slr2002*	CphA	cyanophycin synthetase
sll1758	GlmM	MrsA protein homolog	*slr2003*	Slr2003	hypothetical protein
sll1761	Sll1761	unknown protein	*slr2024*	Slr2024	two-component response regulator CheY subfamily
sll1787	RpoB	RNA polymerase beta subunit	*slr2032*	Ycf23	hypothetical protein YCF23
sll1789	RpoC2	RNA polymerase beta prime subunit	*slr2051*	CpcG	phycobilisome rod-core linker polypeptide LRC
sll1801	RplW	50S ribosomal protein L23	*slr2058*	TopA	DNA topoisomerase I

sll1802	RplB	50S ribosomal protein L2	*slr2067*	ApcA	allophycocyanin alpha subunit
sll1803	RplV	50S ribosomal protein L22	*slr2070*	Slr2070	hypothetical protein
sll1804	RpsC	30S ribosomal protein S3	*slr2072*	IlvA	L-threonine deaminase
sll1808	RplE	50S ribosomal protein L5	*slr2073*	SepF	hypothetical protein YCF50
sll1811	RplR	50S ribosomal protein L18	*slr2075*	GroES	10kD chaperonin
sll1812	RpsE	30S ribosomal protein S5	*slr2076*	GroL1	60kD chaperonin
sll1815	Adk1	adenylate kinase	*slr2077*	#N/A	#N/A
sll1816	RpsM	30S ribosomal protein S13	*slr2094*	Fbpl	fructose-1,6-/sedoheptulose-1,7-bisphosphatase
sll1821	RplM	50S ribosomal protein L13	*slr2098*	Hik21	two-component hybrid sensor and regulator
sll1823	PurA	adenylosuccinate synthetase	*slr2102*	FtsY	cell division protein FtsY
sll1830	Sll1830	unknown protein	*slr2115*	#N/A	#N/A
sll1833	FtsI	penicillin-binding protein	*slr2118*	#N/A	#N/A
sll1841	OdhB	pyruvate dehydrogenase dihydrolipoamide acetyltransferase component (E2)	*slr5016*	#N/A	#N/A
sll1852	Ndk	nucleoside diphosphate kinase	*slr5018*	Slr5018	hypothetical protein
sll1862	Sll1862	unknown protein	*slr5051*	Slr5051	unknown protein
sll1863	Sll1863	unknown protein	*slr6001*	#N/A	#N/A
sll1865	PrfB	peptide chain release factor 2	*slr6012*	#N/A	#N/A
sll1867	#N/A	#N/A	*slr6028*	#N/A	#N/A
sll1873	Sll1873	unknown protein	*slr6031/slr6090*	#N/A	#N/A
sll1879	Crr23	two-component response regulator	*slr6039*	#N/A	#N/A
sll1893	HisF	cyclase	*slr6040*	#N/A	#N/A
sll1908	SerA	D-3-phosphoglycerate dehydrogenase	*slr6050*	Slr6050	hypothetical protein
sll1911	Sll1911	hypothetical protein	*slr6106*	Slr6106	hypothetical protein

sll1921	Sll1921	hypothetical protein	*slr6110*	Slr6110	putative signalling protein
sll1931	GlyA	serine hydroxymethyltransferase	*slr7010*	#N/A	#N/A
sll1932	DnaK3	DnaK protein	*slr7060*	Slr7060	hypothetical protein
sll1945	Dxs	1-deoxyxylulose-5-phosphate synthase	*slr8016*	ParB	plasmid partitioning protein, ParB
sll1967	Sll1967	probable RNA methyltransferase	*ssl0483*	Ssl0483	hypothetical protein
sll1973	PlsY	hypothetical protein	*ssl0563*	PsaC	photosystem I subunit VII
sll2012	RpoD; SigD	group2 RNA polymerase sigma factor SigD	*ssl0601*	RpsU	30S ribosomal protein S21
sll5042	Sll5042	probable sulfotransferase	*ssl0707*	GlnB	nitrogen regulatory protein PII
sll5059	Crr43	two-component response regulator	*ssl1046*	Ssl1046	hypothetical protein
sll5066	Sll5066	probable plasmid partitioning protein, ParA family	*ssl1498*	Ssl1498	hypothetical protein
sll5079	Sll5079	probable short chain dehydrogenase	*ssl1552*	Ssl1552	unknown protein
sll7063	Sll7063	unknown protein	*ssl1633*	HliC	high light-inducible polypeptide HliC, CAB/ELIP/HLIP superfamily
sll8031	#N/A	#N/A	*ssl1707*	Ssl1707	hypothetical protein
slr0009	CbbL	ribulose bisphosphate carboxylase large subunit	*ssl1784*	RpsO	30S ribosomal protein S15
slr0012	CbbS	ribulose bisphosphate carboxylase small subunit	*ssl2084*	AcpP	acyl carrier protein
slr0032	IlvE	probable branched-chain amino acid aminotransferase	*ssl2420*	Ssl2420	unknown protein
slr0038	Slr0038	hypothetical protein	*ssl2982*	RpoZ	DNA-directed RNA polymerase omega subunit
slr0040	CmpA	bicarbonate transport system substrate-binding protein	*ssl3093*	CpcD	phycobilisome small rod linker polypeptide LR10
slr0041	CmpB	bicarbonate transport system permease protein	*ssl3177*	RepA	hypothetical protein
slr0067	Mrp	MRP protein homolog	*ssl3335*	SecE	preprotein translocase SecE subunit
slr0072	RsmG	glucose inhibited division protein B	*ssl3364*	CP12	CP12 polypeptide

slr0073	Hik36	two-component sensor histidine kinase	*ssl3445*	RpmE	50S ribosomal protein L31
slr0075	Ycf16	ABC transporter ATP-binding protein	*ssl5113*	Ssl5113	unknown protein
slr0076	Slr0076	hypothetical protein	*ssr0680*	#N/A	#N/A
slr0096	#N/A	#N/A	*ssr1176*	#N/A	#N/A
slr0121	Slr0121	hypothetical protein	*ssr1528*	Ssr1528	hypothetical protein
slr0145	Slr0145	unknown protein	*ssr1600*	Ssr1600	similar to anti-sigma f factor antagonist
slr0148	Fed5	ferredoxin-like protein	*ssr1789*	HliD	CAB/ELIP/HLIP-related protein HliD
slr0149	Slr0149	hypothetical protein	*ssr2708*	#N/A	#N/A
slr0151	Slr0151	unknown protein	*ssr2723*	Ssr2723	hypothetical protein
slr0152	SpkG	serine/threonine kinase SpkG	*ssr2831*	PsaE	photosystem I subunit IV
slr0161	PilT	twitching motility protein PilT	*ssr3189*	Ssr3189	hypothetical protein
slr0164	ClpR	ATP-dependent Clp protease proteolytic subunit	*ssr3383*	ApcC	phycobilisome small core linker polypeptide LC
slr0165	ClpP3	ATP-dependent Clp protease proteolytic subunit	*ssr3451*	PsbE	cytochrome b559 alpha subunit
slr0168	Slr0168	unknown protein			

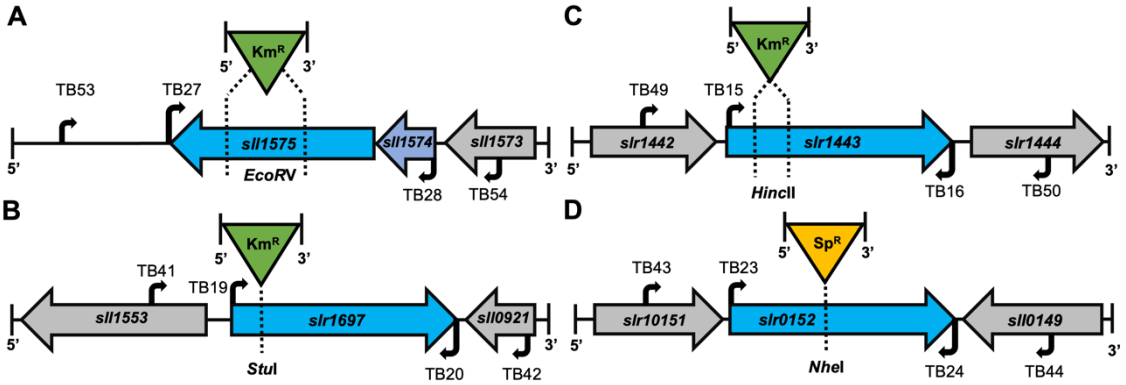

Appendix Figure 1: Cloning strategies for protein kinase mutants. Mutated protein kinase coding genes were amplified in null mutants together with 500 bp up- and downstream of the GOI in a PCR. DNA regions were subcloned into pJET1.2/blunt and re-sequenced. Cloning strategies could be clarified for Δ*spkA* (**A**), Δ*spkB* (**B**), Δ*spkE* (**C**) and Δ*spkG* (**D**). Indicated are primer pairs, restriction enzymes and antibiotic resistances employed during cloning. (Km^R= kanamycin resistance; Sp^R= spectinomycin resistance)

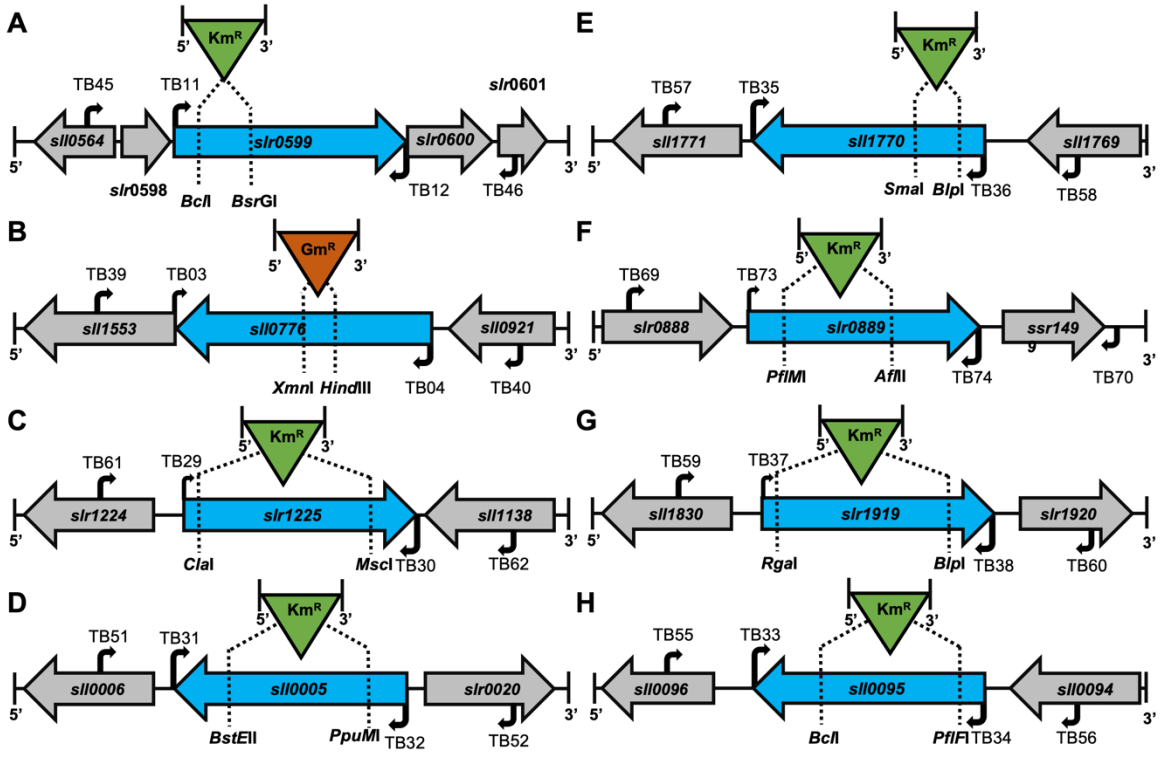

Appendix Figure 2: Cloning strategies for newly established protein kinase mutants. Protein kinase gene were amplified together with 500 bp up- and downstream of the GOI. DNA fragments were ligated into either pJET1.2/blunt or pGEMT for propagation and sequencing. Naturally occurring exonuclease cutting sided were employed to remove parts of the gene sequence. Removed parts were replaced with antibiotic resistance genes. Indicated are primer pairs, restriction enzymes and antibiotic resistances employed during cloning. Mutation constructs were generated for spkC (**A**), spkD (**B**), spkF (**C**), spkH (**D**), spkI (**E**), spkJ (**F**), spkK (**G**) and spkL (**H**). Created mutation constructs were used to transform *Synechocystis* WT (F) and WT (M). (Km^R= kanamycin resistance; Gm^R= gentamycin resistance)

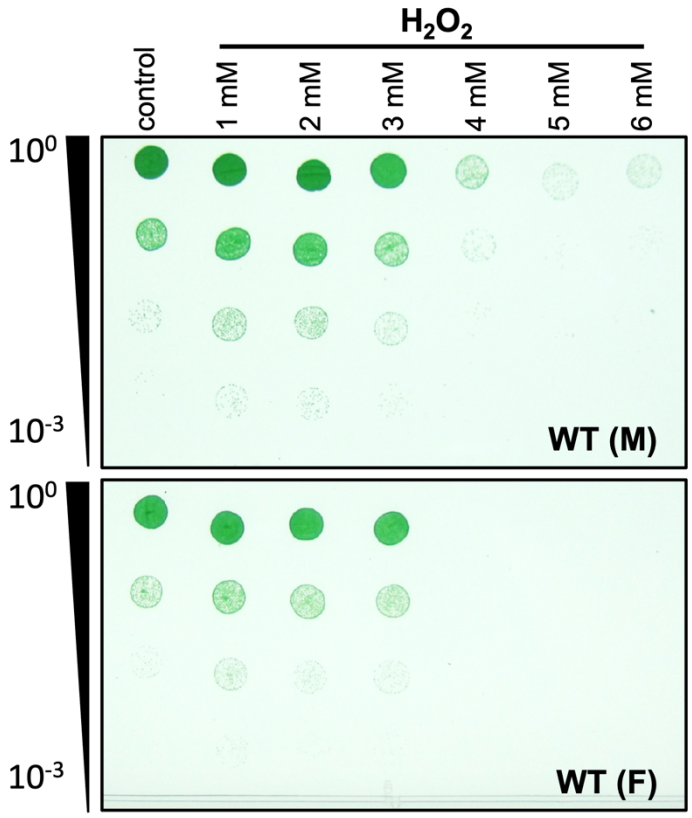

Appendix Figure 3: Preliminary experiment to evaluate critical external H_2O_2 concentration for WT (M) and WT (F). Cultures were adjusted to OD750 of 0.4 and probed with increasing amount of H_2O_2 (1; 2; 3; 4; 5; 6 mM) and exposed to light for 1 h at 30 °C and 100 µmol m^{-2} s^{-1}. Upon survival assay, *Synechocystis* was adjusted to the OD750 of 0.2 with BG11 (TES pH 8.0). Further, the suspension was diluted in serial dilution to 1:10, 1:100 and 1:1000. 2 µl of the dilution series were spotted on solid BG11 plates (TES pH 8.0; 1.5 % bacto agar). Cultures were allowed to recover for 4 d under constant light (at 30 °C and 100 µmol m^{-2} s^{-1})

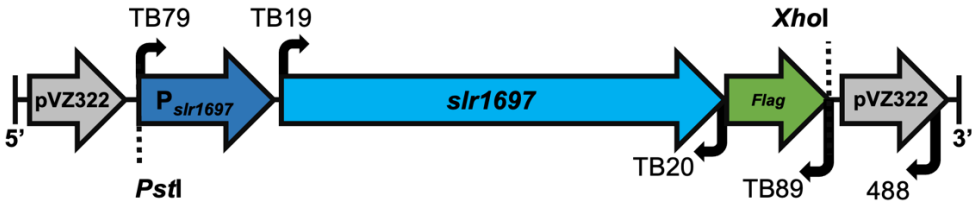

Appendix Figure 4: Generation of Δ*spkB*^{C}. Native *slr1697* was amplified together with its native promoter ($P_{slr1697}$, TB79/80) in a PCR reaction. C-terminally a 3x Flag-tag was added for immunodetection. Through blunt end cloning (*Pst*I; *Xho*I) the complementation construct was ligated into the autonomous plasmid pVZ322 generating pTB29.

Acknowledgement

At first and foremost, I would like to thank Prof. Dr. Martin Hagemann for giving me the opportunity to work on this project under his guidance. He did not only provide valuable input in the field of science but also for life in general. I am grateful that he always kept a positive outlook on this project even when I lost hope. Further, I am grateful for introducing me into the research consortium “SCyCode”, which funded my work and granted me access to this remarkable network of scientists.

Further, I like to say thank you to the entire PUR team for welcoming me into their group and being supportive throughout the entire journey. A special thanks goes out to Klaudia Michl for her kindness and the lively conversations we had about topics beyond science. You made the “little lab” a warm place to work in. Same goes out to Peter Walke and his talent in entangling me into conversations at our daily tea rounds. My love goes out to Luna Alvarenga-Lucius and Stefan Lucius and our time we had in our office talking about life, future plans and sometimes even talking about science. You became dear friends of mine. Same goes out for Oliver Mantovani for his amazing cookouts and Mariano Santoro for just being himself.

I’d like to thank my family, especially my sister for always believing in me in pursing this path of life. I would like to thank my parents who unfortunately hadn’t had the chance to be with me on this journey however, they built the foundation which eventually led into this thesis. Additionally, I am grateful for having Petra Redekop and Eileen Basse in my life. For many years you supported me, and I found not only friends in you but also family. Finally, I would like to convey my sincere appreciation to my partner Konstantinos Fourlakis. Kostas you have always been on my side and coped with me at every point along this journey. We went through three theses together and you are still with me. This must be love!

Curriculum vitae

Name: Thomas Barske

Date of Birth: 03.06.1990 in Neustrelitz

Email: thomasbarske@gmx.de

Phone : +491520456955

Academic Background

07.2019-10.2022	PhD Student; University of Rostock Dep: Plant physiology (Prof Dr. M. Hagemann) Dissertation: The role of protein phosphorylation in acclimation processes in the cyanobacterium *Synechocystis* sp. PCC 6803 Consortium “SCyCode” (FOR2816)
04.2017-08.2019	Master of Science; University of Duesseldorf Dep: Plant biochemistry (Prof Dr. A. Weber) Master Thesis: Studies on manganese homeostasis in the cyanobacterium *Synechocystis* sp. PCC 6803
10.2011-08.2017	Bachelor of Science; University of Duesseldorf Dep: Plant stress physiology (Prof Dr. P. Jahns) Bachelor Thesis: Characterization of photosynthesis mutants *pgr1* and *mnx2* in *A. thaliana*
09.2001-07.2009	Abitur; Gymnasium Carolinum Neustrelitz

Publications

Barske, T., Spät, P., Schubert, H., Walke, P., Maček, B., & Hagemann, M. (2023). The Role of Serine/Threonine-Specific Protein Kinases in Cyanobacteria-SpkB Is Involved in Acclimation to Fluctuating Conditions in *Synechocystis* sp. PCC 6803. *Molecular & Cellular Proteomics*, ***22***(11). DOI: doi.org/10.1016/j.mcpro.2023.100656

Wang, Y., Chen, X., Spengler, K., Terberger, K., Boehm, M., Appel, J., **Barske, T.**, Timm, S., Battchikova, N., Hagemann, M., Gutekunst, K. (2022) Pyruvate:ferredoxin oxidoreductase and low abundant ferredoxins support aerobic photomixotrophic growth in cyanobacteria. *Elife*, ***11***, e71339. DOI: doi.org/10.7554/eLife.71339

Spät, P., **Barske, T.**, Maček, B., & Hagemann, M. (2021). Alterations in the CO2 availability induce alterations in the phosphoproteome of the cyanobacterium *Synechocystis* sp. PCC 6803. New Phytologist, ***231***(3), 1123-1137. DOI: doi.org/10.1111/nph.17423

Poster Presentations

Thomas Barske & Martin Hagemann: The role of serine/threonine-kinases in the metabolic regulation of carbon metabolism in *Synechocystis* sp. PCC 6803. *Annual Conference of the Association for General and Applied Microbiology (VAAM)*; Leipzig (Deutschland). 2020

Assertion

I hereby declare, that the submitted thesis entitled

'The role of protein phosphorylation in acclimation processes in the cyanobacterium *Synechocystis* sp. PCC 6803'

is my own work. I have only used the sources indicated and have not made unauthorized use of services of a third party. Where the work of others has been quoted or reproduced, the source is always given.

I further declare that the dissertation presented here has not been submitted in the same or similar form to any other institution for the purpose of obtaining an academic degree.

Rostock, 12.12.2024 .....

.....

Thomas Barske